DOI: 10.31577/ahs-2019-0020.02.0013

ACTA HYDROLOGICA SLOVACA

Volume 20, No. 2, 2019, 113–121

EFFECT OF THE DATA LENGHT AND SEASONALITY ON THE ACCURACY OF *T*-YEAR DISCHARGES ESTIMATION: CASE STUDY ON THE TOPĽA RIVER

Veronika Bačová Mitková

The paper deals with the effect of two factors on the accuracy of *T*-year discharge estimation resp. fluctuations in the estimation of these discharges. As input data the series of daily discharges and peak discharges on the Topľa River at Hanušovce nad Topľou for the period of 1931–2015 were used. To estimate the *T*-year maximum discharges, the maximum annual discharges (AM) method was used with theoretical probability distributions that are among the most widely used in Slovak hydrological practice (Log-Pearson III, Gamma and Log-Normal). We analysed the effect of the time series length and the effect of seasonality (winter, summer) on the accuracy of *T*-year maximum discharges estimation.

KEY WORDS: the Topľa River, AM method, peak discharge, data length, seasonality, *T*-year discharge

Introduction

Flood frequency analysis plays a major role in the design of hydraulic structures and flood control management. One way of estimating the design discharges is the flood frequency analysis and solution of the relationship between peak discharges of the flood waves and probability of their return period (*T*). Directive 2007/60/ EC of the European Parliament of 23 October 2007 concerning the assessment and management of flood risks requires member States to draw up flood hazard maps of floods with very long return periods *T* (500 to 1000 years). All methods of estimating floods with a very long return period are associated with great uncertainties. Determining the specific value of a 500- or 1000-year flood for engineering practice is extremely complex. Nowadays hydrologists are required to determine not only the specific design value of the flood, but it is also necessary to specify confidence intervals in which the flow of a given 100-, 500-, or 1000-year flood may occur with probability, for example, 90%. The correct estimations of potential culminations of floods require the inclusion of the longest data series of observations, as well as the inclusion of historic pre-instrumental data to statistically analysed data series (Gaal et al., 2010; Elleder et al., 2013; Kjeldsen et al., 2014). Brazdil et al. (2006) studied historic hydrological materials in order to estimate floods threat in Europe. Estimation of the uncertainty at the design discharges was investigated for example by Merz and Thieken (2009) or Rogger et al. (2012). In addition to this factor, the type of theoretical probability distribution that is used to estimate maximum (extreme) values has an impact on the estimation of *T*-year discharges. Bačová (2019) compared the two most commonly used methods in estimating *T*-year maximum discharges, AM method and POT method. The author analysed effect of the threshold level value and various data set (peaks, mean daily discharges) on estimated values of Q_T. In El Adlouni et all (2008), Malamud and Turcotte showed that, the most commonly used distributions in hydrology can be divided into four groups: the normal family (normal, Lognormal), the general extreme value family (GEV, Gumbel, Fréchet, reverse Weibull), the Pearson type III family (Gamma, Pearson type III, Log-Pearson type III), and the Generalized Pareto distributionIn practice, all these models are fitted to data and compared using conventional goodness-of-fit tests. Having a data set of maximum annual values of discharges different statistical tests, like Kolmogorov-Smirnov, Anderson-Darling and Chi-Squared tests (Ang and Tang, 2007) are used to select the suitable continuous distribution. When the sample volume is not very large, the volume can be extended by numerical simulation of random variable based on the inverse method. The maximum discharges Q_p% corresponding to the probability of exceedance *P*% are not unique values, but they depend on aleatory and epistemic uncertainty (Merz and Thieken, 2009). Aleatory uncertainty is mainly due to the time variability and the length of the maximum discharges series, while the epistemic uncertainty is the consequence of the incomplete knowledge of the hydrological system. The paper presents an estimation of the *T*-year maximum dis-

charges by the AM method and analyses the effect of the time series length and seasonality (winter, summer) on the accuracy of *T*-year maximum discharges estimation. In this approach Log-Pearson theoretical probability distribution type III. was used. Subsequently, estimated *T*-year maximum discharges were compared with other two theoretical distribution types used in Slovakia: Log-normal and Gamma probability distribution. The set of daily discharges and peak discharges on the Topľa River at Hanušovce nad Topľou for the period of 1931–2015 was used as input data for our case study.

Method and material

Annual maximum discharges method (AM)

In estimating *T*-year maximum discharges, the annual maximum method (AM) is generally the first and most widely used method. It aims to estimate the Q_T quantiles, it means such annual maximum discharges that their probability of exceedance is *1/T*, where *T* can be e.g. 10, 20, 50, and 100, 500 or 1000 or more years. These quantiles are determined from the distribution function of the maximum annual discharges. Thus, Q_T is the maximum discharges with a probability *P* that occurs, on average, once every *T*-years. When interpreting the results, it should be borne in mind that the estimated values of *T*-year maximum discharges with very high return periods are extrapolated and that each statistical method is burdened with some uncertainty. Different types of theoretical distributions are used to evaluate the *T*-year maximum discharges. Appropriate choice of the theoretical probability distribution type should represent quite precisely the uncertainty and variability of the problem. In the world literature, there are a number of scientific papers dealing with the selection and testing of the suitability of theoretical probability distributions in estimating the maximum values of hydrological characteristics.

In our analysis we use one type of the theoretical probability distribution the Log-Pearson distribution type III (LP III). The advantage of this particular technique is that extrapolation can be made of the values for events with return periods well beyond the observed flood events. To estimate the distribution parameters, the method described in Bulletin17B was used. Bulletin 17B was issued in USA in 1981, and re-issued with minor corrections in 1982 in the Center for Research in Water Resources of the University of Texas at Austin (IACWD, 1982). Bulletin 17B provided revised procedures for weighting station skew values with results from a generalized skew study, detecting and treating outliers, making two station comparisons, and computing confidence limits about a frequency curve. Bulletin 17B is based on Bulletins 15, 17, 17A (http://acwi.gov/hydrology/ Frequency/minutes/ index.html). The cumulative distribution function and probability distribution function according Hosking and Wallis (1997) are defined as:

If $\gamma \neq 0$ let $\alpha = 4/\gamma^2$ and $\xi = \mu - 2\sigma/\gamma$

If $\gamma > 0$ then:

$$F(x) = G(\alpha, \frac{x-\xi}{\beta})/\Gamma(\alpha), \quad (1)$$

$$f(x) = \frac{(x-\xi)^{\alpha-1} e^{-(x-\xi)/\beta}}{\beta^{\alpha}\Gamma(\alpha)} \quad (2)$$

If $\gamma < 0$ then

$$F(x) = 1 - G(\alpha, \frac{\xi-x}{\beta})/\Gamma(\alpha) \quad (3)$$

$$f(x) = \frac{(\xi-x)^{\alpha-1} e^{-(\xi-x)/\beta}}{\beta^{\alpha}\Gamma(\alpha)} \quad (4)$$

where
μ – location parameter;
σ – scale parameter;
γ – shape parameter;
Γ – Gamma function.

Subsequently, the LP III probability distribution was compared with other recommended probability distributions (Gamma and Log-normal) according to OTN ŽTP 3112-1: 03. To verify the accuracy of theoretical distributions, we used a non-parametric Kolmogorov-Smirnov goodness of fit test for the significance level $\alpha = 0.05$.

Topľa River basin and input data

The Topľa is upland/lowland type of river in eastern Slovakia. The catchment drainage area is 1 506 km² with length of 129.8 km (Fig. 1). The long-term mean daily discharge amounts in Hanušovce nad Topľou was 8.1 $m^3 s^{-1}$ during period 1931–2015 (runoff height was 244.2 mm). The maximum discharge during the analysed period was 449 $m^3 s^{-1}$ (06.04.1932) in the station Hanušovce nad Topľou. Figure 1 also shows the exceeding probabilities of the maximum annual discharges according to Log-Pearson Type III. probability distribution (LPIII). The advantage of this particular technique is that extrapolation can be made of the values for events with return periods well beyond the observed flood events. This theoretical distribution belongs to the family of Pearson distributions, so called three parametric Gamma distributions, with logarithmic transformation of the data. We compared the LPIII distribution with the theoretical probability distributions that were (and still are) most widely used hydrological practice in Slovakia: Gamma distribution and Log-normal distribution Table 1. From Table 1 we can see relatively small differences in the values of estimated *T*-year maximum discharge values in comparison with other two types of theoretical probability distributions used in hydrological analyses of extremes in the Slovakia. The lowest values of estimated *T*-year maximum discharges, achieved Gamma theoretical probability distribution, especially for discharges with high return periods.

Peak annual discharges (points), linear trend (red line), and 4-years moving averages for the Topľa River at Hanušovce nad Topľou during the period 1931–2015 are shown in Figure 2. In the analysed period, two dry periods of 1954–1964 and 1990–1999 were occurred.

While wet periods can be described only as years with extreme flood events (e.g. 1932, 1948, 1952, or 1980), a relatively prolonged wet period was in 2004–2010. Annual maximum discharges show a decreasing trend for the period of 1931–2015.

Results

The effect of time series length on the T-year discharge estimation

For analysing the effect of the length of the data series on the estimation of *T*-year discharges, the period 1931–2015 was divided into two shorter periods: 1931–1973 and 1974–2015. We had chosen this approach because for the frequency analysis is recommended the length of the observation series 5T (FEH, 1999). If T=50 years, then a 250-member observation series is required for a reliable estimate of Q_{50}. Such a length of data series (AM) is practically absent. Therefore, the probability of a reliable estimate of *T*-year maximum discharge for short-range river basins is relatively low. In the case of the 50-year observation series, the probability of Q_{100} is 39% and in the case of the 100-year series is 63% (Viessman et al., 1977).

The estimated values of the Q_{Tmax} for shorter periods of the data series are listed in Table 2. There is compared the LPIII distribution with other frequently used and recommended hydrological distributions in hydrological practice in Slovakia: Log-normal distribution and Gamma distribution. The exceedance probabilities of the annual peak discharges for two shorter periods of the Topľa River at Hanušovce nad Topľou according the LPIII distribution are presented in Figure 3a-b.

The effect of the seasonality on the T-year discharge estimation

For dividing the year into seasons, we proceeded from the analysis of the occurrence of floods and from the evaluation of the Topľa runoff regime during the year. In terms of the type of runoff regime, Topľa belongs to the highland-lowland area with rain-snow runoff with the culmination of river runoffs in the month of March, respectively April. The distributions of the mean monthly discharges in 10-year periods are presented in Figure 4a-b. The Figure 4a-b shows that in some 10-year periods lower values of mean monthly discharges were achieved in months of occurrence of high water levels. The long-term mean monthly discharge in the month of March reached value 11.82 $m^3 s^{-1}$ and in month of September reached value 3.25 $m^3 s^{-1}$ during the period of 1931–2015. The occurrence of annual maximum discharges is presented in Figure 5. The number

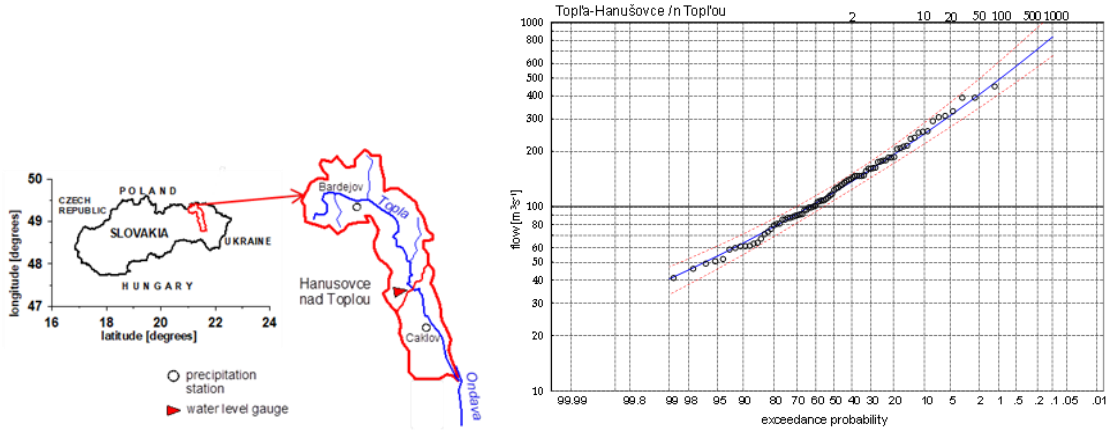

Fig. 1. A scheme of the Topľa River basin (left) and exceedance probability of the annual peak discharges of the Topľa River: Hanušovce nad Topľou within 1931–2015 period (right).

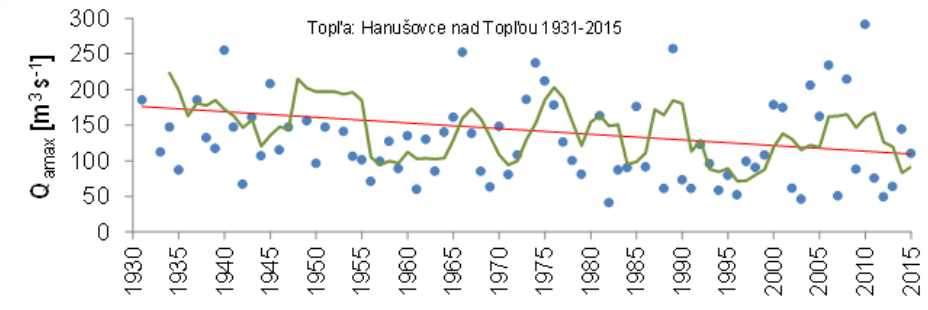

Fig. 2. Peak annual discharges (points), linear trend (red line), and 4-years moving averages for the Topľa River at Hanušovce nad Topľou during the period 1931–2015.

Table 1. ***T*-year maximum discharges Q_{Tmax} [m^3 s^{-1}] on the Topľa River: Hanušovce nad Topľou (1931–2015) estimated from maximum annual discharges Q_{amax}**

T [year]	*2*	*5*	*10*	*50*	*100*	*200*	*500*	*1000*
P [%]	*39*	*18*	*9.5*	*2*	*1*	*0.5*	*0.2*	*0.1*
Log-Pearson III								
Q_{Tmax} [m^3 s^{-1}]	139	193	249	398	473	556	679	783
P_{value} *K-S*	0.999							
Log-normal								
Q_{Tmax} [m^3 s^{-1}]	146	199	252	380	439	502	589	660
P_{value} *K-S*	0.987							
Gamma								
Q_{Tmax} [m^3 s^{-1}]	148	204	255	360	404	446	506	541
P_{value} *K-S*	0.744							

Table 2. **Comparison of the estimated Q_{Tmax} for shorter periods on the Topľa River: Hanušovce nad Topľou**

1931–1973								
T [year]	*2*	*5*	*10*	*50*	*100*	*200*	*500*	*1000*
P [%]	*39*	*18*	*9.5*	*2*	*1*	*0.5*	*0.2*	*0.1*
Log-Pearson III								
Q_{Tmax} [m^3 s^{-1}]	143	198	257	427	519	627	797	949
P_{value} *K-S*	0.813							
Log-normal								
Q_{Tmax} [m^3 s^{-1}]	161	202	249	357	408	457	527	583
P_{value} *K-S*	0.787							
Gamma								
Q_{Tmax} [m^3 s^{-1}]	169	219	272	321	428	472	529	571
P_{value} *K-S*	0.44							
1974–2015								
T [year]	*2*	*5*	*10*	*50*	*100*	*200*	*500*	*1000*
P [%]	*39*	*18*	*9.5*	*2*	*1*	*0.5*	*0.2*	*0.1*
Log-Pearson III								
Q_{Tmax} [m^3 s^{-1}]	125	180	239	408	499	602	760	899
P_{value} *K-S*	0.74							
Log-normal								
Q_{amax} [m^3 s^{-1}]	137	181	233	362	423	488	580	654
P_{value} *K-S*	0.74							
Gamma								
Q_{Tmax} [m^3 s^{-1}]	144	189	236	336	376	416	467	505
P_{value} *K-S*	0.55							

of annual peak discharges during the period of 1931–2015 occurred in the month of March was 31 peaks (Fig. 5). In terms of the Topľa runoff regime, the measured data were divided into two seasons:

- Summer season is from May to October, when peak discharges occur only from heavy rainfall (Fig. 6a).
- Winter season is from November to April, when peak discharges occur by combining heavy rainfall in the form of snow and rain as well as snow melting in the area (Fig. 6b).

The statistical data series were supplemented with maximum discharges in the given season, so that there are 85 measurements per season.

The estimated values of the Q_{Tmax} for summer season and winter season are listed in Table 3. There is compared the LPIII distribution with other frequently used and recommended hydrological distributions in hydrological practice in Slovakia: Log-normal distribution and Gamma distribution. The exceedance probabilities of the maximum seasonal discharges of the Topľa River at Hanušovce nad Topľou according the LPIII distribution are presented in Figure 7a-b.

Comparisons of the estimated maximum discharges with a return period of 100 and 1000 years according to the selected procedures are shown in Figure 8. The highest estimated values of Q_T were achieved according the LPIII distribution.

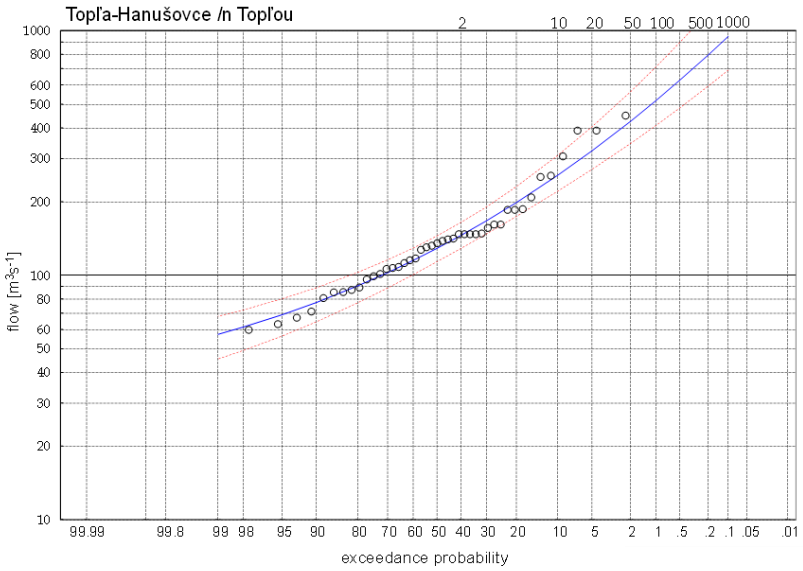

a)

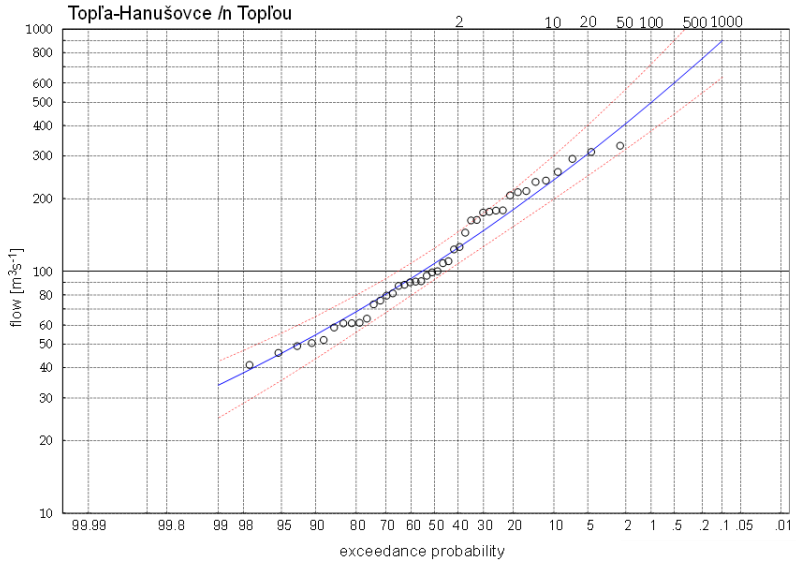

b)

Fig. 3. The exceedance probabilities of the annual maximum discharges according to Log-Pearson Type III. probability distribution (LPIII) a) period 1931–1973 and b) period 1974–2015 on the Topľa River: Hanušovce nad Topľou.

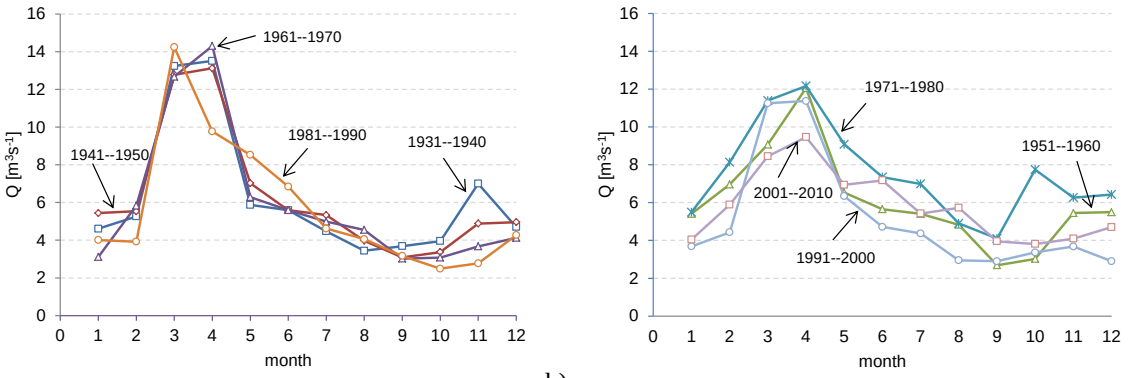

a) b)

Fig. 4. The distributions of the mean monthly discharges in 10-year periods of the Topľa River: Hanušovce nad Topľou.

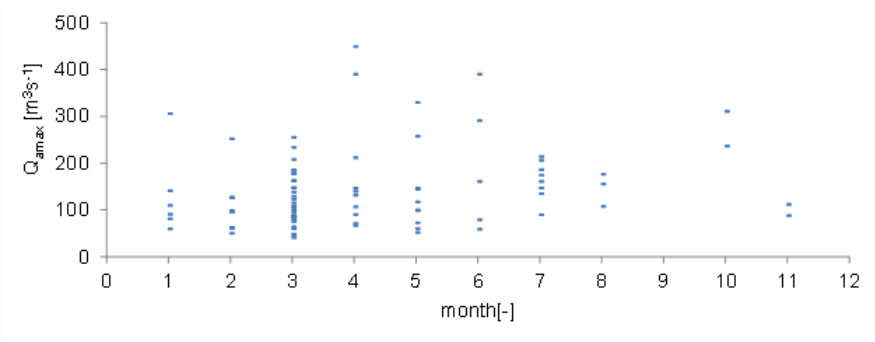

Fig. 5. Month of the annual maximum discharges occurrence (period of 1931–2015) on the Topľa River at Hanušovce nad Topľou.

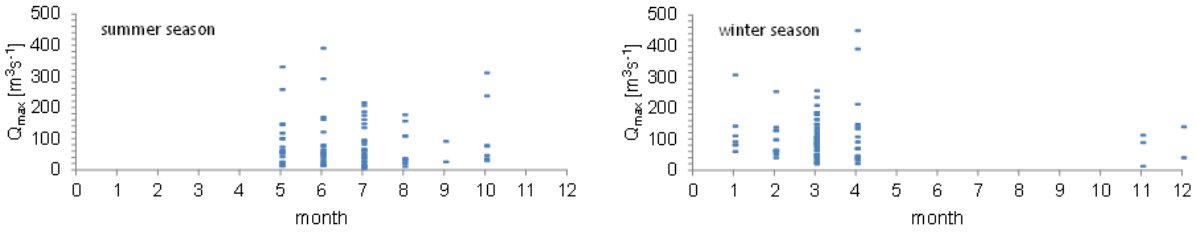

Fig. 6. Occurrence of extreme discharges in month of the summer season (left) and winter season (right), with supplemented maximum discharges in a given season (number of measurements is still 85 per season).

Table 3. Comparison of the estimated Q_{Tmax} in selected two season a) summer and b) winter on the Topľa River: Hanušovce nad Topľou

Summer season								
T [year]	*2*	*5*	*10*	*50*	*100*	*200*	*500*	*1000*
P [%]	*39*	*18*	*9.5*	*2*	*1*	*0.5*	*0.2*	*0.1*
Log-Pearson III								
Q_{Tmax} [m^3 s^{-1}]	68	124	194	423	558	718	975	1209
P_{value} *K-S*	0.953							
Log-normal								
Q_{Tmax} [m^3 s^{-1}]	75	124	193	422	555	714	971	1202
P_{value} *K-S*	0.922							
Gamma								
Q_{Tmax} [m^3 s^{-1}]	86	134	189	318	373	428	501	556
P_{value} *K-S*	0.79							
Winter season								
T [year]	*2*	*5*	*10*	*50*	*100*	*200*	*500*	*1000*
P [%]	*39*	*18*	*9.5*	*2*	*1*	*0.5*	*0.2*	*0.1*
Log-Pearson III								
Q_{Tmax} [m^3 s^{-1}]	117	172	228	372	443	518	626	715
P_{value} *K-S*	0.94							
Log-normal								
Q_{Tmax} [m^3 s^{-1}]	108	151	204	347	419	498	613	710
P_{value} *K-S*	0.73							
Gamma								
Q_{Tmax} [m^3 s^{-1}]	115	159	208	315	360	404	462	504
P_{value} *K-S*	0.78							

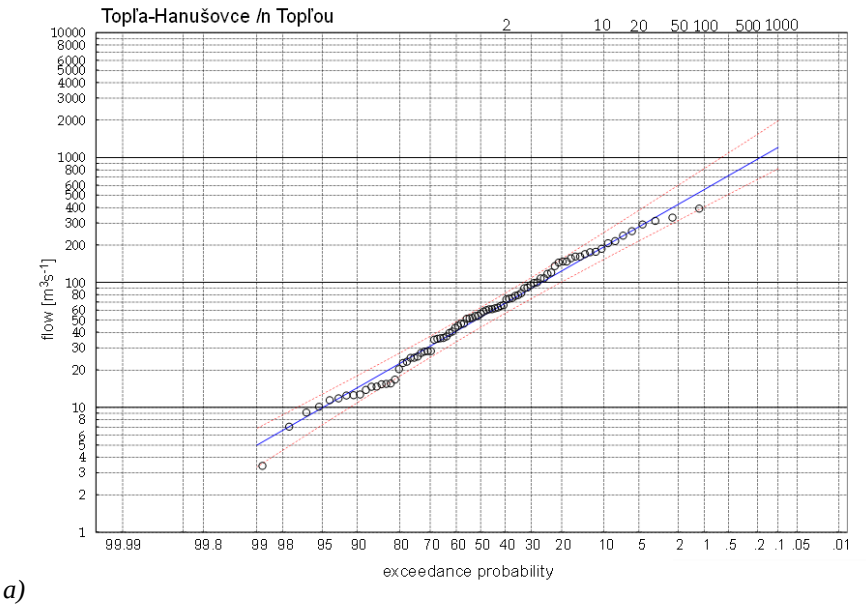

a)

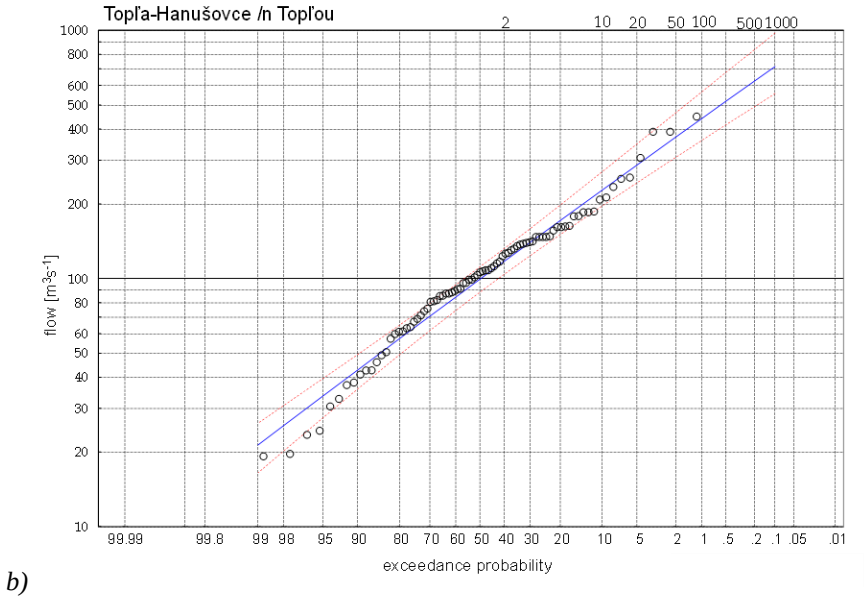

b)

Fig. 7. Exceedance probabilities of the maximum discharges according to Log-Pearson Type III. probability distribution (LPIII) a) summer season and b) winter season on the Topľa River: Hanušovce nad Topľou.

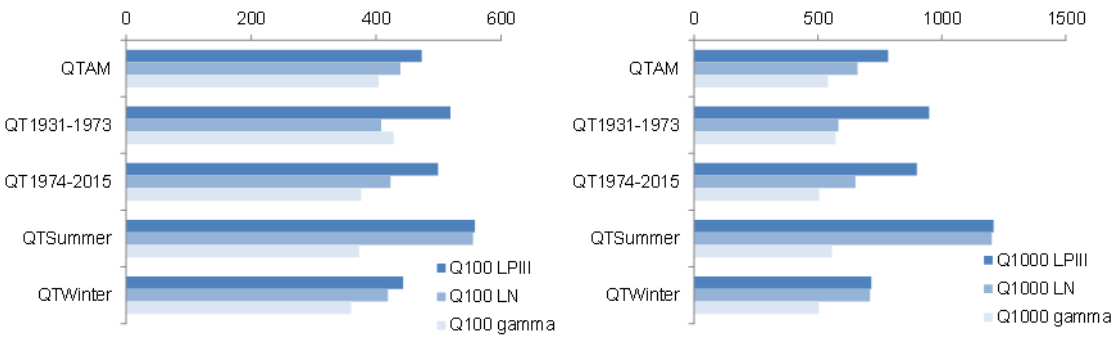

Fig. 8. Comparisons of the estimated maximum discharges with a return period of 100 and 1000 years according to the selected procedures.

Conclusions and discussion

The first part of the paper deals with the estimation of the Q_T from annual peak discharges on the Topľa River at Hanušovce nad Topľou (1931–2015). Results of this part showed relatively small differences in the values of estimated *T*-year maximum discharge values in comparison with other two types of theoretical probability distributions used in hydrological analyses of extremes in the Slovakia. The lowest values of estimated *T*-year maximum discharges, achieved Gamma theoretical probability distribution, especially for discharges with high return periods. Phien and Jivajirajah (1984) dealt with the use of the Log-Person III distribution to estimate the maximum annual rainfall and discharges. They concluded that this distribution is more suitable for discharges with a higher return period, but for the annual floods the existence of an upper bound of the distribution, in some cases may cause some higher uncertainties. Comparing the suitability of several types of probability distributions (GEV, LPIII and Gumbel) for estimating *T*-year discharges was discussed in Millington et al. (2011). Authors do not prefer any of the selected distributions as better and recommend further research. Results of our analysis indicate that the LPIII distribution is suitable distribution for *T*-year discharge estimation with a higher return period.

Estimation of flood magnitudes to be used as a basis to design the hydraulic structures and flood control management is therefore of crucial importance. Therefore the paper also presented an estimation of the *T*-year maximum discharges by the AM method and analysed the effect of the time series length and seasonality (winter, summer) on the accuracy of *T*-year maximum discharges estimation. Results showed that not only the selection of the distribution function to estimate *T*-year discharges but also the processing of the statistical series affect the results of the estimation. The shorter periods showed higher estimations of the *T*-year discharges. The highest estimated values according the LPIII distribution was achieved for summer season. The lowest estimated value according the LPIII distribution was achieved for winter season. When interpreting the results, it should be borne in mind that the *T*-year maximum discharges are related to the length of the analysed series and therefore estimated values with very high return periods are extrapolated and that each statistical method is burdened with some uncertainty that may be caused by alone method, but also the data, which may be burdened by a certain measurement error.

Acknowledgements:

This work was supported by the project VEGA 2/0004/19 and results from the project implementation of the "Centre of excellence for integrated flood protection of land" (ITMS 26240120004) supported by the Research & Development Operational Programme funded by the ERDF.

References

Ang, A. H-S., Tang, W. H. (2007): Probability Concepts in Engineering, Emphasis on Application to Civil and Environmental Engineering, John Wiley & Sons, 427 p., ISBN 978-0-471-72064-5.

Bačová Mitková, V. (2019): The peak over threshold method and its uncertainty in determining of T-year maximum discharges: Case study at the Topľa River. In Acta Hydrologica Slovaca, 2019, Vol. 20, No. 1, 32–43, ISSN 1335–6291. (In Slovak)

Brazdil, R., Kundzewicz, Z. W., Benito, G. (2006): Historical hydrology for studying flood risk in Europe. Hydrological Science J., 51(5), 739–764, DOI:10.1623/hysj.51.5. 739.

El Adlouni, S., Bobée, B., Ouarda, T. B. M. J. (2008): On the tails of extreme event distributions in hydrology. Journal of Hydrology. vol. 355, issues 1–4, 16–33.

Elleder, L., Herget, J., Roggenkamp, T., Nießen, A. (2013): Historic floods in the city of Prague – a reconstruction of peak discharges for 1481–1825 based on documentary sources, Hydrology Research, 44(2), 202–214.

FEH (1999): Flood estimation handbook. Wallingford (Institute of Hydrology), ISBN 0 948540 94 X.

Gaal, L., Szolgay, J., Kohnova, S., Hlavcova, K., Viglione, A. (2010): Inclusion of historical information in flood frequency analysis using a Bayesian MCMC technique: A case study for the power dam Orlik, Czech Republic, Contribut. to Geophysics and Geodesy, 40(2), 121–147.

Hosking, J. R. M., Wallis, J. R. (1997): Regional Frequency Analysis. Cambridge University Press. Cambridge. 244 p. ISBN 0521019400, 9780521019408.

IACWD (1982): Guidelines for determining flood flow frequency, Bulletin 17-B. Technical report, Interagency Committee on Water Data, Hydrology Subcom. 194 p.

Kjeldsen, T. R., Macdonald, N., Lang, M., Mediero, et al. (2014): Documentary evidence of past floods in Europe and their utility in flood frequency estimation, Journal of Hydrology, 517, 963–973. ISSN 0022-1694.

Merz, B., Thieken, A. H. (2009): Flood risk curves and uncertainty bounds. Natural Hazards, vol. 51, issue, 3, 437–458, DOI: 10.1007/s11069-009-9452-6.

Millington, N., Das, S., Simonovic, S. P. (2011): The Comparison of GEV, Log-Pearson Type 3 and Gumbel Distributions in the Upper Thames River Watershed under Global Climate Models. Water Resources Research Report. Department of Civil and Environmental Engineering the University of Western Ontario London, Ontario, Canada, September 2011, 1–54.

OTN ŽP 3112–1: 03 ME SR (2003): Quantities of surface and groundwater. Hydrological data of surface waters. Quantification of the flood regime. Part 1: Determination of T-year flow rates and T-year flow waves at larger flows Branch technical standard OTN ŽP 3112–1: 03, Ministry of Environment SR, Bratislava, 31 p. (in Slovak)

Phien, H. N., Jivajirajah, T. (1984): Applications of the log Pearson type-3 distribution in hydrology. J. Hydrol., 73, 359–372.

Rogger, M., Kohl, B., Pirkl, H., Viglione, A., Komma, J., Kirnbauer, R., Merz, R., Blöschl, G. (2012): Runoff models and flood frequency statistics for design flood estimation in Austria – Do they tell a consistent story? Journal of Hydrology, 456–457, 16 August 2012, 30–43.

Viessman, J. R. W., Knapp, J. W., Lewis, G. L, Harbaugh, T. E. (1977): Introduction to hydrology. New York (Harper and Row), 704 p., ISBN 0700224971.

Ing. Veronika Bačová Mitková, PhD.
Institute of Hydrology SAS,
Dúbravská cesta 9
84104 Bratislava
Slovak Republic
E-mail: mitkova@uh.savba.sk

DOI: 10.31577/ahs-2019-0020.02.0014

ACTA HYDROLOGICA SLOVACA

Volume 20, No. 2, 2019, 122–130

LONG-TERM TREND CHANGES OF MONTHLY AND EXTREME DISCHARGES FOR DIFFERENT TIME PERIODS

Dana Halmová, Pavla Pekárová, Veronika Bačová Mitková

Nowadays, we are more frequently faced to the information about the extremes in discharge regime (floods and droughts) and their catastrophic consequences. Because of this, the first aim of hydrologists should be to verify these hypotheses and identify sources of mentioned changes. Rating extreme discharges is very important for example for assessing the impact of air temperature on the discharge. The upper parts of river basins are suitable for studying the effect of potential climate change or increased air temperature on drainage conditions in the basin. Analysis of trends in minimum discharges can predict its development and minimize its negative impacts on society and the environment. The contribution deals with the analysis of monthly discharges regime at gauging stations Bela-Podbanske (1929–2014) and Vah-Liptovsky Mikulas (1922–2014) and also analysis the minimum/maximum discharges in Bela River basin. Discharge analysed trends in mean monthly discharges and extreme discharges for selected time period to determine whether there is any significant change in the trend. We used the Mann-Kendall nonparametric test, which is one of the most widely used non-parametric tests to detect significant trends in time series.

KEY WORDS: trend analysis, MANN-KENDALL test, extreme and monthly discharges, Vah River basin, Bela River basin

Introduction

Currently, we are more frequently faced to the information about the hydrological extremes and their catastrophic consequences. Because of this, the first aim of hydrologists should be to verify these hypotheses and identify sources of mentioned changes (e.g. the natural variability of runoff). Analysis of trends in minimum discharges can predict its development and minimize its negative impacts on society and the environment. It is important to note that the minimum discharge is one of the characteristics that can define hydrological drought. So that we can answer these questions, it is necessary to statistically analyse long and high quality time series of hydrological observations from the river basins, which are little affected by anthropogenic activities. The upper part of the Bela River Basin is particularly suitable for studying the effect of potential climate change on drainage conditions in the basin. Regular, continuous evaluation of average daily discharges began in 1927/1928. Attention was also paid to the precipitation, including winter. Based on the measured data originated a number of studies, (Burn et al., 2004; Demeterová and Škoda, 2009; Majerčáková et al., 2007). Analysis of trends in long-term series of hydrological data are an important tool for finding and understanding of the changes in the development of a rainfall-runoff process and the results are useful in the water planning and flood protection. The main reasons for the runoff changes are considered global climate change in combination with different types and degree of human activities. The trend analysis used different methods. Specific examples of analyses of trends in rainfall-runoff time series can be found in several works of authors Falarz (2004), Fu et al. (2004), Franke et al. (2004), Kundzewicz and Robson (2004), Helsel and Frans (2006); Schoner et al. (2009), Onoz, Bayazit, (2003), Pekárová, (2003), etc.
The aim of this article is analysis of monthly discharges regime at gauging stations Bela-Podbanske and Vah-Liptovsky Mikulas for the selected time periods and analysis of minimum discharges in Bela River basin.

Methods and data

At the trend analysis of the time series, generally, the null hypothesis *H0* that there is no trend is to be tested against the alternative hypothesis *H1*, that there is a trend. The parametric and non-parametric tests can be used for this purpose. The parametric test considers the linear regression of the random variable x_i on time. The parameters of the trend line are calculated by using standard method for estimation of the parameters of a simple linear regression model, i.e. by using least square method.

Mann-Kendall nonparametric test

The Mann-Kendall nonparametric test (M-K test) is one of the most widely used non-parametric tests for signifycant trends detection in time series. The nonparametric tests are more suitable for the detection of trends in hydrological time series, which are usually irregular, with many extremes (Hamend, 2008; Yue et al., 2003; Gilbert, 1987; Blahušiaková et al., 2016; Lettenmaier et al., 1994; Sonali et al., 2013). The study performs two types of statistical analyses: 1) the presence of a monotonic increasing or decreasing trend, and 2) the slope of a linear trend is estimated with the non-parametric Sen's method, which uses a linear model to estimate the slope of the trend and the variance of the residuals should be constant in time.

By M-K test, we want to test the null hypothesis H_0 of no trend, i.e. the observations x_i are randomly ordered in time, against the alternative hypothesis H_1, where there is an increasing or decreasing monotonic trend. The data values are evaluated as an ordered time series. Each data value is compared with all subsequent data values. If a data value from a later time period is higher than a data value from an earlier time period, the statistic S is incremented by *1*. On the other hand, if the data value from a later time period is lower than a data value sampled earlier, S is decremented by *1*. The net result of all such increments and decrements yields the final value of S (Shahid, 2011).

For n (number of tested values) ≥ 10, the statistic S is approximately normally distributed with the mean and variance as follows

$$E(S) = 0 \tag{1}$$

$$VAR(S) = \frac{1}{18}\left[n(n-1)(n-2) - \sum_{p=1}^{q} t_p (t_p - 1)(2t_p + 5) \right] \tag{2}$$

where:

q – number of tied groups,

t_p – number of data values in the p group.

The standard test statistic Z is computed as follows

$$Z = \begin{cases} \dfrac{S-1}{\sqrt{VAR(S)}} & if \quad S \rangle 0 \\ 0 & if \quad S = 0 \\ \dfrac{S+1}{\sqrt{VAR(S)}} & if \quad S \langle 0 \end{cases} \tag{3}$$

The presence of a statistically significant trend is evaluated using Z value. A positive (negative) value of Z indicates an upward (downward) trend. The statistic Z has a normal distribution. To test for either an upward or downward monotone trend (a two-tailed test) at α level of significance, hypothesis H_0 (no trend) is rejected if the absolute value of Z is greater than Z_1-α/2, where Z_1- α/2 is obtained from the standard normal cumulative distribution tables. The M-K test detects trends at four levels of significance: α=0.001, 0.01, 0.05, and α=0.1. Significance level of 0.001 means that there is a 0.1% probability that the value of x_i is from a random distribution and are likely to make a mistake if we reject the hypothesis H_0; Significance level of 0.1 means that there is a 10% probability that we make a mistake if we reject the hypothesis H_0. If the absolute value of Z is less than the level of significance, there is no trend.

For the four tested significance levels the following symbols are used in the template:

*** if trend at α=0.001 level of significance – H_0 seems to be impossible,

** if trend at α=0.01 level of significance,

* if trend at α=0.05 level of significance – 5% mistake if we reject the H_0,

\+ if trend at α=0.1 level of significance,

Blank: the significance level is greater than 0.1, cannot be excluded that the H_0 is true.

Study area and data

River Vah is the biggest left-side Danube River tributary and the second biggest river in Slovakia. The Bela River (93.49 km^2), tributary of the Vah River, is situated in the High Tatra Mountains with the highest degree of protection and it can be considered as the basin unaffected by human activity. Gauging station Vah-Liptovsky Mikulas is the final profile above the water reservoir Liptovska Mara, one of the largest reservoirs in Slovakia and the basin are is 1107.21 km^2. Also for that reasons, it is useful to know the hydrological changes in the discharge profiles, (Fig. 1).

In this study the average daily discharges from above mentioned water gauges were used (Vah River: 1922–2014, Bela River 1929–2014). These basins were selected according of the homogeneity of the discharge time series. In order to perform the homogeneity analyses of data, two different tests of homogeneity were applied on each series, the standard normal homogeneity test (Alexandersson, 1986) and the Mann-Whitney-Pettit test (Pettit, 1979). Software Anclim (Štěpánek, 2007) was used to perform both tests (Pekárová and Miklánek ed., 2019).

The Figure 2 shows the long-term percentiles of daily discharges, which gives a basic overview of the hydrology regime in the area. E.g. green line means the mean of daily discharges, percentile P50. Yellow line represent 99th percentile. According to classification method by Pardé (1947), the Bela River and Vah River have snow-meltwater (nival) runoff regimes, single-peak with a maximum in April-May due to snowmelt and a minimum in winter when the water is retained in form of ice and snow.

Results

Changes of the monthly and extreme discharge from the long-term point of view

Variation in average monthly discharges

We quantify the variation in average monthly discharges from long-term point of view and analysed the monthly discharges regime at both profiles Bela-Podbanske and Vah-Liptovsky Mikulas for the whole selected time periods and for five shorter periods, see Table 1 and

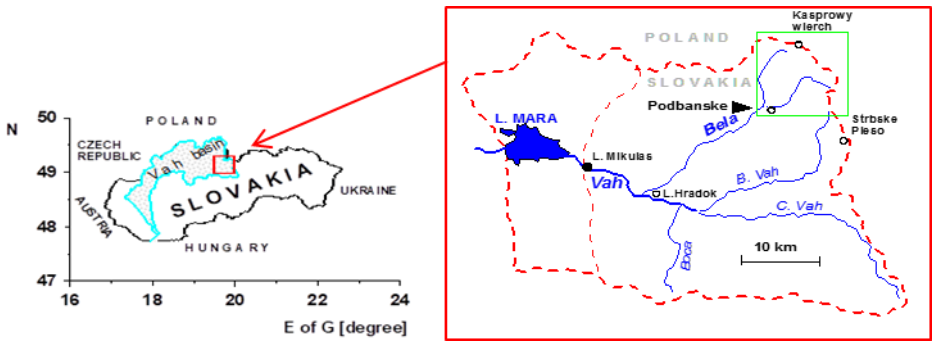

Fig. 1. Location of the Vah River in Slovakia (left), scheme of the Vah River Basin up to Liptovsky Mikulas gauge; green square represents Bela River basin up to gauging station Bela-Podbanske (right).

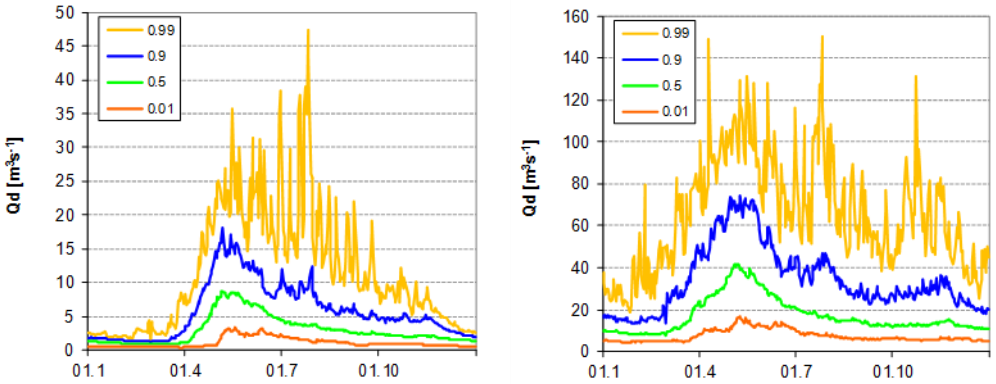

Fig. 2. Long-term percentiles of daily discharges, Bela - Podbanske (left), Vah - Liptovsky Mikulas (right).

Table 2, for both profiles, were average monthly discharges subsequently analysed too. The results show that the maximum monthly discharge in each period occurred in May at both river basins. Minimum discharges occurred in February and March at Bela-Podbanske. Minimum discharge occurred in January and February at Vah-Liptovsky Mikulas. This mode of maximum and minimum discharges coincides with the regime discharges in these altitudes. Mean monthly discharge in gauging stations Bela-Podbanske and Vah-Liptovsky Mikulas for selected time periods is in Table 1 and Table 2, maximal and minimal monthly values are highlighted. The shorter time series distribution was chosen with respect to the recommended minimum lengths of time series for hydrological analyses (Viessman et al., 1977).

Trend analysis of monthly and extreme discharge characteristics

The results of the slope of trend lines analysis for individual months give us the information about ***monthly discharge trend changes*** for different periods (Fig. 3). Directive of trend lines for individual months for the selected time periods suggest that a change in trend (from decreasing to increasing trend) occurs in the second half of the year (from July to December) at Bela-Podbanske (Fig. 3a). Conversely, in the month of May, when occurring in those watersheds maximum discharges, trend remains growing for both periods at the Bela River Basin, but during the period of 1960–2014 is three times higher than during the period of 1929–2014. On the contrary at the Vah River Basin trend remains downward. Clearly declare upward or downward trend in the flow, it is necessary to analyse the longest series of observations at any station. In the profile Vah-Liptovsky Mikulas change in trend occurs in different months of the calendar year in the months January, March, August, September and November (Fig. 3b). However, in some months (April, June, July, October) there is a situation where the trend does not change, but in the period 1960–2014 it is several times higher.

Trends changes of monthly discharges for two different time periods and selected months can be clearly seen in Fig. 4; Fig. 4a applies to the station Bela-Podbanske, months: May, September to November and Fig. 4b. applies to the station Vah-Liptovsky Mikulas, months: March, September and November.

The upper part of the Bela River Basin is particularly suitable for studying the effect of potential climate change on drainage conditions in the basin. Analysis of ***trends in several discharge characteristics*** (***minimum and maximum, 1-day, 3-day, 7-day and 30-day minimum,***

Table 1. **Mean monthly discharge for selected time periods at gauging stations Bela-Podbanske (maximal monthly discharge – bold; minimal monthly discharge – grey color)**

Bela - Podbanske						
Time period	1929–2014	1960–2014	1929–1948	1949–1968	1969–1988	1989–2014
January	1.205	1.205	1.063	1.304	1.244	1.208
February	0.988	1.017	0.777	1.120	1.018	1.027
March	1.037	1.001	1.039	1.118	0.920	1.065
April	3.394	3.291	3.577	3.498	2.843	3.598
May	**8.432**	**8.418**	**8.207**	**8.211**	**8.372**	**8.823**
June	6.300	6.274	6.419	6.589	6.156	6.100
July	4.553	4.436	4.630	4.482	4.607	4.506
August	3.401	3.240	3.720	3.382	3.415	3.160
September	2.852	2.816	3.263	2.288	2.709	3.081
October	2.522	2.450	2.897	2.243	2.381	2.556
November	2.338	2.072	1.945	1.802	2.412	2.430
December	1.639	1.535	1.631	1.488	1.651	1.632

Table 2. **Mean monthly discharge for selected time periods at gauging stations Vah-L. Mikulas (maximal monthly discharge – bold; minimal monthly discharge – grey color)**

Vah-Liptovsky Mikulas						
Time period	1922–2014	1960–2014	1922–1941	1942–1961	1962–1981	1982–2014
January	9.640	9.550	10.190	9.306	9.640	9.508
February	9.184	9.226	9.045	9.066	10.125	8.770
March	14.772	13.954	16.950	14.560	14.829	13.545
April	30.010	30.107	26.740	32.563	33.325	28.435
May	**39.131**	**38.689**	**42.535**	**35.070**	**41.436**	**38.132**
June	26.762	27.380	26.815	25.035	30.872	25.287
July	20.173	20.009	19.745	21.308	20.406	19.604
August	16.379	16.277	17.930	15.488	17.021	15.591
September	14.128	13.934	18.028	10.423	14.199	13.967
October	14.372	14.533	16.755	11.123	17.700	12.881
November	15.485	13.687	21.908	14.172	13.768	13.624
December	12.377	11.477	14.316	12.488	11.883	11.095

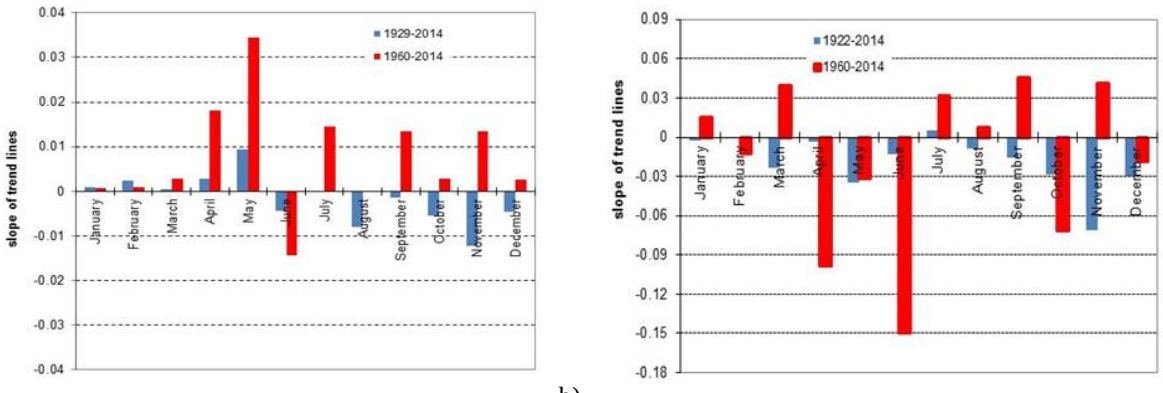

a) b)

Fig. 3. Slope of trend lines of individual months; a) Bela-Podbanske the time periods 1929–2014 and 1960–2014; b) Vah-L. Mikulas, the time periods 1922–2014 and 1960–2014.

as well as maximum, and day of minimum/maximum discharge occurrence) can predict its development and minimize its negative impacts on society and the environment (fauna and flora of the river basin). It is important to note that the minimum discharge is one of the characteristics that can define hydrological drought.

Trends changes of discharge characteristics for period 1929–2014 in gauging station Bela-Podbanske and period 1922–2014 Vah-Liptovsky Mikulas is shown in Fig. 5a and Fig. 5b.

Results clearly declare increasing (Bela-Podbanske) or decreasing (Vah-Liptovsky Mikulas) trend in the *Q_1-day minimum* or *Q_1-day maximum* flow. For further analysis it is clear that trend in time period 1960–2014 is decreesing.

The trend of other extreme discharges (*Q_3-day min/max*, *Q_7-day min/max*, and *Q_{30}-day min/max*) at gauging station Bela-Podbanske during the longer period 1929–2014 is slightly increasing. While the trend of shorter observation period (1960–2014) suggests that individual extreme discharges remain unchanged or very slightly decreasing. The trend of these characteristics at gauging station Vah-Liptovsky Mikulas during the longer period 1922–2014 remain unchanged or very slightly increasing in minimum and decreasing in maximum values.

According to these differences in trends for shorter and longer measurement periods is necessary to analyse the longest series of observations at any station.

Non-parametric tests for significant trends detection in time series at Bela and Vah

Examples of the evaluation of monthly and extreme discharge trends for selected time periods at gauging stations Bela-Podbanske (time periods 1929–2014, 1960–2014, and 1989–2014) and Vah-Liptovsky Mikulas (time periods 1922–2014, 1960–2014, and 1989–2014) are given in Table 3 and Table 4.

The results for the Bela River Basin (profile Bela-Podbanske) indicate trends at α=0.05 level of significance *(marking symbol – *)* in November, and trends at α=0.1 level of significance *(marking symbol – +)* in December for the time period 1929–2014. Guest shorter period 1960–2014 showed no significant trend. The trend at α=0.1 level of significance in November was established for the Vah River Basin (profile Vah-Liptovsky Mikulas) for the evaluation period 1922–2014. When evaluating a shorter time period 1960–2014 no signify-cant trend was detected, and we cannot reject the hypothesis H_0.

According to the M-K test, there was a change in the trend at the significance level α=0.05 for both stations in the analysis of whole periods of measurement (Bela-Podbanske 1929–2014, Vah-Liptovsky Mikulas 1922–2014) in the month of November. Figure 6 presents comparison of the long-term trend – as the conclusions of M-K trend test – of discharge in gauging station Bela-Podbanske and Vah-Liptovsky Mikulas in November for two time periods (1929/1922–2014, and 1960–2014) are shown.

Conclusion and discussion

In this study the average daily discharges from above mentioned water gauges were used (Vah River: 1922–2014, Bela River 1929–2014). These basins were selected according of the homogeneity of the discharge time series. In order to perform the homogeneity analyses of data, two different tests of homogeneity were applied on each series, the standard normal homogeneity test (Alexandersson, 1986) and the Mann-Whitney-Pettit test (Pettit, 1979). Software Anclim (Štěpánek, 2007) was used to perform both tests (Pekárová and Miklánek ed., 2019).

According to the M-K test, The Mann-Kendall nonparametric test (M-K test), which is one of the most widely used non-parametric tests for significant trends detection in time series, results showed a change in the trend at the significance level α=0.05 for both stations in

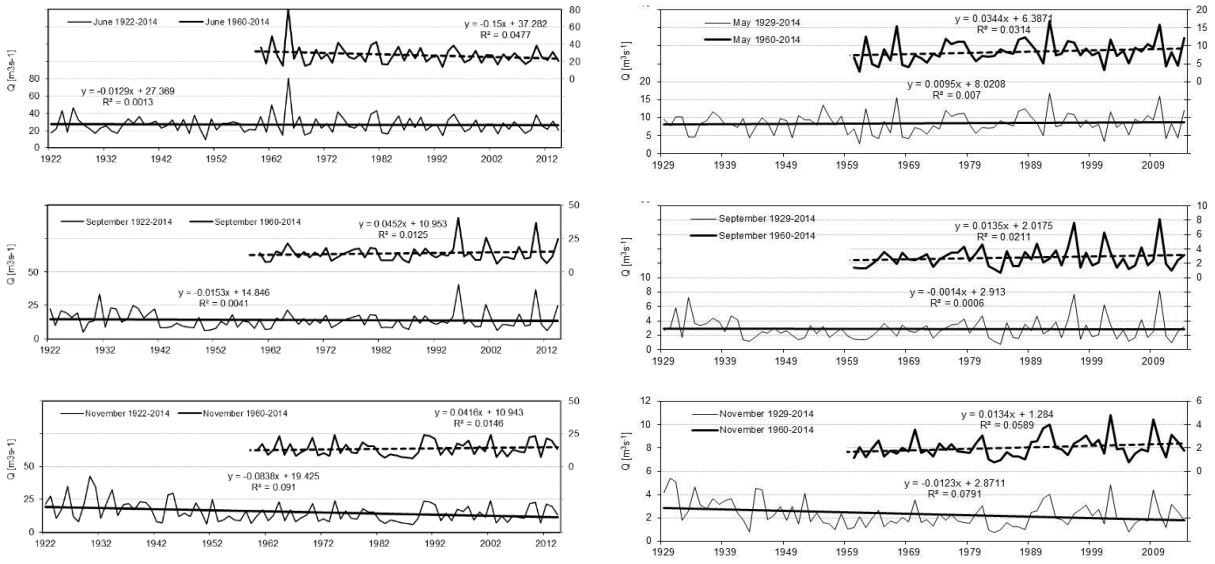

a) *b)*

Fig. 4. Linear trend of discharges in selected months: a) Bela-Podbanske: time periods 1929–2014 and 1960–2014; months June, September and November, b) Vah-Liptovsky Mikulas: time periods 1922–2014 and 1960–2014, months March, September and November.

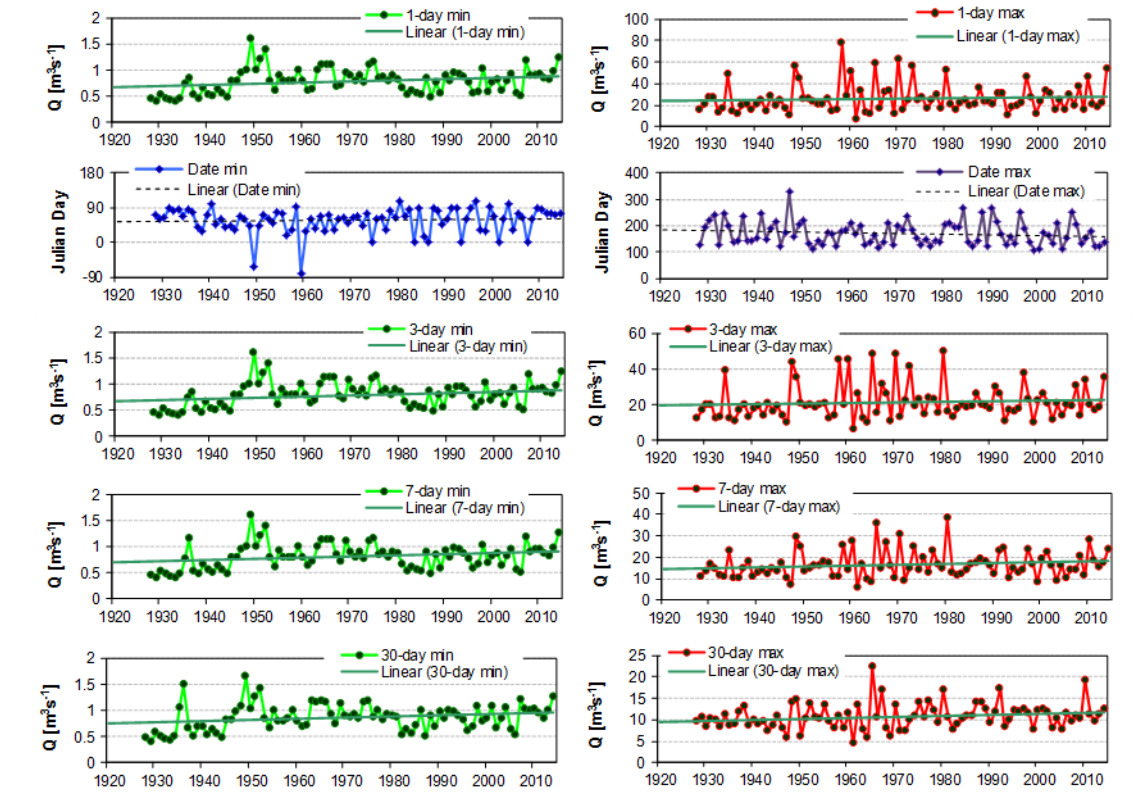

a)

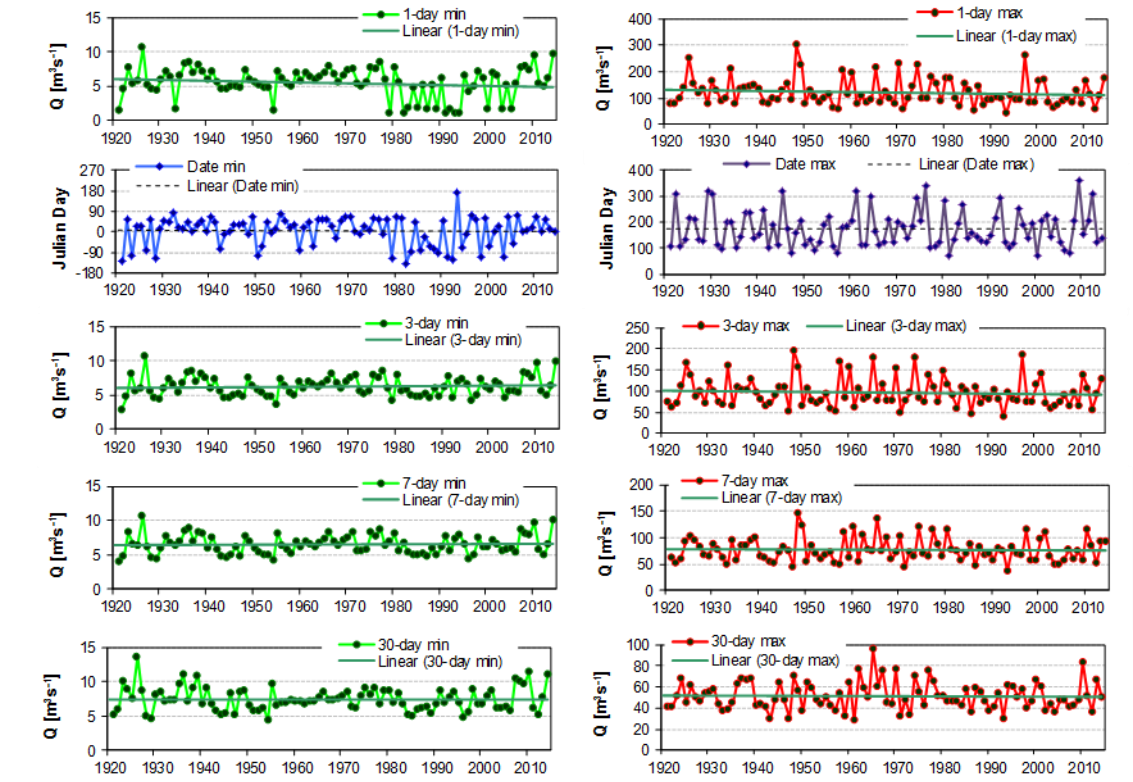

b)

Fig. 5. Linear trend of minimum (left figures) and maximum (right figures) discharge characteristics in particular years, a) station Bela-Podbanske, period: 1929–2014; b) station Vah-L. Mikulas, period 1922–2014.
Julian day means: 1=January 01, 30=January 30, –30 is 336 day=December 06.

Table 3. **Results of monthly and extreme discharge M-K trend tests for selected time periods, gauging station Bela-Podbanske** ***(** – level of significance α=0.01, * – level of significance α=0.05, +-α=0.1 level of significance)***

	1929–2014			1960–2014			1989–2014		
Discharge characteristics	Test Z	Signf.	Sen's A slope estimate	Test Z	Signf.	Sen's A slope estimate	Test Z	Signf.	Sen's A slope estimate
January	-0.31		0.000	-0.70		-0.002	0.14		0.002
February	1.33		0.002	-0.31		-0.001	0.50		0.004
March	1.13		0.002	-0.07		0.000	1.21		0.007
April	0.99		0.009	0.70		0.012	1.57		0.072
May	1.25		0.016	1.23		0.040	-0.82		-0.050
June	-0.19		-0.002	-0.50		-0.012	-1.18		-0.064
July	-0.44		-0.004	-0.91		-0.017	0.96		0.036
August	-1.82	+	-0.011	-0.46		-0.006	1.07		0.039
September	-0.40		-0.002	0.36		0.004	-0.75		-0.025
October	-0.93		-0.004	-0.10		-0.002	0.32		0.011
November	-2.40	*	-0.013	1.39		0.009	0.55		0.015
December	-1.92	+	-0.005	0.38		0.002	-0.07		-0.003
1-day min	2.55	*	0.002	-0.07		0.000	2.11	*	0.008
3-day min	2.73	**	0.002	-0.02		0.000	1.96	*	0.009
7-day min	2.62	**	0.002	-0.04		0.000	1.78	+	0.008
30-day min	2.36	*	0.003	-0.12		0.000	1.53		0.007
90-day min	0.68		0.001	-0.54		-0.001	1.25		0.008
1-day max	1.01		0.046	0.00		0.000	0.43		0.098
3-day max	1.42		0.040	0.03		0.007	0.14		0.020
7-day max	1.60		0.037	0.33		0.021	0.00		0.004
30-day max	1.89	+	0.021	0.80		0.020	-1.07		-0.046
90-day max	0.99		0.007	0.00		0.000	-0.75		-0.017

Table 4. **Results of monthly and extreme discharge M-K trend tests for selected time periods, gauging station Vah-Liptovsky Mikulas** ***(** - level of significance α=0.01, * - level of significance α=0.05, +-α=0.1 level of significance)***

	1922–2014			1960–2014			1989–2014		
Discharge characteristics	Test Z	Signf.	Sen's A slope estimate	Test Z	Signf.	Sen's A slope estimate	Test Z	Signf.	Sen's A slope estimate
January	0.451		0.005	0.886		0.026	1.106		0.091
February	-0.793		-0.011	0.537		0.018	1.534		0.123
March	-0.704		-0.018	1.031		0.043	2.070	*	0.213
April	-0.913		-0.045	-0.900		-0.100	0.571		0.142
May	-0.959		-0.047	-0.494		-0.070	-1.035		-0.299
June	-0.813		-0.028	-1.016		-0.090	-0.856		-0.157
July	-0.010		0.000	-0.290		-0.025	1.570		0.246
August	-1.381		-0.042	-0.552		-0.032	1.338		0.199
September	-0.803		-0.021	-0.138		-0.014	-0.303		-0.052
October	-1.603		-0.038	-0.145		-0.006	1.070		0.105
November	-2.546	*	-0.075	-0.073		-0.010	0.749		0.100
December	-1.646	+	-0.033	-0.508		-0.020	-0.660		-0.063
1-day min	-0.853		-0.006	-0.719		-0.010	3.055	**	0.159
3-day min	0.428		0.002	-0.327		-0.005	2.035	*	0.064
7-day min	0.156		0.001	-0.421		-0.005	2.248	*	0.071
30-day min	-0.571		-0.004	-0.116		-0.001	2.034	*	0.091
90-day min	-0.999		-0.012	0.987		0.023	2.570	*	0.111
1-day max	-1.640		-0.252	-0.937		-0.280	0.357		0.431
3-day max	-0.959		-0.113	-1.263		-0.306	0.036		0.061
7-day max	-0.451		-0.039	-1.314		-0.264	0.500		0.227
30-day max	-0.438		-0.020	-1.307		-0.178	0.321		0.056
90-day max	-0.949		-0.033	-1.336		-0.102	0.000		0.002

the analysis of whole periods of measurement (Bela-Podbanske 1929–2014, Vah-L. Mikulas 1922–2014) in the month of November. Figure 6 presents comparison of the long-term trend – as the conclusions of M-K trend test – of discharge in gauging station Bela-Podbanske and Vah-Liptovsky Mikulas in November for two time periods (1929/1922–2014, and 1960–2014).

We quantified the variation in average monthly discharges from long-term point of view and analysed the monthly discharges regime at both profiles Bela-Podbanske (1929–2014) and Vah-Liptovsky Mikulas (1922–2014) for the whole selected time periods and for five shorter periods. The mode occurrence of maximum and minimum discharges coincides with the regime discharges in these altitudes. We analysed the slope of trend lines analysis for individual months. This analysis

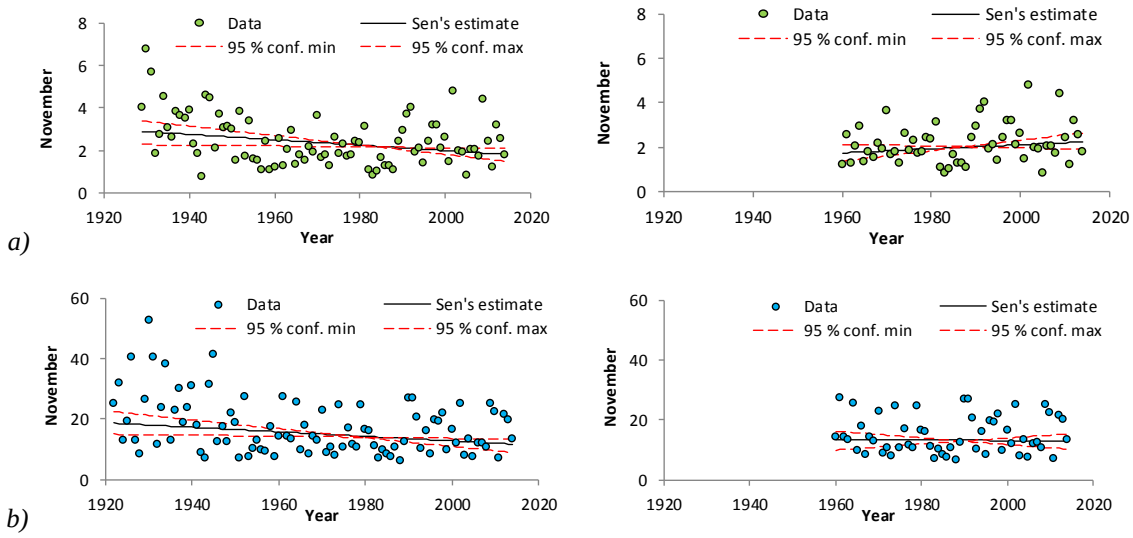

Fig. 6. Long-term trend – conclusions of Mann-Kendall trend test for discharge in November.a) Bela-Podbanske, b) Vah-L. Mikulas; whole period (left side figures) and 1960–2014 (right side figures).

gave us the information about ***monthly discharge trend changes*** for the whole year and also for different time periods. We analysed ***trends of several discharge characteristics*** (***minimum and maximum, 1-day, 3-day, 7-day and 30-day minimum, as well as maximum, and day of minimum/maximum discharge occurrence***) for shorter and longer time periods. Results showed that according to differences in trends for shorter and longer measurement periods is necessary to analyse the longest series of observations at any station. We aim to process the longest series of data flow and then evaluate their trends. Then we can evaluate the trend changes in the event of changes in the basin (climate change, water management construction, etc.).

The results of such analysis can be helpful in predicting of their development and minimizing their negative impacts on society and the environment (fauna and flora of the river basin). It is important to note that the minimum discharge is one of the characteristics that can define hydrological drought. In future, trend analysis should be linked to the climate change scenarios. Addressing the observed and potential future changes in runoff will require careful planning by water resource managers and policy makers, that should ensure the sustainable development of water management in the area of interest or mitigate the effects of potential drought periods.

Acknowledgements:

This work was supported by the project VEGA 2/0004/19 and results from the project implementation of the "Centre of excellence for integrated flood protection of land" (ITMS 26240120004) supported by the Research & Development Operational Programme funded by the ERDF.

References

Alexandersson H. (1986): A homogeneity test applied to precipitation data. J. Climatol., 6, 661–675.

Blahušiaková, A., Matoušková, A. (2016): Rainfall and runoff regime trends in mountain catchments (Case study area: the upper Hron River basin, Slovakia). J. of Hydrology Hydromech. 63: 3. 183–192.

Burn, D. H., Cunderlik, J. M., Pietroniro, A. (2004): Hydrological trends and variability in the Liard River basin. Hydrological Science Journal, 49(1), 53–68, doi.org/10.1623/hysj.49.1.53.53994.

Demeterová, B., Škoda, P. (2009): Low flow in selected streams of Slovakia. J. Hydrol. Hydromech., 57(1), 55–69.

Falarz, M. (2004): Variability and trends in duration and depth of snow cover in Poland in the 20th century. International Journal of Climatology, 24, 1713–1727.

Franke, J., Goldberg, V., Eichelmann, U., Freydank, E., Bernhofer, C. (2004): Statistical analysis of regional climate trends in Saxony, Germany. Climate Research, 27, 2004, 145–150, DOI: 10.3354/cr027145.

Fu, G., Chen, S., Liu, C., Shepard, D. (2004): Hydro-climatic trends of the Yellow River basin for the last 50 years. Climatic Change, 65, 2004, 149–178, doi.org/10.1023/B:CLIM.0000037491.95395.bb.

Kundzewicz, Z., Robson, A. (2004): Change detection in hydrological records – a review of the methodology. Hydrological Science Journal, 49(1), 7–20, doi.org/10.1623/hysj.49.1.7.53993.

Gilbert, R. O.(1987): Statistical Methods for Environmental Pollution Monitoring. John Wiley & Sons, Inc., New York.

Hamed, K. H. (2008): Trend detection in hydrologic data: The Mann-Kendall trend test under the scaling hypothesis. Journal of Hydrology, 349 (3–4), 350–363, doi.org/10.1016/j.jhydrol.2007.11.009.

Helsel, D. R., Frans, L. M. (2006): Regional Kendall Test for Trend. Environmental Science and Technology, 40, 2006, 13 p.

Lettenmaier, D. P, Wood, E. F., Wallis, J. R. (1994): Hydro-Climatological Trends in the Continental United States, 1948-1988. Journal of Climate. 7. 586–607.

Majerčáková, O., Škoda, P., Danáčová, Z. (2007): Development of selected hydrological and rainfall characteristics for the periods 1961–2000 and 2001–2006 in the High Tatras. Meteorological Jour. (in Slovak), 10(4), 205–210.

Onoz, B., Bayazit, M. (2003): The power of statistical tests for trend detection. Turkish J. Eng. Environ. Sci., 27, 247–251., <http://journals.tubitak.gov.tr/engineering/issues/muh-03-27-4/muh-27-4-5-0206-6.pdf>

Pardé, M. (1947): Fleuves et Riviéres. Paris.

Pekárová, P. (2003): Identification of long-term trends and fluctuations of hydrological time series (Part II, Results). Journal of Hydrol. and Hydromech., 51(2), 2003, 97–108.

Pekárová, P., Miklánek, P. (ed): Flood regime of rivers in the Danube River basin. IH SAS, Bratislava, CD ROM, 215 pp. + 450 pp. app., ISBN 978-80-89139-43-9

Pettitt A. N. (1979): A non-parametric approach to the change-point problem. Appl. Stat., 28, 126–135.

Schoner, W., Auer, I., Bohm, R. (2009): Long term trends of snow depth at Sonnblick (Austrian Alps) and its relation to climate change. Hydrological Processes, 23, 2009, 1052–1063, DOI: 10.1002/hyp.7209.

Shahid, S. (2011): Trends in extreme rainfall events of Bangladesh. Theoretical and Applied Climatology, 104, 489–499, DOI: 10.1007/s00704-010-0363-y.

Sonali, P., Nagesh Kumar, D. (2013): Review of trend detection methods and their application to detect temperature changes in India. Journal of Hydrology. 47: 6. 212–227.

Štěpánek P. (2007): AnClim - software for time series analysis (for Windows). Dept. of Geography, Fac. of Natural Sciences, Masaryk University, Brno. 1.47 MB

Viessman, J. R. W., Knapp, J. W., Lewis, G. L, Harbaugh, T. E. (1977): Introduction to hydrology. New York (Harper and Row), 704 p., ISBN0700224971.

Yue, S., Pilon, P., Phinney, B. (2003): Canadian streamflow trend detection: impacts of serial and cross-correlation. Hydrological Sciences Journal, 48(1), 51–64, doi.org/10.1623/hysj.48.1.51.43478.

Ing. Dana Halmová, PhD.
Ing. Veronika Bačová Mitková, PhD.
RNDr. Pavla Pekárová, DrSc.
Institute of Hydrology SAS,
Dúbravská cesta 9
84104 Bratislava
Slovak Republic
E-mail: halmova@uh.savba.sk

DOI: 10.31577/ahs-2019-0020.02.0015

ACTA HYDROLOGICA SLOVACA

Volume 20, No. 2, 2019, 131–138

TESTING OF AN ALTERNATIVE APPROACH TO CALIBRATION OF A HYDROLOGICAL MODEL UNDER VARYING CLIMATIC CONDITIONS

Patrik Sleziak, Michal Danko, Ladislav Holko

Conceptual rainfall-runoff models are routinely used in practical water resources investigations. Common uncertainties associated with these models (in addition to the uncertainty related to schematization and structure of the models) include for example errors in the inputs, calibration/validation uncertainties (e.g., choice of the suitable lengths of the two periods), uncertainties related to the use of the models in other climatic conditions, etc. This study addresses the uncertainties related to the choice of calibration/validation periods for the long data sets with varying climatic inputs. It is conducted in the pilot catchment of the Jalovecký Creek (area 22.2 km^2) in Slovakia and uses data from the 30-years long period 1989–2018. A HBV type model (the TUW model) is used for the modelling. Two different approaches to selection of calibration period are compared. In the first approach, the calibration period is determined by division of the available data into three equally long periods (each of them is then used in model calibration and validation). Such an arbitrary division is the common practice in hydrological modelling. In the second approach, the selection of calibration periods is based on the cycles found in the measured data. The wavelet transform method revealed cyclical components in air temperature with period of 6-years. Periods in other data sets were less significant. In accordance with this finding, the model is calibrated for five 6-years long periods. Model performance for the two approaches to selection of the calibration periods is evaluated by visual comparison of measured and simulated monthly flows in different climatic periods and by the Nash-Sutcliffe efficiency coefficient. The two approaches to the selection of calibration period provided similar results. However, the model calibrated in colder period represents monthly flows more reliably than the model that was calibrated in warmer period. In terms of predictions related to climate change impacts it would mean that hydrological models calibrated in current period should provide reasonable simulations for warmer climate.

KEY WORDS: hydrological model calibration, method of wavelet transform, climate change

Introduction

Conceptual rainfall-runoff (r-r) models are routinely used in various practical water resource investigations (for example, flow forecasting, flood impact assessment, climate impact studies, etc.). Common problem linked with the use of these models is their calibration (i.e. the way to deal with uncertainties in parameter estimation, choice of the suitable length of calibration and validation periods, etc.). Previous studies (e.g., Merz et al., 2009; Perrin et al., 2007) showed that the length of the calibration period may significantly affect model calibration and model performance (for example, if the calibration period is too short). Merz et al. (2009) calibrated a semi-distributed conceptual r-r model for periods of 1, 3, 5, 10, 15, 30 years and analyzed the effect of the length of the calibration period on model performance. Their study was performed for 269 catchments in Austria. They found that the model performance during calibration period decrease and the model performance during validation period increase with the number of years available for calibration. Their results suggest that minimum calibration period to achieve good model performance is five years. Other authors suggest that the optimal length for the model calibration may vary from two to ten years (Anctil et al., 2004; Brath et al., 2004). Generally, the calibration period should be long enough to capture the variability of climatic and flow conditions (Sorooshian et al., 1983).

Previous studies (e.g., Vaze et al., 2010; Merz et al., 2011; Coron et al., 2012; Fowler et al., 2016; Saft et al., 2016; Sleziak et al., 2017, 2018) demonstrated that the r-r models show significant reductions in performance when used in climatic conditions that differ from the conditions for which were the models calibrated. For example, in Australia, Vaze et al. (2010) and Coron et al. (2012) observed that the hydrological model had a tendency to overestimate mean runoff when the calibretion period was wetter (i.e., a wet to dry parameter transfer). On the contrary, in Austria, Merz et al. (2011) and Sleziak et al. (2018) showed that a HBV model calibrated in a colder/drier decade (e.g., 1981–1990)

tended to overestimate the runoff in a warmer and wetter decade (e.g., 2001–2010), particularly in flatland basins. Such findings naturally indicate problems with model schematization or structure. In theory, the performance of a model that captures the dominant hydrological processes correctly, should not depend too much on the climatic (i.e. input) data. However, changing climate may result in a change of the dominant processes. Numerous studies were carried out on this topic, but the results are not always consistent among them due to different regions, physiographic conditions, etc. Proper approaches in hydrological modelling under changing climate therefore remains a great challenge for the modelers.

The objective of this article is to test an alternative approach to calibration of a lumped HBV model for the use in changing (or changed) climate. Specifically, we asked two research questions: (1) Can the determination of calibration periods based on natural cycles defined by the data result in better simulation results? (2) Can hydrological models that are calibrated in current climatic conditions achieve satisfactorily results in the future warmer climate?

The paper is organized as follows. The data section describes the study area and data. The methods section gives the details on determination of natural cycles in the data series, the TUW model and its application. The results section summarizes the results of this study. The discussion section discuss and compares the results to other studies. The last section presents conclusions.

Study area and data

This study is carried out in the mountain catchment of the Jalovecký Creek in Slovakia (Fig. 1). The catchment is representative for the hydrological cycle of the highest part of the Western Carpathians. Catchment area is 22.2 km^2. Elevations in the catchment range from 800 to 2178 m a.s.l. (mean 1500). Mean slope is 30º. Soil cover is represented by Cambisoils, Podsol, Ranker and Lithosoils. Forests dominated by spruce cover 44% of catchment area, dwarf pine covers 31% and alpine meadows and bare rocks cover the rest 25%.

Daily catchment precipitation daily air temperature, discharge and potential evapotranspiration from the period 1989–2018 are used. Point precipitation and air temperature measurements were interpolated to obtain catchment values. Potential evapotranspiration was calculated by the Blaney-Criddle method (Schrödter, 1985).

Methods

Two approaches to division of input data for the model (precipitation and air temperature as climatic drivers and runoff used for the validation of simulation) are used. First, the data are divided arbitrarily into equal periods, i.e. decades (1989–1998, 1999–2008, 2009–2018). Second, the data are divided into periods identified by the analysis of data carried out by the wavelet transform method. The idea is to use the data from the same natural cycle in hydrological modelling.

Method of wavelet transform

It is well know that the natural processes occur in cycles (e.g., Hurst, 1951; Klemeš 1974; Pekárová and Pekár, 2007). The WT method is a simple method to estimate the changes in cyclical components and variability of the time series (e.g., Sabo 2012). We apply the method to daily time series of air temperature, precipitation, and discharges of the of Jalovecký Creek catchment. The R software environment (R Development Core Team,

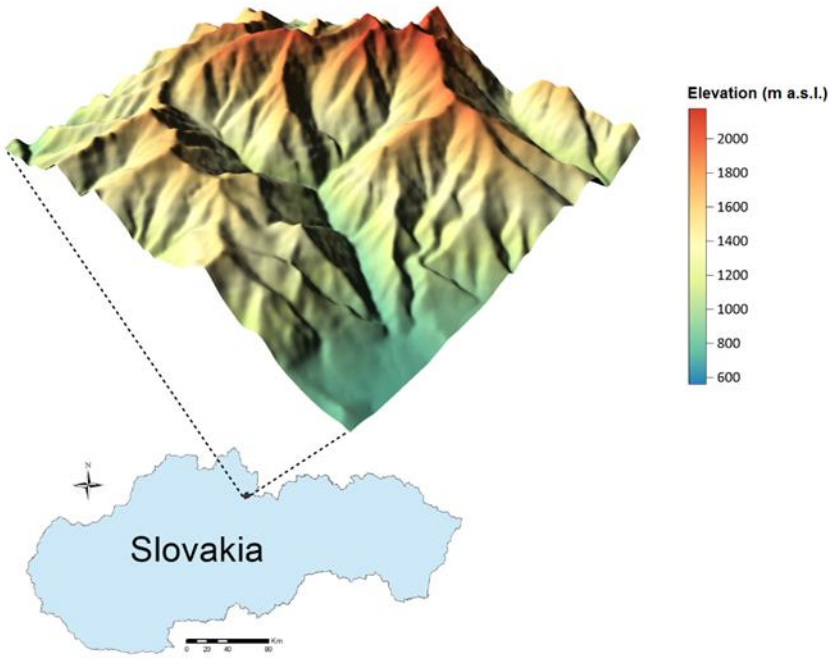

Fig. 1. The location and topography of the Jalovecký Creek catchment.

2011) and the package WaveletCo (Tian and Cazelles, 2011) are used to conduct the analysis that consists of four steps. First, the database of hydrometeorological time series (daily air temperature, precipitation, discharges) is created. Then, the work package is started and the models for the descriptions of changes in the cyclical components and the variability of the time series are created. In the last step, the structural changes in hydrometeorological time are analyzed/interpreted. For the interpretation of the results the scalogram used (see the Results).

Modelling

We apply the simple lumped model TUW (Viglione and Parajka, 2014), which follows the structure of a widely used Swedish HBV model (Bergström, 1995). The model simulates daily discharge using daily precipitation, air temperature, and potential evapotranspiration as inputs. It has 15 parameters that need to be calibrated. The model involves three modules (i.e., snow, soil, runoff module). In the snow module, the accumulation and melt are computed by the degree-day method. Groundwater recharge and actual evaporation are functions of actual water storage in the soil module. In runoff module, the runoff formation is represented by two linear reservoir equations. Channel routing is simulated by a triangular weighting function. More details about the model are given in Parajka et al. (2007).

The model is automatically calibrated using a differential evolution algorithm Deoptim (Ardia et al., 2015). The objective function consists of the combination of the Nash-Sutcliffe coefficient (NSE, Nash and Sutcliffe, 1970) and the logarithmic Nash-Sutcliffe coefficient (logNSE, Merz et al., 2011). The function is used in the form of (NSE + logNSE)/2.

Calibration and validation periods determined by the two approaches, i.e. the arbitrary and cycles-based divisions are used in the modelling. The model is in both cases calibrated and validated consecutively for each period and the comparison of results represent the Differential Split-Sample Test (DSST) proposed by Klemeš (1986) for model performance testing. Because the climatic characteristics in individual periods differ, the DSST evaluates model performance in periods with contrasting climate. The commonly used Nash–Sutcliffe Efficiency (NSE) is used to evaluate the model performance. A good simulation result will have NSE close to 1 (the best match between observed and simulated flows).

Results

Identification of cyclical components

Significant cyclical component was determined only for the air temperature data. The result is presented in the form of scalogram in Fig. 2. The scalogram provides an information about two parameters: scale (i.e., frequency) and time. The horizontal axis denotes time (i.e., duration of the signal) and the vertical axis denotes period (i.e., cyclical components). The size of the wavelet coefficients (used to receive an estimation of power spectrum) can be identified by the intensity of color. Significant periods are identified by the white line drawn around the intense colors. The section of the scalogram outside the cupola shape is considered problematic. The right side of the scalogram shows the global wavelet spectrum (averaged scalogram). The scalogram shown in Fig. 2 identifies significant periods in a range of 6–8 years, which occurred between the years 1995–2010. Because scalograms for precipitation and discharge did not show any significant cycles, the 6 years long period obtained from the air temperature data was used to split the data for the modelling into five periods.

Comparison of air temperature, precipitation and discharge in the periods determined arbitrarily and according to cycles identified in the data is shown in Fig. 3. It is clear that the period 1999–2008 is colder. The values of the mean annual air temperatures decrease on average by 0.7°C between periods 1989–1998 and 1999–2008 and 0.4°C between periods 1999–2008 and 2009–2018. Precipitation shows a slightly decreasing trend over the entire study period while the mean annual discharge does not change. The right part of Fig. 3 shows that air temperature has decreasing trend approximately until the year of 2006 with decrease of about 1.5°C between

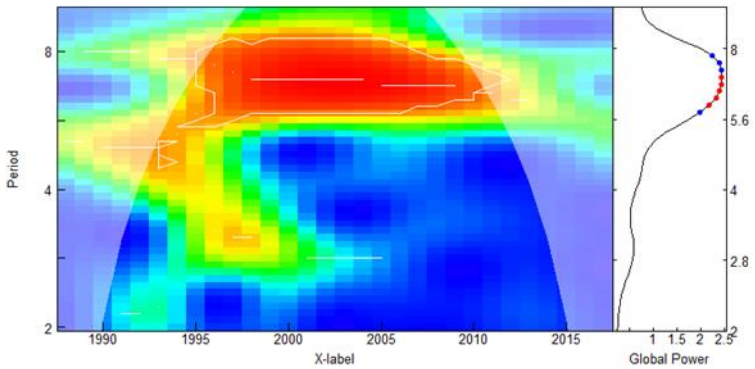

Fig. 2. Scalogram of air temperatures at Jalovecký Creek catchment. The data indicate significant cycles with period of 6-8 years that occurred approximately in 1995–2010.

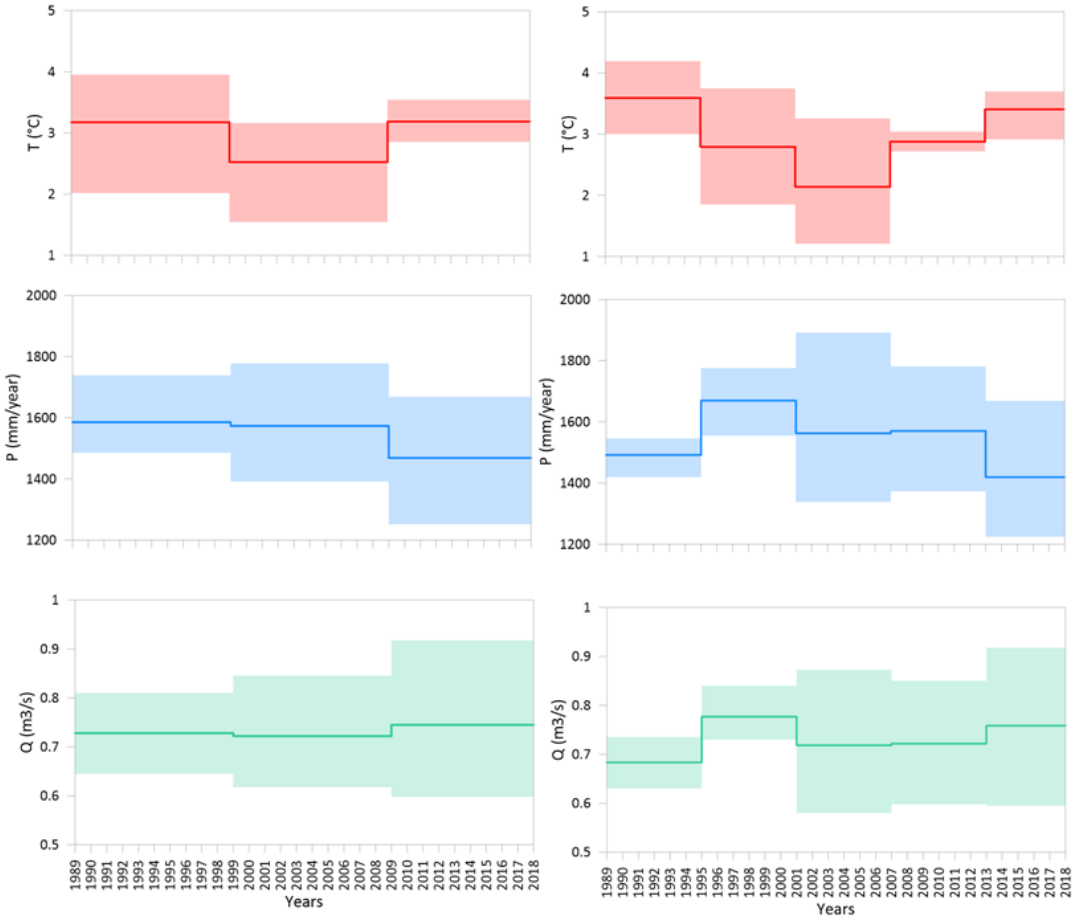

Fig. 3. Changes in the hydroclimatic characteristics (annual precipitation, mean annual air temperatures and annual flows) over three/five specific periods. The line shows the mean value of the hydroclimatic characteristics in a particular period. The coloured area indicates the range of 75 and 25 percentiles.

periods 1989–1994 and 2001–2006. The values of the air temperatures decreased from 3.6°C to 2.9°C between 1989–1994 and 2007–2012. Based on this analysis the periods 1999–2008 and 1995–2000/2001–2006/2007–2012 are considered as colder and period 1989–1998/2009–2018 and 1989–1994/2013–2018 as warmer.

Assessment of the model performance for two approaches to selection of calibration/validation periods

Results of model calibration and validation (in terms of different calibration lengths) are summarized in Tables 1 and 2. The results show that the model performed better in calibration periods. For the first calibration approach (i.e., the calibration periods are determined arbitrarily, Table 1), the NSE values in calibrations are on average 0.67 (1989–1998), 0.75 (1999–2008), and 0.76 (2009–2018). For the second calibration approach (i.e., determination of calibration periods based on naturally cycles, Table 2), the NSE values in calibrations are on average 0.63 (1989–1994), 0.75 (1995–2000), 0.73 (2001–2006), 0.74 (2007–2012) and 0.80 (2013–2018). The NSE values in the validation periods are generally lower than in the calibration periods. Different length or periods obtained by the two approaches did not result in significant differences.

Performances in the colder calibration period (1999–2008) are satisfactory, with NSE of 0.75. The NSE in the warmer validation period is 0.73 (Table 1). Similar result in terms of NSE is also achieved in the calibration period 2007–2012 (Table 2). Generally, the model calibrated in colder decade gives more satisfactorily results. This is also demonstrated in comparison of simulated and measured monthly flows (Figures 4 and 5). For the simulations we used parameters from colder calibration periods (i.e., period 1999–2008 and period 2007–2012). Comparison of measured and simulated monthly flows indicates that the model provided reasonable simulation of flows in different calibration and validation periods. Our results suggest that the model calibrated in colder decade more reliably represent the monthly flows. This implies that hydrological models calibrated in current climate (2013–2018) could provide reasonable predictions for the changed climate (i.e., for future warmer conditions).

Table 1. **Values of the Nash-Sutcliffe coefficient (NSE) in calibration and validation periods with length of 10 years; shaded area indicates the NSE values obtained in the calibrations; WP is warmer period and CP is colder period.**

Nash-Sutcliffe coefficient (NSE)		
WP 1989–1998	**CP 1999–2008**	**WP 2009–2018**
0.67	0.70	0.63
0.59	0.75	0.73
0.48	0.68	0.76

Fig. 6 presents measured and simulated snow water equivalent (SWE). Measured data are represented by point measurements of SWE at catchment mean elevation (1500 m a.s.l.). Simulated SWE with simulated SWE from the period of 1999–2008 and the period of 2007–2012. The simulations are also compared with the simulations obtained by using distributed model MIKE SHE (Danko et al., 2015). By visual comparison is clear that the simulations are close to real measurements. In some cases (e.g., years 1989, 1990, 2002) the model underestimated measured SWE.

Discussion

We evaluated the influence of selection of calibration and validation periods on performance of a lumped hydrological model. Length of the data series used in calibration and validation was 10 years and 6 years, respectively. Visual examination and the model performance efficiency indicator (NSE) show that the differences are small. Several studies (e.g., Merz et al. 2009; Perrin et al., 2007) addressed the question how much data are needed for model calibration. Merz et al. (2009) in their study showed that the calibration period of five years would be the minimum for achieving a good model performance. Other results suggest that the optimal length for the model calibration may vary from two to ten years (Anctil et al., 2004; Brath et al., 2004). Our results indicate that the length of calibration periods 6 and 10-years are both appropriate achieving similar simulations. It suggests that if the calibration period is long enough to cover periods of natural cycles in the input data, the arbitrary splitting of data into calibration and validation periods does not produce worse simulations. This conclusion should be verified in other catchments.

Studies show that the r-r models provide poor simulations when are applied in changing climate (e.g., Merz et al., 2011; Vaze et al., 2010; Coron et al., 2012; Sleziak et al., 2018). Merz et al. (2011) found that the model calibrated

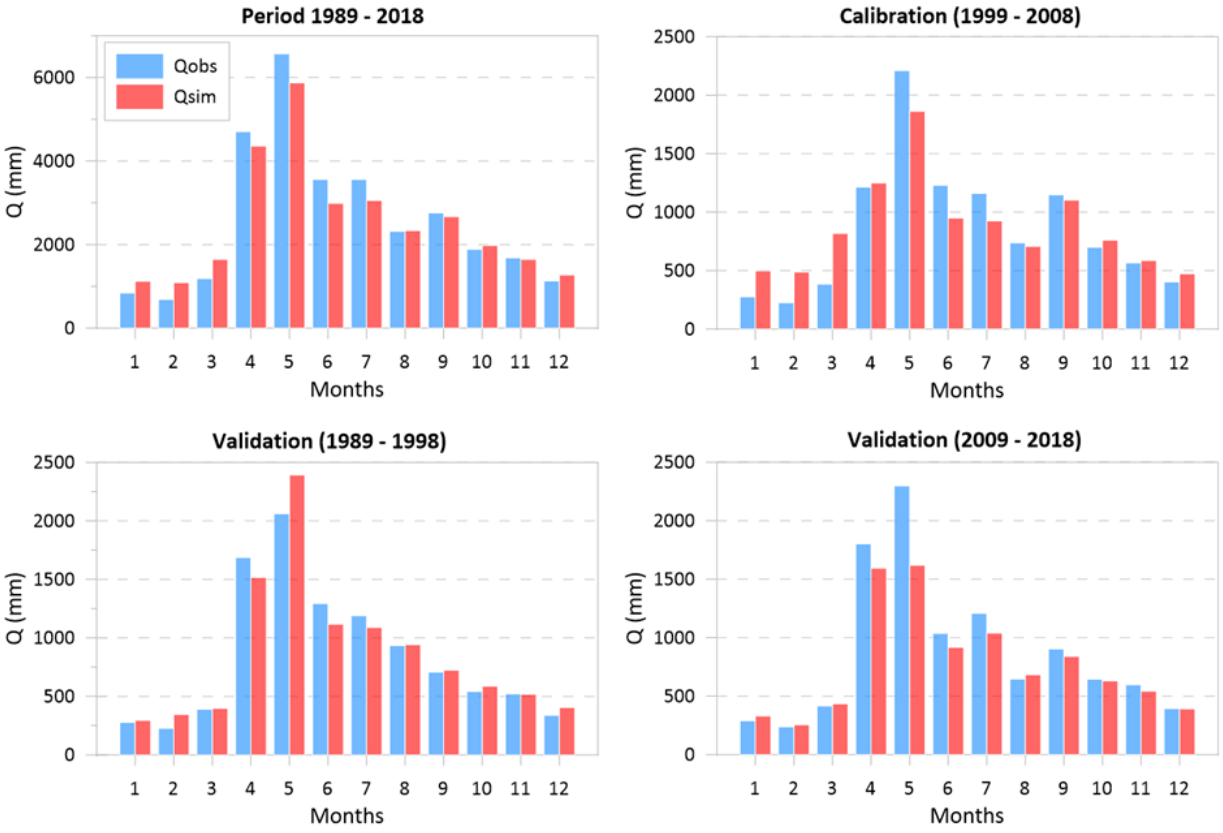

Fig. 4. Comparison of the observed (blue colour) and simulated (red colour) monthly flows for simulations based on arbitrary division of the data (i.e., into three decades). The simulations were performed with the parameters obtained in the calibration period of 1999–2008.

Table 2. **Values of the Nash-Sutcliffe coefficient (NSE) and in calibration and validation periods with length of 6 years; shaded area indicates the NSE values obtained in the calibrations; WP is warmer period and CP is colder period**

Nash-Sutcliffe coefficient (NSE)				
WP 1989–1994	**CP 1995–2000**	**CP 2001–2006**	**CP 2007–2012**	**WP 2013–2018**
0.63	0.69	0.62	0.65	0.58
0.57	0.75	0.61	0.62	0.56
0.56	0.65	0.73	0.65	0.65
0.51	0.64	0.63	0.74	0.73
0.23	0.34	0.39	0.60	0.80

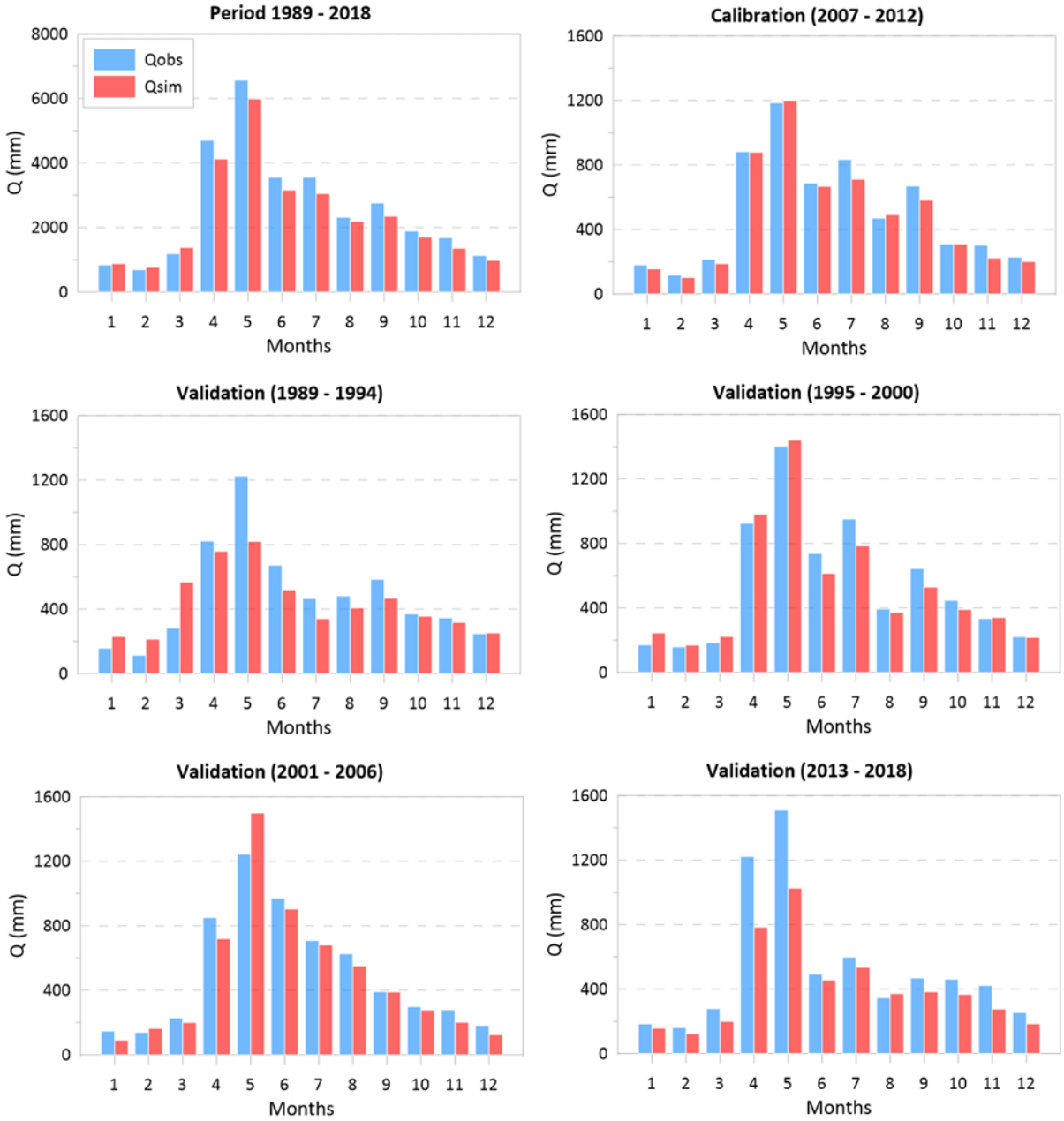

Fig. 5. Comparison of the observed (blue colour) and simulated (red colour) monthly flows for simulations based on the cycles-based division of the data (i.e., into five 6-years long periods). The simulations were performed with the parameters obtained in the calibration period of 2007–2012.

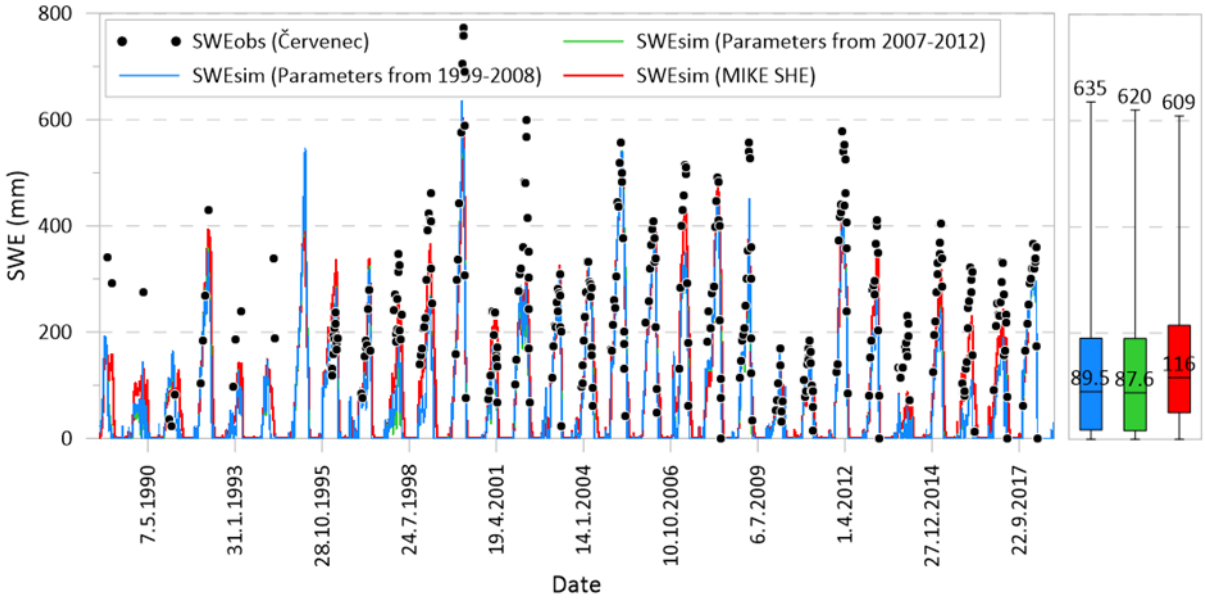

Fig. 6. Measured SWE at catchment mean elevation (points), simulated catchment SWE with the parameters from 1999–2008 (blue colour) and from 2007–2012 (green colour) and simulated catchment SWE obtained by the spatially distributed simulation of model MIKE SHE (red colour). The comparisons of the simulated SWE values are also shown in the box plots (right panel).

in a colder time period had tendency to overestimate the runoff (Q95 by about 12%, Q50 by about 15%, Q5 by about 35%) in a warmer/wetter period. Sleziak et al. (2018) observed overestimation of mean runoff when the calibration period was colder too. Coron et al. (2012) and Vaze et al. (2010) for Australian catchments observed a tendency to overestimate runoff when the calibration period was wetter. Our results indicate that the model calibrated in colder periods (i.e., 1999–2008 and 2007–2012) provided better simulation of catchment runoff. According to the results, the best Nash-Sutcliffe efficiency was achieved in calibration period of 2013–2018 (warmer period) (Table 2), but validation in years 1989–1994, 1995–2000, 2001–2006 showed worse results compared with those from the first selection of calibration periods (Table 1). This can be related to (a) different length of calibration periods, (b) algorithm used in the calibration strategy. Underestimation of measured flows in spring months (April and May) indicate the need to think about the improvement of the snowmelt-rainfall phase of runoff formation.

Conclusions

In this study, we have assessed the uncertainties related to the choice of calibration/validation periods. For the modelling purposes, we used a popular HBV model. From our results the following conclusions can be drawn. The model's uncertainties are associated with the climatic characteristics. In other words, the difference in climatic characteristics between the calibration and validation periods affects the performance of hydrological model. We found that the model calibrated in colder periods (i.e., 1999–2008 and 2007–2012) provided better representation of flows. This finding point to the fact that hydrological models calibrated in current climatic conditions could work reasonably also in the future warmer climate. These results should be validated in other catchments. In the future we plan (a) to extend such analysis to other regions (e.g., Slovakia vs. Austria), (b) to include other data (e.g., soil moisture data, MODIS data, etc.) to calibration strategy and thus better represent the hydrological components, (c) to use HBV vs. spatially distributed based models.

Acknowledgement

This study was supported by the grants from the Slovak Academy of Sciences (project VEGA No. 2/0065/19) and from the Slovak Research and Development Agency (project APVV No. 15- 0497).

References

Anctil, F., Perrin, C., Andréassian, V. (2004): Impact of the length of observed records on the performance of ANN and of conceptual parsimonious rainfall–runoff forecasting models. Environ. Model. Software 19(4), 357–368.

Ardia, D., Mullen, K. M., Peterson, B. G., Ulrich, J. (2015): DEoptim: Diferential evolution in R. Version 2. 2–3.

Bergström, L. (1995): The HBV model. Computer models of watershed hydrology, edited by V.P. Singh. Water. Resour. Publ., 443–476.

Brath, A., Montanari, A., Toth, E. (2004): Analysis of the effects of different scenarios of historical data availability on the calibration of a spatially-distributed hydrological model. J. Hydrol. 291(3/4), 232–253.

Coron, L., Andréassian, V., Perrin, C., Lerat, J., Vaze, J., Bourqui, M., Hendrickx, F. (2012): Crash testing

hydrological models in contrasted climate conditions: An experiment on 216 Australian catchments, Water Resour. Res., 48, W05552.

Danko, M., Holko, L., Kostka, Z., Tachecí, P. (2015): Simulation of snow water equivalent, snowmelt rate and runoff in mountain catchment during winter period. (In Slovak) Acta Hydrologica Slovaca, 16, 1, 42–50.

Fowler, H. J. A., Peel, M. C., Western, A. W., Zhang, L., Peterson, T. J. (2016): Simulating runoff under changing climatic conditions: Revising an apparent deficiency of conceptual rainfall-runoff models. Water Resources Research, 52, 1820–1846.

Hurst, H., E. (1951): Long-term storage capacity of reservoirs, Trans. Amer. Soc. Civil Eng. 116, 770–808.

Klemeš, V. (1986): Operational testing of hydrological simulation models, Hydrol. Sci. J., 31(1), 13–24.

Klemeš, V. (1974): The Hurst phenomenon: A puzzle? Water Resources Research, 10, 4, 675–688.

Merz, R., Parajka, J., Blöschl, G. (2011): Time stability of catchment model parameters: Implications for climate impact analyses, Water Resour. Res., 47, W02531.

Merz, R., Parajka, J., Blöschl, G. (2009): Scale effects in conceptual hydrological modeling, Water Resour. Res., 45, W09405.

Nash, J.E., and Sutcliffe, J.V. (1970): River flow forecasting through conceptual models, part 1. A discussion of principles. Journal of Hydrology, 10, 282–290.

Parajka, J., Merz, R., Blöschl, G. (2007): Uncertainty and multiple calibration in regional water balance modelling case study in 320 Austrian catchments. Hydrol. Process, 21, 435–446.

Pekárová, P., Pekár, J. (2007). Teleconections of Inter-Annual Streamflow Fluctuation in Slovakia with Arctic Oscillation, North Atlantic Oscillation, Southern Oscillation, and Quasi-Biennial Oscillation Phenomena. Advances in Atmospheric sciences, 24, 4, 655–663.

Perrin, C., Oudin, L., Andréassian, V., Rojas-Serna, C., Michel, C., Mathevet, T. (2007): Impact of limited streamflow data on the efficiency and the parameters of rainfall–runoff models. Hydrol. Sci. J. 52(1), 131.

R Development Core Team, 2011. R: A language and environment for statistical computing. R Foundation for Statistical Computing, Vienna, Austria. ISBN 3-900051-07-0, URL http://www.R-project.org/.

Sabo, M., 2012. How to analyze time series with wavelet transform. (in Slovak) Acta Hydr. Slov., 13, 1, 233–241.

Saft, M., Peel, M. C., Western, A. W., Zhang, L. (2016): Predicting shifts in rainfall-runoff partitioning during multiyear drought: Roles of dry period and catchment characteristics. Water Resour. Res., 52.

Schrödter, H. (1985): Verdunstung - Anwendungsorientierte Meßverfahren und Bestimmungsmethoden, Springer Verlag.

Sleziak, P., Szolgay, J., Hlavčová, K., Danko, M., Parajka, J. (2018): Factors controlling alterations in the performance of a runoff model in changing climate conditions. J. Hydrol. Hydromech., 66(4), 381–392.

Sleziak, P., Hlavčová, K., Szolgay, J., Parajka, J. (2017): Závislosť kvality simulácie odtoku pomocou zrážkovo-odtokového modelu od rozdielnosti hydroklimatických podmienok kalibračného a validačného obdobia. (in Slovak). Acta Hydrologica Slovaca, 18(1), 23–30.

Sorooshian, S., Gupta, V. K., Fulton, J. L. (1983): Evaluation of maximum likelihood parameter estimation techniques for conceptual rainfall–runoff models: influence of calibration data variability and length on model credibility. Water Resour. Res. 19(1), 251–259.

Tian, H. and Cazelles, B., (2013): WaveletCo: Wavelet Coherence Analysis. http://www2.uaem.mx/r-mirror/web/packages/WaveletCo/WaveletCo.pdf.

Vaze, J., Post, D. A., Chiew, F. H. S., Perraud, J. M., Viney, N. R., Teng, J. (2010): Climate nonstationarity – Validity of calibrated rainfall-runoff models for use in climatic changes studies. J. Hydrol., 394 (3–4), 447–457.

Viglione, A., Parajka, J. (2014): TUWmodel: Lumped hydrological model for educational purposes, R package version 0.1-4, dostupné na: http://CRAN.R-project.org/package=TUWmodel (posledná úprava 13.9.2016).

Ing. et Ing. Patrik Sleziak, PhD.
Ing. Michal Danko, PhD.
RNDr. Ladislav Holko, CSc.
Institute of Hydrology SAS,
Dúbravská cesta 9
841 04 Bratislava
Slovak Republic
E-mail: sleziak@uh.savba.sk

DOI: 10.31577/ahs-2019-0020.02.0016

ACTA HYDROLOGICA SLOVACA

Volume 20, No. 2, 2019, 139–144

BATHYMETRIC SURVEYS OF TATRAS GLACIAL LAKES: CASE STUDY – BATIZOVSKE PLESO

Valentín Sočuvka, Yvetta Velísková

The Tatras Mountain, located on the border between Slovakia and Poland, are the highest and the most significant mountains range within the Carpathian Mountains of Central Europe. Because of their altitude and former glaciations the Tatras Mountain are classified as an alpine massif. The most important and interesting natural elements of the Tatras Mountain alpine landscape represent glacial lakes. There are about 87 lakes of glacial origin in the Slovak part of the Tatras Mountain, the most of them are situated in the alpine zone (1 800–2 200 m a.s.l.) above the upper forest line. Hydrographic research of the glacial lakes in the Tatras Mountain has a long history since 1925, however the results of the surveys were different over the years due to technical limits of the survey instruments, their low precision as well as the extreme climate conditions with high altitude. The aim of this paper is to demonstrate the application of modern hydrographic and geodetic instruments for bathymetric survey in the condition of the Tatras Mountain, which unlike the traditional instruments and techniques are characterized by high precession and efficiency. In the case study we demonstrate yet the most precise digital terrain model (DTM) of the glacial lake Batizovske pleso, created in software environment ArcGIS and based on the data from the bathymetric survey performed in 2018 by Autonomous Underwater Vehicle (AUV) EcoMapper and geodetic instrument GNSS Stonex.

KEY WORDS: bathymetry, lake, Tatras Mountain, EcoMapper, DTM

Introduction

The Tatras Mountain are the part of Western Carpathians and they are situated on the territory of two states – the Slovak Republic and the Polish Republic along the border between 20°10′ E and 49°10′ N. The Tatras Mountain stretch longitudinally over a distance of 50 km and occupy about 778 km^2 of area divided between Slovakia (78%) and Poland (22%) (Fig. 1). The Tatra range can be divided into four geomorfological unit: the High Tatra, the Western Tatra, the Belianske Tatra and Reglowe Tatra (Klimaszewski, 1988). In Pleistocene, the Tatras Mountain were covered several times with ice and the glaciation imprinted the present shape to the mountains on both sides of the state border by forming peaks, glacial valleys, cirques, amphitheatres; waterfalls and lakes. The alpine glacial lakes – as the relicts of the last Ice Age, which ended up some 10 to 8 thousand years ago, are the typical elements of the Tatras Mountains nature. Many small and larger lakes form the alpine scenery of the Tatras, while the majority of them indicate the closure of individual glaciers' branches, the formation of which started in cirques. Considering the genesis; the glacial lakes had been either hollowed out (kar lakes) or dammed by moraines (moraine lakes). However, the majority of the Tatras lakes were formed by the combination of both genesis types, when the originally hollowed out lakes were later dammed by the moraine detritus (UNESCO, 2002).

Nowadays, there is about 150–230 lakes of various sizes and depths (depending on the size and periodicity criteria) in the Tatras. Approximately half of them are periodic. In addition, there is a significant number of already extinct, fully overgrown lakes and peat bogs. Mostly, there are small lakes with a surface of less than 1 ha and depth up to 2 m (Gregor and Pacl, 2005), (Kapusta et al., 2018). The lakes are situated mainly in the West Tatras Mountain and the High Tatras Mountain at elevations between 1089 and 2189 m above sea level (a.s.l.). About 70% of the lakes are in an alpine zone above 1800 m a.s.l., 19% in subalpine zone and 11% in mountain zone. The total area of the glacial lakes in Slovak part of Tatras Mountain is 3 km^2 and they have volume of about 10 million cubic meters (Štefkova et al., 2001). The largest lake of the Slovak part of the Tatras Mountain and also the deepest one is Velke Hincovo pleso. The highest located lakes are Modre pleso (2192 m a.s.l.), and Baranie pliesko (2 207 m a.s.l.). However, Baranie pliesko dries up at the end of the summer and has no water. It should also be noted that 20 lakes of the total number are located in the Western Tatras, however they are shallower and relatively small (2.1 ha max.). Altitu-

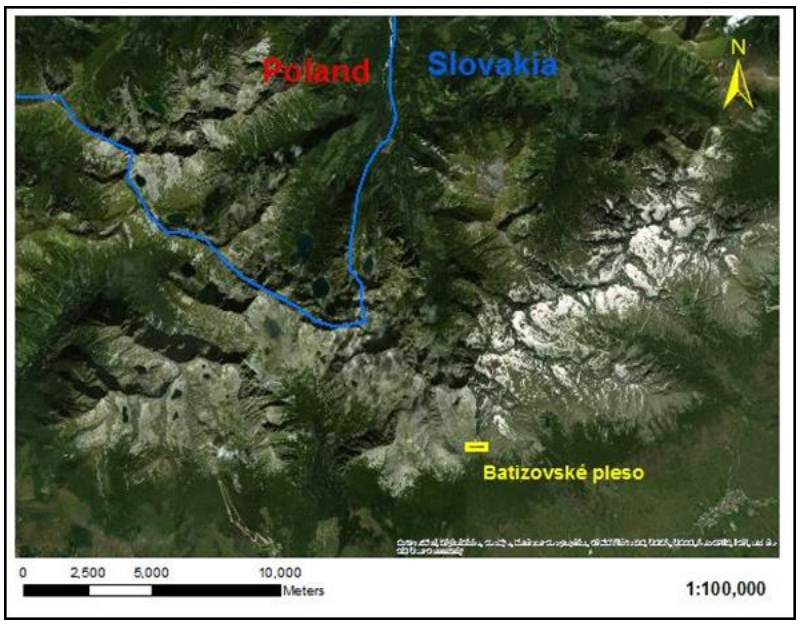

Fig. 1. The Tatras Mountain – location of representative lakes.

des of the Tatras lakes are connected with individual stages of valley glaciers. Therefore, the highest located lakes are the youngest ones and the lowest located are lakes in the advanced stage of the development. The fluctuation of the kar lakes water level with the surface runoff is small, max 0.5 m (UNESCO, 2002).

Previous research

Bathymetric measurements of the Tatras Mountain lakes commenced by Josef Schaffer in 1927 and Franz Stummer in 1931. The cooperation of these two explorers resulted in the Atlas of the High Tatras lakes that was published in three volumes (Schaffer & Stummer 1929, 1930, 1932). It comprises bathymetric plans of 31 Tatras lakes with a number of longitudinal and cross sections. Another researcher who dealt with the lakes of the West Tatras was Eduard Kříž in his doctoral thesis. He carried out plan and depth measurement of twelve lakes in the area. It was the first survey of morphographical and hydrographical conditions (Kříž, 1970). In the years 1961–1964 measurements were performed by Gregor and Pacl (2005) on the areas, depths and altitudes. In 2001, bathymetric measurements of some High Tatras lakes were carried out within the EMERGE project and in 2006 measurement of eighth lakes were performed by Šobr and Česák (2006). To construct these maps a series of transects were run across the lake using the manual method or an echo sounder to measure water depth. Depth was transcribed onto a corresponding transect map. When all the depths had been transcribed, then the points of equal depth were joined on the map to create contours. The quality of the maps depended on a variety of factors including the number of transects that were run, the accuracy of the transect map, the number of depths transcribed and the interpretive skills of the drawer. At the best, only a moderately accurate bathymetric map could be produced and it was inevitable that many underwater features would be missed (Monroe and Betteridge, 2000). In the recent years, a new technology became available that was used in the collection of bathymetric data. Applying GPS (Global Positioning System) technology significantly improved the efficiency and speed of data collection. The quality of data also improved from using GPS, and the integration with GIS to produce maps also became much more efficient. Combination of the GPS unit and single beam echo sounder for hydrographic measurement of selected Tatras lakes used Kapusta (2018) in his dissertation thesis which deals detailed analysis of changes of glacial lakes in the High Tatras Mts.

Material and methods

For the hydrographic research and data mapping, the Autonomous Underwater Vehicle (AUV) Eco Mapper device was used. AUVs represent devices which are currently used in a wide range of hydrographic research, marine geosciences, and the military, comercial, and policy sectors. EcoMapper was developed by YSI Company (USA) and is designed for the quick and easy collection of bathymetric, sonar, and water quality data. EcoMapper is capable of moving on surface and subsurface water levels independently and performing data logging. This device is ideal for coastal and shallow water applications such as hydrographic surveys and spatial environmental monitoring. A survey mission by EcoMapper can be performed in water with a depth of more than one meter, and it is fully capable of subsurface operations down to 100 m. The EcoMapper device consists of a hardware part and the Vector Maps software program, which is designed for mission planning and for

the partial analysis of measured data. Physically, the vehicle can be divided into 3 distinct parts. The bow section contains water quality sensors that interact with the aquatic environment and a Doppler Velocity Log (DVL) for navigation under water surface. The middle section includes an onboard computer, electronic components, batteries, and weights to balance the vehicle. The tail section contains a propulsion system and GPS antennas for navigating on the water's surface. The device uses a frequency of 500 kHz and has a range of measurement depth from 0.5 to 100 m and a measurement accuracy ±0.003 m. While it is measuring (its mission), the EcoMapper collects predetermined parameters in one second intervals and they are automatically associated with geographic coordinates (latitude, longitude). Water quality measurements include information such as the water temperature, dissolved oxygen, turbidity, pH, chlorophyll, salinity, etc.

Acoustic bathymetry profiling

The EcoMapper follows a predefined mission plan preprogrammed by the operator. The mission plan is created in the graphic user environment of the Vector Map Software. Geo-referenced charts, maps or satellite images are imported into the Vector Maps planning software and the mission plan continues by setting positions of waypoints for the vehicle's navigation. The mission planning includes set points for each leg to a waypoint, speed, depth or undulates for data collection (Fig. 2). This parameter programming tool can be separately utilized for vehicle and sensors preprogramming of each leg or for a complete survey. The software output of the mission planning is an ASCII file that is uploaded to the EcoMapper via a wireless interface prior to the mission's start. Once the vehicle has started its mission, it operates independently and uses GPS waypoints and DVL navigation to complete its preprogrammed course. Throughout the course, the vehicle constantly steers toward the line drawn in the mission planning software and essentially follows more accurate course of coordinates instead of traversing waypoint-to-waypoint. Upon completing its mission, the vehicle uses Windows Remote Desktop to relay the collected data via a WiFi connection, which is facilitated by the Communications Box, to the user's computer.

Two missions in total were planned for Batizovske pleso. First mission were planned in transverse direction and second mission in longitudinal direction. The navigation path was created by linking 61 waypoints for the first mission and 53 waypoints for the second mission (Table 1). The average vehicle speed was set to 3.7 km/hour and the acquisition frequency to 1 point per second, resulting in 7,886 points. Total length of both survey missions was 7493 m and duration 121 minutes. The position fixing was guaranteed by an average of nine satellites.

In addition a combination of GNSS Stonex S9II and control unit Ashtech Mobile Mapper 100 was used for the data collecting of the Batizovske pleso shore line and the altitude of the lake surface. Phase measurements

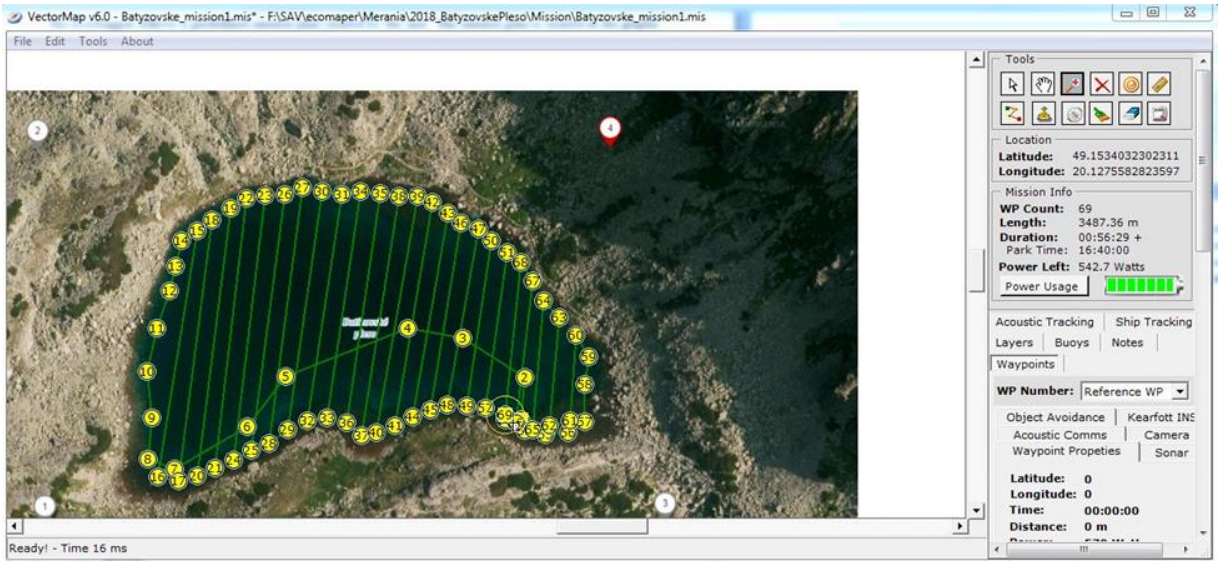

Fig. 2. Mission planning in software program Vector Map.

Table 1. Type of performed mission for location Batizovske pleso and measured parameters

No. of mission	No. of waypoint	Total length of survey [m]	Duration [min]	No. of measured points
Mission 1 (EcoMapper)	69	3487	56:29:00	4177
Mission 2 (EcoMapper	53	4006	64:54:00	3709
GNSS (Stonex SII)	-	-	-	142

SKPOS were used for higher accuracy. SKPOS service provides differential corrections for real-time phase measurements (RTK) in the virtual reference station (VRS) concept. To use this service a dual-frequency GNSS receiver is necessary, which is able to process RTK corrections in one of RTCM 2.3, RTCM 3.1, CMRx, CMR+formats. The service delivers 0.020–0.040 m level accuracy. During the data collection, only measured parameter which fulfilled the accuracy <0.025 were saved. Total number of measured points by GNSS Stonex was 142. Trajectory of both mission and measured points by EcoMapper and GNSS Stonex shows Fig. 3.

Post-processing

Post processing and data analysis were accomplished using Esri's ArcGIS software. The majority of data obtained was in point form and imported as *x, y, z* files. The vertical datum and horizontal projection were provided with the metadata and were assigned to the ESRI ArcGIS 10.1 working files. The optimum gridded resolution was determined based on the density of the data. ArcGIS provides advanced and various options to interpolate surfaces using two extensions: Spatial Analyst and Geostatistical Analyst. Digital Elevation Model (DEM) of Batizovske pleso was created by geostatistical analyst tool through the Topo to Raster. Topo to Raster provides the functionality of incorporating other types of geographic features, which can assist in the creation of a DEM. The parameters required for topo to raster are mostly optional to change from the default. Spot elevation, contours, cliffs, lakes, coasts and other boundary information can be inputted and can be utilized in creation of the final raster surface. The drainage enforcement within the tool will ensure a mostly hydrological correct surface. Overall, these interpolation methodologies provide the basic requirements of testing the integration of the topographic and bathymetric point elevation values in order to create a single raster elevation surface (Rodriguez 2015).

Results and discussion

Based on the analysis and post-processing of measured data in GIS software ArcGIS 10.1 Digital Elevation Models of the lake Batizovske pleso was produced (Fig. 4, Fig. 5). The area and volume were calculated with the 3-D surface analysis package in ArcGIS 10.1. For each altitude, the triangulated irregular network was examined to determine the area and volume of each triangle contained within the limits of that particular altitude. The sum of these triangles is used for the output of area and volume (Baskin, 2005). The output from the calculations of area and volume is shown in Table 2. The calculations of area and volume for the Batizovske pleso show the maximum area of 33 011 square meters and the maximum volume of 158 787 cubic meters at a water-surface altitude of 1 884.7 meters above sea level.

Another outcome was a comparison (Table 2) of our

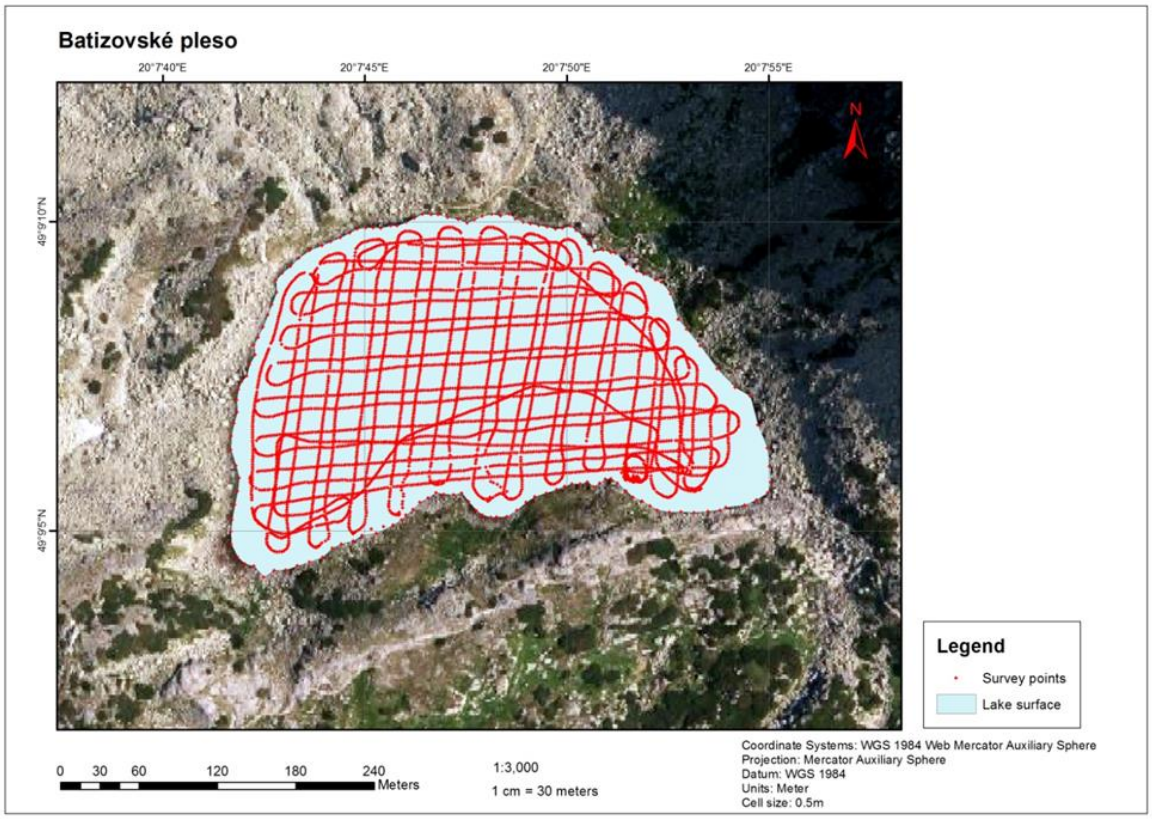

Fig. 3. Trajectory of the survey and measured bottom points.

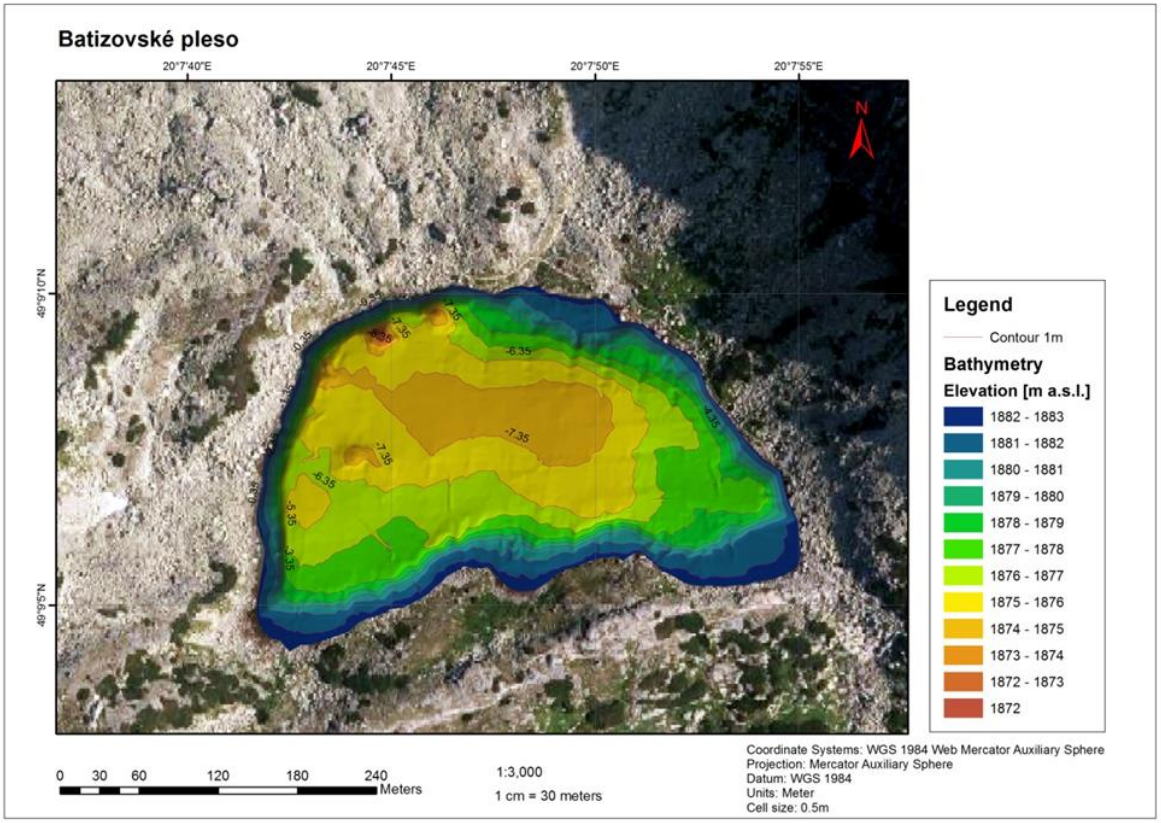

Fig. 4. Digital elevation model (bathymetry) of the Batizovske pleso.

Table 2. Comparison of the survey results performed by Gregor and Pacl (2005) and by our measurements in 2018

Author	Water surface [m a.s.l.]	Surface Area [m^2]	Circumference - shape length [m]	Max. depth [m]	Lake volume [m^3]
Gregor, Pacl, (2005)	1884.2	34775	885	10,5	232089
Our measurements (2018)	1884.7	33011	783	10.4	158787

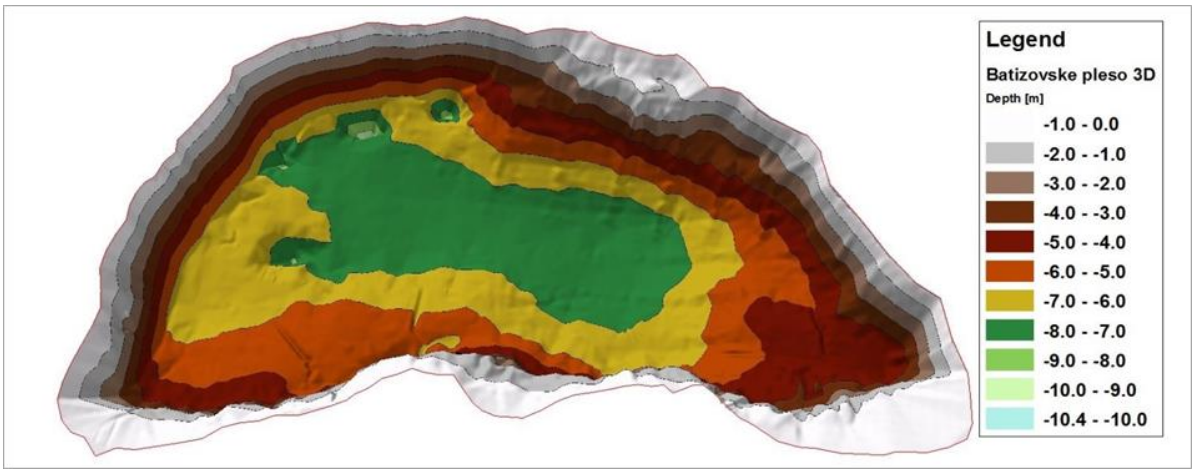

Fig. 5. 3D model of the lake Batizovske pleso.

results with 50 year old measurements performed by Gregor and Pacl (2005). Differences between lakes morphometrical characteristics are mostly in volume calculation. The difference at lake volume is very likely result of different methods and density of depth measurements. It is very disputable how many depth measurements used Gregor and Pacl to bathymetric maps construction. Difference of elevation of water surface is 0.5 m so differences at calculation of lake area and circumference should be caused by different water level in lake at the time of both measurements.

Conclusion

The purpose of bathymetric survey is to describe the physical characteristics of the water body bottom. Bathymetric data are used to produce a map showing depth contours, underwater structure, maximum and minimum depth. Data are used to calculate lake volume and mean depth, too. This information is important for understanding the ecology of lake systems, evaluating the limnology process in lakes or for evaluating habitat suitability of lakes for various aquatic species. However, gaining access to these data especially from the mountains terrain is often challenging. Significant potential for the bathymetric survey mountain lakes is application autonomous survey vehicles which are characterized by high precession and efficiency of the survey. The survey had two objectives: (1): to acquire a modern bathymetric dataset of lake Batizovske pleso that can serve as a reference for future investigations of the lake dynamics and (2) to demonstrate application of Autonomous Underwater Vehicle EcoMapper in condition of alpine mountain terrain. The outcomes of the bathymetric survey in this case study deliver the high precious results with utilization of the newest bathymetric instruments and post-processing software methods.

Acknowledgement

This work was supported by the Slovak Research and Development Agency under Contract No. APVV–18–0205 and the VEGA Grant Agency No.1/0805/16.

References

Baskin, R. L. (2005): Calculation of area and volume for the south part of Great Salt Lake, Utah: U.S. Geological Survey OpenFile Report 2005–1327, accessed 08/16/06 at http://pubs.usgs.gov/of/2005/1327/

Gregor, V., Pacl, J. (2005): Hydrológia tatranských jazier. Acta Hydrologica Slovaca. 2005, roč. 6, č. 1, 161–187.

Kapusta, J. (2018): Metodika rekonštrukcie brehovej čiary tatranských plies. Dizertačná práca, UKF Nitra.

Kapusta, J., Hreško, J., Petrovič, F., Tomko-Králo, D., Gallik, J. (2018): Water surface overgrowing of the Tatra's lakes. Ekológia (Bratislava), Vol. 37, No. 1, p. 11–23, 2018.

Klimaszewski, M. (1988): Rzeźba Tatr Polskich. Warszawa: State Publisher. 668 p.

Kříž, E. (1970): Jezera Západních Tater. Rigorózní práce, PřF UK Praha, 156 p.

Monroe, B., Betteridge, G. (2000): The Algonquin Fisheries Assessment Unit Real-time GPS Lake Bathymetry System. Algonquin Fisheries Assessment Unit, Algonquin Park.

Rodriguez, R. R. (2015): Integration of Topographic and Bathymetric Digital Elevation Model using ArcGIS Interpolation Methods: A Case Study of the Klamath River Estuary

Schaffer, J., Stummer, F. (1929). Atlas der Seen der Hohen Tatra I. Arbeiten d. Geogr. Institutes der Deutschen Univ. In Prag, 1929.

Schaffer, J., Stummer, F. (1930). Atlas der Seen der Hohen Tatra II. Arbeiten d. Geogr. Institutes der Deutschen Univ. In Prag, 1930.

Schaffer, J., Stummer, F. (1932): Atlas der Seen der Hohen Tatra III. Arbeiten d. Geogr. Institutes der Deutschen Univ. In Prag, 1932.

Šobr, M., Česák J., (2006): Methodology and Results of Bathymetric Measurements of the Selected High Tatras Glacila Lakes. Acta Universitatis Carolinae. 2006, Vol. 20, Nos 1-2, s. 109–120.

Štefková E., Šporka F., (2001): Long-term ecological research of High mountain lakes in the High Tatras (Slovakia) Ekologia, Vol.20, Supplement 2/201.,p. 101–106.

UNESCO (2002) Natural Reserves of Tatras Mountain: Available from: https://whc.unesco.org/en/tentativelists/1737/

Ing. Valentín Sočuvka, PhD.
Ing. Yvetta Velísková, PhD.
Institute of Hydrology SAS,
Dúbravská cesta 9
841 04 Bratislava
Slovak Republic
E-mail: socuvka@uh.savba.sk

DOI: 10.31577/ahs-2019-0020.02.0017

ACTA HYDROLOGICA SLOVACA

Volume 20, No. 2, 2019, 145–150

FIELD STUDY FOR DETERMINE MANNING´S ROUGHNESS COEFFICIENT WITH DIFFERENT FLOW CONDITIONS

Schügerl Radoslav

Vegetation growing in the water along streams has been the subject of several studies since it was recognized that it could have a significant impact on the water flow. It may increase resistance to flow and cause higher water levels. Also, it has an effect on the velocity profiles. The purpose of this paper is to investigate, and determine how aquatic vegetation influences flow resistance, water depth and discharge in the Malina stream at the Záhorská lowland area. Vegetation causes resistance to flow; it reduces flow velocities, discharge and increases water depth. Measurements performed during three years at this stream were used for an evaluation of vegetation impact on flow conditions. The Manning´s coefficient was used as one way of quantifying this impact. The results show variation of this parameter during the growing season.

KEY WORDS: Manning´s roughness coefficient, flow conditions, water-level, aquatic vegetation

Introduction

Research of the impact of aquatic vegetation is based on the investigation of the problem in laboratory conditions (Green, 2005; Manes et al., 2011). On the other side, examination of the research issues in the field conditions is more problematic (Nikora et al., 2008).

Vegetation affects fluvial processes and is key in current river management and river hydraulics. Advances in understanding the behavior of flow over vegetation allow us to improve both the knowledge of flow-velocity profiles and flow resistance (James et al., 2004; Cheng, 2011; Nehal et al., 2013).

The flow regime in channels or in surface water at lowland territories during the growing season is often very strongly influenced by the occurrence of aquatic vegetation. From a hydrodynamic point of view, water plants alter the size and distribution of flow velocities at a large rate; they increase the stream bed roughness and decrease the discharge capacity of a stream. As the development of water plants progresses, the coefficient of roughness value is changed. In general, this parameter determines the extent of roughness and impacts the flow capacity of channels or watercourses. For correct design or computation of flow in an open channel, it is necessary to evaluate the channel resistance to flow, which is typically represented by a roughness parameter, such as Manning's n (Velísková et al., 2017). Its determination is not easy for natural streams, because the characteristics of channels and the factors that affect channel capacity can vary greatly; furthermore, the combinations of these factors are numerous. Therefore, the selection of roughness for natural and constructed channels is often based on field judgment and personal skill, which are acquired mainly through experience. Determination of the roughness coefficient *n*, according a seasonal variation, is an important tool in hydraulic modelling (De Doncker et al., 2009; Korichi & Hazzab, 2012).

The aim of this contribution is to demonstrate, on the basis of results from experimental field measurements on the Malina stream (Slovakia), how the sprouting of stream bed vegetation influences channel's flow conditions and its capacity.

Theoretical background

In describing the vegetation resistance, differences have been made between submerged, emergent, flexible and rigid vegetation. It is important to distinguish between definitions of the terms 'roughness' and 'resistance'.

Resistance accounts for the (boundary) turbulence caused by surface properties, geometrical boundaries, obstructions and other factors causing energy losses. Therefore, a resistance coefficient reflects the dynamic behaviour in terms of momentum or energy losses in resisting the flow of the fluid. Here, flow resistance is considered to be made up of four parts: skin drag, shape drag, form drag and some other factors.

Roughness reflects the influence of the surface on the momentum and energy dissipation in resisting the flow of the fluid. Therefore, with a roughness factor the actual or effective unevenness of the boundary sur-

face is meant. Shape drag occurs as a result of the geometry of the channel. The flow has a tendency to form vortices. Form drag arises because of the form of the object. Other factors, which can influence the resistance of the flow are the presence of suspended material in the flow, wave and wind resistance from free surface distortion etc.

We know several descriptions to describe the resistance of vegetation, ranging from general roughness descriptions, to descriptions that account for various vegetation characteristics. Roughness description with constant roughness coefficient, for example Chézy formula, Dardy-Weisbach equation, Manning´s equation or roughness coefficient dependent on flow characteristics, for example Strickler and Keulegan approach. In addition we know new approach for describe the resistance of vegetation, mainly for flexible submerged vegetation (Kutija & Hong, 1996; Stone & Shen, 2002; Wilson, 2007).

Hydraulic resistance can be found in literature as:

Manning´s equation: $$v = \frac{1}{n} R^{2/3} i_o^{1/2} \quad (1)$$

Darcy-Weisbach equation: $$v = \sqrt{\frac{8g}{f}} \sqrt{R i_o} \quad (2)$$

Chézy´s equation: $$v = C \sqrt{R i_o} \quad (3)$$

where
v – mean flow velocity [m s^{-1}],
R – hydraulic radius [m],
i_o – water level slope,
n – Manning´s roughness coefficient [s m$^{-1/3}$],
g – gravity acceleration [m s^{-2}],
C – Chézy´s coefficient [m$^{1/2}$ s^{-1}].

Manning's equation is the most widely used resistance measure among these, in particular with respect to vegetated channel. Although it expresses the resistance at the reach scale and reflects only the influence of the boundary shear on flow depth and averaged velocity, Manning's coefficient n is often used as a lumped parameter accounting for all the various influences in a river reach. It is commonly estimated through experience from simple verbal or photograph descriptions of channels. A more advanced method is to split channel resistance into its component parts, and to determine the final value of Manning's *n* from knowledge of the separate, smaller scale contributing effects using table.

The determination of spatial parameters of a stream, such as the discharge area, stream bed slope, and hydraulic radius, is quite easy, but the stream bed roughness assessment could be a problem. During a year, the various degrees of in-channel sprouting could be found, and the different kinds of water plants usually grow up in stream cross-section profiles. On small longitudinal slopes, the extension of aquatic vegetation is conditional and accordingly, also on small flow velocities. The height of the vegetation with respect to the water level is important in describing vegetation resistance, because it influences the flow velocity profile (Velísková et al., 2017).

There are many vegetation characteristics that affect the hydraulic resistance in vegetated channels. The first important vegetation characteristic that affects the flow resistance is the geometry of the vegetation itself, concerning the taxonomy of the species as the branching index, the density of the shoots, the maximum level of growth that each species can reach in a cross section, the seasonal presence of the plant. In addition to this, there is a hydraulic parameter which considers the characteristic dimension of the vegetation in relation to flow conditions. One of the main problems in vegetated channel is the determination of the vegetation height. This can be solved if the flexural and drag properties of the vegetation are known. Flow over flexible vegetation induces bends and reduces the height of the vegetation stems. As a result, the flow-vegetation interactions are reduced. The vegetation configuration depends on flexural rigidity and density of the vegetation itself. These characteristics depend essentially on the species. The blockage factor B is the parameter that measures the portion of the channel blocked by vegetation, or equivalently the proportion of the channel containing vegetation. Several types of blockage factors have been proposed in the literature (Boscolo, 2014).

All factors mentioned above can be quantified only under laboratory conditions. Evaluation of the impact of water plants on flow conditions in a lowland stream is complicated. Nevertheless, it is possible to determine the value of the roughness coefficient n for a stream reach by using the Chézy–Manning equation for steady uniform flow condition (Eq. 4):

$$n_m = \frac{A_m R_m^{2/3} i_{om}^{1/2}}{Q_m} \quad (4)$$

where
i_o – water level slope,
A – discharge area [m^2],
R – hydraulic radius [m],
Q – discharge [m^3 s^{-1}],
m – means a measured value.

Material and methods

Field measurements, related to the investigation of aquatic vegetation impact on flow in a lowland stream, were performed along the Malina stream in the Záhorská lowland. Záhorská lowland area – and Malina stream - was chosen, it is one of the most productive agricultural areas of Slovakia. Malina stream is a sewer river in Záhorie low-land, flows through the territory of Malacky district. It is a left tributary of Morava river, has a length of 47.75 km. Catchment area is 516.6 km² and her discharge is 0.828 m^3 s^{-1} in Jakubov village 2.234 m^3 s^{-1} in the estuary. Four observing cross-section profiles were selected along the Malina stream, their locations are shown in Fig. 1. Measurement were carried out in the first section with distance 1140 meters (from gas profile to Suchý stream profile) and in the second section with distance 2140 meters (from railway bridge profile to road bridge profile). Cross-section profiles parameters (channel width, distribution of water depth along

the cross-section profile width), water levels (by levelling device), discharges and velocity distribution along the cross-section profile width (by ADV – Acoustic Doppler Velocimeter device Flow Tracker) were measured. Measurements were performed in the channel segments with steady uniform flow conditions. In general, field measurements were done in April, during summer time (July–August) and during autumn (October) and winter (November and February). Accordingly, we try to detect if any changes occur in different periods of the growing season.

Results and discussion

As it was mentioned, there exists a number of ways how to evaluate the influence of aquatic vegetation on flow in lowland streams. Quantification of the impact of aquatic vegetation through the roughness coefficient is one of the practically suitable methods. This roughness coefficient represents a parameter influencing discharge capacity of streams. Ranges of measured data from each year are condensed in Table 1 for section 1 (from gas profile to Suchý stream profile) and Table 2 for section 2 (from railway bridge profile to road bridge profile). Tables contain mean flow velocity (v), discharge area (A), wetted perimeter (l), hydraulic radius (R), water level change (Δh), water level slope (i_o) and Manning´s roughness coefficient (n).

The roughness coefficient value in the sprouted stream bed is changing during the growing season depending on aquatic vegetation growth. In consequence of raised roughness, the velocity profile is changing and thereafter the discharge capacities are also changed. The rate of the vegetations impact on flow regime during the vegetation season differed in each year. The reason is that each year had different climatic conditions, which stimulated aquatic vegetation growth to a different extent. Furthermore, the activities concerning the maintenance of the channel network (mowing, water level regulation, etc.) also influenced the degree of aquatic vegetation growth, as it was mentioned above. For example, in the third year of observation, the differences of n values along the channel varied in the most extensive range (0.021–0.195) for the first section, for the second sector the differences of n values along the channel varied in the most extensive range (0.020–0.138 vs. 0.015–0.133) in the second and third year.

Aquatic vegetation recording by means of camera during the year 2018 (april vs. august) are shown in Fig. 4 (gas profile) and Fig. 5 (railway bridge profile). The mean flow velocity values decrease with increasing roughness coefficient and are lower during the summer season than during spring or autumn for the same discharge subrange.

Value of Manning´s roughness coefficient by Chow (1959) belong to channels not maintained, weeds and brush uncut with dense weeds, high as flow depth is from 0.050 to 0.120 or with dense brush, high stage is from 0.080 to 0.140. Calculated datas are in the our case is higher.

Change of discharge and water-level during three years for section one (from gas profile to Suchý stream profile) and section two (from railway bridge profile to road bridge profile) are shown in Fig. 2 and Fig. 3. Ranges of measured data for section 1 and section 2 are condensed in Table. The results show, that when is recorded biggest discharge value, then water-level value is smallest (for all measured cross-section profile). On the other side, when discharge value is smallest, water-level value is not biggest.

Figure 4 and figure 5 show growing of aquatic vegetation in the Malina stream during the season from april 2018 and from august 2018 (figure 4 for gas profile and figure 5 for railway bridge profile).

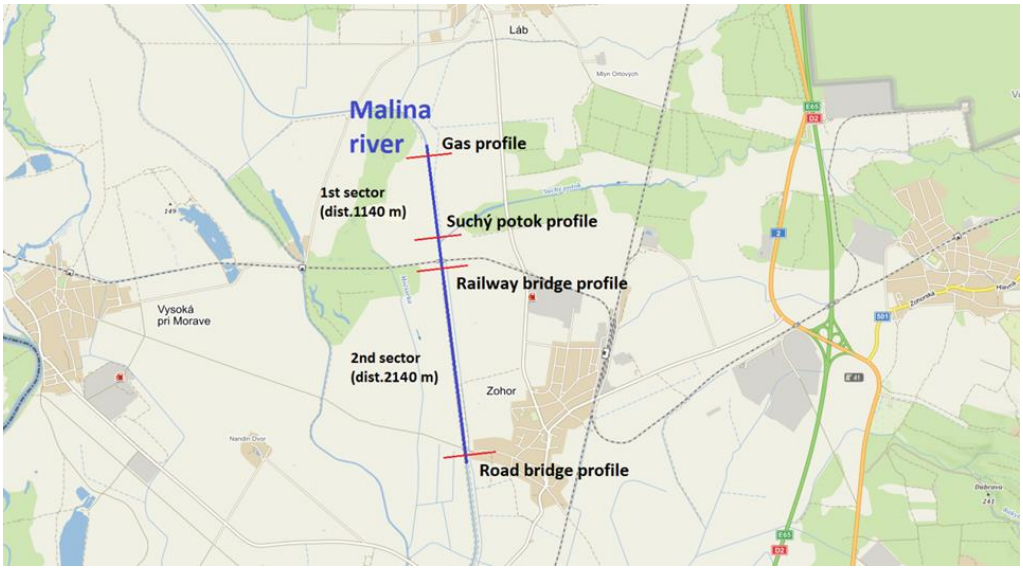

Fig. 1. Location of observed cross-section profiles along the Malina stream.

Table 1. Summary of measured and calculated data of first section experiment (from gas profile to Suchý stream profile)

Date of measur.	gas profile				Suchý stream profile				Δh [m]	i_o	n
	v [m s^{-1}]	A[m^2]	l [m]	R [m]	v [m s^{-1}]	A[m^2]	l [m]	R [m]			
08/2016	0.095	4.09	5.8	0.705	0.091	3.75	6.49	0.578	0.048	0.000422	0.156
11/2016	0.153	3.96	6.7	0.59	0.158	2.52	6.59	0.382	0.028	0.000246	0.052
02/2017	0.315	2.92	5.67	0.515	0.351	2.62	6.8	0.385	0.014	0.000128	0.017
07/2017	0.061	2.83	5.64	0.502	0.059	2.39	6.31	0.379	0.020	0.000171	0.115
04/2018	0.221	1.46	5.08	0.287	0.262	1.25	5.91	0.211	0.029	0.000257	0.021
08/2018	0.052	3.73	5.99	0.622	0.045	4.22	8.55	0.493	0.023	0.000198	0.195
12/2018	0.128	3.58	6.32	0.566	0.35	2.71	6.63	0.408	0.035	0.000309	0.027
04/2019	0.201	2.71	5.35	0.505	0.375	1.45	5.79	0.25	0.056	0.000492	0.023

Table 2. Summary of measured and calculated data of second section experiment (from railway bridge profile to road bridge profile)

Date of measur.	railway bridge profile				road bridge profile				Δh [m]	i_o	n
	v [m s^{-1}]	A[m^2]	l [m]	R [m]	v [m s^{-1}]	A[m^2]	l [m]	R [m]			
08/2016	0.096	4.24	6.21	0.632	0.085	3.341	7.108	0.471	0.056	0.000263	0.115
11/2016	0.15	4.74	6.46	0.733	0.188	3.86	8.466	0.455	0.065	0.000303	0.054
02/2017	0.401	2.79	6.03	0.463	0.393	2.928	5.824	0.502	0.036	0.000169	0.020
07/2017	0.069	2.57	6.35	0.404	0.059	3.021	6.508	0.464	0.040	0.000185	0.138
04/2018	0.243	1.52	6.01	0.253	0.239	1.708	7.456	0.229	0.021	0.000011	0.015
08/2018	0.047	4.102	7.79	0.526	0.052	3.668	9.044	0.405	0.034	0.000016	0.133
12/2018	0.131	3.714	6.31	0.588	0.14	3.519	7.604	0.462	0.045	0.000211	0.061
04/2019	0.248	2.295	6.71	0.342	0.283	2.045	6.627	0.307	0.068	0.000318	0.028

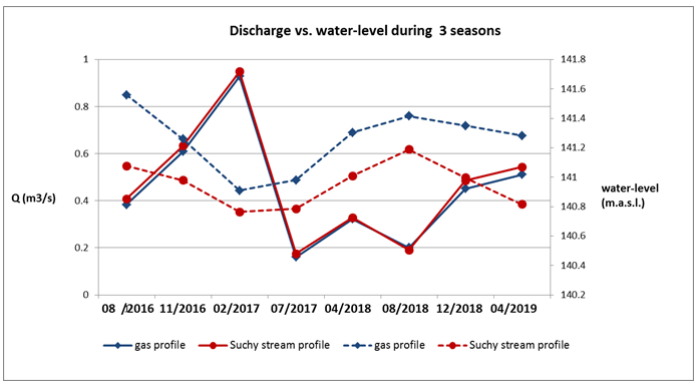

Fig. 2. Change of discharge and water-level of the Malina stream during three years for section one.

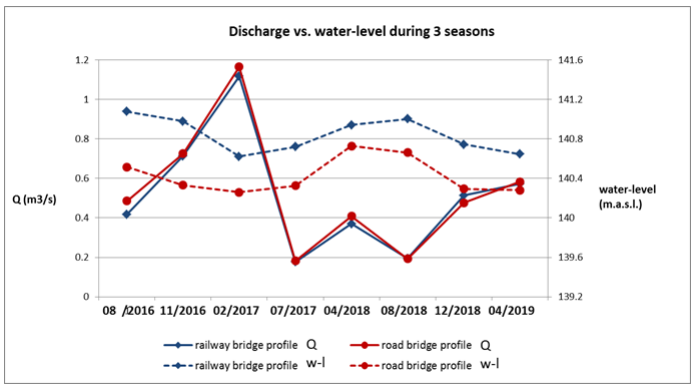

Fig. 3. Change of discharge and water-level of the Malina stream during three years for section two.

Table 3. Summary of measured data of the discharge and water-level on the four cross-section profile

Date of measur.	gas profile		Suchý stream profile		railway bridge profile		road bridge profile	
	Q [$m^3 s^{-1}$]	w-l [m a.s.l.]	Q [$m^3 s^{-1}$]	w-l [m a.s.l.]	Q [$m^3 s^{-1}$]	w-l [m a.s.l.]	Q [$m^3 s^{-1}$]	w-l [m a.s.l.]
08/2016	0.384	141.559	0.408	141.077	0.418	141.077	0.486	140.514
11/2016	0.609	141.260	0.633	140.979	0.714	140.979	0.726	140.331
02/2017	0.929	140.910	0.949	140.764	1.117	140.621	1.165	140.260
07/2017	0.161	140.981	0.175	140.785	0.177	140.721	0.182	140.325
04/2018	0.323	141.304	0.328	141.010	0.370	140.942	0.409	140.727
08/2018	0.201	141.415	0.191	141.189	0.194	141.003	0.193	140.661
12/2018	0.451	141.350	0.486	140.997	0.513	140.745	0.476	140.293
04/2019	0.511	141.282	0.543	140.815	0.572	140.646	0.583	140.281

Fig. 4. Aquatic vegetation in the Malina stream during season (april 2018 versus august 2018) –gas profile.

Fig. 5. Aquatic vegetation in the Malina stream during season (april 2018 versus august 2018)–railway bridge profile.

Conclusion

Vegetation in natural streams influences the flow field and related characteristics and phenomena, such as discharge capacity, velocity profile, roughness, but also erosion and sedimentation, pollutant transport and water biota. The aim of this paper was to investigate and determine the impact rate of aquatic vegetation on flow conditions, based on field measurements along the Malina stream. The roughness coefficient n was used as a way of quantifying the impact. A summary of relevant measured and calculated values is given in Tables 1 and 3.
An analysis of the obtained data revealed that the roughness coefficient value changes during the growing season. A consequence of vegetation growth in the channel is a changing velocity profile and water level. The rate of these hydraulic parameters divergences, in comparison to summer and non-summer seasons, decreases with increasing discharge. The analyses of measured data showed and confirmed the complexity of the impact of in-channel vegetation on stream flow, and the necessity to continue investigation into this problem.

Acknowledgement

This paper was prepared with the support of the project No. VEGA 2/0025/19.

References

Boscolo, V. (2014): Effect of in-stream vegetation on hydraulic resistance in regulated rivers. Master thesis, Universita degli Studi di Padova, Aberdeen, 2014, 117 p.

Cheng, N. (2011): Hydraulic radius for evaluating resistance induced by simulated emergent vegetation in open-channel flows. Journal of Hydraulic Engineering, vol. 137, 2011, p. 995–1004.

Chow, V. T. (1959): Open channel hydraulics. McGraw-Hill, 1959.

De Doncker, L., Verhoeven, R., Bal, K., Meire, P., Quintelier, J. (2009): Determination of the Manning roughness coefficient influenced by vegetation in the river Aa and Biebrza river. Environmental Fluid Mechanics, vol. 9, no. 5, 2009, 549–567. https://doi.org/10.1007/s10652-009-9149-0.

Green, J. C. (2005): Modelling flow resistance in vegetated streams: review and development of new theory. Hydrological processes, vol. 19, no. 6, 2005, p. 1245–1259.

James, C. S., Birkhead, A. L., Jordanova, A. A., O'Sullivan, J. J. (2004): Flow resistance of emergent vegetation. Journal of Hydraulic Research, vol. 42, no. 4, 2004, p. 390–398.

Korichi, K., Hazzab, A. (2012): Hydrodynamic investigation and numerical simulation of intermittent and ephemeral flows in semi-arid regions: Wadi Mekerra, Algeria. Journal of Hydrology and Hydromechanics, vol. 60, no. 2, 2012, p. 125–142.

Kutija, V., Hong, H. T. M. (1996): A numerical model for assessing the additional resistance to flow introduced by flexible vegetation. Journal of Hydraulic Research, vol. 34, no. 1, 1996, 99–114.

Manes, C., Pokrajac, D., Nikora, V. I., Ridolfi, L., Poggi, D. (2011): Turbulent friction in flows over permeable walls. Geophysical Research Letters, vol. 38, no. 3, 2011. https://doi.org/10.1029/2010GL045695.

Nehal, L., Hamimed, A., Khaldi, A. (2013): Experimental study on the impact of emergent vegetation on flow, p. 6. In: Proc. 7th International Water Technology Conference, IWTC17, Istanbul, (http://iwtc.info/wp-content/uploads/2013/11/94.pdf).

Nikora, V., Larned, S., Nikora, N., Debnath, K., Cooper, G., Reid, M. (2008): Hydraulic resistance due to aquatic vegetation in small streams: Field study. Journal of Hydraulic Engineering, vol. 134, no. 9, 2008, 1326–1332. ISSN 0733-9429.

Stone, M. B., Shen, H. T. (2002): Hydraulic resistance of flow in channels with cylindrical roughness. Journal of Hydraulic Engineering, vol. 128, no. 5, 2002, 500–506.

Velísková, Y., Dulovičová, R., Schügerl, R. (2017): Impact of vegetation on flow in a lowland stream during the growing season. Biologia, vol. 72, no. 8, 2017, 840–846. DOI: 10.1515/biolog-2017-0095.

Wilson, C. A., Hoyt, J., Schnauder, I. (2007): Flow resistance models for flexible submerged vegetation. Journal of Hydrology, vol. 134, no. 7, 2007, 213–222.

Mgr. Radoslav Schügerl, PhD.
Institute of Hydrology, SAS,
Dúbravská cesta 9
841 04 Bratislava, SR
Slovak Republic
E-mail: schugerl@uh.savba.sk

DOI: 10.31577/ahs-2019-0020.02.0018

ACTA HYDROLOGICA SLOVACA

Volume 20, No. 2, 2019, 151–159

TRANSFORMATION OF BED SILTS ALONG LOWLAND CHANNEL GABČÍKOVO-TOPOĽNÍKY AND COMPARISON OF THEIR SATURATED HYDRAULIC CONDUCTIVITY VALUES

Renáta Dulovičová

This contribution deals with the evaluation of bed silts permeability on channel Gabčíkovo-Topoľníky (G-T channel), the one from three great channels of channel network at Žitný ostrov (ŽO). The bed silts permeability in ŽO channel network significantly impacts on mutual interaction between channel network and groundwater at ŽO and it is expressed by parameter their saturated hydraulic conductivity (SHC). The paper compares the values of bed silts SHC which were extracted from G-T channel during period 1993–2018. The bed silts were extracted and obtained by two ways, as a disturbed samples and as an undisturbed samples. From disturbed samples on G-T channel were obtained bed silts SHC calculated according to empirical formulas of Bayer-Schweiger and Špaček, the valid values of SHC – K_p reached from $4.3\ 10^{-07}$–$4.5\ 10^{-05}$ m s^{-1}. From undisturbed samples of silts which were extracted along G-T channel from top, middle and bottom layer of silts, were determined the values SHC – K_n by measurement in laboratory – by the laboratory falling head method. The acquired values K_n for G-T channel reach from $5.2\ 10^{-08}$–$4.2\ 10^{-03}$ m s^{-1}. The current state of longitudinal distribution of bed silts SHC along the G-T channel was demonstrated as numerically and graphically, too.

KEY WORDS: channel network, bed silts, granularity, silt permeability, saturated hydraulic conductivity

Introduction

The area of ŽO formed as a flat plain with only small differences in altitude. Its surface decreases in the southeast direction. Its average slope is about 0.25‰ and it was one of the reasons for building channel network here (as a drainage system) – Fig. 1 and therefore is ŽO densely interlocked by quantity of channels. The longitudinal slopes of these channels are also very small forasmuch as whole area of ŽO has very little slopes. This fact had impact to production of silts on the channel bottom. These silts has been created by wash out from adjacent territory in consequence manipulation with the existing structures at channel network and also from decomposition of water vegetation. The thickness and structure of bed silts are factors which influence the groundwater and channel network interaction. Therefore was checked up the impact of channel network silting up on it and determined necessary characteristic – the permeability of silts expressed by its saturated hydraulic conductivity.

This paper deals with results of field measurements on G-T channel in the period from 1993 to 2018 with aim to sketch the current state of silting up at this channel, its influence to interaction between channel and groundwater and to compare the results obtained by two ways of bed silts extraction (disturbed and undisturbed samples).

Material and methods

Groundwater at ŽO is strongly related to water regime of channel network. The problem of water level regulation at this area is complex. Therefore, many specialists were interested in solution of it (Kosorin, K. 1997; Burger and Čelková, 2004; Mucha, Šestakov, 1983; Mucha et al., 2006; Štekauerová et al., 2009; Baroková and Šoltész, 2011; Baroková and Šoltész, 2014; etc.). Channels, manipulating objects and pumping stations as basic elements of this channel network allow to control water level in channels to achieve optimal position of groundwater table during vegetation period when water vegetation affects flow conditions in channels.

The G-T channel is the biggest one from three main channels of the channel network at ŽO (besides Chotárny and Komárňanský channel) – see Fig.1 (right) and Fig. 2. G-T channel was built primary for drainage, now it is used also for irrigation function. The length of the G-T channel is about 30 km. Its width oscillated between 8–17 m during monitored period, the last measurements of channel depth registered maximal values up to 2.6 m (according to located cross-section profiles). The values of saturated hydraulic conductivity in aquifers nearby

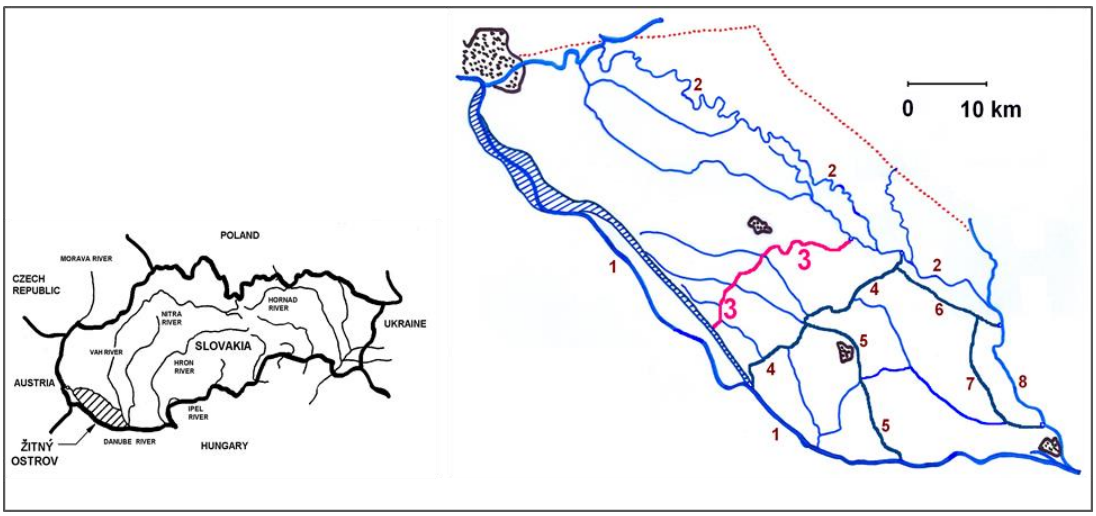

Fig. 1. Situation of ŽO (left), scheme of channel network at ŽO (right): 1 – Danube; 2 – Small Danube; ***3 – channel Gabčíkovo–Topoľníky****; 4 – Chotárny channel; 5 – Čalovo–Holiare–Kosihy; 6 – Aszód–Čergov; 7 – Čergov–Komárno; 8 – Dudváh; 9 – Komárňanský channel.*

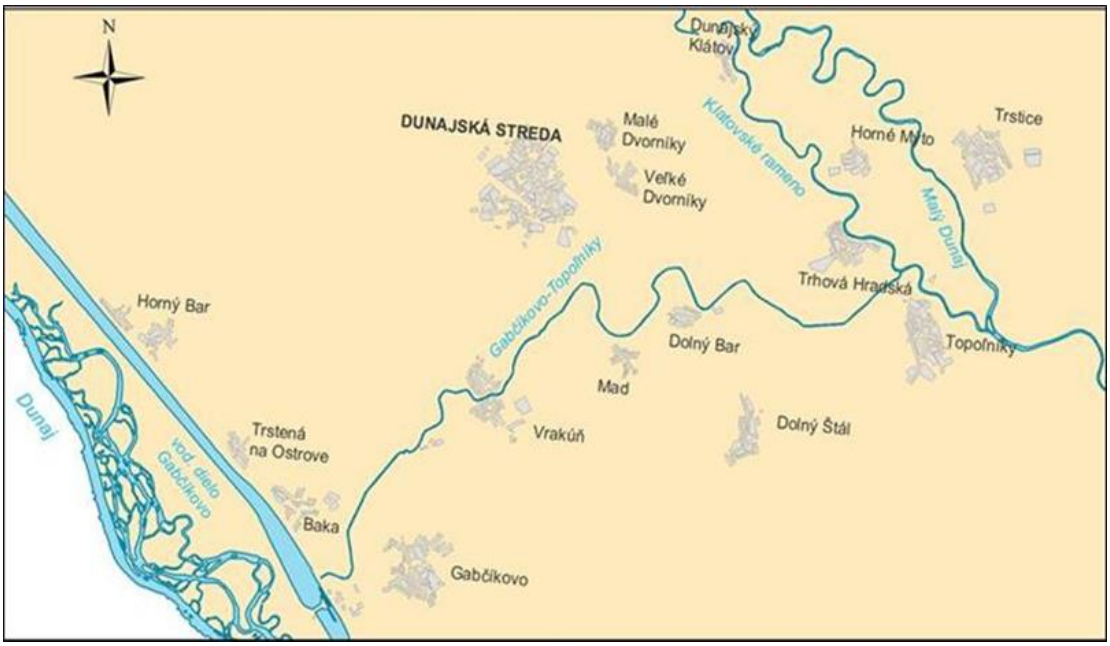

Fig. 2. Position of G-T channel.

this channel k_{fp} are 0.55–7.3 10^{-3} m s^{-1} (Mišigová, 1988). The first measurements of silting up at ŽO channel network were performed in 1993, at first from the displaceable inflatable dinghy with special equipments – first by simple drill hole, then by echo-sounder Lowrance HDS-10 and EA400/SP – see at Fig. 3. The measurements were performed along the whole length of the G-T channel. The distance of cross-sections along the channel varied between 1.0–1.5 km. In all channel cross-section profiles there was measured the water depth and silt thickness with step 1.0–2.0 m along the channel width. The measurements of channels silting up are restated periodically from 2004 up to now.

From 2004 were started measurements with the extraction of silts in single channel cross-section profiles. The extraction of silt samples was performed by two sorts of equipment – by auger (as disturbed samples of silts) and by sediment beeker sampler (also as undisturbed samples of silts) – Fig. 4. It was need for determination of bed silts granularity and consecutively for determination of saturated hydraulic conductivity value of bed silts. The silt samples were extracted from top, middle and bottom layer of silt.

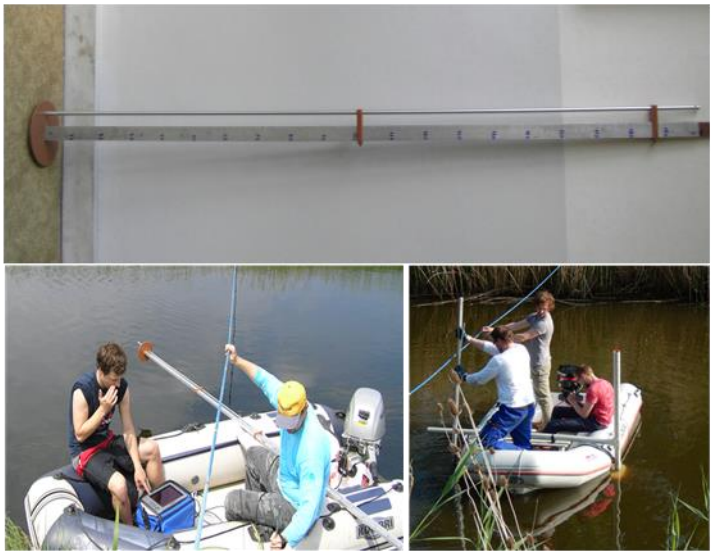

Fig. 3. Equipments for measurement of silt thickness – drill hole probe (up), echo-sounder Lowrance HDS-10 (left down) and EA400/SP (right down).

Fig. 4. Measuring equipment for silt samples extraction in 1993–2014 – auger (up) and beeker sampler (down).

Saturated hydraulic conductivity of bed silts

As was mentioned, the silt samples were extracted as disturbed and as undisturbed samples. The values of saturated hydraulic conductivity (SHC) from disturbed samples of silts were calculated by empirical formulas coming out from granularity curves. The several empirical relationships for determination of SHC from granularity of silts exist, but we had applied them very carefully for their limited validity. As we could take disturbed samples of silts, we could apply only the relationships by Beyer-Schweiger and Špaček (Špaček, 1987). These relationships are functions of d_{10} – particle diameter in 10% of soil mass [m] and d_{60} – particle diameter in 60% of soil mass [m]. Both of them were determined from granularity curves of the extracted silts. The formulas of Beyer-Schweiger and Špaček were used for assessment of SHC from disturbed samples from G-T channel – K_p:

Beyer-Schweiger formula [m.s^{-1}]

$$K_p = 7.5\ 10^6\, C\,(d_{10})^2 \tag{1}$$

where

$$C = 1.5961\ 10^{-3}\left(\frac{d_{60}}{d_{10}}\right)^{-0.20371}$$

d_{10} – particle diameter in 10% of soil mass [m]
d_{60} – particle diameter in 60% of soil mass [m]

and conditions of validity are:

$$0.06 \le d_{10} \le 0.6 \quad ; \quad 1 \le \frac{d_{60}}{d_{10}} \le 20$$

Špaček formulas [m d^{-1}]

$$K_{p\,I.} = 20.77\,(d_{10})^{1.013}\left(\frac{0.5}{d_{60}-d_{10}}\right)^{0.059} \quad (2)$$

$$K_{p\,II.} = 108.4386\,(d_{10})^{0.8866}(d_{60})^{0.7726} \quad (3)$$

where
conditions of validity for application of eq. (2) are:
1. $d_{10} < 0.01\text{mm}$
or
2. $0.01 \le d_{10} < 0.13 \;\wedge\; d_{60} < 0.0576 + 0.5765 d_{10}$

conditions of validity for application of eq. (3) are:
1. $d_{10} \ge 0.13\text{mm}$
or
2. $0.01 \le d_{10} < 0.13 \;\wedge\; d_{60} > 0.0576 + 0.5765 d_{10}$

The values of SHC from disturbed samples K_p along the G-T channel are summed and marked in Table 1.

In 2014–2016 we were able to extract also some undisturbed samples of silts (by beeker sampler). These undisturbed samples were transposed from extracting cylinder of sediment beeker sampler to sampling tube and then were assessed the values of SHC by direct measurement in laboratory – falling head method. There was used simplified equipment for measuring of SHC from undisturbed samples – see Fig. 5 (methodology of measurement and calculation is described e.g. Šurda et al., 2013; Dulovičová et al., 2016, 2018, etc.).
The relation for calculation of average SHC according to scheme on Fig. 5. (Šurda et al., 2013), is:

$$K_{priem} = \frac{l}{\Delta t}\, ln\, \frac{h2}{h1} \quad [\text{cm s}^{-1}] \quad (4)$$

where
K_{priem}– saturated hydraulic conductivity of undisturbed samples,
l – height of sample,
h_1, h_2 – see at Fig. 5.

Based on this relation were determined the values of silts SHC as undisturbed samples extracted from selected cross-section profiles of G-T channel during 2018. The values of SHC from undisturbed samples K_n along the G-T channel are summed and marked in Table 2.

Results and discussion

The area of ŽO is very flat and flow velocities in the channels are very slow. This was main reason of silts deposition. Its distribution along the channel depends also on flow conditions in channels junction. As logically expected, most of the silts deposited at the bottom of the channel and much less was observed at the sides. Otherwise the data does not seem to show clear and simple relationship between the silt thickness and any of variables which we believed would influence the silt depositions. The deposition of the silts is certainly attributed the low velocities in the channel. At the same time, the velocities do not seem to control whether the heaviest deposition of the silts occurred in the down-stream, middle or upstream segments of the channel. It was confirmed that primarily the low velocities influenced the silt depositions, then also in consequence manipulation with the existing structures at channel network and also from decomposition of water vegetation and its successive deposition. We started to measure also the velocities and discharges from 2016 during our field measurements of channels silting up – by using the River

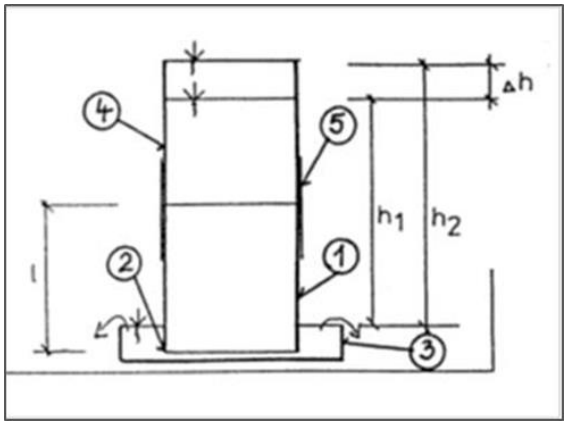

Fig. 5. Simplified equipment for measuring saturated hydraulic conductivity of undisturbed sample (Šurda et al., 2013). 1 – sampling tube, 2 – filter paper and woven wired sieve, 3 – Petri dish, 4 – extension piece, 5 – confining ring.

Surveyor S5/M9 from SONTEK. The files from these measurements confirmed that the velocities (measured in 9 points of channel cross-sections) are very low.
Even at some places where the channel was overgrown by very wild vegetation also inside the channel (under water level) then was impracticable to gauge this parameter. The solution of this question (the values of velocities and discharges in channel) will be subject of another scientific contribution which will deal with silt depositions and from that reason I do not mention about the exact velocity values in this paper.
We assumed the smaller amounts of the silt deposition in the upstream and downstream parts of the G-T channel (by manipulating with pumping station) and larger amounts in the middle part and we assumed this increase to be gradual and linear. These assumptions were confirmed in part. The largest silt thicknesses on G-T channel during monitored period 1993 to 2018 were noticed in its middle parts – Fig. 6.

Results of SHC from disturbed samples of silts

Silts permeability, expressed as SHC value, was calculated for disturbed samples of silts through relationships of Beyer-Schweiger and Špaček. Each of them determines SHC as a function of d_{10} – particle diameter in 10% of soil mass and d_{60} – particle diameter in 60% of soil mass because conditions of validity for application of these formulas also depend on value of d_{10} and d_{60}. The characteristics d_{10} and d_{60} were determined for top, middle and bottom layer of silt samples. The valid values of silts SHC on G-T channel ranged 4.3 10^{-07} – 4.5 10^{-05} m s^{-1}. In comparison with SHC values of surrounding aquifer K_{fp} near G-P channel the values of silts SHC are severalfold lower.
From comparison of structure of extracted silt samples in its single layers (top, middle and bottom) during period 2004 to 2014 we saw (according Table 1) that in 2004 the structure of silt samples in bottom and top layer was same – loamy sand. In 2008 on this place the structure of silt sample in middle layer has been changed from loamy sand, sandy loam, loam to clay loam, together the calculated valid values of SHC decreased to 10^{-07}. In 2014 the structure of silt samples has been changed from sand and sandy loam in top layer through sandy loam, loam and clay loam in the middle layer right to sandy loam and clay loam in bottom layer of silt samples. As is evident from next values in Table 1, the calculated valid values of SHC along the G-T channel have been changed from 2004 to 2014 from 10^{-05} to 10^{-07}.

Results of SHC from undisturbed samples of silts

The values of silts SHC from undisturbed samples K_n extracted from selected cross-section profiles of G-T channel during 2018 were determined on the base of relation (4) according to scheme on Fig. 5. The valid values of silts SHC on G-T channel K_n ranged 5.2 10^{-08}–4.2.10^{-03} m s^{-1}. In comparison with SHC values of surrounding aquifer K_{fp} near G-P channel the values of silts SHC from undisturbed samples are also severalfold lower.
The another values K_n along the G-T channel shows Table 2.
At comparison of structure of undisturbed silt samples in its single layers it notes that the differences between top, middle and bottom layer are nearly inconsiderable – the values 10^{-06} 10^{-07} predominates in all three layers.
Furthermore we tried to compare the values of SHC for disturbed a undisturbed samples of bed silts on G-T channel. The remarkable results came up from this comparison. As was mentioned before the values of SHC from disturbed samples on G-T channel K_p run into 10^{-07} to 10^{-05}, over against the values of SHC from undisturbed samples K_n run into 10^{-08} to 10^{-03}. This fact confirmed our assumption that the values from undisturbed samples K_n will be lower than the values from disturbed samples K_p, they tenfold decreased. At comparison of single layers of silts, extracted as disturbed and undisturbed samples, we identify that between top, middle and bottom layers did not appear considerably noticeable differences. They were similar, practically comparable as demonstrates Table 1 and 2 (besides occasional cases). The order of magnitude ranged predominant from 10^{-06} to 10^{-07}. The graphical interpretation of comparison results is shown on Fig. 7.

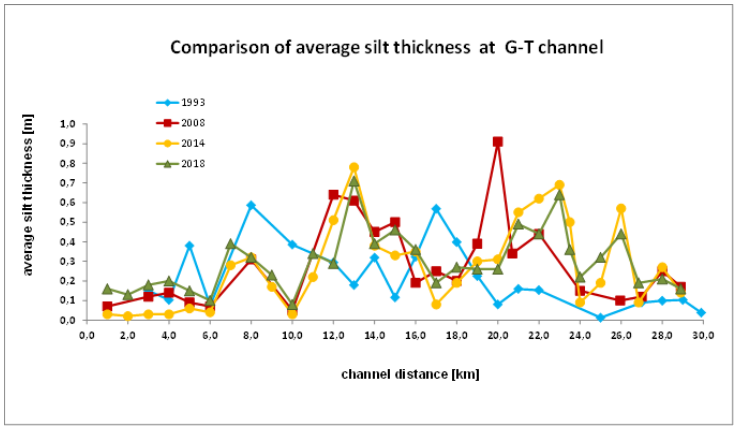

Fig. 6. Average silt thicknesses along G-T channel in 1993–2018.

Table 1. Gabčíkovo-Topoľníky channel – valid values of K_p from disturbed samples of silts in year 2004–2014

Channel:			**Gabčíkovo – Topoľníky**		
Year:			**2004**		
Channel distance [km]	Silt layer	Type of sample	Saturated hydraulic conductivity K_p [m s^{-1}]		
			Bayer-Schweiger	Špaček I.	Špaček II.
26.0	top – LS	disturbed	-	-	2.7 10^{-06}-
	bottom – LS		-	-	7.6 10^{-06}
Year:			**2008**		
Channel distance [km]	Silt layer	Type of sample	Saturated hydraulic conductivity K_p [m s^{-1}]		
			Bayer-Schweiger	Špaček I.	Špaček II.
8.0	middle – LS		-	-	2.6 10^{-06}
12.0	middle – SL		-	1.2 10^{-06}	-
15.0	middle – SL	disturbed	-	1.3 10^{-06}	-
20.0	middle – L		-	8.5 10^{-07}	-
26.0	middle – CL		-	5.9 10^{-07}	-
28.9	middle – CL		-	4.6 10^{-07}	-
Year:			**2014**		
Channel distance [km]	Silt layer	Type of sample	Saturated hydraulic conductivity K_p [m s^{-1}]		
			Bayer-Schweiger	Špaček I.	Špaček II.
1.0	top – S		4.5 10^{-05}	-	4.3 10^{-05}
7.0	top – CL		-	-	1.3 10^{-05}
	bottom – CL		-	-	1.9 10^{-06}
8.0	top – S		4.3 10^{-05}	-	3.8 10^{-05}
	middle – S		-	-	1.7 10^{-05}
	bottom – CL		-	4.3 10^{-07}	-
11.0	top – S		-	-	1.5 10^{-05}
	bottom – S		-	-	1.3 10^{-05}
12.0	top – SL	disturbed	-	6.9 10^{-07}	-
	middle – SL		-	1.0 10^{-06}	-
	bottom – SL		-	1.0 10^{-06}	-
13.0	top – SL		-	8.8 10^{-07}	-
	middle – SL		-	9.1 10^{-07}	-
	bottom – SL		-	6.5 10^{-07}	-
17.0	top – LS		-	-	3.7 10^{-06}
19.0	top – SL		-	1.0 10^{-06}	-
	middle – SL	disturbed	-	9.1 10^{-07}	-
	bottom – SL		-	-	1.7 10^{-06}
21.0	top – L		-	1.0 10^{-06}	-
	middle – L		-	1.1 10^{-06}	-
	bottom – SL		-	7.0 10^{-06}	-
22.0	top – SL		-	1.2 10^{-06}	-
	middle – SL		-	1.2 10^{-06}	-
	bottom – LS		-	2.1 10^{-06}	-
24.0	top – SL		-	-	2.3 10^{-06}
	middle – SL	disturbed	-	-	1.3 10^{-06}
	bottom – SL		-	1.5 10^{-06}	-
25.0	top – SL		-	-	3.0 10^{-06}
	bottom – SL		-	-	8.4 10^{-06}
26.0	top – CL		-	4.9 10^{-07}	-
	middle – LS		-	2.0 10^{-06}	-
	bottom – S		3.1 10^{-05}	-	2.1 10^{-05}
28.0	bottom – CL		-	4.4 10^{-07}	-

LS – loamy sand; SL – sandy loam; S – sand; CL – clay loam; L – loam
– unkept conditions of validity

Conclusion

Aim of this paper was to evaluate the influence of silt permeability to mutual interaction between surface water of channel system and nearby groundwater on ŽO, exactly to the G-T channel and its surroundings. The permeability of silts is expressed by SHC of silts and it was reason why we wanted to know how this parameter has modified along the G-T channel during monitored period from 1993 to 2018. According to results of distribution of average silts thickness along the G-T channel in period 1993 to 2018 (Fig. 6) is evident that

silting up of G-T channel has been changed, the biggest one was in the middle part and it was also transposing during monitored period (2014–2018 in comparison by 1993).

The SHC values of silts were calculated by two ways as bed silts were extracted and obtained as disturbed samples and as undisturbed samples from top, middle and bottom layer of silts. From disturbed samples in G-T channel were obtained SHC values of bed silts calculated according to Bayer-Schweiger and Špaček formulas and they are presented in Table 1, the valid values K_p reach from 4.3 10^{-07}–4.5 10^{-05} m s^{-1}. From undisturbed samples of silts which were extracted along G-T channel, were determined values of SHC K_n by falling head method and they are demonstrated in Table 2. The values K_n for G-T channel reached values from 5.2 10^{-08}–4.2 10^{-03} m s^{-1}. The extant silting up by fine-grained silt substances along this channel at time caused that the less permeable channel bottom has been gradually created. This "clogging of channel bottom" can affect adversely to the interaction between surface water in channel and groundwater in its surroundings, because it reduces the exchange of water amounts between them (this reduction could have adverse impact during the hydrological extremes).

The information about silting up of G-T channel, supplemented by SHC values of silts, will be helpful for regulation of groundwater level in surroundings of this channel and they are very useful for plant water supplying. The SHC characteristics were used also for simulation of interaction between channel network and groundwater at ŽO area and for determination of surface water impact on reserves of soil water at this area.

Acknowledgement

This work was supported by the contract VEGA-02/0025/19 and APVV-14-0735.

Table 2. Gabčíkovo-Topoľníky channel – valid values of K_n from undisturbed samples of silts in year 2018

Channel:	**Gabčíkovo-Topoľníky**		
Year:		**2018**	
Channel distance [km]	Silt layer	Type of sample	SHC – K_n [m s^{-1}]
1.0	top	undisturbed	1.6 10^{-06}
	middle		1.3 10^{-06}
	bottom		1.0 10^{-06}
12.0	top		2.6 10^{-07}
	middle		1.6 10^{-07}
	bottom		2.4 10^{-06}
14.0	top		8.7 10^{-07}
	middle		2.1 10^{-06}
	bottom		3.5 10^{-06}
19.0	top		4.6 10^{-06}
	middle		5.8 10^{-05}
	bottom		4.2 10^{-03}
23.0	top		1.9 10^{-07}
	middle		3.7 10^{-07}
	bottom		1.8 10^{-07}
23.5	top		3.2 10^{-07}
26.0	top		5.2 10^{-08}
	middle		2.2 10^{-07}
	bottom		2.3 10^{-06}
28.0	top		1.1 10^{-07}
	bottom		1.6 10^{-07}

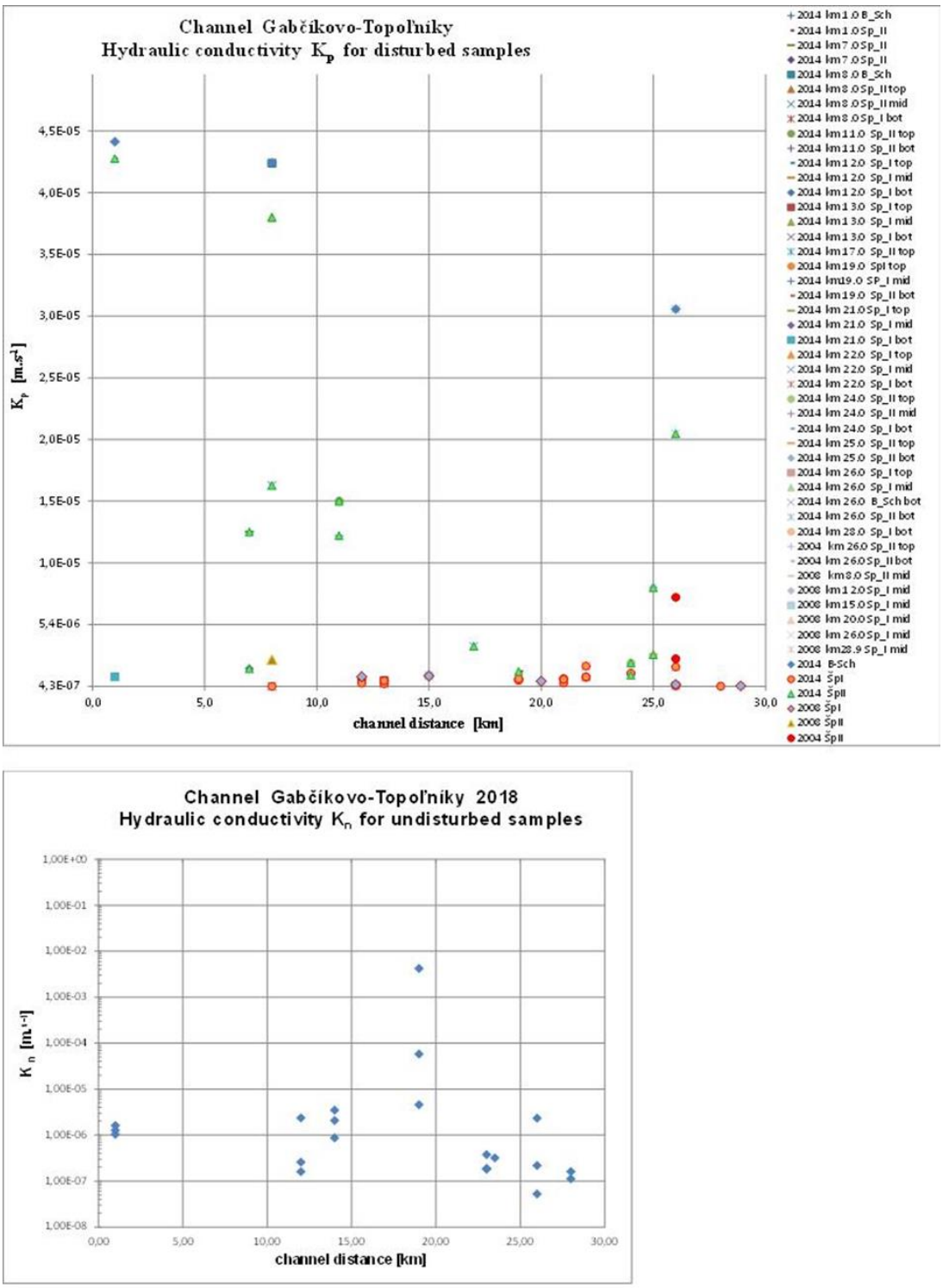

Fig. 7. Graphic representation of longitudinal distribution of silt saturated hydraulic conductivity values on G-T channel - comparison for disturbed (up) and undisturbed (down) samples.

References

Baroková, D., Šoltész, A. (2011): Drainage and Infiltration Resistance of Rivers – Element of Interaction Between Surface and Groundwater. In: Current events in hydraulic engineering. Wydawnictwo Politechniki Gdańskiej, Gdańsk.

Baroková, D., Šoltész, A. (2014): Analysis of surface and groundwater interaction in the Danube river branch system, SGEM Conference Proceedings, 14th SGEM Geo-

Conference on Water Resources. Forest, Marine And Ocean Ecosystems, Vol. I., www.sgem.org, ISBN 978-619-7105-13-1/ ISSN 1314-2704, 51–58.

Burger, F., Čelková, A. (2004): Simulation of aquifer feeding processes during dry period. Acta Hydrologica Slovaca, Vol.5, No.2, 348–357. (in Slovak)

Dulovičová, R., Velísková, Y., Schűgerl, R. (2016): Hydraulic conductivity of silts in Chotárny channel at Žitný ostrov, Acta Hydrologica Slovaca, vol. 17, No. 2, 149–156. ISSN 1335-6291

Dulovičová, R., Velísková, Y., Schügerl, R. (2018): Hydraulic conductivity of bed silts in Komárňanský channel – Žitný ostrov, Acta Hydrologica Slovaca, vol. 19, No. 1, 117–125. ISSN 1335-6291

Kosorin, K. (1997): Spatial groundwater dynamics of the Rye Island aquifer. J. Hydrol. Hydromech., 45, 348–364.

Mucha, I., Banský, Ľ., Hlavatý, Z., Rodák, D. (2006): Impact of riverbed clogging colmatation on ground water, Riverbank Filtration Hydrology: Impacts on System Capacity and Water Quality, 43–72. NATO Science Series: IV. Earth and Environmental Sciences – Vol. 60. Springer, Printed in the Netherlands.

Mucha, I., Šestakov, V. M. (1983): Hydraulics of groundwaters (Hydraulika podzemních vod). Bratislava 1983.

Mišigová, I. (1988): Methods of regional assessment of hydraulic properties of the rocks on the Žitný ostrov, Report IHH SAS. (in Slovak)

Špaček, J. (1987): Determination of filtration coefficient from total grain-size curves. J. Meliorace, 23, No.1: 1–13. (in Czech)

Šurda, P., Štekauerová, V., Nagy, V. (2013): Variability of the saturated hydraulic conductivity of the individual soil types in the area of the Hron catchment, Nővénytermelés, vol. 62, supplement, 323–326. ISSN 0546-8191

Štekauerová, V., Nagy, V., Šútor, J., Milics, G., Neményi, M. (2009): Influence of groundwater level on soil water regime of Žitný ostrov. In V. Növénytermesztési Tudományos Nap – Növénytermesztés: Gazdálkodás – Klímaváltozás – Társadalom, Akadémiai Kiadó, Budapest, 197–200.

Ing. Renáta Dulovičová
Institute of Hydrology SAS,
Dúbravská cesta 9
84104 Bratislava
Slovak Republic
E-mail: dulovicova@uh.savba.sk

DOI: 10.31577/ahs-2019-0020.02.0019

ACTA HYDROLOGICA SLOVACA

Volume 20, No. 2, 2019, 160–165

WATER BALANCE ESTIMATION UNDER A CHANGING CLIMATE IN THE TURIEC RIVER BASIN

Peter Rončák, Peter Šurda

The article deals with the estimation of water balance components under a changing climate in selected catchments in Slovakia. Climate change has a significant impact on the hydrological cycle and water resources. In this research, the GIS-based, spatially distributed WetSpa rainfall-runoff model was used to simulate mean daily discharges in the outlet of the basin as well as the individual components of the water balance. The WetSpa model simulations are often used to evaluate the impact of changes on the generation of runoff and water balance. The parameters of the model were estimated using climate data and three digital map layers: a land-use map, soil map and digital elevation model. In this research, the KNMI and MPI regional models with SRES A1B (moderate) emission scenario were used. Outputs from the KNMI and MPI climate scenarios (as input data) were used to estimated future behavior of characteristics of water balance as an actual evapotranspiration and soil moisture. The results showed an increase of actual evapotranspiration and decrease of soil moisture in future horizons in comparison with the reference period of 1981–2010.

KEY WORDS: water balance, climate change scenarios, rainfall-runoff modelling

Introduction

Climate change is a phenomenon that deals with countless numbers of scientific researches. Problematic changes in runoff conditions due to climate change are currently one of the main sources of uncertainty in the long-term planning of water resources and flood protection. The problematics of climate change have also been dealt with by several authors from Slovakia (Rončák et al., 2016). Changing the environment (including changing land use and climate change) and its impact on water resources has been a relatively hot topic in recent years. The direct or indirect consequences on the hydrological regime due to changes in land use and climate have undoubtedly contributed to problems such as water scarcity, proliferation of lightning floods, or damage caused by massive deforestation. Rainfall-runoff models are often used as a tool for assessing the impacts of climate and land use change on the hydrological cycle. While modeling of climate change can be used especially for conceptual rainfall-runoff models, simulating the influence of land use change on the runoff processes in the river basin requires models with spatially distributed parameters. The climate change is caused by increasing concentrations of greenhouse gases in the atmosphere may affect the hydrological cycle and human availability of water and therefore affect agriculture, forestry and other industries (Rind et al., 1992). Changes in the hydrological cycle may cause more incidence of floods in some areas.

Actual evapotranspiration and soil moisture are important in many hydrological conditions. Actual evapotranspiration, reflects complex interactions between climate, vegetation, soil and catchment hydrological processes (Donohue et al., 2006), and is one of the most important variables to diagnose the changes of water regime in the basin scale (Liu and Yang, 2010). Soil moisture has an important effect on the partitioning of precipitation in surface runoff, infiltration and groundwater recharge, and is also a key factor for plant growth, land degradation, flood generation and drought mitigation (Tavakoli and De Smedt, 2013). Decreasing of soil moisture may causes generation of floods as a principal soil threat and soil erosion as an additional soil threat mainly on arable lands of hillslope areas (Hlavčová et al., 2019).

Particularly interesting, as important indicators of global warming, are the projected trends of climate variables such as temperature and rainfall on the Central Europe area. Not only in this region, annual mean temperatures will rise and the warming is likely to be largest in summer (Christensen et al., 2013). Moreover, the majority of the general circulation models (GCMs) foresee an increase, in frequency, of extreme daily precipitation, despite a decrease in total values. Thus, this tendency can lead to longer dry periods, increasing the risks of droughts, interrupted by extreme intense precipitation, enhancing the flood risk (Ayanshola et al., 2018; Wani et

al., 2017; Bates et al., 2008). Average runoff in Slovakian rivers is projected to decrease with increasing temperatures and decreasing precipitation. In particular, some river basins may see decreases below today's levels in the future.

Distributed hydrological models (spatially distributed models) take into account the spatial variability of atmospheric processes and the physical-geographic characteristics of river basins that control rainfall-runoff processes. In this paper, we are focusing on a physically based model with spatially distributed parameters. These models are based on a physical description of rainfall-runoff processes and seek to respect the laws of conservation of matter, momentum and energy. The physically based distributed hydrological models are directly capable using geospatial information. The intense development of computer programs promotes the ability to exploit the rich content of information describing land use or soil moisture. Physically-based distributed models are a constantly evolving tool in the hydrology, particularly in the flood protection, or the estimation of the impact of climate and land use change on the runoff processes. Conceptual models are also used to estimate the impact of climate change on components of water balance (Sleziak et al., 2016).

In this paper we evaluated the possible impacts of climate change on the components of water balance in the selected river basins, where the simulation of future changes in rainfall-runoff processes were based on the outputs of the KNMI and MPI regional climate models (RCMs).

Data and methodology

In this research the WetSpa model was used for estimating the impact of global climate change on the components of water balance in the selected river basins in Slovakia. This work contains scenarios of global climate change. Outputs from the KNMI and MPI climate scenarios were used to simulation components of water balance. Both types of scenarios of changes were prepared, and the components of water balance under the new conditions was simulated. Then, the calculation of actual evapotranspiration and soil moisture were made. After that, we compared the components of water balance between the reference period 1981–2010 and the climate change scenarios.

Rainfall-runoff model

For simulations of water balance components under changed conditions, the distributed rainfall-runoff WetSpa model was used (Rončák et al., 2016). This research was made for 5 selected basins in Slovakia. For this paper the Turiec River catchment was chosen as example (Fig. 1).

The model uses geospatially referenced data as the input for deriving the model parameters, which includes most data types supported by ArcGIS, such as coverage, shape files, grids and ASCII files. An image can be used for reference within a view, but is not used directly by the model. Digital maps of the topography, land use and

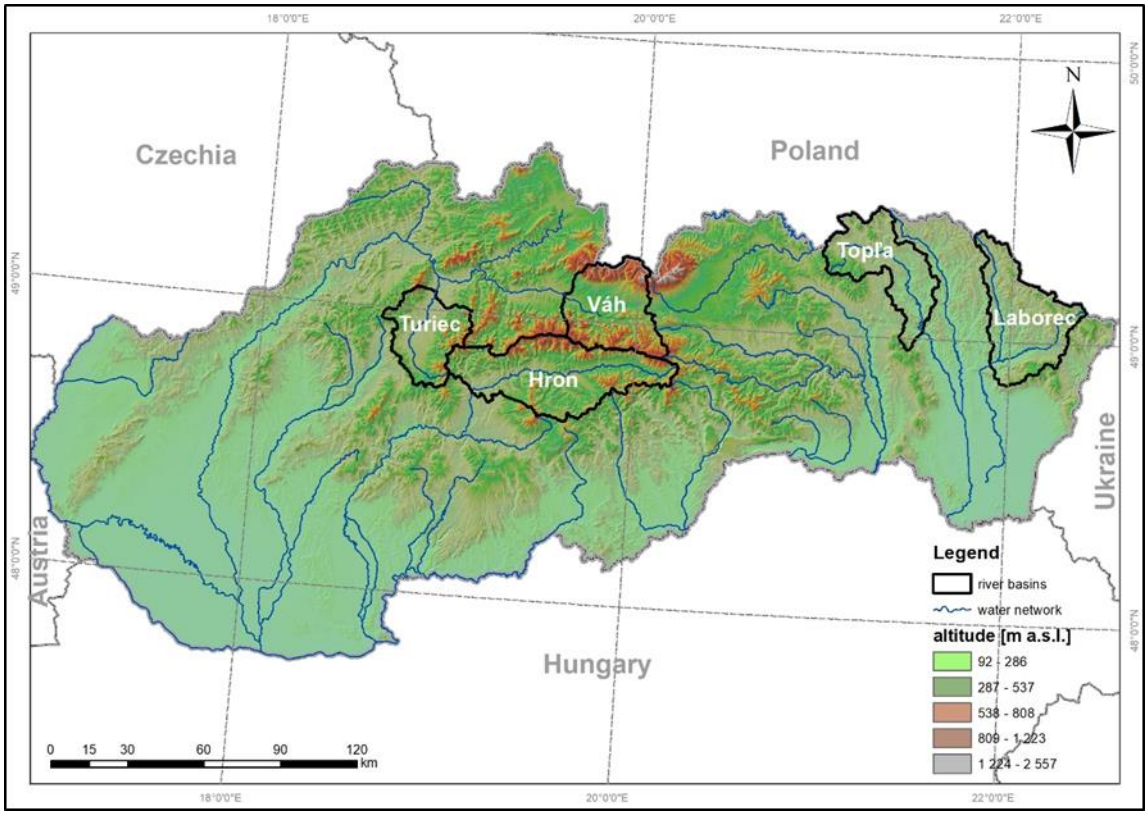

Fig. 1. The location of the selected catchments within Slovakia.

soil types are the 3 base maps used in the model, while other digital data are optional, depending upon the data available, the purpose, and the accuracy requirements of the project (Wang et al., 1996). The following hydrometeorological data were used in the model: daily precipitation totals from spot measurements at 17 stations, and the average daily values for the air temperature at 5 climatological stations. The flow data consisted of the average daily flows at the Turiec-Martin profile. The calibration period was from 1981–1995. Twelve parameters for which a range of admissible values set were optimized.

The climate change scenarios

Climate scenarios Dutch KNMI (with A1B emission scenario) and German MPI (with A1B emission scenario) were used for this research. These regional circulation models take over boundary conditions for the solution of equations from the outputs of ECHAM5 global model. Both models are coupled, i.e., atmosphere-ocean circulation models with greenhouse gasses and aerosols influence on change in radiative forcing. The latest climate change scenarios for the territory of Slovakia were processed on the basis of outputs from climatic atmospheric models at the Department of Astronomy, Earth Physics and Meteorology at the Faculty of Mathematics, Physics and Informatics of Comenius University (Lapin et al., 2012).

Table 1 illustrates the long-term mean monthly values of the air temperatures and precipitation for the reference period 1981–2010 in the Turiec River basin and their differences for the three future time horizons according to the KNMI and MPI regional climate change scenarios. According to the individual climatic models, as seen in Table 1, a decrease in mean monthly precipitation in the summer period can be expected. On the other hand, the winter period should be more humid in comparison with the current conditions. The mean monthly air temperature will rise, without exception, in the catchment at about the same rate. The mean monthly air temperatures will increase with the increasing time horizons.

Actual evapotranspiration (average actual evapotranspiration losses [mm])

Evapotranspiration from the soil and vegetation is calculated based on the relationship developed by (Thornthwaite and Mather, 1955):

$$ES_{i(t)} = \begin{cases} [c_v EP - EI_i(t) - ED_i(t)]\left[\frac{\theta_i(t) - \theta_{i,w}}{\theta_{i,f} - \theta_{i,w}}\right] & for\ \theta_{i,w} \le \theta_i(t) < \theta_{i,f} \\ c_v EP - EI_i(t) - ED_i(t) & for\ \theta_i(t) \ge \theta_{i,f} \end{cases} \quad (1)$$

where

$ES_{i(t)}$ – actual soil evapotranspiration for the time increment [mm],

c_v – vegetation coefficient determined by land use classes varying throughout the year,

$\theta_{i(t)}$ – cell average soil moisture content at time t [m³ m⁻³],

$\theta i_{,f}$ – soil moisture content at field capacity [m³ m⁻³],

$\theta_{i,w}$ – soil moisture content at plant permanent wilting point [m³ m⁻³].

Table 1. Long-term mean monthly values of air temperatures and precipitation of reference period and their differences for the future time horizons in the Turiec River basin

air temperature [°C]		I	II	III	IV	V	VI	VII	VIII	IX	X	XI	XII
1981–2010		-3.7	-2.6	1.1	6.5	11.7	14.4	16.4	15.9	11.3	6.8	1.7	-2.6
KNMI	2025	0.3	1.4	1.5	0.9	1.4	1.3	1.4	1.5	1.4	1.9	0.9	0.6
	2055	1.8	3.1	1.8	1.5	2	2.4	2.3	2.4	2	2.3	1.8	2.3
	2085	3.2	3.4	2.7	2.1	3.1	3.9	4.2	3.8	2.9	3.4	3.4	3.8
MPI	2025	0.4	1.3	0.8	0.7	1	1.1	1.2	1.5	1.4	1.9	1.2	0.7
	2055	2.4	3.4	1.8	1.2	1.6	1.6	2	2.7	2.2	2.2	2.2	2
	2085	3.7	4	2.4	1.8	2.5	3.4	3.3	4	3.6	3.6	3.7	3.9
precipitation [mm]		I	II	III	IV	V	VI	VII	VIII	IX	X	XI	XII
1981–2010		60.3	51.3	60.2	57.7	92.3	95.5	100.2	87.4	76.2	62.5	69.5	67.4
KNMI	2025	-3.1	0.2	-4.5	-8.5	-13.4	-4.4	-23.4	-3.9	30.1	-6.3	-1	21.9
	2055	2.1	3.7	9.1	12.9	-4.1	-13.4	-21.4	0.4	14	6.2	-0.5	24.8
	2085	16.5	14.4	23.7	7.8	-20.1	-33.2	-32.9	-5.5	30.1	9.5	5.8	28.6
MPI	2025	-0.5	7.1	-0.9	-5.6	-14.9	16.3	-0.2	-10.4	22.1	-7.4	1.6	11.1
	2055	2.5	3.7	13.4	19.1	-13.3	9.3	-12	-10.9	13.1	4.3	-7.1	19
	2085	12.7	11.8	22.5	14.1	-17	0.8	-19.5	-10.8	22.6	12.7	4.8	11.6

Soil moisture (average soil moisture in the root zone [mm])

For each grid cell, the root zone water balance is modelled by equating inputs and outputs (Liu and De Smedt, 2004):

$$D\frac{d\theta}{dt} = P - I - S - E - R - F \quad (2)$$

where
D – root depth [L],
θ – soil moisture content of the root zone [$L^3\ L^{-3}$],
t – time [T],
P – precipitation intensity [$L\ T^{-1}$],
I – initial loss due to interception and depression storage [$L\ T^{-1}$],
S – surface runoff [$L\ T^{-1}$],
E – evapotranspiration [$L\ T^{-1}$],
R – percolation to groundwater [$L\ T^{-1}$],
F – interflow [$L\ T^{-1}$].

Results and discussion

In simulating, the expected parameters of the model were obtained from model calibration in period 1981–1995. For the reference period has been selected 1981–2010. The simulated long-term mean monthly actual evapotranspiration and soil moisture were compared with long-term mean monthly values of the reference period. Then, the comparison between the reference period and the climate change scenarios was made.
Figs. 2 and 3 show the calculated values of the components of water balance and their comparison between the reference period and future time horizons.
Looking at Fig. 2 and Table 2, there is an increase in long-term average monthly actual evapotranspiration in selected river basin in each future time horizons. The increase in actual evapotranspiration depends mainly on the increasing air temperature, which directly affects the evapotranspiration value, and whose increase will be characteristic of future time horizons. The increase in long-term average monthly actual evapotranspiration is

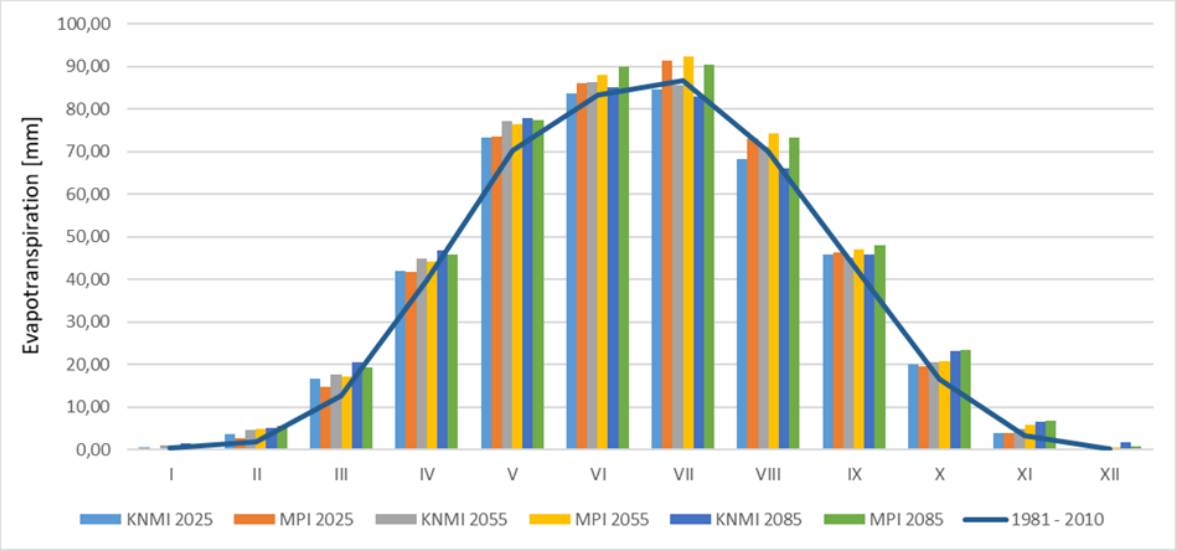

Fig. 2. Comparison of the long-term mean monthly values of actual evapotranspiration in the reference period and in the future time horizons.

Table 2. Simulated long-term mean monthly actual evapotranspiration using the parameters from the 1981–1995 calibration period in the Turiec River basin and its changes for the 3 future time horizons [%]

	period/scenario		I	II	III	IV	V	VI	VII	VIII	IX	X	XI	XII	Øyear [mm]
	1981–2010 [mm]		0.30	1.80	12.80	39.61	70.26	83.18	86.70	69.98	42.95	16.50	3.17	0.18	427
Turiec	KNMI [%]	2025	47	100	29	6	4	0	-2	-3	7	22	24	44	4
		2055	203	163	37	13	10	4	-1	2	5	24	55	272	8
		2085	377	178	61	18	11	2	-4	-6	7	40	109	844	8
	MPI [%]	2025	-30	53	14	5	5	4	5	4	8	18	23	22	6
		2055	147	169	34	11	9	6	7	6	10	26	80	178	10
		2085	290	206	51	16	10	8	4	5	11	41	116	383	13

practically every month. The largest increase (in relative values) is visible in winter period.
Based on Fig.3 and Table 3, there is a modest decrease in long-term mean monthly values of soil moisture in Turiec River basin in each future time horizon. The reduction in long-term average monthly soil moisture is mainly related to the summer period. On the contrary, there is a slight increase in winter months.
In future time horizons, it is likely that there will be a reduction in the sum of precipitation totals in the summer months and an increase in precipitation in the winter period. Consequently, while in the winter months the soil moisture will grow slightly, it will decline in the summer period.

Conclusion

This paper describes the possible impact of climate change on the components of water balance. Actual evapotranspiration and soil moisture are important in many hydrological processes. Therefore, it is important to know their behaviour in the future, especially how the climate change affect them.

The KNMI and MPI climate change scenarios represent less extreme changes (the A1B emission scenario). Based on a scenarios of long-term average components of water balance of future horizons and their comparison with a reference period 1981–2010 it shows that in the future we can expect some change (but not significant) of the long-term mean monthly actual evapotranspiration and soil moisture in the simulated catchments. These changes are predominantly due to the increase of air temperature and decline in precipitation total. This change may reflect differently, depending on several climate change scenarios. Of the considered scenario it suggests that practically all simulated basins could be at risk from the summer or the autumn drought. Based on the simulated watershed in this work it is likely that this effect will apply to the whole territory of Slovakia. On the other hand, it is possible that it runoff will be increase in the winter and the loss precipitation of natural snow accumulated.
For an interpretation of these findings, however, one should not forget the limits of rainfall-runoff modeling. Computer simulation models are inherently uncertain, and even more so when considering future projections.

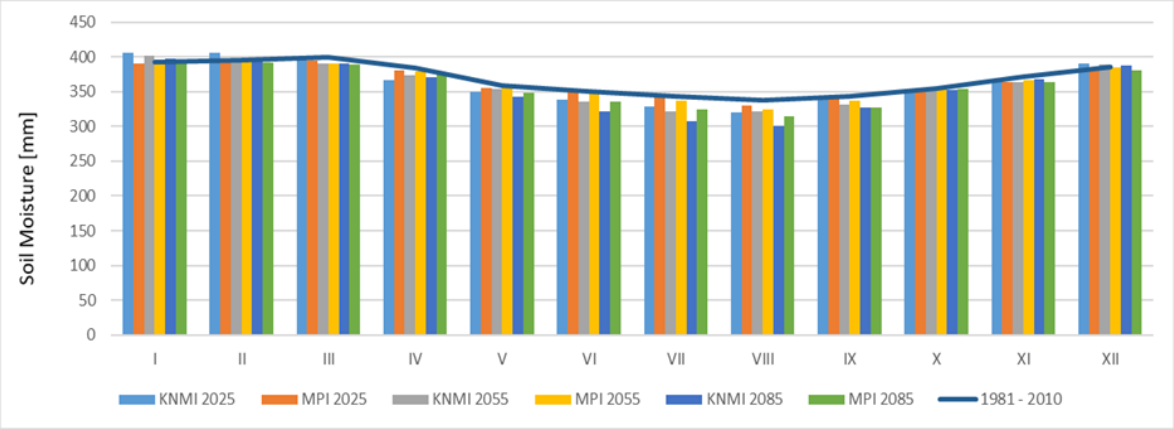

Fig. 3. Comparison of the long-term mean monthly values of soil moisture in the reference period and in the future time horizons.

Table 3. Simulated long-term mean monthly soil moisture using the parameters from the 1981–1995 calibration period in the Turiec River basin and its changes for the 3 future time horizons [%]

	period/scenario		I	II	III	IV	V	VI	VII	VIII	IX	X	XI	XII	Øyear [mm]
	1981–2010 [mm]		392	395	399	384	359	351	343	337	344	355	372	385	368
Turiec	KNMI [%]	2025	4	3	-1	-4	-3	-3	-4	-5	-1	-1	-2	1	-1
		2055	2	0	-2	-3	-1	-4	-7	-5	-4	-1	-2	1	-2
		2085	1	1	-2	-3	-5	-9	-11	-11	-5	-1	-1	1	-4
	MPI [%]	2025	0	1	-1	-1	-1	-1	1	-2	0	-1	-2	0	-1
		2055	1	0	-2	-1	-1	-1	-2	-4	-2	0	-2	0	-1
		2085	-1	-1	-3	-2	-3	-4	-5	-7	-5	0	-2	-1	-3

Acknowledgements

This work was supported by the Slovak Scientific Grant Agency VEGA Project 2/0189/17.

References

Ayanshola, A., Olofintoye, O., Obadofin, E. (2018): The Impact of Global Warming on Precipitation Patterns in Ilorin and the Hydrological Balance of the Awun Basin. Slovak Journal of Civil Engineering, 26(1), 40–46.

Bates, B. C., Kundzewicz, Z. W., Wu, S., Palutikof, J. P. (2008): Climate change and water. International Panel on Climate Change Tech. Rep. 6, 214 p.

Christensen, J. H., Kanikicharla, K. K., Marshall, G., Turner, J. (2013): Climate phenomena and their relevance for future regional climate change. 1217–1308.

Donohue, R. J., Roderick, M. L., McVicar, T. R. (2006): On the importance of including vegetation dynamics in Budyko's hydrological model. Hydrology and Earth System Sciences Discussions, 3(4), 1517–1551.

Hlavčová, K., Danáčová, M., Kohnová, S., Szolgay, J., Valent, P., Výleta, R. (2019): Estimating the effectiveness of crop management on reducing flood risk and sediment transport on hilly agricultural land–A Myjava case study, Slovakia. Catena, 172, 678–690.

Lapin, M., Bašták, I., Gera, M., Hrvoľ, J., Kremler, M., Melo, M. (2012): New climate change scenarios for Slovakia based on global and regional general circulation models. Acta Meteorologica Universitatis Comenianae, 37, 25–73.

Liu, Y. B., De Smedt, F. (2004): WetSpa extension, documentation and user manual. Department of Hydrology and Hydraulic Engineer., Vrije Universiteit Brussel, Belgium.

Liu, Q., Yang, Z. (2010): Quantitative estimation of the impact of climate change on actual evapotranspiration in the Yellow River Basin, China. Journal of Hydrology, 395(3–4), 226–234.

Rind, D., Balachandran, N. K., Suozzo, R. (1992): Climate change and the middle atmosphere. Part II: The impact of volcanic aerosols. J. Climate, 5, 189–208.

Rončák, P., Hlavčová, K., Látková, T. (2016): Estimation of the effect of changes in forest associations on runoff processes in basins: case study in the Hron and Topla river basins, Slovak Journal of Civil Engineering, 24(3), 1–7.

Sleziak, P., Szolgay, J., Hlavčová, K., Parajka, J. (2016): The impact of the variability of precipitation and temperatures on the efficiency of a conceptual rainfall-runoff model. Slovak Journal of Civil Engineering, 24(4), 1–7.

Tavakoli, M., De Smedt, F. (2013): Validation of soil moisture simulation with a distributed hydrologic model (WetSpa). Environmental earth sciences, 69(3), 739–747.

Thornthwaite, C. W., Mather, J. R. (1955): The water balance publications in Climatology, 8 (1). DIT, Laboratory of climatology, Centerton, NJ, USA.

Wang, Z., Batellan, O., De Smedt, F. (1996): A Distributed Model For Water And Energy Transfer Between Soil, Plants And Atmosphere (Wetspa), Phys. Chem. Earth, 21, pp. 189–193.

Wani, J. M., Sarda, V. K., Jain, S. K. (2017): Assessment of Trends and Variability of Rainfall and Temperature for the District of Mandi in Himachal Pradesh, India. Slovak Journal of Civil Engineering, 25(3), 15–22.

Mgr. Peter Rončák, PhD.
Ing. Peter Šurda, PhD.
Institute of Hydrology SAS,
Dúbravská cesta 9
84104 Bratislava
Slovak Republic
E-mail: roncak@uh.savba.sk
surda@uh.savba.sk

DOI: 10.31577/ahs-2019-0020.02.0020

ACTA HYDROLOGICA SLOVACA

Volume 20, No. 2, 2019, 166–171

IMPACT OF GRAPEVINE BIOCHAR ON SOME HYDRO-PHYSICAL CHARACTERISTICS OF SILT LOAM SOIL – LABORATORY MEASUREMENTS

Justína Vitková, Ján Gaduš, Kamil Skic, Patrycja Boguta, Tomáš Giertl

This study is focused on some hydro-physical characteristics of silt loam soil and their changes after biochar amendment. The used biochar was produced from wooden parts of grapevine (*Vitis*) in UNIPYR reactor in AgroBioTech Research Center in Nitra, Slovakia. There were established 4 sets in laboratory: pure soil and soil-biochar mixtures with 20, 40 and 80 t ha^{-1} biochar amendment. Our results confirmed more scientific studies that adding biochar into the soil decreased soil bulk density, particle density and increased porosity. Saturated hydraulic conductivity increased only for higher biochar concentrations in our research. Based on our measurements the optimal amount of grapevine biochar for improving hydro-physical characteristics of silt loam soil was 40 t ha^{-1}.

KEY WORDS: grapevine biochar, soil characteristics, silt loam soil

Introduction

Biochar application to agricultural soils has been proposed as a way to increase crop production by improving soil chemical and physical properties. The growth of plants is determined among others by the physical state of the soil environment. Biochar may also improve soil performance by altering soil physical characteristics such as porosity, bulk density, hydraulic conductivity, and water holding capacity (Githinji, 2013; Tárník, 2019) and by changing soil chemical properties including pH, cation exchange capacity, and nutrient availability (Deal et al., 2012; Liu et al., 2012). Biochar particles can have high initial hydrophobicity if they are produced at low temperatures (<400°C) (Kinney et al., 2012). Hydrophobic biochar has positive water entry pressure (Wang et al., 2000) which means that an applied pressure is required for water to enter intrapores. If the hydrostatic pressure is less than the water entry pressure, water will not enter these intrapores, therefore reducing their effectiveness of water flow and water storage (Masiello et al., 2015).

In this paper, we focused on impact of biochar amendment on some hydro-physical characteristics described below.

Soil bulk density (BD), also known as dry bulk density, is the weight of dry soil divided by the total soil volume. The total soil volume is the combined volume of solids and pores which may contain air or water, or both. The average values of air, water and solid in soil are easily measured and are a useful indication of a soils physical condition. Soil BD and porosity reflects the size, shape and arrangement of particles and voids (soil structure). Both BD and porosity give a good indication of the suitability for root growth and soil permeability and are vitally important for the soil-plant-atmosphere system (Cresswell and Hamilton, 2002; McKenzie et al., 2004).

Particle density (PD) of a soil indicates the mass of a soil sample in a given volume of particles (mass divided by volume). PD focuses on just the soil particles and not the total volume that the soil particles and pore spaces occupy in the soil. PD differs from BD because bulk density includes the volume of the solid (mineral and organic) portion of the soil along with the spaces where air and water are found. In general, PD represents the average density of all the minerals composing the soil. The density of the minerals depends on their elementary composition, so PD of a soil is certainly also dependent on its chemical bulk composition. It other words, density summarizes the interaction of soil chemical constituents within the environment (Di Giuseppe et al., 2016).

Hydraulic conductivity is the volume of water that flows through a unit cross-section of soil per unit time. Hydraulic conductivity plays important role in water resources development, planning and management as well as environmental protection. Saturated hydraulic conductivity (*K*) is a quantitative characteristic for the ability of porous system to transfer water in a saturated state. In soils, this characteristic depends mainly on its structure and texture. The heterogeneity of

soil significantly influences the spatial manifestation of hydraulic conductivity in both vertical and horizontal directions. On the other hand, the transformation of organic matter causes the changes of hydraulic conductivity in time (Fodor et al., 2011). *K* is one of the most important physical characteristics of soil that has significant effect on salt, pesticide, nutrient leaching, water infiltration and consequently, controlling surface runoff (Mohsenipour and Shahid, 2016).

A soil's *porosity* and pore-size distribution characterize its pore space, that portion of the soil's volume that is not occupied by solid material. The basic character of the pore space governs critical aspects of almost everything that occurs in the soil: the movement of water, air, and other fluids; the transport and the reaction of chemicals; and the residence of roots and other biota. By convention the definition of pore space excludes fluid pockets that are totally enclosed within solid material – vesicles or vugs, for example that have no exchange with the pore space that has continuity to the boundaries of the medium. Thus we consider a single, contiguous pore space within the body of soil. In general it has fluid pathways that are tortuous, variably constricted, and usually highly connected among themselves (Nimmo, 2005).

Material and methods

Grapevine biochar production

The biochar, used in this research was obtained from wooden parts of grapevine (*Vitis*) in UNIPYR reactor by pyrolysis at 520°C. The size of biochar was 0–10 mm. This reactor is part of AgroBioTech Research Center of the Slovak University of Agriculture in Nitra and consists of set of equipment for the production of synthesis gas and biogenic fuels in liquid and solid phase. The basic principle of the plant operation is continuous thermal decomposition of biomass and dendromass, eventually other materials of organic origin (such as paper, textiles), free of inert impurities (such as metal, glass, soil, sand), with a raw material processing capacity up to 60 kg per hour. The process of biochar production is described by Gaduš and Giertl (2019). Elemental analysis of biochar carbon (C), hydrogen (H), nitrogen (N) and sulfur (S) was performed using a CHNSO elemental analyzer (Perkin Elmer 2400 Series II CHNSO Elemental Analyzer) at Institute of Agrophysics of the Polish Academy of Sciences in Lublin (Poland). C, H, N and S results were expressed in weight percentage. Before the analysis samples were ground in a mortar and then dried at 105°C by 24 hours. Elemental composition of the biochar characteristics is listed in Table 1.

Table 1. Some chemical characteristics of biochar

	C	H	N	S
	[%]	[%]	[%]	[%]
Biochar	78.43	2.21	1.22	0.24

Soil mixtures

In this research in laboratory conditions was used the same type of soil as in our previous research in field conditions with soil particles diameter ≤2 mm. The soil type was classified as the Haplic Luvisol with content of sand 15.2%, silt 59.9% and clay 24.9% – silt loam (Šimanský and Klimaj, 2017). In our field research, biochar was applied into the depth of 10 cm below soil surface, that's why we considered the same depth of biochar application in laboratory measurements. The biochar was mixed to the soil at a ratio of 20, 40 and 80 t ha^{-1} (in dry weight basis). Measurements were provided on samples with volume of 100 cm^3 (Kopecky rings). Four different sets were established: a soil without biochar (soil), soil amended with biochar of 20 t/ha (G20), soil amended with biochar of 40 t ha^{-1} (G40) and soil amended with biochar of 80 t ha^{-1} (G80). Each set was prepared with 3 replicates.

Soil bulk density

The dry soil bulk density (ρ_d) is defined as the mass of dry soil (m_s) of the total volume (V):

$$\rho_d = \frac{m_s}{V} \quad [\text{g cm}^{-3}] \tag{1}$$

The soil bulk density was established based on core method (volumetric cylinder method). This method requires a volumetric cylinder. The total volume of the soil is estimated as the internal volume of the cylinder (in our measurements it was 100 cm^3). Samples are dried at 105°C and then the mass of the dry soil sample is measured (Velebný, 1981).

Particle density

The particle density (ρ_s) is defined as the mass (m_s) of the unit volume of the solid soil phase (V_s):

$$\rho_s = \frac{m_s}{V_s} \quad [\text{g cm}^{-3}] \tag{2}$$

In this research was used pycnometric method with pycnometer volume of 100 ml. Density determination by pycnometer is a very precise method. It uses a working liquid with well-known density, such as water. We used distilled water. The pycnometer is a glass flask with a close-fitting ground glass stopper with a capillary hole through it. This fine hole releases a spare liquid after closing a top-filled pycnometer and allows for obtaining a given volume of measured and/or working liquid with a high accuracy. The laboratory measurement was described by e.g. Velebný (1981).

Saturated hydraulic conductivity

Hydraulic methods come from supposed certain flow conditions, with boundary and initial conditions and with use of Darcy's Law (respectively Darcy-Buckingham Law in a case of unsteady state flow in unsaturated zone)

and with use of equation of continuity. Final formulas for direct calculations (approximation) of *K*-values were received by analytical solution of initial fundamental equations. *K* was measured by the falling head method in laboratory conditions based on formula (3) (Velebný, 1981):

$$K = \frac{L}{\Delta t} \ln \frac{h_1}{h_2} \quad [\text{cm day}^{-1}] \tag{3}$$

where
L – cylinder length [cm]
Δt – time elapsed [day],
h_1 – initial head from water surface to sample bottom [cm],
h_2 – final head from water surface to sample bottom [cm].

This method was described by e.g. Zvala et al. (2017).

Porosity

Porosity (P) is the fraction of pore volume (V_p) per total sample volume V (pores plus solids):

$$P = \frac{V_P}{V} \quad [-] \tag{4}$$

Using known ρ_d and ρ_s the formula (4) can be replaced with (Velebný, 1981):

$$P = 1 - \frac{\rho_d}{\rho_s} . 100 \quad [\%] \tag{5}$$

Porosity of surface soil typically decreases as particle size increases and porosity of subsurface soil is lower than in surface soil due to compaction by gravity. Soil bulk density influences the soil porosity and porosity can be proportional to hydraulic conductivity. Soil porosity is affected by soil particle texture, soil structure, soil compaction and quantity of organic material.

Results and discussion

Our measurements of soil bulk density, particle density, and porosity confirmed the scientific studies results that with higher rate of biochar the soil bulk density and particle density decrease and porosity and saturated hydraulic conductivity increased.
Average soil bulk density (Fig. 1) significantly decreased for G20, G40 and G80 about 10, 18 and 26%, respectively in comparison to pure soil. Biochar may affect soil bulk density indirectly by influencing aggregation. Increasing biochar concentration in soils resulted in decreasing soil bulk density (Verheijen et al., 2019).
Average particle density (Fig. 2) also decreased in comparison to pure soil. The smallest difference was between soil and G20, only 0.71%. For G40 and G80 it was about 4.5 and 7.4%, respectively. In general, particle density represents the average density of all the minerals composing the soil. The density of the minerals depends on their elementary composition, so particle density of a soil is certainly also dependent on its chemical bulk composition.
Average measured saturated hydraulic conductivity (Fig. 3) decreased for G20 about 49%, but for G40 and G80 increased about 25 and 195%, respectively in comparison to pure soil. These results confirmed results by Liu et al. (2016) who found that when biochar particles were finer than soil particles, *K* value more decreased with less biochar rate. In our case the mixtures of G20 contained smaller biochar particles than G40 and G80. Esmaeelnejad et al. (2017) founded that biochar's effect on *K* was mainly controlled by interpores. When fine-grained particles applied to soil, they filled interpores resulting in a creation of smaller pores and

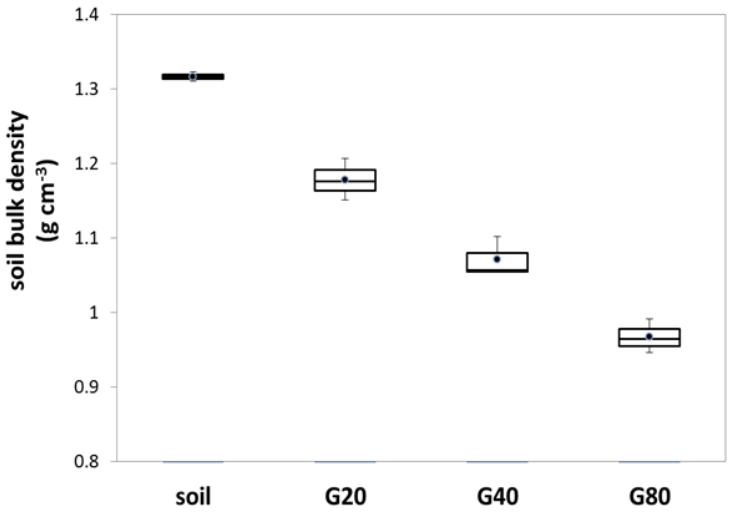

Fig. 1. Measured soil bulk density using core method at pure soil samples (soil) and mixtures soil with biochar rate of 20 t ha^{-1} (G20), 40 t ha^{-1} (G40) and 80 t ha^{-1}(G80). Value range: minimum, 25th percentile, median, 75th percentile, maximum and circles represent average value.

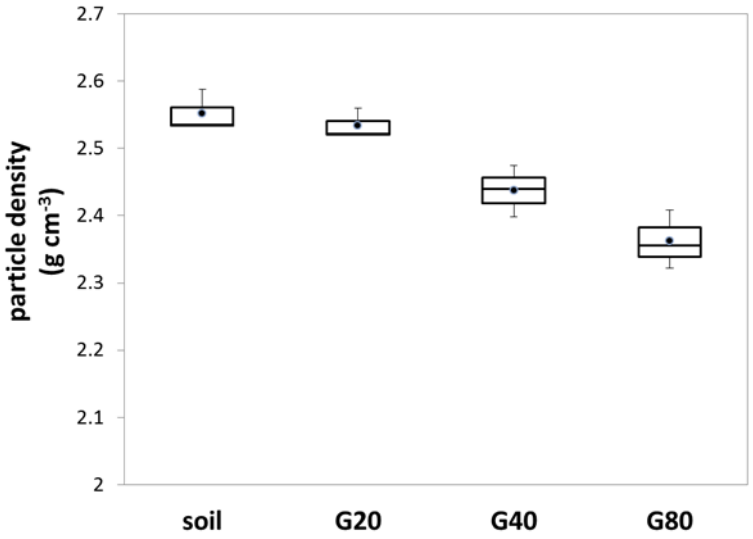

Fig. 2. Measured particle density using pycnometric method at pure soil samples (soil) and mixtures soil with biochar rate of 20 t ha^{-1}(G20), 40 t ha^{-1}(G40) and 80 t ha^{-} (G80). Value range: minimum, 25th percentile, median, 75th percentile, maximum and circles represent average value.

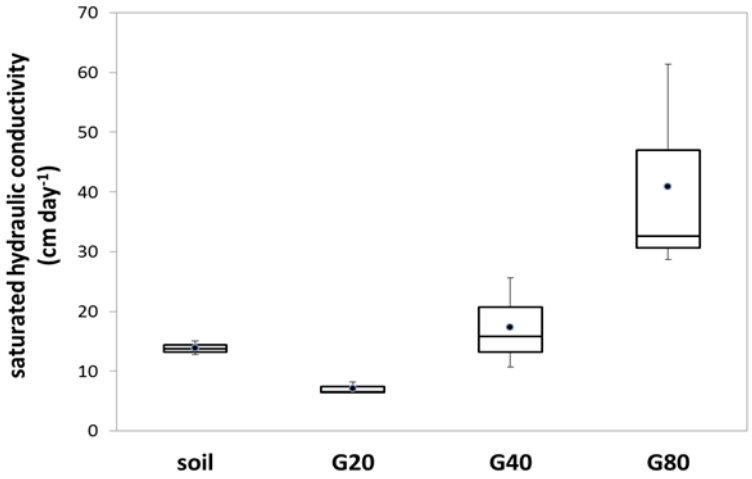

Fig. 3. Measured saturated hydraulic conductivity using falling head method at pure soil samples (soil) and mixtures soil with biochar rate of 20 t ha^{-1} (G20), 40 t ha^{-1}(G40) and 80 t ha^{-1}(G80).
Value range: minimum, 25th percentile, median, 75th percentile, maximum and circles represent average value.

an increase of tortuosity, thus decreasing *K*. Degree of permeability for G20 was *very low* (7 cm day^{-1}) and for soil, G40 and G80 *low* (13, 17 and 40 cm day^{-1}, respectively). The range values were higher in G40 and G80 mixtures. Previous studies showed that amending soil with biochar can either increase (Hlaváčiková et al., 2016) or decrease *K* (Liu et al., 2016).

Average porosity, calculated based on formula (5), increased with biochar rate (Fig. 4). For G20 was higher at 10%, for G40 at 15% and for G80 at 22% in comparison to pure soil. When pores are connected, water moves faster in larger pores than in smaller pores and thus larger pores dominate water flow through porous media. Amending soil with biochar will likely change porosity, pore size, pore connectivity, and hydrophobicity of soil because of the dual porosity of the system, changes in the particle size distribution, and hydrophobicity of biochar (Liu et al., 2016).

Soil samples and mixtures prepared in laboratory conditions, had similar compaction as this type of soil in field conditions, as well as mixture of this type of soil and biochar in rate of 20 t ha^{-1} in field conditions, applied in Malanta area, where our previous research was done. Differences between samples in the same type of set were

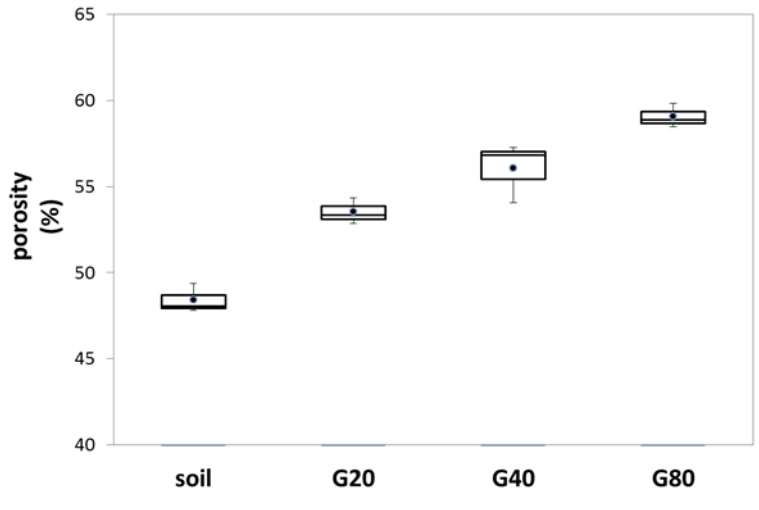

Fig. 4. Calculated porosity at pure soil samples (soil) and mixtures soil with biochar rate of 20 t ha^{-1} (G20), 40 t ha^{-1} (G40) and 80 t ha^{-1}(G80).
Value range: minimum, 25th percentile, median, 75th percentile, maximum and circles represent average value.

insignificant during measurements.
Results of soil bulk density and porosity measurements were significant between pure soil and G20. Conversely, by particle density were insignificant and by saturated hydraulic conductivity were opposite than other measurements, in this content it means negative. There were measured big differences in all analyzed characteristics between pure soil and G80. The question now is, how much organic matter, in this case the biochar, is needed add into the silt loam soil to prepare its optimal hydro-physical conditions for vegetation root system. Based on results in our study, the biochar amendment in rate of 80 t ha^{-1} is too much and differences between G40 and G80 were small. Amount of 20 t ha^{-1} of biochar had a negative effect on saturated hydraulic conductivity, so the optimal amount of grapevine biochar for improving hydro-physical characteristics of silt loam soil was 40 t ha^{-1}.

Conclusions

In this study we tried to analyze some hydro-physical characteristics after biochar application on samples prepared in laboratory conditions. We measured soil bulk density, particle density, and calculated porosity to help understand the physical mechanisms that may cause changes in saturated hydraulic conductivity. The results in all studied characteristics varied with biochar concentration. Adding biochar decreased soil bulk density, particle density and increased porosity. Depending on the soil type and particle size of biochar, results are more or less similar in many scientific studies and our study confirmed these conclusions. Measurements of saturated hydraulic conductivity were different, because adding biochar into soil may affect saturated hydraulic conductivity of soil by changing pore characteristics. Past studies have reported that biochar addition increases saturated hydraulic conductivity as a result of its high surface area and large internal pore volume. We confirm it only for higher biochar concentrations. Decreasing of saturated hydraulic conductivity for G20 was caused by big count of very small particles of biochar. This type of grapevine biochar in amount of 40 t ha^{-1} is enough to improve hydro-physical characteristics of silt loam soil.

Acknowledgement

This work was supported by Scientific Grant Agency No. VEGA 2/0053/18 and by AgroBioTech Research Centre built in accordance with the project Building „AgroBioTech" Research Centre ITMS 26220220180.

References

Cresswell, H. P., Hamilton, P. (2002): Particle Size Analysis. Soil Physical Measurement and Interpretation for Land Evaluation. (Eds. N. J. McKenzie, H. P. Cresswell and K. J. Coughlan), CSIRO Publishing: Collingwood, Victoria. 224–239.

Deal, C., Brewer, C. E., Brown, R. C., Okure, M. A. E., Amoding, A. (2012): Comparison of kiln-derived and gasifier-derived biochars as soil amendments in the humid tropics. Biomass Bioenergy, vol. 37, 161–168.

Di Giuseppe, D., Melchiorre, M., Tessari, U., Faccini, B. (2016): Relationship between particle density and soil bulk chemical composition. J. Soil Sediments, vol. 16, 909–915. https://doi.org/10.1007/s11368-015-1275-3.

Esmaeelnejad, L., Shorafa, M., Gorji, M., Hosseini, S. (2017): Impacts of Woody Biochar Particle Size on Porosity and Hydraulic Conductivity of Biochar-Soil Mixtures: An Incubation Study. Communications in Soil Science and Plant Analysis, vol. 48, 1710–1718. http://dx.doi.org/10.1080/00103624.2017.1383414.

Fodor, N., Sándor, R., Orfánus, T., Lichner, L., Rajkai, K.

(2011): Evaluation method dependency of measured saturated hydraulic conductivity. Geoderma, vol. 165. no. 1, 60–68.

Gaduš, J., Giertl, T. (2019): Production of biofuels by thermochemical conversion /Výroba biopalív termochemickou konverziou/ in Slovak. In Vykurovanie 2019. 27. medzinárodná konferencia Smart technológie a inovácie pri zásobovaní teplom, 1.–5.4.2019, Podbanské, Slovakia.

Githinji, L. (2013): Effect of biochar application rate on soil physical and hydraulic properties of a sandy loam. Arch. Agron. Soil Sci., vol. 60, 457–470. https://doi.org/10.1080/03650340.2013.821698.

Hlaváčiková, H., Brezianská, K., Novák, V. (2016): Influence of a biochar application on a sandy-loam soil water retention properties (in Slovak). Acta Hydrologica Slovaca, vol. 17, no. 2, 279–286.

Kinney, T. J., Masiello, C., Dugan, B., Hockaday, W. C., Dean, M. R. (2012): Hydrologic properties of biochars produced at different temperature. Biomass Bioenergy, vol. 41, 34–43. https://doi.org/10.1016/j.biombioe.2012.01.033.

Liu, J., Schulz, H., Brandl, S., Miehtke, H., Huwe, B., Glaser, B. (2012): Short-term effect of biochar and compost on soil fertility and water status of a Dystric Cambisol in NE Germany under field conditions. Journal of Plant Nutrition Soil and Science, vol. 175, 698–707. https://doi.org/10.1002/jpln.201100172.

Liu, Z., Dugan, B., Masiello, C. A., Barnes, R. T., Gallagher, M. E., Gonnermann, H. (2016): Impacts of biochar concentration and particle size on hydraulic conductivity and DOC leaching of biochar–sand mixtures. Journal of Hydrology, vol. 533, 461–472.

Masiello, C., Dugan, B., Brewer, C. E., Sorrenti. G. (2015): Biochar effects on soil hydrology: Biochar for environmental management science, technology and implementation. 2nd ed. United Kingdom: Routledge, 928 p.

McKenzie, N. J., Jacquier, D. J., Isbell, R. F., Brown, K. L. (2004): Australian Soils and Landscapes: An Illustrated Compendium. CSIRO Publishing: Collingwood, Victoria, 432 p.

Mohsenipour, M., Shahid, S. (2016): Estimation of saturated hydraulic conductivity: a review. 25 p.

Nimmo, J. R. (2005): Encyclopedia of Soils in the Environment. Chapter: Porosity and pore-size distribution. Elsevier, New York, 2200 p.

Šimanský, V., Klimaj, A. (2017): How does biochar and biochar with nitrogen fertilization influence soil reaction? Journal of Ecological Engineering, vol. 5, 50–54.

Tárník, A. (2019): Impact of Biochar Reapplication on Physical Soil Properties. IOP Conf. Ser.: Mater. Sci. Eng. 603 022068.

Velebný, V. (1981): Hydropedology /Hydropedológia/ in Slovak. Slovak University of Technology in Bratislava. 173 p.

Verheijen, F. G. A., Zhuravel, A., Silva, F. C., Amaro, A., Ben-Hur, M., Keizer, J. J. (2019): The influence of biochar particle size and concentration on bulk density and maximum water holding capacity of sandy vs sandy loam soil in a column experiment. Geoderma, vol. 347, 194–202.

Wang, Z., Wu, L., Wu, Q. J. (2000): Water entry value as an alternative indicator of soil water-repellency and wettability. Journal of Hydrology, vol. 231, 76–83. https://doi.org/10.1016/S0022-1694(00)00185-2.

Zvala, A., Orfánus, T., Stojkovová, D., Nagy, V. (2017): Hydraulic conductivity of forest floor soil layer /Hydraulická vodivosť pokrývkových horizontov lesnej pôdy/ in Slovak. Acta Hydrologica Slovaca, vol. 18, no. 1, 112–119.

Ing. Justína Vitková, PhD.
Institute of Hydrology SAS
Dúbravská cesta 9
841 04 Bratislava
Slovak Republic
E-mail: vitkova@uh.savba.sk

prof. Ing. Ján Gaduš, PhD.
Ing. Tomáš Giertl, PhD.
Department of Regional Bioenergy
Faculty of European Studies and Regional Development,
Slovak University of Agriculture in Nitra
Tr. A. Hlinku 2
949 76 Nitra, Slovak Republic

Kamil Skic, PhD.
Patrycja Boguta, PhD.
Department of Physical Chemistry of Porous Materials
Institute of Agrophysics, Polish Academy of Sciences
Doświadczalna 4
20-290 Lublin, Poland

DOI: 10.31577/ahs-2019-0020.02.0021

ACTA HYDROLOGICA SLOVACA

Volume 20, No. 2, 2019, 172–179

DETERMINATION OF ACTUAL SOIL WATER CONTENT, MATRIX POTENTIAL AND WATER REPELLENCY IN SANDY SOIL DURING A DEHYDRATION EXPERIMENT

Peter Šurda, Anežka Čelková, Justína Vitková, Anton Zvala

Soil water repellency (SWR) diminishes the affinity of soils towards the water and may resist wetting for durations ranging from a few seconds to hours or days depending on its persistence. It has been proposed that the origin of natural SWR is caused by organic compounds released from different plant species and sources, due to resins, waxes and other organic substances in their tissues. SWR may vary nonlinearly with soil moisture content (SMC), showing complex responses. It has been observed that small variations in water potential may have significant impacts on the wettability of water-repellent soils, and concluded that maximum soil water repellency does not necessarily occur in oven-dry soils, but at certain specific soil water potentials. The aims of this work were: i. to determine the values of SMC and corresponding values of soil matrix potential and persistence of SWR in forest soil samples during the drying process under laboratory conditions; ii. graphically analyze and quantify the drying process of the water-repellent soil surface.

KEY WORDS: soil water repellency, soil moisture content, soil matrix potential, dune sand

Introduction

Soil water repellency (SWR) has been observed in forest soils under different climatic conditions, soil types and vegetation covers (Doerr et al., 2000). It has been proposed that the origin of natural SWR is caused by organic compounds released from different plant species and sources, due to waxes and other organic substances in their tissues. SWR diminishes the affinity of soils towards the water and may resist wetting for durations ranging from a few seconds to hours or days depending on its persistence (Doerr and Thomas, 2000). SWR is normally characterized by a high spatial variability in persistence, with wettable and water repellent patches next to each other (Lozano et al., 2013).

SWR can alter infiltration and water storage capacity of soils. Reduced infiltration increases the surface runoff generation (overland flow) and associated erosion, and uneven wetting leads to the development of fingered flow (Keizer et al., 2005; Leighton-Boyce et al., 2007; Ritsema and Dekker, 1994; Shakesby et al., 1993; Kobayashi and Shimizu, 2007).

A large number of authors have indicated a variety of factors influencing SWR, such as soil moisture content (SMC) (Chau et al., 2014; Ferreira et al., 2016), incidence of fires (DeBano, 2000; Mataix-Solera and Doerr, 2004), presence of fungi and bacteria species (Schaumann et al., 2007), soil texture and structure (Urbanek et al., 2007; Giovannini and Lucchesi, 1983), surface roughness (Shirtcliffe et al., 2006), aggregation (Jordán et al., 2011; Mataix-Solera et al., 2011; Zavala et al., 2010), organic matter content and chemical composition (Atanassova and Doerr, 2010), acidity, soil type and mineralogy of the clay fraction (Dlapa et al., 2004; Mataix-Solera et al., 2008; Zavala et al., 2009), microbiology (Jex et al., 1985; Savage et al., 1969), and soil organic carbon content (Wijewardana et al., 2016).

Under high SMC, SWR is reduced, and a critical soil moisture threshold exists above which the soil becomes wettable. This threshold ranges from 5% (sandy soils) to >30% (clay soils) (Bodí et al., 2012; Poulenard et al., 2004; Regalado and Ritter, 2005). According to Dekker and Ritsema (1994) the critical soil water content varies between 4.75% at 5–10 cm and 1.75% at 45–50 cm depth in this sandy soil.

But other authors have reported contradictory results, showing that SWR may vary nonlinearly with SMC, showing complex responses (de Jonge et al., 2007; King, 1981). Goebel et al. (2004) observed that small variations in water potential may have significant impacts on the wettability of subcritical water-repellent soils, and concluded that maximum soil water repellency does not necessarily occur in oven-dry soils, but at certain specific soil water potentials.

As the soil dries out, SWR tends to be restored, which causes intra-annual, short-term variations in SWR driven by SMC (Keizer et al., 2008).

The temperature both in situ and in the laboratory con-

ditions affects also water repellent characteristics of soils. Dekker et al. (1998) reported that potential water repellency was greater after drying soils at 65°C relative to those drying at 25°C. In contrast, some soils show higher water repellency at low temperature (20°C) conditions than those at comparatively high temperature (40°C) conditions (Whelan et al. 2014).

The aims of this work were: i. to determine the values of SMC and corresponding values of soil matrix potential and persistence of SWR during the drying process in water-repellent soil columns under laboratory conditions; ii. graphically analyze and quantify the drying process of the water-repellent soil surface.

Material and methods

Field-soil and soil sampling

The experimental area Pine 1 was located near Sekule (48°37'10'' N, 16°59'50'' E) in the Borská nížina lowland (southwest Slovakia). The altitude of study site is 150 m above sea level. The climate is continental with less annual temperature fluctuations than on the neighboring Podunajská nížina lowland. Mean annual temperature is 9°C. Mean annual precipitation is 550 mm, and it is mainly summer-dominant (Klimatický atlas Slovenska, 2015). Aeolian sandy soil from these sites is classified as an Arenosol (WRB, 2006) and sandy texture was measured for whole soil profile (Soil Survey Division Staff, 1993).

The experimental site was the stand of about 20-year old pine trees (*Pinus sylvestris*), under which occurred bryophytes (*Polytrichum piliferum*), followed by lichens (*Cladonia sp.*) and sporadically occurred also higher plants (*Corynephorus canescens*). The growth of mosses and lichens was evenly covered with fallen needles. The soil was known to be severely to extremely water repellent during dry periods (Lichner et al., 2005; Šurda et al., 2013).

Disturbed soil samples were taken from depth 0–10 cm in 1.5 m vertical transect on 20 August, 2019, after a period of 4 days without rainfall. Soil was sampled using little gardening steel shovel with a 5 cm blade and transported in closed plastic bag. In laboratory was sandy material homogenized and spreaded as a 5 cm layer. Four Kopecký steel cylinders (100 cm^3) were filled with same weight of sandy material and had been oven-dried and weighed to calculate actual volumetric SMC.

Soil columns preparation and hydration

Four soil columns with bulk density 1.625 g cm^3 were prepared in laboratory, using 800 ml transparent plastic cylinders with a height of 13 cm (height of sand in cylinder was 11.1 cm) and diameter of 10 cm. The lower parts of the cylinders were perforated to ensure water drainage. 300 ml of water was applied on each of soil column surface in 3 x 100 ml irrigation doses. Applied water entered the soil through the process of falling head ponded infiltration. Water leakage through the bottom part of soil column was measured after each irrigation dose.

Table 1. Physical and chemical properties of the top (0–10 cm) soil taken from the experimental site Pine1 (stand of pine trees) near Sekule, Slovakia

	Depth [cm]	Sand [%]	Loam [%]	Clay [%]	$CaCO_3$ [%]	C [%]	pH [H_2O]	pH [H_2O]
Pine 1	0–10	95.1	2.3	2.6	<0.05	0.83	5.65	4.39

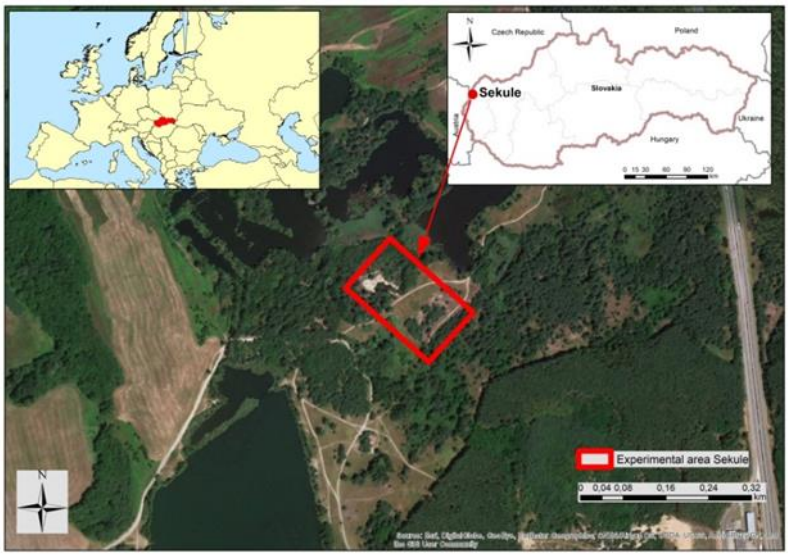

Fig. 1. Experimental area Pine 1 near Sekule.

Measurement of matrix potential and SMC during dehydration

Two of these columns were equipped with moisture probes 5TM (Decagon Devices, Inc.) and two others with matrix potential sensors MPS6 (Decagon Devices, Inc.). Continuous measurements at 5 minute intervals were recorded using EM50 data loggers (Decagon Devices, Inc.). SMC of all soil columns during drying process was determined gravimetrically. Prepared columns were dried in a laboratory oven at 35°C. The drying process of soil column surfaces was captured using a Canon EOS 600d camera.

Water drop penetration time (WDPT) test

The stability or persistence of the repellency was measured by the water drop penetration time (WDPT) test – a measure of the time required for the drop to enter the soil. Five drops of distilled water from a standard medicine dropper were placed on the surface of a soil sample, and the time that elapsed before the drops were absorbed was registered. We measured the persistence of water repellency of the soil samples in the laboratory under controlled conditions at a constant temperature of 22°C.

In general, a soil is considered to be water repellent if the WDPT exceeds 5 s. Soils with WDPT=5–60 s were considered slightly water repellent, WDPT=60–600 s strongly water repellent, WDPT=600–3600 s severely water repellent, and WDPT≥3600 s extremely water repellent (Bisdom et al., 1993).

Image analysis

For the digital photo analysis we used GIMP and also ImageJ (http://imagej.net/ImageJ), open source Java image processing program inspired by NIH Image. JPEG digital photography was calibrated through the function "Set scale". Defined number of pixels was assigned to a real known distance on picture. Then it was transformed into 8 bit format (black and white). Next step was a use of "Bandpass filter" function, which filtered structures smaller or bigger as defined size in pixels. Then we used a "Treshold" function which gives us images, usable for counting black and white pixels within the 10 cm diameter of soil surface.

Results and discussion

Soil moisture content and matrix potential in the soil columns during dehydration

The persistence of SWR at the initial air-dried conditions of the all prepared soil columns surface was determined through WDPT test and soil was classified as extremely water repellent in all cases. The results of WDPT test and hydration process of four soil columns are in Table 2.

According to the Table 2, soil samples were able to hold only very limited amount of water from the applied irrigation dose. Applied water entered the soil columns through the process of falling head infiltration (which lasted overall ca. 12 hours). After each application of 100 ml irrigation dose, a 1 cm water layer was formed on the surface. Water percolated through the soil columns through the process of preferential (fingered like) flow and the SMC increased only in the spaces around the preferential flow paths. Maximal amount of applied water held the Column 1 (61 ml), the smallest amount Column 3 (13 ml). The surface layers of soil columns were exposed to water, which reduced the SWR and thin surface layer of soil (with thickness of 2–3 mm) becomes wettable. Analysis of the soil surface drying process results are stated in next subchapter.

Drying process of soil samples started at various initial SMC (from 0.11 to 0.051). Decrease in SMC over time is shown in Figure 2. As it can be seen at the Fig. 2, the curve of SMC decrease can be divided into two parts according to the slope; to the first part with higher rate of evaporation (from 0.47 ml h^{-1} in Column 1 to 0.26 ml h^{-1} in Column 3) and second part with lower evaporation intensity (from 0.08 ml h^{-1} in Column 1 to 0.03 ml h^{-1} in Column 3). Breakpoint between two slopes of curve, or threshold value, approximately coincides with the time when SWR of the whole soil surface was restored. The decrease in evaporation rate is mainly due to a decrease in SMC, but since the initial SMC level is also low, the recovery of the surface SWR can also be important.

SWR of whole sample soil surface in all columns was recovered after 42 hours of drying process by constant temperature of 35°C and decrease of SMC by 0.027 in 1, 0.020 in 4, 0.022 in 2 and 0.015 in 3.

Relation between measured values of SMC and soil matrix potential is displayed at Fig. 3. The authors do not

Table 2. Persistence of SWR of prepared samples (examined through the WDPT test with five repetitions) at the initial air-dried conditions (± represents standard deviation); values of SMC before wetting (SMC_{0ML}); applied irrigation dose; leakage through the bottom and SMC after application of 300 ml of water (SMC_{300ML})

	WDPT [s]	SMC_{0ML} [m^3 m^3]	Applied water [ml]	Leakage [ml]	SMC_{300ML} [m^3 m^3]
Soil column 1	10200 ±1296	0.035	300	239	0.1118
Soil column 2	13200 ±1132	0.035	300	272	0.0705
Soil column 3	10800 ±1836	0.035	300	287	0.0511
Soil column 4	11400 ±2452	0.035	300	282	0.0573

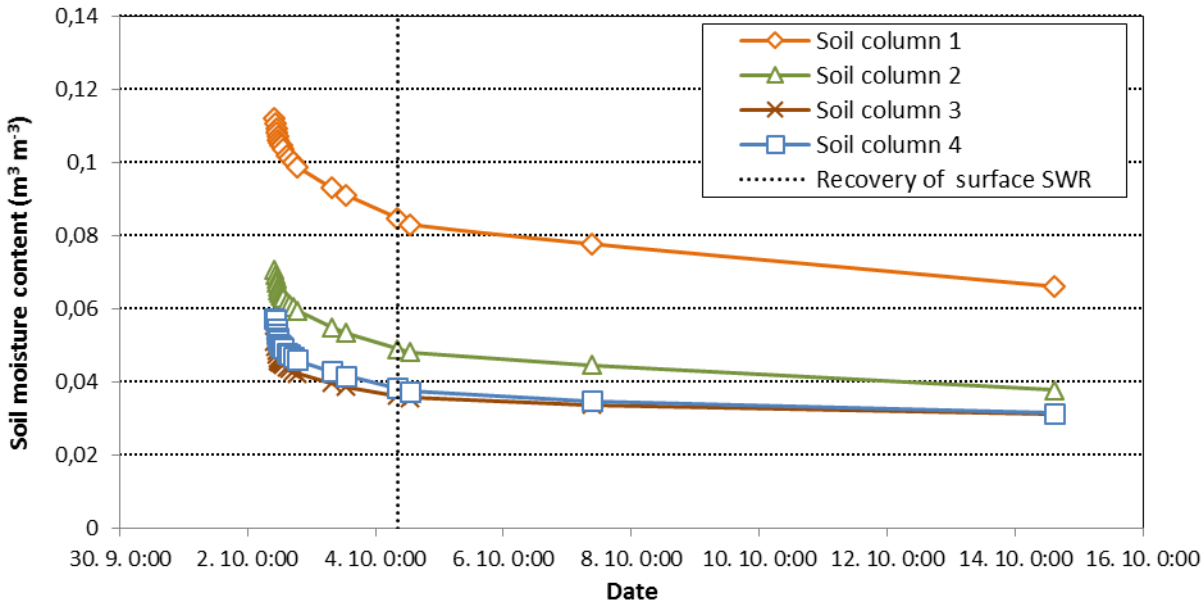

Fig. 2. Decrease of soil moisture content during dehydration of soil columns (1, 2, 3 and 4); dotted line represents the threshold, beneath which are whole surfaces of soil columns water repellent.

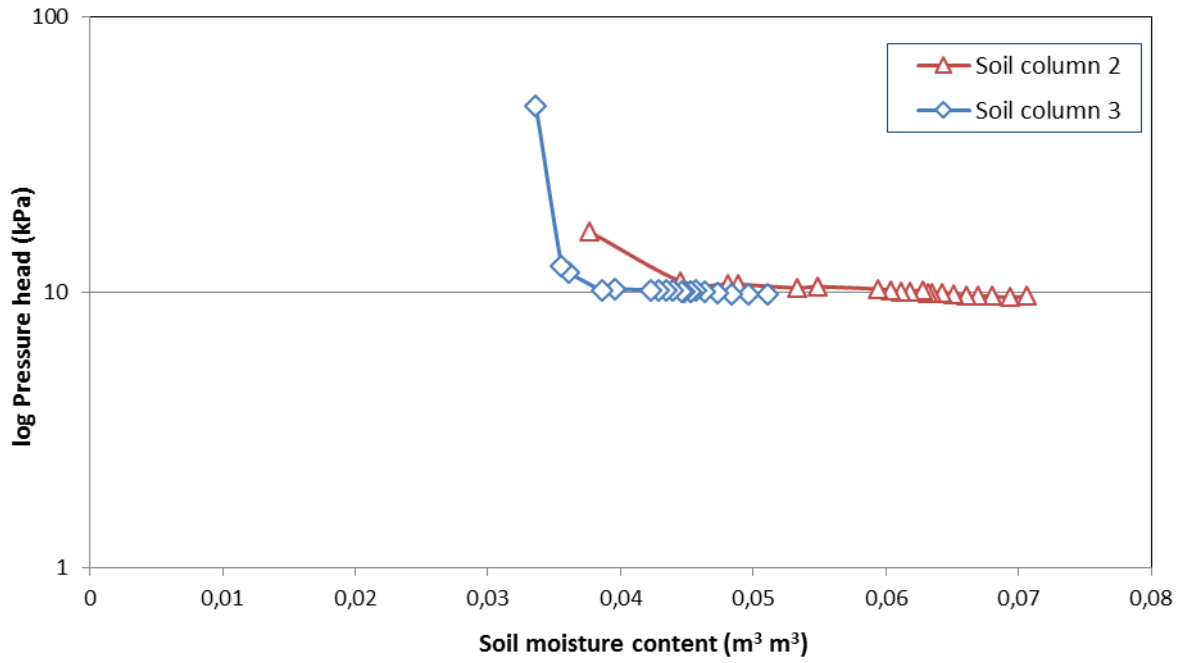

Fig. 3. Values of soil matrix potential (kPa) and soil moisture content [m^3 m^3], measured during drying experiment.

consider the depicted potential – SMC dependence a retention curve, nor have they attempted to fit it with existing models.

Soil columns under the conditions of the experiment cannot be fully saturated and the authors believe that this does not happen even in normal filed conditions in the top layer (10 cm) of the extreme repellent soil profile. Therefore, the highest measured potential was -9.8 kPa in 3 and -9.7 kPa in 2, which corresponds with the value of SMC of 0.051 in 3 resp. 0.071 in 2. Minimal values of matrix potential, -47.6 kPa in 3 and -16.7 kPa in 2, corresponding with the SMC of 0.034 resp. 0.037, were measured after 5 days (119 hours) resp. after 12 days (293 hours) of drying process.

Drying process of the water-repellent soil surface

After infiltration process, whole surface area of soil columns (with thickness of 2–3 mm) became wettable. The drying process of the wettable soil columns surfaces are displayed in Fig. 4 (first pictures were taken after ca 30 minutes of drying).

The surface of each soil column was visually dried (according to analysis of photographs) approximately two and a half hours after the start of dehydration. All dark (wetter) surfaces were always wettable (WDPT <5 s). Visually lighter and drier part of the surface behaved differently; some of them act as wettable and some as water-repellent. SWR was completely restored (WDPT>5 s) after 42 hours of dehydration at the entire surface of the all soil columns. Enlargement of the dry area during the dehydration process was evaluated from the binary pictures made from sequence of photographs displayed in Fig. 4. Increasing ratio of white pixels (dried area) to the total number of pixels (surface of soil column) during drying process is shown in Figure 5.

According to Fig. 4 and 5, enlargement of the dried surface area of the soil columns during the drying process was relatively uniform. The largest relative increase in the dried area was detected after ca. two and a half hours in all soil columns. The surface of columns 1 and 2 dried slowly, while the strong and severe SWR at surface of these columns was recovered faster than in columns 3 and 4. This may be related to the delay of the water layer (and hence the exposure time to water) on the soil surface which could be caused by the different rate of the hydraulic conductivity (*Ks*) of the prepared soil columns. The necessity of the *Ks* measurement is important for the realization of the future experiments.

Conclusions

The values of SMC and corresponding values of soil matrix potential and persistence of SWR were measured in sandy soil columns under laboratory conditions. Drying process of samples started at various initial SMC (from 0.11 to 0.051). The curve of SMC decrease can be divided into two parts according to the slope; to the first part with higher rate of evaporation (from 0.47 ml h^{-1} to 0.26 ml h^{-1}) and second part with lower evaporation intensity (from 0.08 ml h^{-1} to 0.03 ml h^{-1}).

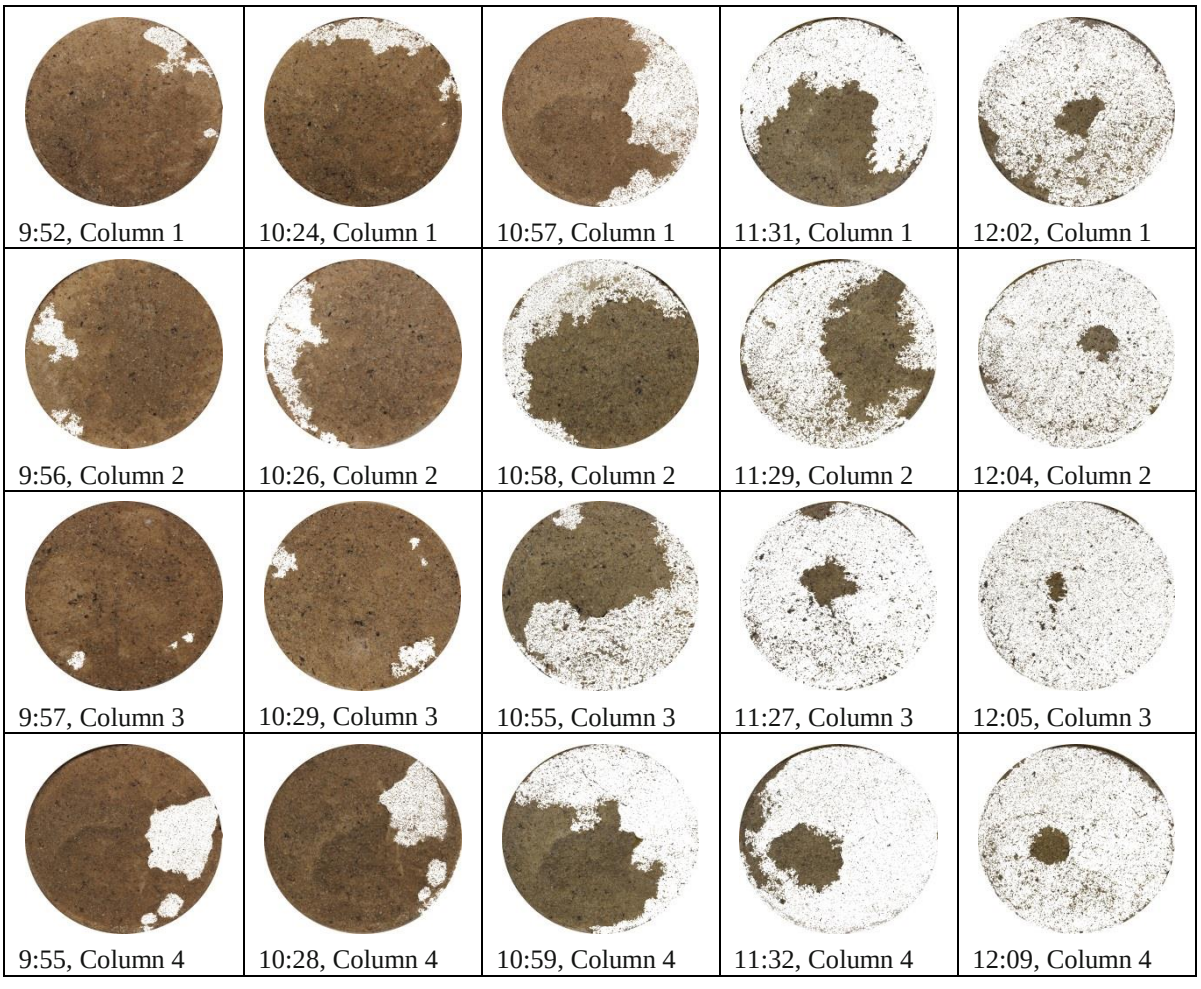

Fig. 4. Sequence of photographs graphically depicting the drying process of soil samples surface (brown color represents wettable parts of surface, white area represents dried part of soil surface, below is time the photo was taken).

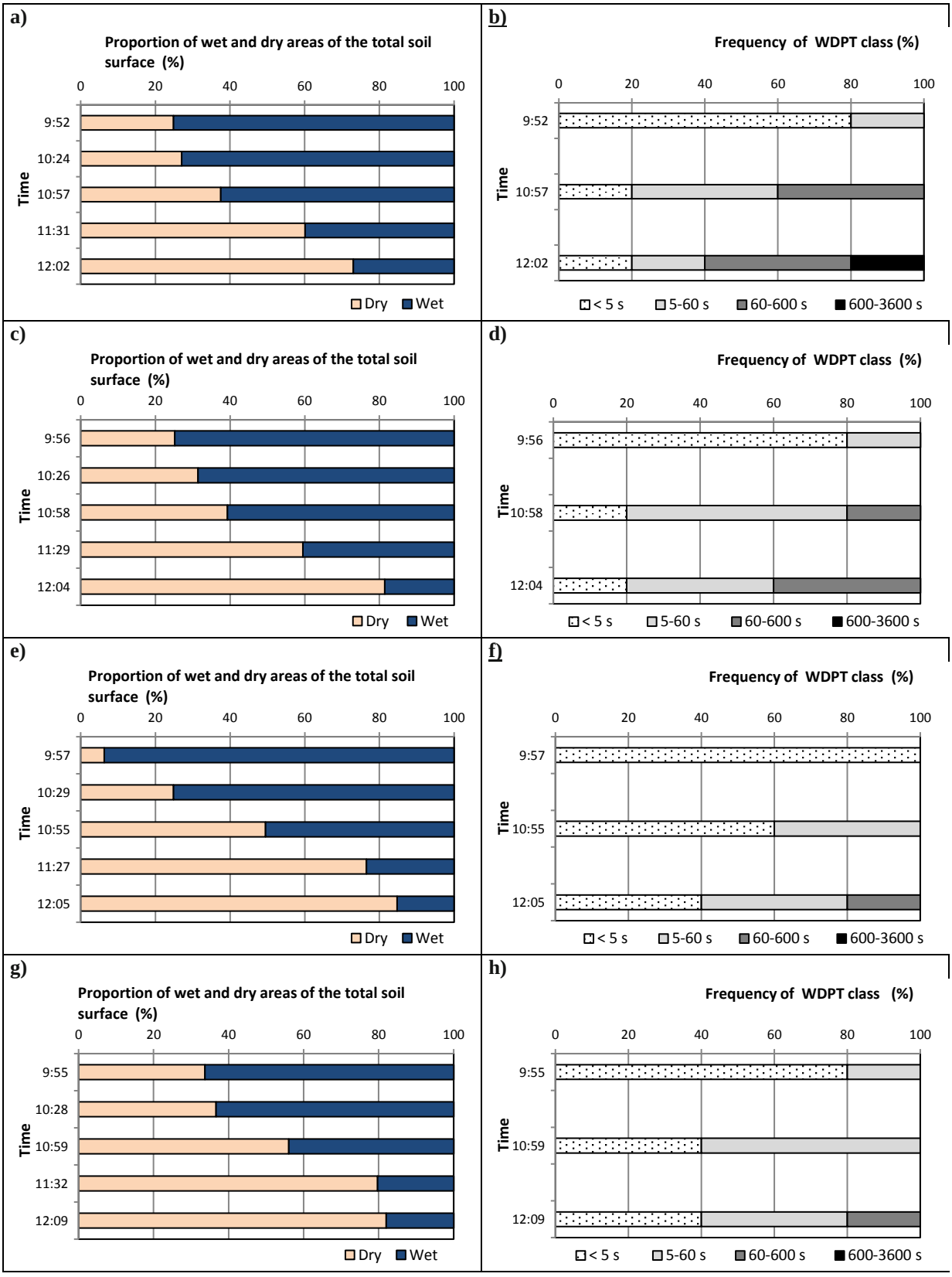

Fig. 5. Proportion of wet and dry areas of the total soil surface on the five measuring dates and relative frequency of the persistence of actual water repellency (WDPT class) on the three measuring dates (N=5) of the column 1 (a, b), column 2 (c, d), column 3 (e, f) and column 4 (g, h).

Soil columns under the conditions of the experiment were not fully saturated, due to the extreme SWR. Therefore, the highest measured potential was -9.8 kPa, which corresponds with the value of SMC of 0.05. Minimal value of matrix potential, -47.6 kPa, corresponding with the SMC of 0.03 was measured after 5 days (119 hours) of drying process.

The surface of each soil column was visually dried approximately two and a half hours after the start of dehydration, while the enlargement of the dried surface area was relatively uniform. The surface of columns 1 and 2 dried slowly, while the strong and severe SWR at surface of these columns was recovered faster than in columns 3 and 4.

Acknowledgement

This work was supported by the Slovak Scientific Grant Agency VEGA Project 2/0189/17.

References

Atanassova, A., Doerr, S. H. (2010): Organic compounds of different extractability in total solvent extracts from soils of contrasting water repellency. European Journal of Soil Science 61, 298–313.

Bisdom, E. B., Dekker, L. W., Schoute, J. T. (1993): Water repellency of sieve fractions from sandy soils and relationships with organic material and soil structure. Geoderma, 56, 105–118.

Bodí, M. B., Doerr, S. H., Cerdà, A., Mataix-Solera, J. (2012): Hydrological effects of a layer of vegetation ash on underlying wettable and water repellent soils. Geoderma 191, 14–23.

DeBano, L. F. (2000): The role of fire and soil heating on water repellency in wildland environments: a review. Journal of Hydrology. 231–232, 195–206.

De Jonge, L. W., Moldrup, P., Jacobsen, O. H. (2007): Soil-water content dependency of water repellency in soils: effect of crop type, soil management, and physical–chemical parameters. Soil Science 172, 577–588.

Dekker, L. W., Ritsema, C. J. (1994): How water moves in a water repellent sandy soil. 1. Potential and actual water repellency. Water Resources Research 30, 2507–2517.

Dlapa, P., Doerr, S. H., Lichner, L., Sir, M., Tesar, M. (2004): Alleviation of soil water repellency: effect of kaolinite and Ca-montmorillonite. Plant, Soil and Environment 50, 358–363.

Doerr, S. H., Shakesby, R. A.,Walsh, R. P. D. (2000): Soil water repellency: its causes, characteristics and hydro-geomorphological significance. Earth-Science Reviews 51, 33–65.

Doerr, S. H., Thomas, A. D. (2000). The role of soil moisture in controlling water repellency: new evidence from forest soils in Portugal. J Hydrol 231–232:134–147.

Ferreira, C. S. S., Walsh, R. P. D., Shakesby, R. A., Keizer, J. J., Soares, D., González-Pelayo, O., Coelho, C. O. A., Ferreira, A. J. D. (2016). Differences in overland flow, hydrophobicity and soil moisture dynamics between Mediterranean woodland types in a periurban catchment in Portugal. J. Hydrol. 533, 473–485.

Goebel, M.-O., Bachmann, J., Woche, S. K., Fischer, W. R., Horton, R. (2004): Water potential and aggregate size effects on contact angle and surface energy. Soil Science Society of America Journal 68, 383–393.

Dekker, L. W., Ritsema, C. J., Oostindie, K., Boersma, O. H. (1998): Effect of drying temperature on the severity of soil water repellency. Soil Science 163, 780–796.

Giovannini, G., Lucchesi, S. (1983): Effect of fire on hydrophobic and cementing substances of soil aggregates. Soil Science 136, 231–236.

Chau, H. W., Biswas, A., Vujanovic, V., Si, B. C. (2014): Relationship between the severity, persistence of soil water repellency and the critical soil water content in water repellent soils. Geoderma 221–222, 113–120.

Jex, G. W., Bleakley, B. H., Hubbell, D. H., Munro, L. L. (1985): High humidity-induced increase in water repellency in some sandy soils. Soil Science Society of America Journal 49, 1177–1182.

Jordán, A., Zavala, L. M., Mataix-Solera, J., Nava, A. L., Alanís, N. (2011): Effect of fire severity on water repellency and aggregate stability on Mexican volcanic soils. Catena 84, 136–147.

Keizer, J. J., Doerr, S. H., Malvar, M. C., Prats, S. A., Ferreira, R. S. V., Oñate, M. G., Coelho, C. O. A., Ferreira, A. J. D. (2008): Temporal variation in topsoil water repellency in two recently burnt eucalypt stands in north-central Portugal. Catena 74, 192–204.

Keizer, J. J., Coelho, C. O. A., Shakesby, R. A., Domingues, C. S. P., Malvar, M. C., Perez, I. M. B., Matias, M. J. S., Ferreira, A. J. D. (2005): The role of soil water repellency in overland flow generation in pine and eucalypt forest stands in coastal Portugal. Soil Res. 43, 3, 337–349.

King, P. M. (1981): Comparison of methods for measuring severity of water repellence of sandy soils and assessment of some factors that affect its measurement. Australian Journal of Soil Research 19, 275–285.

Klimatický atlas Slovenska (2015): Climate Atlas of Slovakia (in Slovak). Bratislava: Slovenský hydrometeorologický ústav. 132 s. ISBN 978-80-88907-90-9.

Kobayashi, M., Shimizu, T. (2007): Soil water repellency in a Japanese cypress plantation restricts increases in soil water storage during rainfall events. Hydrol Process 21, 2356–2364.

Leighton-Boyce, G., Doerr, S. H., Shakesby, R. A.,Walsh, R. P. D. (2007): Quantifying the impact of soil water repellency on overland flow generation and erosion: a new approach using rainfall simulation and wetting agent on in situ soil. Hydrol. Process. 21, 17, 2337–2345.

Lichner, Ľ., Nižnanská, Z., Faško, P., Šír, M., Tesař, M. (2005): Vplyv rastlinného pokryvu a počasia na infiltráciu do vodoodpudivej pôdy. Acta Hydrologica Slovaca, 6, 2, 321–329.

Lozano, E., Jiménez-Pinillaa, P., Mataix-Soleraa, J., Arceneguia, V., Bárcenasb, G. M., González-Pérezc, J. A., Mataix-Beneyto, J. (2013): Biological and chemical factors controlling the patchy distribution of soil water repellency among plant species in a Mediterranean semiaridforest. Geoderma, 207–208, 5, 212–220.

Mataix-Solera, J., Doerr, S. H. (2004): Hydrophobicity and aggregate stability in calcareous topsoils from fire-affected pine forests in southeastern Spain. Geoderma 118, 1–2, 77–88.

Mataix-Solera, J., Cerdà, A., Arcenegui, V., Jordán, A., Zavala, L. M. (2011): Fire effects on soil aggregation: a review. Earth-Science Reviews 109, 44–60.

Mataix-Solera, J., Arcenegui, V., Guerrero, C., Jordán, M., Dlapa, P., Tessler, N., Wittenberg, L. (2008): Can terra rossa become water repellent by burning? A laboratory approach. Geoderma 147, 178–184.

Poulenard, J., Michel, J., Bartoli, F., Portal, J., Podwojewski, P. (2004): Water repellency of volcanic ash soils from

Ecuadorian paramo: effect of water content and characteristics of hydrophobic organic matter. European Journal of Soil Science 55, 487–496.

Regalado, C. M., Ritter, A. (2005): Characterizing water dependent soil repellency with minimal parameter requirement. Soil Science Society of America J. 69, 1955–1966.

Ritsema, C. J., Dekker, L. W. (1994): How water moves in a water repellent sandy soil: 2. Dynamics of fingered flow. Water Resour. Res. 30, 9, 2519–2531.

Savage, S. M., Martin, J. P., Letey, J. (1969): Contribution of some soil fungi to natural and heat-induced water repellency in sand. Soil Science Society of America Proceedings 33, 405–409.

Shakesby, R. A., Coelho, C. O. A., Ferreira, A. D., Terry, J. P., Walsh, R. P. D. (1993): Wildfire impacts on soil erosion and hydrology in wet Mediterranean forest, Portugal. International Journal Wildland Fire 3, 2, 95–110.

Shirtcliffe, N. J., McHale, G., Pyatt, F. B., Newton, M. I., Doerr, S. H. (2006): Critical conditions for the wetting of soils. Applied Physics Letters 89.

Schaumann, G. E., Braun, B., Kirchner, D., Rotard, W., Szewzyk, U., Grohmann, E. (2007): Influence of biofilms on the water repellency of urban soil samples. Hydrol. Process. 21, 17, 2276–2284.

Šurda, P., Rodný, M., Nagy, V., Matula, S., Miháliková, M., Chala, A. T. (2013): Horizontálna a vertikálna priestorová variabilita hydraulickej vodivosti pôdy s biologickým povlakom. Acta Hydrologica Slovaca, 14, 2, 466–472.

Urbanek, E., Hallett, P., Feeney, D., Horn, R. (2007): Water repellency and distribution of hydrophilic and hydrophobic compounds in soil aggregates from different tillage systems. Geoderma 140, 1–2, 147–155.

Whelan, A., Kechavarzi, C., Coulon, F., Doerr, S. H. (2014): Experimental characterization of the impact of temperature and humidity on the breakdown of soil water repellency in sandy soils and composts. Hydrol. Process 29, 2065–2073.

Wijewardana, N. S., Müller, K., Moldrup, P., Clothier, B., Komatsu, T., Hiradate, S., de Jonge, L.W., Kawamoto, K. (2016): Soil-water repellency characteristic curves for soil profiles with organic carbon gradients. Geoderma 264, 150–159.

Zavala, L. M., Granged, A. J. P., Jordán, A., Bárcenas-Moreno, G. (2010): Effect of burning temperature on water repellency and aggregate stability in forest soils under laboratory conditions. Geoderma 158, 366–374.

Zavala, L. M., González, F. A., Jordán, A. (2009): Intensity and persistence of water repellency in relation to vegetation types and soil parameters in Mediterranean SW Spain. Geoderma 152, 361–374.

Ing. Peter Šurda, PhD.
Ing. Anežka Čelková
Ing. Justína Vitková, PhD.
Mgr. Anton Zvala, PhD.
Institute of Hydrology SAS,
Dúbravská cesta 9
84104 Bratislava
Slovak Republic
E-mail: surda@uh.savba.sk

DOI: 10.31577/ahs-2019-0020.02.0022

ACTA HYDROLOGICA SLOVACA

Volume 20, No. 2, 2019, 180–188

IMPACT OF FOREST SOIL INTERFACE DEPTH ON VALUE OF SATURATED HYDRAULIC CONDUCTIVITY OF SUPERIMPOSED ORGANIC HORIZON

Anton Zvala, Tomáš Orfánus, Anežka Čelková

The paper examines the impact of the interface depth between the superimposed organic horizon and the organomineral A- horizon of forest soil on the water infiltration from the Guelph infiltrometer into forest soil. The superimposed organic horizon forms the surface layer of forest soil and it has specific physical properties such as high porosity, low bulk density, released structure and high values of hydraulic conductivity. The decomposing organic matter of the superimposed organic horizon causes the water repellency of organomineral A-horizon lying under it. In model Hydrus 2D/3D simulations with different interface depths between the superimposed organic horizon and the organomineral A-horizon of forest soil a slowdown of vertical component of infiltration from the Guelph infiltrometer and a preference of horizontal component of infiltration was detected in the case when the interface was in the bottom of borehole in which the Guelph infiltrometer was located, or when the interface has been moved higher than the bottom of borehole. By the increase of interface above the bottom of borehole, the increase of saturated hydraulic conductivity value from K_s=0.0041 cm s^{-1} to K_s=0.109 cm s^{-1} was detected.

KEY WORDS: forest soil, saturated hydraulic conductivity, superimposed organic horizon, model Hydrus 2D/3D

Introduction

The climatic conditions largely impact on the amount of water in the soil but also by the physical and chemical properties of the soil. These properties are impacted by the type of plant cover, especially in the top of forest soil layers. The forests (deciduous, coniferous), meadows and pastures, vegetation of spring areas, tree strips and groves in agricultural land, etc. impact the development of soils under these stands. Priority for the development of superimposed organic horizons of forest soils are dead underground and above ground (litter) organs of plants and animals. Dead organisms change over time, subject to the interaction of microbial soil component (bacteria, actinomycetes) through various degradation and synthetic processes of mainly biochemical nature. The composition, properties and amount of organic matter are constantly changing, the degree of decomposition is varies. Organic material of superimposed forest soil is very specific in terms of its physical properties. Several authors report mainly high porosity of this material, low bulk density, released structure and high values of hydraulic conductivity (Butorova and Bedrna, 2012; Lauren and Manerrkoski, 2001; Kosugi, 1997).

These specific physical properties would logically predetermine the superimposed organic horizons of forest soils to stimulate rainwater infiltration and prevent surface runoff. However, the hydraulics of these materials is not really trivial. Dead organic matter can cause an increase in the contact angle between water and the solid phase of soil matrix, especially in the organomineral A-horizon. The soil material then behaves as water repellency, which is caused mainly by waxes from biological litter, by the presence of fungi, mosses, lichens and other types of organic matter (Neris et al., 2013). The research of soil organic matter is a demanding discipline due to various continuous and parallel transformation processes that cause their very variable overall biochemical composition and habitus across a range of spatial scales. Water repellency and cohesion of soil particles are the key factors in soil hydrological processes. Even in the soil species with generally high infiltration capacity and low runoff generation, the litter accumulation and leaching can to lead to significant changes in the values of these parameters. Organic water repellency limits water infiltration into the soil matrix, while superimposed organic horizon aggregation limits the presence of preferential flows that allow rainwater to reach subsurface soil horizons.

Water infiltration into soil is the most important initiation process in the distribution of rainwater among the components of the hydrological cycle; surface and subsurface runoff, evapotranspiration, soil water supply regime and replenishment of deep water reservoirs in the river basin. Despite the relatively great interest in this processes in the scientific literature of the last decades (Capuliak et

al., 2010; Ritsema and Dekker, 2000; Jury and Horton, 2004), our ideas of water infiltration, especially in mountainous areas are many times very simplified and not seldom unrealistic. It is caused by historical development of hydrological models, which did not take into account the real physical properties of the soil, with a large number and variability of relevant factors that determine these soil properties. The infiltration of water into the soil is usually not uniform, the water transfer is inhomogeneous and uneven, and the water flow rate is very spatially and temporally variable, even when is saturated. Among the other factors influencing the infiltration of water into the soil are two very important characteristics: the vegetation cover and the pedogenic substrates resp. the maternal rocks from which the soil cover was evolved (Orfánus et al., 2018). The saturated hydraulic conductivity (K_s) is a quantitative characteristic of the ability to transfer water in a water saturated soil or other porous medium. Its value depends mainly on the structure and texture of the soil. Hydraulic conductivity measurements are significantly influenced by the heterogeneity of the soil composition. The spatial variability of hydraulic conductivity is manifested in both horizontal and vertical directions. The higher hydraulic conductivity in the vertical direction than in the horizontal direction was detected in the structural soils. On the contrary, the prevailing horizontal conductivity was observed in layered and compacted soils (e.g. forest roads) (Šurda et al., 2013).

The aim of this paper is to examine the impact of interface depth between the superimposed organic horizon and the organomineral A-horizon of forest soil on the water infiltration. The Hydrus 2D/3D model was applied for the modelling of water infiltration into forest soil from the Guelph infiltrometer at a different level of interface between superimposed organic horizon and the organomineral A-horizon.

Material and methods

The research locality with a working name at "Kokava meadows" is located on a wooded slope near the meadow in a typical cultural mountain spruce forest in the Western Tatras near community Liptovska Kokava. The coordinates of the research area are: 49° 6' 30.8" northern latitude and 19° 51' 53.4" eastern longitude. The average altitude is 878 m. The measurement places (1–6 in Table 3) were situated in area where the raining experiment was carried out in the past (Orfánus and Fodor, 2011), in a part with more developed superimposed organic horizon. All measurements were performed in an uneven pattern choosing the sites on naturally flat (not inclined) segments of relief and best developed forest floor horizons, without human intervention, within the 15x45 meter plot. The tributary of the Dovalovec stream, which flows near the research locality, is unlikely to have any effect on measurements. The research locality is located at the top of the slope and the tributary of the Dovalovec stream flows at the bottom of the slope, 30 meters below the measurement locality. For saturated hydraulic conductivity measurement by the Guelph infiltrometer method six places was selected at locality and forest soil moisture was measured by the Frequency domain reflectometry method. The average angle of the examined slope is 25°. The observed soil is cambisol modal, acidic with an A- horizon (16–25 cm) covered by superimposed organic horizon (0–16 cm deep) which was composed of layer of plant litter (mainly needles) at different degree of decomposition. This superimposed organic horizon in the bottom layer shown a significant degree of water repellency depending on the water content of the forest soil (Orfánus and Bedrna, 2012). The previous research in the year 2010 revealed that the organomineral A- horizon has also significant hydrophobic properties in the dry season. The transition A/B horizon is located at a depth of 25–45cm with the Bvs horizon below it. The plant cover of soil consists of spruce forest (different age structure) with discontinuous undergrowth of blueberries and mosses.

At selected places, the saturated hydraulic conductivity was measured by a Guelph infiltrometer of the upper soil layer, which consisted mostly of the superimposed organic horizon and partially encroached into the organomineral A-horizon. Guelph infiltrometer is an experimental field method applying the principle of Mariotte container which was inserted into the borehole with adjustable level of pond. The measured values of K_S express the integrally vertical and horizontal hydraulic conductivity of saturated soil and by pond influence it includes also the preferential pathways (Štekauerová et al., 2010). The measurements were realized in 6 cm and 11 cm deep of boreholes at six selected places at the research locality. The deep of pond was set to 5 cm and 10 cm. To calculate the steady water discharge (Q) and consequently the K_S, the equations 1–7 were use. The parameter α was determined according to soil structure and then inserted into the equations together with water head height H_1=5 cm and H_2=10 cm and than calculated the shape factors C_1 and C_2 as follows:

$$C_1 = \left(\frac{\frac{H_1}{\alpha}}{2.074 + 0.093\left(\frac{H_1}{\alpha}\right)} \right)^{0.754} \quad (1)$$

$$C_2 = \left(\frac{\frac{H_2}{\alpha}}{2.074 + 0.093\left(\frac{H_2}{\alpha}\right)} \right)^{0.754} \quad (2)$$

where
C_1, C_2 – shape factor,
H_1, H_2 – water head height [L],
α – radius of borehole into soil [L].

After inserting C_1 and C_2 into equations (3) and (4), we calculate G_1 and G_2.

$$G_1 = \frac{H_2 C_1}{\pi\left(2H_1H_2\left(H_2 - H_1\right) + \alpha^2\left(H_1C_2 - H_2C_1\right)\right)} \quad (3)$$

$$G_2 = \frac{H_1 C_2}{\pi\left(2H_1H_2\left(H_2 - H_1\right) + \alpha^2\left(H_1C_2 - H_2C_1\right)\right)} \quad (4)$$

where
G_1, G_2 – two head, combined reservoir,
H_1, H_2 – water head height [L],
π – constant (Ludolf number),
α – radius of borehole into soil [L].

The measurement data of steady flow rate R_1 and R_2 obtained from the Guelph infiltrometer we insert into equations Q_1 and Q_2:

$$Q_1 = R_1\ 35.22 \tag{5}$$

$$Q_2 = R_2\ 35.22 \tag{6}$$

where
Q_1 – steady state infiltration flow rate [$L^3\ T^{-1}$] for setting water head height H_1,
Q_2 – steady state infiltration flow rate [$L^3\ T^{-1}$] for setting water head height H_2,
R_1, R_2 – steady flow rate from the Guelph infiltrometer [$L\ T^{-1}$].

The saturated hydraulic conductivity K_s we calculate by using Q_1, Q_2 and G_1, G_2 (7):

$$K_s = G_2\ Q_2 - G_1\ Q_1 \tag{7}$$

where
K_s – saturated hydraulic conductivity [$L\ T^{-1}$].

Hydrus 2D/3D (Šimůnek et al., 2012a) was used to estimate the soil hydraulic parameters via numerical inversion and simulate the observed saturated hydraulic conductivity of forest soil. The Hydrus model (Šimůnek et al., 2008, Šimůnek et al., 2012b, Šimůnek et al., 2016) is a mathematical deterministic model that allows the simulation of water movement, heat and solutes transport in porous materials that are variable saturated. Preferably it was designed to simulate the transport of chemicals, but it is possible separately to simulate the movement of water in a one-dimensional or two-dimensional environment by incorporating a double porosity or double permeability model. The model has a very good user interface and is continually improved based on the current demands of its users.
The single-porosity model was used to simulate the hydraulic parameters of the superimposed organic horizon from the cumulative water infiltration into the forest soil measured by the Guelph infiltrometer. We created a network in the Hydrus 2D/3D (Šejna et al., 2014) model for an axially symmetrical quasi-three-dimensional runoff domain. The drainage domain contained axially symmetrical holes in a superimposed organic horizon with a radius of 2.5 cm and a depth of 12 cm. The simulated domain is composed of two materials with different values of θ_r–residual soil moisture, θs–saturated soil moisture, α–alpha parameter, n–parameter, K_s–saturated hydraulic conductivity, detected from the retention curve and from the measurements of saturated hydraulic conductivity K_s (Table 1).
During the infiltration of water into the forest soil, a free drainage was set as boundary condition. The Hydrus 2D/3D modelling consisted of changing parameters (the depth of interface of two horizons, the depth borehole and the applied pond). The saturated hydraulic conductivity K_s of the superimposed organic horizon was calibrated by inverse modelling while maintaining the other parameters as determined by measurements.
Forest soil moisture was measured by the Frequency Domain Reflectometry method. The electrical capacitance of a capacitor that uses the soil as a dielectric depends on soil water content θ. When this capacitor, which is made of metal plates or rods imbedded in the soil, is connected to an oscillator to form an electrical circuit, changes in soil moisture can be detected by changes in the circuit operating frequency (Báťková et al., 2013). These changes form the basis of the Frequency Domain Reflectometry sensors.

Results and discussion

From the measurements of saturated hydraulic conductivity K_s in two summer seasons (in the year 2015 and 2016) at the locality near Kokava meadows was detected, that the values of K_s measured with the Guelph infiltrometer were higher unlike other methods of measuring saturated hydraulic conductivity, when the values of K_s were lower in the year 2016 (Zvala, 2018). After considering of possible causes of this condition, we decided to verify one of the most likely hypotheses by mathematical model (Hydrus 2D/3D). The hypothesis was based on the assumption that in the second year (2016) the depth of boreholes for measurement by the Guelph infiltrometer was near to the boundary of the superimposed organic horizon with a significantly water repellency organomineral A-horizon. The K_s value of superimposed organic horizon was calibrated by the inverse model. The depth of the interface was changed, all other parameters remained unchanged. By using of Guelph infiltrometer the higher values of saturated hydraulic conductivity in the year 2016 compared to the previous year were measured. It was in average of 0.023 cm s^{-1}, four times more than the previous year (Table 2.). How is it possible if the measurements were carried out at the efficacy of the same factors (lower water content, volume changes, water repellency), which in other methods caused the decrease of K_s? The answer to this question is to be found in one of the other factors which overlaps the effect of the above mentioned parameters in this method and which is not present in disk infiltrometer and single-ring method respectively is much less active. The most likely parameter will be the depth of boundary between the superimposed organic horizon and water repellency organomineral A-horizon. The reason why we decided to simulate the measurement of saturated hydraulic conductivity of forest soil by Guelph infiltrometer was the increase in the value of saturated hydraulic conductivity in year 2016 compared to year 2015. The 2016 simulation provided us with an answer to the beginning of the question. Table 2. contains the average values of saturated hydraulic conductivity calculated from the six measured values for each method. Six measurements for each method correspond to six diffe-

rent measurement points at the research locality. The decrease moisture of forest soil in 2016 (Table 3), the volume changes of forest soil and increased water repellency (decrease of forest soil moisture causes the increased water repellency of organomineral A- horizon) and they are therefore the most likely cause of a significant decrease of K_S in 2016 compared to 2015 for single ring method and disk infiltrometer method. The forest soil moisture and their average values on all six places at the research locality of measurement are presented in Table 3. Forest soil moisture were measured before the measurement of saturated hydraulic conductivity by various methods. They are identical to the measurement points for saturated hydraulic conductivity. At each of the six points, the measurement of forest soil moisture was performed five times. From the five measured values was calculated average value for each point. Measured by frequency domain reflectometry method.

The Guelph infiltrometer measurements were apparently installed below or just below the interface between the superimposed organic horizon and water repellency organomineral A-horizon in the year 2015. The presence or the proximity of this interface to the bottom of the boreholes for the Guelph infiltrometer caused a much more significant slowdown in the vertical component of water infiltration in 2015.

The model simulations using the Hydrus 2D/3D model include various changing parameters: the interface of two materials, the depth of borehole and the height of pond, which are described in each example for water infiltration into forest soil from the Guelph infiltrometer. The soil hydraulic parameters for superimposed organic horizon such as: residual soil moisture, saturated soil moisture, alpha parameter, n – parameter and saturated hydraulic conductivity, were unchanged and their values were: θ_r=0.057 cm^3 cm^{-3}, θ_s=0.7 cm^3 cm^{-3}, α=0.03 cm^{-1}, n=1.6, K_s=0.0041 cm s^{-1} and for organomineral A-horizon: θ_r=0.089 cm^3 cm^{-3}, θ_s=0.43 cm^3 cm^{-3}, α=0.01 cm^{-1}, n=1.23, K_s=0.000019 cm s^{-1}.

In model simulation no. 1 (Fig. 1) the following model domain was setting: the interface between superimposed organic horizon and organomineral A-horizon was at the borehole bottom for the Guelph infiltrometer, the depth of borehole was 12 cm, the height of pond was10 cm. The value of saturated hydraulic conductivity of the superimposed organic horizon obtained by inverse modelling was: K_s=0.04026 cm s^{-1}.

In model simulation no. 2 (Fig. 2) the following simulation model domain was setting: the interface between superimposed organic horizon and organomineral A- horizon was under borehole bottom in depth of 50 cm,

Table 1. The soil hydraulic parameters of forest soil

Soil horizon	θ_r [cm^3 cm^{-3}]	θ_s [cm^3 cm^{-3}]	α [cm^{-1}]	n	K_s [cm s^{-1}]
Superimposed organic horizon	0.057	0.7	0.03	1.6	0.0041
Organomineral A-horizon	0.089	0.43	0.01	1.23	0.000019

Table 2. The average values of saturated hydraulic conductivity K_s measured in 2015 and 2016 at the locality Kokava meadows (Zvala et al., 2017)

Year of measurement	Guelph infiltrometer K_s [cm s^{-1}]	Single ring method K_s [cm s^{-1}]	Disk infiltrometer K_s [cm s^{-1}]
2015	0.0056	0.033	0.086
2016	0.023	0.0061	0.0032

Table 3. The forest soil surface moistures measured by Frequency Domain Reflectometry method at Kokava meadows locality in the years 2015 and 2016

Place of measurement at the research locality	Year	Forest soil moisture [%]					Average forest soil moisture [%]
1.	2015	8.6	11.6	12.6	13	11.2	9.5
	2016	8.8	7.3	8.2	9.4	7.2	6.8
2.	2015	8.1	17.3	16.0	11.3	10.2	10.5
	2016	11.9	9.4	9.2	8.6	10.7	8.3
3.	2015	14.6	15.7	20.0	9.8	11.0	11.9
	2016	6.0	6.4	6.9	7.0	6.3	5.4
4.	2015	26.3	15.3	17.0	10.2	13.6	13.7
	2016	4.0	2.3	5.0	5.6	8.9	4.3
5.	2015	10.5	13.5	11.6	9.0	12.4	9.5
	2016	6.9	7.3	7.8	5.8	6.3	5.7
6.	2015	12.6	12.8	15.0	15.3	13.5	11.5
	2016	10.7	7.0	16.1	12.3	14.7	10.1

the depth of borehole was 12 cm, the height of pond was 10 cm. The value of saturated hydraulic conductivity of the superimposed organic horizon obtained by inverse modelling was: K_s=0.02566 cm s^{-1}.

In model simulation no. 3 (Fig. 3) the following simulation model domain was setting: the interface between

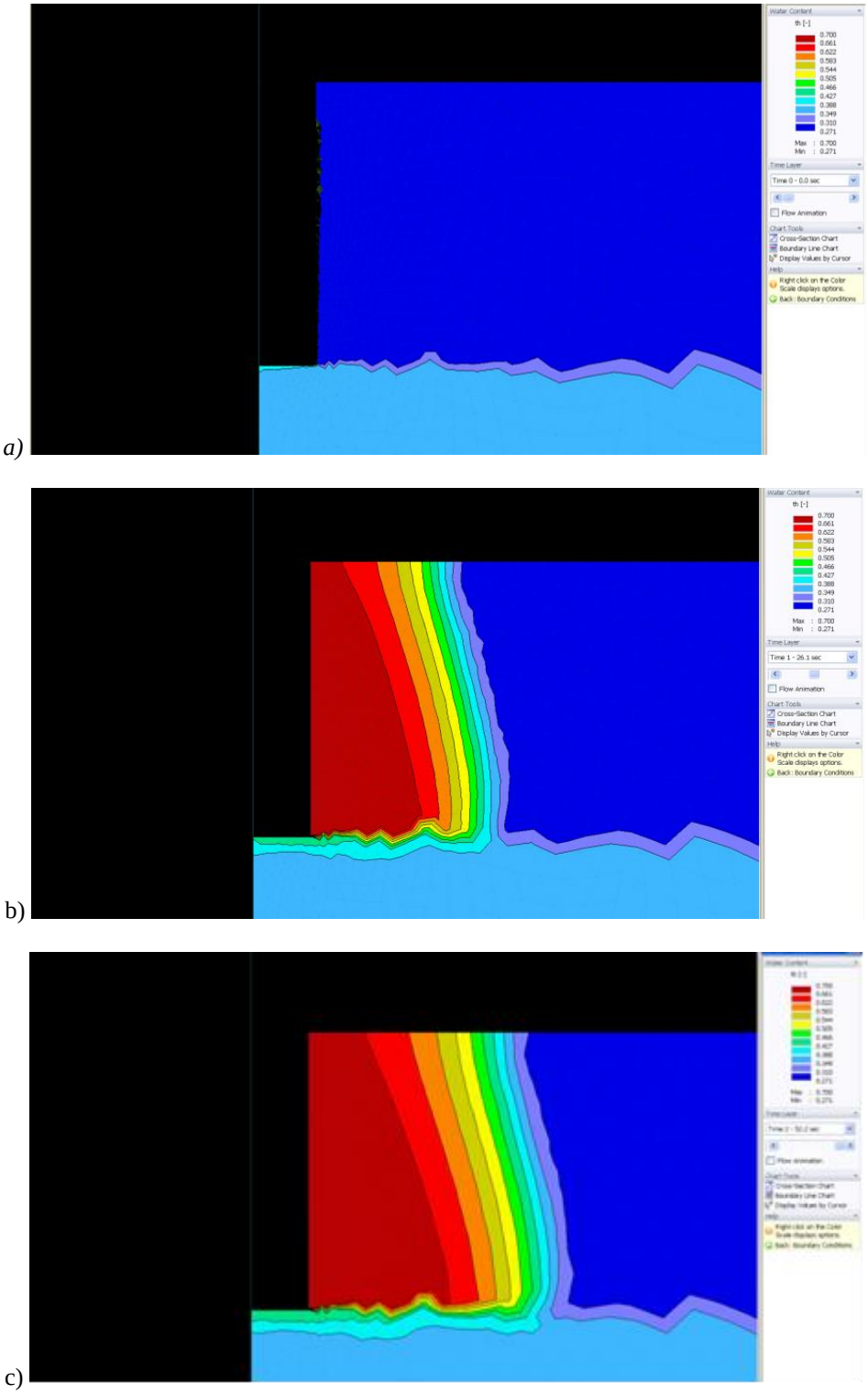

Fig. 1. Model simulation of water infiltration into forest soil by use Guelph infiltrometer in Kokava meadows locality (6/15/2016): a) the forest soil before the start of infiltration (0 s), b) the infiltration after 26 s, c) the infiltration after 52 s. (Model simulation no. 1).

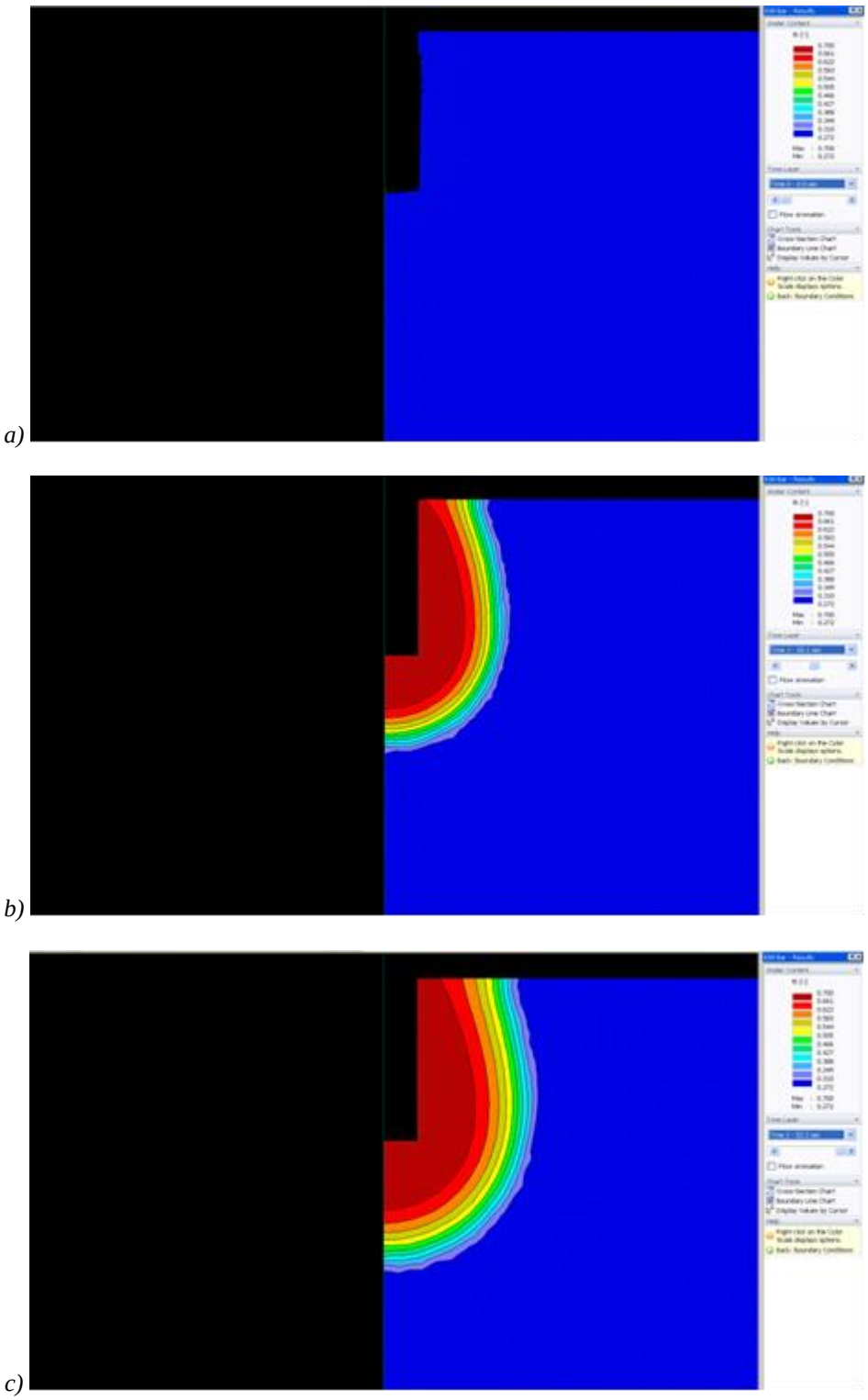

Fig. 2. Model simulation of water infiltration into forest soil by use Guelph infiltrometer in Kokava meadows locality (6/15/2016): a) the forest soil before the start of infiltration (0 s), b) the infiltration after 26 s, c) the infiltration after 52 s. (Model simulation no. 2).

superimposed organic horizon and organomineral A- horizon was in a depth of 7 cm, i.e. above borehole bottom, the depth borehole was 12 cm, the height of pond was 10 cm. The value of saturated hydraulic conductivity of the superimposed organic horizon obtained by inverse modelling was: K_s=0.109 cm s^{-1}.

From the measured and modelled results we detected the differences in the values of saturated hydraulic conductivity. In model simulation no. 1, when the interface between superimposed organic horizon and organo-mineral A-horizon was at the borehole bottom, we detected an increase of saturated hydraulic conductivity value from K_s=0.0041 cm s^{-1} to K_s=0.04026 cm s^{-1}, and preferring of horizontal infiltration into superimposed

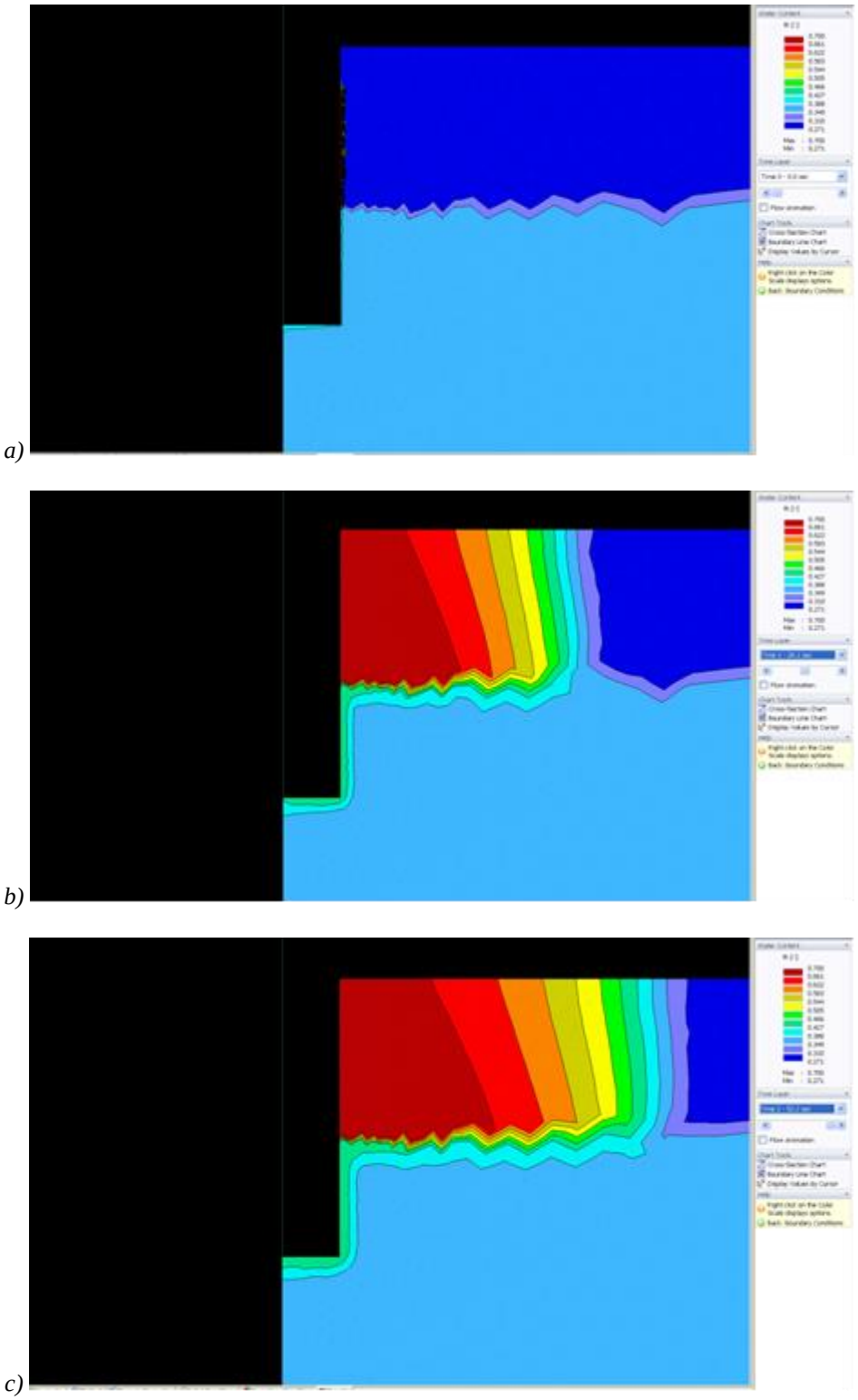

Fig. 3. Model simulation of water infiltration into forest soil by use Guelph infiltrometer in Kokava meadows locality (6/15/2016): a) the forest soil before the start of infiltration (0 s), b) the infiltration after 26 s, c) the infiltration after 52 s. (Model simulation no. 3).

organic horizon. In simulation model no. 2., when the interface between superimposed organic horizon and organomineral A-horizon was under borehole bottom in depth of 50 cm, we detected the increase of K_s value from K_s=0.0041 cm s^{-1} to K_s=0.02566 cm s^{-1}, and almost no influence on vertical and horizontal components of water infiltration into forest soil. In model simulation model no. 3, when the interface between superimposed organic horizon and organomineral A-horizon was above the borehole bottom, at a depth of 7 cm, we detected the highest increase of saturated hydraulic conductivity value from K_s=0.0041 cm s^{-1} to K_s=0.109 cm s^{-1} and the highest preference of horizontal component of infiltration into the forest soil due to the water repellency interface. Simulation model Hydrus 2D/3D revealed a significant impact of the interface depth on the calibrated value of the saturated hydraulic conductivity of the forest soil. The increase of interface above the bottom of borehole, the increase of saturated hydraulic conductivity and preferring of horizontal component of infiltration was detected. Figures 1–3 determine the water content of forest soil from θ_{min}=0,271 cm^3 cm^{-3} (dark blue color) to θ_{max}=0,700 cm^3 cm^{-3} (dark red color). From the figures we can observe the change in the water content of the soil as a function of time and the movement of water in the soil, which is influenced by the water repellency interface.

Conclusions

The Hydrus 2D/3D model was applied for the modelling of water infiltration into forest soil from the Guelph infiltrometer. The macropores and released structure of superimposed organic horizon create a prefered pathways for water infiltration. In model simulations with different interface depths between the superimposed organic horizon and the significantly water repellency organomineral A-horizon of forest soil a slowdown of vertical component of infiltration from the Guelph infiltrometer and a preference of horizontal component of infiltration was detected in the case when the interface was in the bottom of borehole in which the Guelph infiltrometer was located, or when the interface has been moved higher than the bottom of borehole. The depth of interface between the superimposed organic horizon and the organomineral A-horizon of forest soil significantly impacted the calibrated value of saturated hydraulic conductivity. By the increase of interface above the bottom of borehole, the increase of saturated hydraulic conductivity value was detected.

From the point of view of hydrological processes in forested river basins, a significant slowdown of infiltration at the water repellency interface between superimposed organic horizon and organomineral A-horizon. It can cause the shallow subsurface runoff, which accelerates the runoff during floods and causes significant washing of superimposed organic horizon can be optically observed in the forest after extreme rainfall events. It can be stated that a significantly larger part of the water flows through the macropores and the preferred pathways than the through the soil matrix.

Acknowledgement

The contribution was supported by the VEGA Grant Agency Issue 2/0096/19.

References

Báťková, K., Matula, S., Miháliková, M. (2013): Multimedial Study Guide of Field Hydropedological Measurements. 2nd revised edition [on-line]. English version. Czech University of Life Sciences Prague. Prague, Czech Republic. No pagination. Available at: http://hydropedologie.agrobiologie.cz. ISBN: 978-80-213-2434-3.

Bútorová, J., Bedrna, Z. (2012): Contribution to the determination of soil organic horizons texture. Phytopedon (Bratislava), Vol. 7. 51–58. ISSN: 1336-1120.

Capuliak, J., Pichler, V., Flühler, H., Pichlerová, M., Homolák, M. (2010): Beech Forest Density Control on the Dominant Water Flow Types in Andic Soils. Vadose Zone Journal August 01, 2010, Vol.9, 747–756. doi:10.2136/ vzj2009.

Jury, W., Horton, R. (2004): Soil physics. 6th ed. Hardcover March 2004 ISBN 0-471-05965-X.

Kosugi, K. (1997): New Diagrams to Evaluate Soil Pore Radius Distribution and Saturated Hydraulic Conductivity of Forest Soil. Journal of Forest Research, Vol. 2, 95–101. ISSN 1610-7403.

Lauren, A., Manerrkoski, H. (2001): Hydraulic properties of more layers in Finland. Scandinavian Journal of Forest Research 16 (5), 429–441, January 2001 DOI: 10.1080/ 02827580152632829.

Neris, J., Tejedor, M., Rodriguez, M., Fuentes, J., Jimenéz, C. (2013): Effect of forest floor characteristics on water repellency, infiltration, runoff and soil loss in Andisols of Tenerife Spain), Catena 108, September 2013, 50–57. DOI: 10.1016/j.catena.2012.04.011.

Orfánus, T., Fodor, N. (2011): On the issue of flood protection function of the forest in the Tatras. Studies on the Tatra National Park. 10 (43), 99–108. ISBN 978-80-89309-09-2.

Orfánus, T., Bedrna, Z. (2012): New classification of soil texture and its importance for hydropedology. First part. Classification. Acta Hydrologica Slovaca, 13, 3–8. ISSN 1335-6291.

Orfánus, T., Zvala, A., Nagy, V. (2018): Water infiltration into forest soil - what do the measurements signal? Current problems of the soil aeration zone under conditions of ongoing climate change. Science, Bratislava 2018, 54–79. ISBN 978-80-224-1690-0.

Ritsema, C. J., Dekker, L. W. (2000): Preferential flow in water repellent sandy soils: principles and modelling implications. Journal of Hydrology, Vol. 231–232, 308–319. DOI: 10.1016/S0022-1694(00)00203-1.

Šejna, M., Šimůnek, J., Van Genuchten, M. Th. (2014): The HYDRUS Software Package for Simulating the Two- and Three-Dimensional Movement of Water, Heat, and Multiple Solutes in Variably-Saturated Porous Media, User manual, PC Progress, Prague, Czech Republic, 305 p., 2014.

Šimůnek, J., Van Genuchten, M. Th., Šejna, M. (2008): Development and applications of HYDRUS and STANMOD software packages and related codes. Vadose Zone Journal, 7: 587–600. doi:10.2136/vzj2016.04.0033.

Šimůnek, J., Van Genuchten, M. Th., Šejna, M. (2012a): HYDRUS: Model Use, Calibration and Validation, Special Issue on Standard / Engineering Procedures for Model Calibration and Validation, Transactions of

the ASABE Vol. 55(4): 1261-1274 © 2012 American Society of Agricultural and Biological Engineers ISSN 2151-0032.

Šimůnek, J., Van Genuchten, M. Th., Šejna, M. (2012b) The HYDRUS Software Package for Simulating Two- and Three Dimensional Movement of Water, Heat, and Multiple Solutes in Variably Saturated Porous Media, Technical Manual, Version 2.0, PC Progress, Prague, Czech Republic, 258 p.

Šimůnek, J., Van Genuchten, M. Th., Šejna, M. (2016): Recent developments and applications of the HYDRUS computer software packages, Vadose Zone Journal, 15 (7), p. 25. doi:10.2136/vzj2016.04.0033.

Štekauerová, V., Šútor, J., Nagy, V., Breznianska, K. (2010): Measurement of saturated hydraulic conductivity by Guelph permeameter, Acta Hydrologica Slovaca, 11., no. 2, 349–352, ISSN 1335-6291

Šurda, P., Štekauerová, V., Nagy, V. (2013): Statistical analysis of soil hydraulic conductivity in the Hron river basin. In: Rožnovský, J., Litschmann, T., Středová, H., Středa, T. (eds): Water, soil and plants, Křtiny. 29.–30.5. 2013, ISBN 978-80-87577-17-2

Zvala, A., Orfánus, T., Stojkovová, D., Nagy, V. (2017): Hydraulic conductivity of superimposed organic horizons. Acta Hydr. S. roč. 18., no.1, 112–119. ISSN 1335-6291.

Zvala, A. (2018): Impact of specific properties of forest soils on hydrological processes in the basin. Dissertation thesis, Svf-104305-77077, 127p.

Mgr. Anton Zvala, PhD.
RNDr. Tomáš Orfánus, PhD.
Ing. Anežka Čelková
Institute of Hydrology SAS,
Dúbravská cesta 9
84104 Bratislava
Slovak Republic
E-mail: zvala@uh.savba.sk

DOI: 10.31577/ahs-2019-0020.02.0023

ACTA HYDROLOGICA SLOVACA

Volume 20, No. 2, 2019, 189–194

QUANTIFICATION OF SOIL WATER BALANCE COMPONENTS DURING THE VEGETATION PERIOD IN 2018

Lucia Balejčíková, Branislav Kandra, Andrej Tall

Hydrological processes in the atmosphere – plant cover – soil aeration zone – groundwater system are most affected by global climate changes, which influence the distribution and intensity of rainfall. These changes need to be monitored and forecasted for their future development, which is of great importance for human activities, especially agriculture and forestry. Data for the evaluation of soil water regime are obtained from field monitoring. Interpretation of temporal and spatial movement of water in the aeration zone is made by constantly improving computing techniques using various algorithms applied in mathematical simulation models. In our work we used the GLOBAL software, developed at the Institute of Hydrology of SAS, to simulate the individual components of the water balance in rigid soils in the locality Milhostov (Eastern Slovakia Lowland). The paper aims to quantify water balance components of a given soil system. Numerical simulation results were compared with data obtained from field monitoring during the vegetation period in 2018.

KEY WORDS: precipitation, soil aeration zone, groundwater level, evapotranspiration, numerical simulation

Introduction

The soil fertility is very important for agriculture. Its management is associated with nutrients, soil and water exchanges. Soil water regime depends on climate change. The major reason for global climatic changes in the last decades is increasing in solar irradiation, which contributes to the increase of global temperature and decrement in the global sea-ice extent (Bhargawa and Singh, 2019). Changes in water distribution, evaporation increasing and variation in intensity and amount of precipitation are also related to the temperature increasing. Deviations from normal soil water content necessary for the development of vegetation over some time as a result of changes in meteorological elements can cause complications (such as soil drought). Therefore it is necessary to deal with the prognosis that can serve to design adaptation measures to mitigate the adverse effects of climate change on the biosphere. Soil water regime forecasts can be simulated using various mathematical water balance models through input parameters characterizing soil hydrological processes, including precipitation, runoff, plant interception, evaporation, transpiration, infiltration, redistribution, and drainage or deep percolation (Ranatunga et al., 2008). The soil water movement is driven by the water potential, composed of the matrix potential and gravitational potential in the unsaturated zone (Mao et al., 2018). Simulation of the saturated-unsaturated soil water movement at various temporal and spatial scales was modeled using various numerical methods, developed since the 1970s (Bastiaanssen et al., 2007; Ranatunga et al., 2008; Pan et al., 2015; Mao et al., 2018). Many commercial software, such as HYDRUS (Šimunek et al., 2008), SWIM (Huth et al., 2012), FEFLOW (Diersch, 2013), MIKE-SHE (Graham and Butts, 2005), and TOUGH (Xu et al., 2012; Gu and Riley, 2010) use Richards' equation for description of unsaturated flows. Numerical solutions of the Richards' equation have been widely applied in studies of groundwater resources assessment, groundwater pollution, seawater intrusion, land subsidence, soil water and salt transport, and agricultural water management (Yang et al., 2016). Software GLOBAL, developed at the Institute of Hydrology of SAS, belongs to the group of numerical methods based on the solution of the Richards' equation (Majerčák and Novák, 1992). GLOBAL uses the finite element method. The basis of the software is the approximation of dependent variables, e.g. humidity potential, resp. soil moisture; finite series of base functions with time-dependent coefficients. The variables are substituted into the original equation describing the movement of water in a porous medium. Changes of various algorithms can describe water regime of plants, different schemes of water extraction by root system for individual plant species, as well as submodels using meteorological elements. Simulation using GLOBAL can also be performed with a one-day step, allowing the model to be used as an effective means of

monitoring the current soil moisture conditions at a given location. In our work, we aimed at the study of Milhostov station localized in the Eastern Slovakia Lowland (ESL) (Fig. 1). The main objective of this paper is to quantify soil water balance components in the soil profile of Milhostov locality using numerical simulation of GLOBAL software in the vegetation period of 2018.

Material and methods

Once a week, the water storage was monitored to a depth of 0.8 m and at the same time, the groundwater level is measured. The soil type is characterized by a heavy, clay-loamy to clay-like fluvial glaze, which is specific for its two-layer composition. For numerical simulation of the water storage in a given soil, a wide database used by the model in the form of input files is needed. The first group of inputs consisted of daily courses of meteorological elements obtained from the Slovak Hydrometeorological Institute (SHMI), Slovakia. The next part, phenological characteristics, was based on real grown crops on the experimental field no. 9 (for 2018 it was spring barley). The vegetation cover forms an important part of the atmosphere – plant cover – soil aeration zone – groundwater level system (Štekauerová et al., 2001). There are complex interactions between these subsystems within the hydrological cycle, resulting in the temporal and spatial distribution of water in the soil (Tall, 2007). The different crops have their individual physiological and agrotechnical specifics, the investigation of which is well-founded for a better understanding of the processes taking place between soil and plant. This fact is also taken into account by GLOBAL simulating the water regime of soils through input parameters of the stand (e.g. leaf area index, the roughness of evaporating stand surface, root system depth, etc.). The lower boundary condition consisted of a weekly GWL (groundwater level) course measured in the hydrological well and the initial condition included hydrophysical characteristics of the soil. Soil water storages calculated in a one-day step to the depth of 0.8 m were evaluated for the vegetation period 2018. Since monitoring was performed once a week, the same model days were selected for comparison. The model verification included calculation of the linear regression coefficient and deviations, which expresses the degree of dependence of measured and calculated values.

Quantification of soil water balance components during the vegetation period in 2018 was investigated in the locality Milhostov, which is located in the central part of the ESL. The daily course of soil water storage and water balance elements during the vegetation period in 2018 were analyzed. The daily courses of the water balance elements and the soil water storage were obtained by numerical simulation using GLOBAL software.

The results of the numerical simulation were verified on the results of the field monitoring carried out in 2018. After successful verification of the model, the water regime was simulated to a depth of 3 m. The top layer of the soil profile with a thickness of 0.8 m was analyzed. Also, the daily courses of potential (ET_0) and actual evapotranspiration (ET_a) were calculated using the model simulation (Penman, 1948; Monteith, 1965). The baseline database for the analysis consists of daily precipitation totals (P), daily maximum (T_{max}), minimum (T_{min}) and average (T_{avg}) temperatures, wind speed, relative air humidity, and sunshine duration. The GLOBAL software is based on the balance equation (1), which expresses the change in water volume (V_w) over a given soil volume over a given period (t_w):

$$V_w = V_i + P_d - (I + E_e + E_t) \quad (1)$$

where
P_d – capillary inflow from groundwater,
I – downflow,
E_e – evaporation,
E_t – transpiration,
V_i – soil infiltration.

The model simulation is based on the numerical solution of the nonlinear partial differential equation (2) of water movement in the soil aeration zone in the form:

Fig. 1. Area of interest situated in the Milhostov station in the Eastern Slovakia Lowland.

$$\frac{\partial h_w}{\partial t} = \frac{1}{c(h_w)} \frac{\partial}{\partial z} \left[k(h) \left(\frac{\partial h_w}{\partial z} + 1 \right) \right] - \frac{S(z,t)}{c(h_w)} \qquad (2)$$

where
h_w – soil moisture potential,
z – vertical coordinate,
$k(h_w)$ – unsaturated hydraulic conductivity of soil,
$S(z, t)$– intensity of water uptake by plant roots from unit soil volume per unit of time [$cm^3\ cm^{-3}\ d^{-1}$],
$c(hw)=\partial\theta/\partial hw$.

Results and discussion

As a first step, the GLOBAL model was verified in selected vegetation periods (2000–2008 and 2014–2018) (Fig. 2). Figure 2 shows the course of the measured and calculated soil water storage (WS) to a depth of 0.8 m during the verification period i.e. 197 days. It is clear from the figure that the model reliably follows the trend and changes in the soil water storage. However, it tends to underestimate the real state, as seen in the course of the water supply and their absolute error (AE).

The values of absolute errors between the measured and calculated water storages in the soil in the individual vegetation periods of the verification series are collected in Table 1. The mean absolute error (MAE) was in the range between 27.60 mm (2001) and 96.48 mm (2015). The maximum absolute error (MAXAE) during the verification period varies from 44.32 mm (2005) to 126.18 mm (2015) and the minimum absolute error (MINAE) vary from 0.92 mm (2001) to 74.89 mm (2008). Linear dependence showed a high degree of correlation between measurement and model. Except for some growing seasons, high values of the linear regression coefficient R^2 indicate this correlation.

The histogram in Fig. 3 shows the frequency distribution

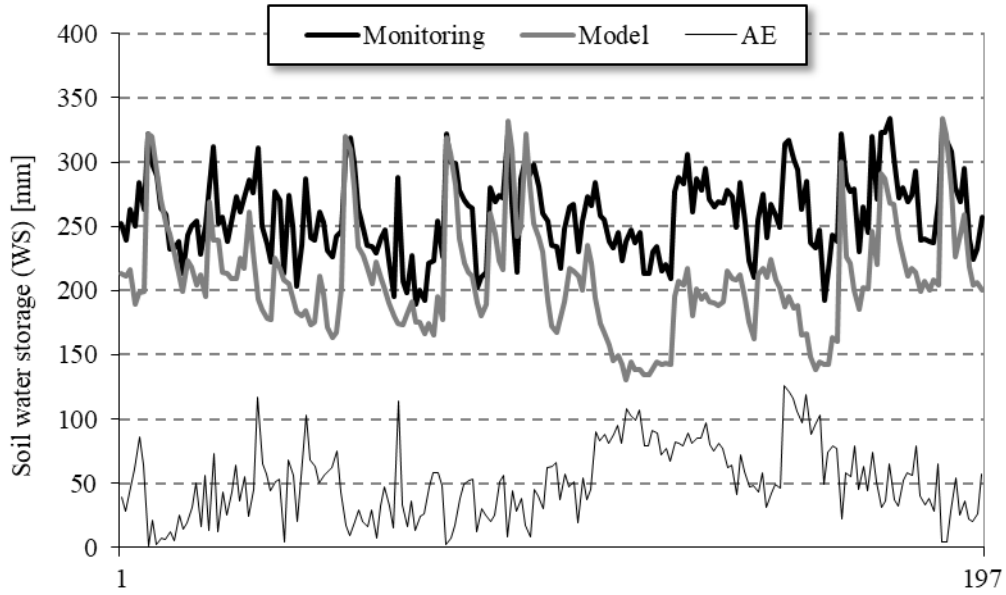

Fig. 2. The course of measured versus calculated soil water storage and their absolute error to a depth of 0.8 m during the verification period.

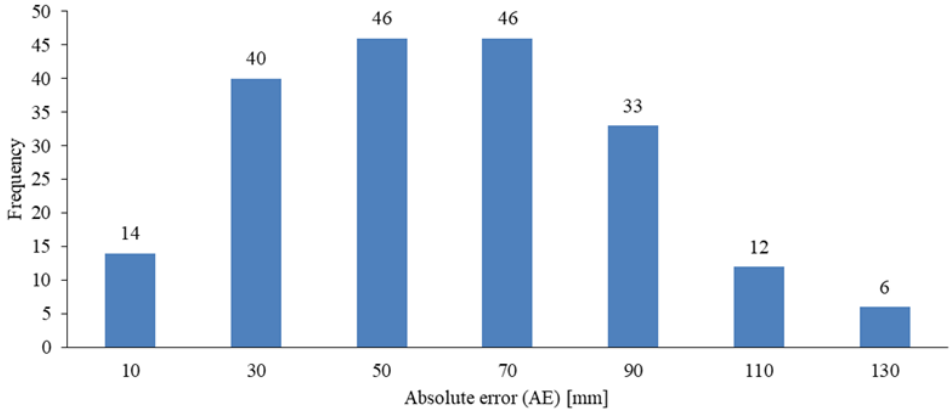

Fig. 3. Histogram of absolute error (AE) between measured and calculated soil water storage over the verification period.

of absolute errors between the measured and calculated water storages in the soil. The absolute errors are divided into 7 intervals. In the evaluated time series there are 54 days with an absolute error value in the interval 0–30 mm, 92 days in the interval 50–70 mm and 51 days in the interval 90–130 mm. The average absolute errors (MAE) over the entire verification period is 51.34 mm. Based on the verification, the highest linear dependence rate between soil water storage in the vegetation period of 2018 was shown. Through the 1:1 line it can be seen that the model underestimates the measurement by 27.73 mm in the average (Fig. 4).

The daily courses of the individual components of the balance equation in the vegetation period of 2018 are plotted in Fig. 5. Here, the interaction between individual subsystems within the atmosphere – vegetation cover – unsaturated soil zone – groundwater level system is visible. Optimum soil moisture conditions in the soil were observed at the beginning of the vegetation period in April and some days of May. In these sections of the growing season, the sums of ET_a were equal to ET_0. The water storage in the analyzed soil profile and the groundwater level was the highest in this period. A significant capillary inflow (P_d) from the groundwater

Table 1. Values of maximum, minimum and mean absolute errors with linear regression coefficient between the measured and calculated water storages in the soil during the verification period

Growing season	MAXAE [mm]	MINAE [mm]	MAE [mm]	R^2
2000	85.72	28.31	54.17	0.0663
2001	73.21	0.92	27.60	0.5072
2002	117.54	4.84	56.57	0.3011
2003	113.72	7.29	32.78	0.6694
2004	56.47	2.73	31.45	0.7837
2005	44.32	7.93	29.63	0.4680
2006	66.63	8.38	42.85	0.7814
2007	107.62	37.03	82.97	0.7496
2008	97.23	74.89	82.62	0.7510
2014	71.92	31.55	51.26	0.7284
2015	126.18	49.47	96.48	0.8370
2016	78.83	22.36	54.78	0.7529
2017	79.27	28.39	46.64	0.7831
2018	56.99	4.21	27.73	0.8513

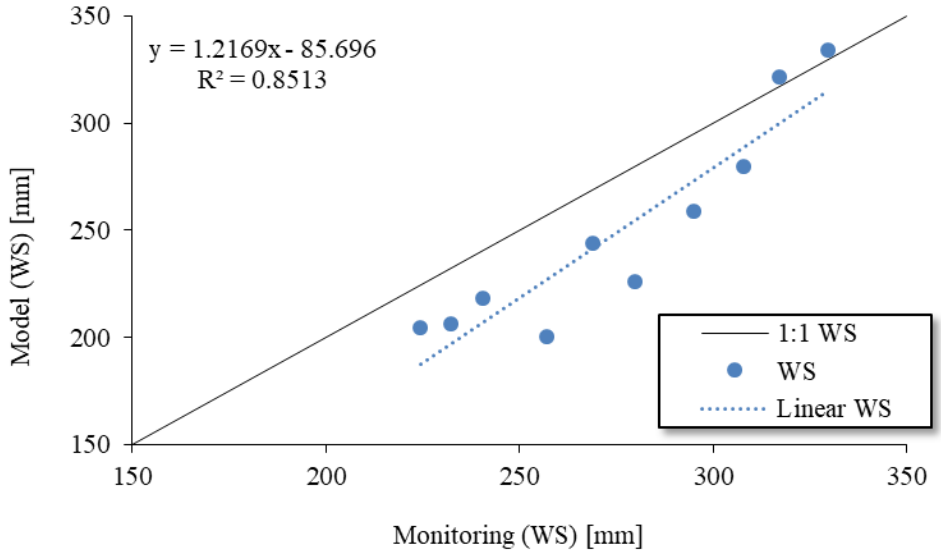

Fig. 4. Linear dependence between measured and calculated soil water storage in the vegetation period of 2018.

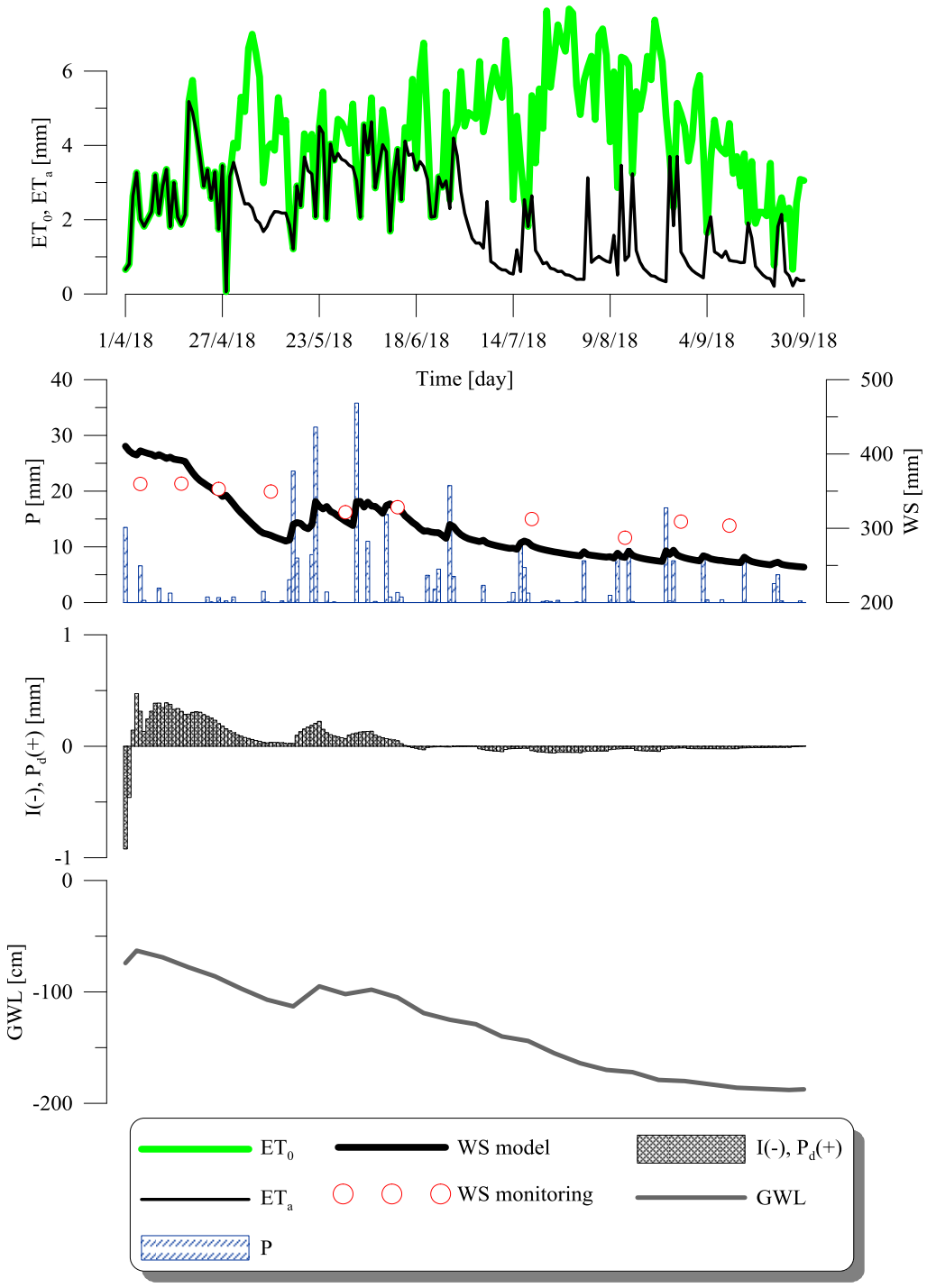

Fig. 5. Modeled daily courses of balance equation components in the vegetation period of 2018.

level into the unsaturated soil zone was found. The water storage in the soil also increased significantly due to the high amount of rainfall in May. From July to the end of the growing season, the water storage gradually decreased as the groundwater level decreased. The capillary inflow of water into the unsaturated soil zone was replaced by the predominant outflow of water from the saturated soil zone to the groundwater level. The precipitation during this period caused a slight increase in the soil water storage, but they were not sufficient to cover the need for water for optimal soil water storage and groundwater level. The result was the evapotranspiration deficit at the end of June, which lasted until the end of the growing season.

Conclusion

Our study was aimed to verify the results of the numerical simulation with the results obtained by field monitoring of the selected locality Milhostov in the investigated

vegetation period of 2018. Under these conditions, using the GLOBAL software, the water storage in the soil aeration zone was simulated to a depth of 0.8 m with a one-day time calculation step. The verification was based on the model's ability to follow the actual trend of water storage development over time, obtained by field monitoring. If the groundwater level interfered with the balance zone, it was supplied with a water capillary inflow. This situation occurred in April and May. At that time, the soil had optimal moisture conditions and the actual evapotranspiration was equal to the potential evapotranspiration. In May, the significant increase in soil water storage was also due to the high amount of precipitation. From July to the end of the growing season, soil water storage and groundwater levels had a decreasing trend. Water outflow from unsaturated soil zone to groundwater prevailed. This was reflected in the evapotranspiration deficit in early July and its duration until the end of the growing season. Based on our results of the verification, it was shown that the mathematical software GLOBAL represents a suitable tool for the quantification of individual components of the water regime of soils in Milhostov conditions. The model simulation reliably follows the trend and changes in the water storage in the soil. However, it tends to underestimate the real state.

Acknowledgement

The work was supported by the project VEGA Slovak Scientific Grant Agency No. 2/0062/16.

References

Bastiaanssen, W. G. M., Allen, R. G., Droogers, P., D'Urso, G., Steduto, P. (2007): Twentyfive years modeling irrigated and drained soils: state of the art. Agricultural Water Management, vol. 92, 111–125.

Bhargawa, A., Singh, A. K. (2019): Solar irradiance, climatic indicators abd climate change – An empirical analysis. Advances in Space Research, vol. 64, 271–277.

Diersch, H. J. (2013): FEFLOW: Finite Element Modeling of Flow, Mass and Heat Transport in Porous and Fractured Media. Springer Science & Business Media, Berlin Heideberg.

Graham, D. N., Butts, M. B. (2005): Flexible, integrated watershed modelling with MIKE SHE. In: Singh, V.P., Frevert, D. K. (Eds.), Watershed Models. Water Resources Public., Highlands Ranch, Colorado. ISBN 0849336090.

Gu, C. H., Riley, W. J. (2010): Combined effects of short term rainfall patterns and soil texture on soil nitrogen cycling-a modeling analysis. Journal of Contaminant Hydrology, vol. 112, 141–154.

Huth, N. I., Bristow, K. L., Verburg, K. (2012): SWIM3: model use, calibration, and validation. Transactions of the ASABE, vol. 55, 1303–1313.

Majerčák, J., Novák, V. (1992): Simulation of the soil-water dynamics in the root zone during the vegetation period. I. The mathematical model. Vodohospodársky Časopis, vol. 40, 299–315.

Mao, W., Yang, J., Zhu, Y., Ye, M., Liu, Z., Wu, J. (2018): An efficient soil water balance model based on hybrid numerical and statistical methods, Journal of Hydrology, vol. 559, 721–735.

Monteith, J. L. (1965): Evaporation and the Environment. 19th Symposia of the Society for Experimental Biology, vol. 19, 205–234.

Pan, F., Nieswiadomy, M., Qian, S. (2015): Application of soil moisture diagnostic equation for estimating root-zone soil moisture in arid and semi-arid regions. Journal of Hydrology, vol. 524, 296–310.

Penman, H. L. (1948): Natural evaporation from open water, bare soil and grass. Proceedings of the Royal Society of London. Series A, Mathematical and Physical Sciences, vol. 193, 120–145.

Ranatunga, K., Nation, E. R., Barratt, D. G. (2008): Review of soil water models and their applications in Australia. Environment. Modelling & Software, vol. 23, 1182–1206.

Šimunek, J., Šejna, M., Saito, H., Sakai, M., van Genuchten, M.Th. (2008): The HYDRUS-1D Software Package for Simulating the Movement of Water, Heat, and Multiple Solutes in Variably Saturated Media, Version 4.0, HYDRUS Software Series 3, Department of Environmental Sciences, University of California Riverside, Riverside, California.

Štekauerová, V., Majerčák, J., Šútor, J. (2001): Kvantifikácia zložiek vodnej bilancie v nenasýtenej oblasti pôdy. Acta Hydrologica Slovaca, vol. 2, 183–190.

Tall, A. (2007): Impact of canopy on the water storage dynamics in soil. Cereal Research Communications, vol. 35, 1185–1188.

Xu, T. F., Spycher, N., Sonnenthal, E., Zhang, G. X., Zheng, L. G., Pruess, K. (2012): TOUGHREACT user's guide: A simulation program for non-isothermal multiphase reactive transport in variably saturated geologic media, version 2.0. Earth Sciences Division, Lawrence Berkeley National Laboratory, Berkeley.

Yang, J. Z., Zhu, Y., Zha, Y. Y., Cai, S. Y. (2016): Mathematical Model and Numerical Method of Groundwater and Soil Water Movement. Science Press, Beijing.

RNDr. Lucia Balejčíková, PhD.
Ing. Branislav Kandra, PhD.
RNDr. Andrej Tall, PhD.
Institute of Hydrology SAS
Dúbravská cesta 9
841 04 Bratislava
Slovak Republic
E-mail: balejcikova@uh.savba.sk

DOI: 10.31577/ahs-2019-0020.02.0024

ACTA HYDROLOGICA SLOVACA

Volume 20, No. 2, 2019, 195–203

ASSESSMENT OF THE PHYSICAL AND CHEMICAL QUALITY OF THE UPPER LAYER OF LOAMY SOIL

Ivana Kameníčková, Šárka Schneiderová, Kateřina Suchá

Healthy soil is a basic prerequisite for the growth and development of plants, animals and humans. It is assessed on the basis of "indicators" of physical, chemical or biological quality. The present paper evaluates the quality of the upper layer of loamy soil using of basic indicators of physical and chemical quality, i.e. texture, density, porosity, maximum water capacity, minimum air capacity, saturated hydraulic conductivity, humus content, pH and conductivity. These indicators were determined by standard laboratory methods from collected intact soil cores and grab samples. Experimental research took place in years 2016–2018 near the village Šardičky (K1) and Bohaté Málkovice (K2) in the South Moravian Region. Upper layer of these plots was cultivated by reduced tillage technology. The plot K1 was sown with poppy seed (*Papaver somniferum L*., 2016) and spring barley (*Hordeum vulgare conv. distichon var. nici*, 2017–2018), the plot K2 with spring barley (*Hordeum vulgare conv. distichon var. nici*, 2016–2017) and sunflower (*Helianthus*, 2018). The long-term reduced tillage technology showed small changes in selected physical and chemical parameters of soil quality in the monitored period 2016–2018, the soil quality was good for both plots. With regard to achieving or exceeding critical values for measured soil quality indicators, the experimental plot K1 has shown a better quality in upper layer of soil than plot K2.

KEY WORDS: soil quality indicators, no-tillage, bulk density, porosity, air capacity, hydraulic conductivity, organic carbon

Introduction

Soil is the natural wealth of our country, an essential element of the food chain and a medium for plant growth. Besides the production function has a many other functions, e.g. filtering, buffering, transformation and socio-economic. Soil quality can be defined as "the capacity of soil to function within ecosystem and land-use boundaries to sustain biological productivity, maintain environmental quality, and promote plant and animal health" (Doran et al., 1996).

An agricultural soil with good quality have all the physical, chemical and biological attributes necessary to promote and sustain good productivity in agriculture with negligible environmental degradation. A soil with poor quality can then aggravate the environmental degradation through wind/water erosion and contaminate surface and subsurface water resources in the landscape.

The quality of agricultural land with regard to the different composition of the soil environment is divided into "physical", "chemical" and "biological" (Dexter, 2004). These components are interconnected and can´t be separated from each other. Physical soil quality refers primarily to the soil´s strength and fluid transmission and storage characteristic in the crop root zone as a result of soil physical properties (e.g. structure and texture), management practices (e.g. technology of soil cultivation, crop types), climate and various chemical and biological processes (faunal activity, mineralization). The upper layer of soil (0–10 cm) is particularly important because it controls many critical agronomic and environmental processes (e.g. seed germination and early growth, impacts of applied technology, erosion, aggregation, surface crusting, aeration, infiltration, and runoff). Soil chemistry is dominated by the interaction between its solid constituents and the water phase, it is the basis for assessing soil fertility and provides the necessary knowledge to understand the differences in fertility of different soils and their response to fertilization. Chemical analysis without knowledge of physical conditions may fail to assess soil fertility if microbial activity is adversely affected.

In practice, we face the problem how to measure and evaluate the quality of the soil. There are established methods for assessing the quality of water and air, but determining standards for assessing soil is complicated with respect to its variability, heterogeneity and an ongoing process. Texture, bulk density, porosity, aeration, saturated hydraulic conductivity, organic carbon content, pH/H_2O and electrical conductivity will form the basic set of parameters indicating the physical and chemical quality of the soil.

The objectives of this study was to measure selected physical and chemical quality parameters in the upper layer of loamy soil processed by reduced tillage in the monitored period 2016–2018, to monitor changes of physical and chemical quality of this soil and to compare the measured parameter values with "ideal, optimal or critical" levels proposed in our and foreign literature.

Materials and methods

Description of experimental plots

Both experimental plots are located in sugar beet production area in the District Vyškov, the plot K1 is close to the village Šardičky and the plot K2 near the road between Bučovice and Bohaté Málkovice (Fig. 1). The plots are approximately 3.2 km apart.
They are a part of the river basin Svratka and the main river basin of Morava. The average altitude for both plots is around 275 m above the sea level.
Data from the meteorological station Bohaté Málkovice were used to characterize climatic conditions. It is a warm area with a mild, humid climate. Annual precipitation and long-term average of precipitation are shown in Table 1, average temperature is around 10.5°C and 8.4°C (1901–1950). If we compare measured precipitation with the long-term average in the growing season, then precipitation was 1/2 (2016) and 3/4 (2017, 2018).
The genetic soil representative is Haplic Chernozem (FAO) and the pedogenic substrate is loess. These soils are very deep with weakly acidic-alkaline soil reaction. Representation of $CaCO_3$ is low.
The co-operative farm Zemo, Bohaté Málkovice, has been processing land with reduced tillage technology (*RT*) since 1992 (e.g. during autumn the cultivation of spring crops is done by vertical hoeing of soil to a depth of 20 cm). Cultivated crops on experimental plot K1: 2016 poppy seed (*Papaver somniferum L.*), 2017–2018 spring barley (*Hordeum vulgare conv. distichon var. nici*). The second plot K2: 2016–2017: spring barley (*Hordeum vulgare conv. distichon var. nici*), 2018 sunflower *(Helianthus).*

Soil quality parameters

The intact soil cores (cylinder of Kopecký with uniform volume 100 cm^3) and accompanying soil grab samples were collected each year from the 0–10 cm depth of each experimental plot. A total of 100 intact soil samples were taken during 10 sampling, ten intact soil samples in each sampling (5 for saturated hydraulic conductivity K_s and 5 for basic soil analysis). The samples were collected

Fig. 1. Experimental plots K1 and K2 with soil sampling points (Mapy.cz, 2015).

Table 1. Precipitation in years 2016–2018 measured in Bohaté Málkovice and long-term average of precipitation in the years 1901–1950 from the station Bučovice (Climate atlas ČSSR, the period 1901–1950)

month/year	precipitation [mm]													
	I	II	III	IV	V	VI	VII	VIII	IX	X	XI	XII	I–XII	IV–IX
2016	15.2	63.6	51.4	44.8	23.8	21.8	70	19.7	6.8	35	21.1	4.8	378	186.9
2017	7	27	25	40	28	37	59.5	25	81	47	29	43	448.5	270.5
2018	45	17	10	48	40	50	39	14	75	29.4	44.1	34.2	367.4	260
1901–1950	28	25	30	36	59	57	74	77	52	52	45	34	569	355

during April–July during active crop growth, and always were taken from the same place (K1: 49° 10' 33.2" N 17° 02' 47.4" E and K2: 49° 10' 42.2" N 17° 00' 07.2"E).
In the pedological laboratory of the Institute of Landscape Water Management at Brno University of Technology, selected soil quality physical and chemical indicators (texture, bulk density, porosity, maximum capillary capacity, minimum air capacity, saturated hydraulic conductivity, organic carbon content, pH/H_2O and electrical conductivity) were analyzed using standard methodology (Jandák et al., 2003).

The texture shows the size and proportional representation of individual soil fractions. It is involved in pedogenetic processes but also in agronomic and ecological characteristics of the soil. It affects virtually all soil properties, especially the water and air ratio, content and composition of edaphon, chemical and biological processes occurring in the soil. A combined method was used to determine the pore size distribution, i.e., sieve analysis and the hydrometer method for smaller fraction. Subsequently, the soil was classified according to Novak and the USDA triangle diagram.
The analysis of the intact soil sample determined the bulk density, porosity, humidity and air characteristics.

Bulk density (BD) is often used to express the degree of compaction or as an index of soil´s mechanical resistance to root growth (Carter, 1988, 1990, Reynolds et al., 2003; Drewry, 2006); and is defined by following equation:

$$BD = \frac{G_F}{V_S} \qquad [\text{g cm}^{-3}] \tag{1}$$

where
G_F – mass of the sample after drying to a constant weight [g],
V_S – bulk volume of intact soil sample [cm^3].

On the basis of bulk density, we can evaluate the critical value expressing the harmful soil compaction (Lhotský et al., 1984), approximately evaluate the structural condition of the humus horizon (Kutílek, 1978) and the growth reduction of roots according to USDA categories (Arshad et al., 1996).

Porosity (P) is characterized by the total pore volume, its shape, size and spatial spacing. It has a decisive influence on the fertility of the soil, it allows the penetration of the roots of plants, water and air into the soil and their movement in the soil and the existence of soil microorganisms. When increasing humidity, it increases, decreasing as the soil dries. Porosity was determining using next equation:

$$P = \frac{\rho_S - BD}{\rho_S} \cdot 100 \quad [\%] \tag{2}$$

where
P – total porosity [%],
ρ_s – particle density of soil [g cm^{-3}],
BD – bulk density [g cm^{-3}].

On the basis of porosity, we can classify compactness of topsoil by Bretfeld (Kutílek, 1978) and assess critical porosity values (Lhotský et al., 1984).

Maximum capillary capacity according Novák (θ_{KMK}) represents the amount of water that the soil in its natural habitat is able to retain for extended periods of time in its capillary pores after the previous saturation. For loamy soils it should not exceed 36%, otherwise soil is damaged and water is poorly absorbed into the soil.

$$\theta_{KMK} = B_2\text{-}C \quad [\%] \tag{3}$$

where
B_2 – state of the intact soil sample after 2 hours of drainage [%],
C – state of the intact sample after drying at 105°C to a constant weight [%].

Minimum air capacity (*AC*) indicates the difference between porosity and maximum capillary capacity. Optimal minimum air capacity values range from 15 to 24%, $AC \geq 10\%$ has traditionally been recommended to achieve minimum susceptibility to crop-damaging aeration deficits in the root (O'Connell, 1975, de Witt and McQueen, 1992) and topsoil is in critical condition and requires agromelioratory intervention (Lhotský et al., 1984). Minimum air capacity is defined as:

$$AC = P - \theta_{KMK} \quad [\%] \tag{4}$$

where
P – total porosity [%],
θ_{KMK} – maximum capillary capacity [%].

Saturated hydraulic conductivity (K_s) is an indicator of the soil's ability to absorb and transfer water to the root zone and to drain excess water out of the root zone (Topp et al., 1997). K_s value in the range, 5 10^{-3} cm s^{-1} to 5 10^{-4} cm s^{-1} may be considered "ideal" for promoting rapid infiltration and redistribution of needed crop-available water, reduced surface runoff and soil erosion, and rapid drainage of excess soil water (Reynolds et al., 2007). For laboratory determination of saturated hydraulic conductivity K_s was used permeameter with constant gradient in which were placed the saturated soil samples with volume of 100 cm^3. The calculation is done using Darcy's relation, 1856:

$$K_s = \frac{V \cdot L}{S \cdot \Delta H \cdot t} \qquad [\text{cm s}^{-1}] \tag{5}$$

where
V – volume of water passed through the soil sample [cm^3],
L – height of soil sample in the direction of water flow [cm],
ΔH – difference of levels before and behind sample [cm],
S – flow area of sample [cm^2],
t – time [s].

Organic carbon (OC) indicates the total amount of organic material in the soil (i.e. living and dead plants, animal and microbial materials, highly stable humic substances). The total humus content, respectively the oxidometric determination of the soil organic matter was done by the Walkley-Black method, by modification of the Novák-Pelíšek. Soil organic matter influences not only the soil quality and soil fertility, but also the physical and chemical properties of the soil. OC range of 3–5 wt % is cited in Reynolds et al. (2007) as being optimal for establishment and maintenance of plant in constructed landscaping soils (e.g. urban parks, sports fields, etc.).

Stability index (SI) indicates the risk of soil degradation (Reynolds et al., 2007), and is calculated according to the following equation:

$$SI = \frac{1{,}72\ \mathrm{OC}}{(\mathrm{clay+silt})} \cdot 100 \quad [wt\ \%] \tag{6}$$

where
SI –soil structural stability index [%],
OC –organic carbon content [wt %],
(clay+silt) –soil´s combined clay and silk content [wt %].

SI ≤ 5% indicates structurally degraded soil due to extensive loss of organic carbon, 5%<SI≤7% shows high risk of structural degradation due to insufficient organic carbon loss, 7%<SI≤9% shows low risk of soil structural degradation and SI > 9% indicates sufficient soil organic carbon to maintain structural stability.

Active soil reaction (pH/H_2O) belongs to significant chemical characteristics, significantly affects the fertility of the soil, it influences soil processes and the presence of soil organisms. The active soil reaction was determined by potentiometrically. Fertility decreases rapidly at pH<5. If pH<3, the plants are generally unable to grow. In the Czech Republic most of the surface layers show a slight to slightly acidic reaction.

Electrical conductivity (EC) characterizes the degree of salt load. Soil salinity greatly influences the chemical and biological properties of the soil and greatly reduces soil fertility. For analysis was used with the electrode pH meter for measuring the electrical conductivity.

Results and discussions

The results of the physical and chemical properties of the soil from the experimental plots K1 and K2 are presented in graphical form (Fig. 2A-H, 3A-H). They represent the average values of measured soil quality indicators from the years 2016–2018.

Locality K1 Šardičky

On the basis of the results obtained, it can be stated that the physical and chemical quality of soil on the plot K1 is good. The average soil texture in the Ap horizon (0–30 cm): 19.23% sand, 69.78% silt and 11% clay. Soil classification: medium heavy loamy soil (Novák) and silt loam (USDA).

The course of bulk density in the monitored period including a critical value according to Lhotský et al. (1984) and Arshad et al. (1996) is seen in Fig. 2A, with average BD values ranging from 1.35 to 1.46 g cm^{-3}. In 2016–2017 the critical value proposed by Lhotský et al. (1.45 g cm^{-3}) was not exceeded and the structural condition of the upper layer was good. In the last year of monitoring, the critical value was exceeded (agricultural machinery travels and natural soil compaction due to various factors), and the structural state was insufficient. Critical value according to Arshad et al. (2002) (1.55 g cm^{-3}) was not reached during the monitored period. The course of porosity, including the critical value for loamy soil, can be seen in Fig. 2B, the average P values ranged from 44.77 to 49.31%. First two years the critical value was not exceeded and the upper layer of the soil, according to Bretfeld, was compact (Kutílek, 1978). In 2018 critical value was exceeded and the upper layer was very compact. The course of maximum capillary water capacity, including reaching or exceeding the critical value for loamy soil is shown in Fig. 2C, the average θ_{KMK} values ranged from 29.05 to 33.69% and the critical value of 36% was not exceeded.

The course of the minimum air capacity including the indication of the optimum range is shown in Fig. 2D, the average AC values ranged from 15.62 to 17.95% and in the monitored period met the condition of optimum air capacity, i.e. in the soil is enough air for the roots of plants.

If we compare the results of the research with the results of the basal monitoring of agricultural soils (Kňákal, 2000: BD=1.4 g cm^{-3}, P=47.08%, θ_{KMK}=35.24%), the achieved values of physical indicators do not show agreement.

The course of K_s including the limit for ideal range K_s is shown in Fig. 2E. In 2016, the average K_s value was high due to preferential flow, in 2017 decreased and stabilized and in 2018 was without significant change. In 2016, the soil was classified according to Kutilek (Holý et al., 1984) as a high permeability soil (2–6 m day^{-1}) and in 2017–2018 was moderately permeable (0.5–2 m day^{-1}). Average values (0.0020–0.0048 cm s^{-1}) fall within the optimal range (5 10^{-3} cm s^{-1} to 5 10^{-4} cm s^{-1}) and can be considered "ideal" (Reynolds et al., 2003).

The chemical properties of the soil can be characterized by a high organic carbon content, the course of which can be seen in Fig. 2F. Humus affects soil fertility and soil function in the ecosystem, average values were higher than 5% (5.66 to 5.68%), i.e. the soil is highly humous (Kutílek, 1978). The high proportion of humus is probably related to the long-term applied reduced tillage technology and to leaving plant residues on the soil surface.

High content of humus is likely to be related to long-term reduced tillage treatment and plant residues in the soil. Based on the humus content and gran size distribution, the stability index SI we used to classify the soil into classes of structural degradation risks. In the monitored period SI values are unchanged (7.0–7.03%), showing low risk of soil structure degradation. The electrical

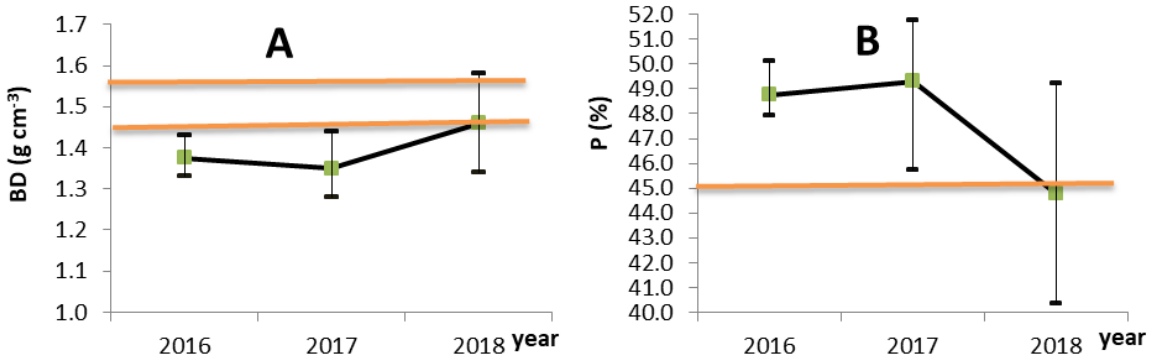

Fig. 2. A) average BD values in the 0–10 cm depth from the plot K1 with RT. The two horizontal lines demark a critical value according Lhotský et al. (1984) and Arshad et al. (1996). B) average P values in the 0–10 cm depth from the plot K1 with RT. The horizontal line demarks a critical value according Lhotský et al. (1984). In both pictures the vertical T- bars indicate range of measured values.

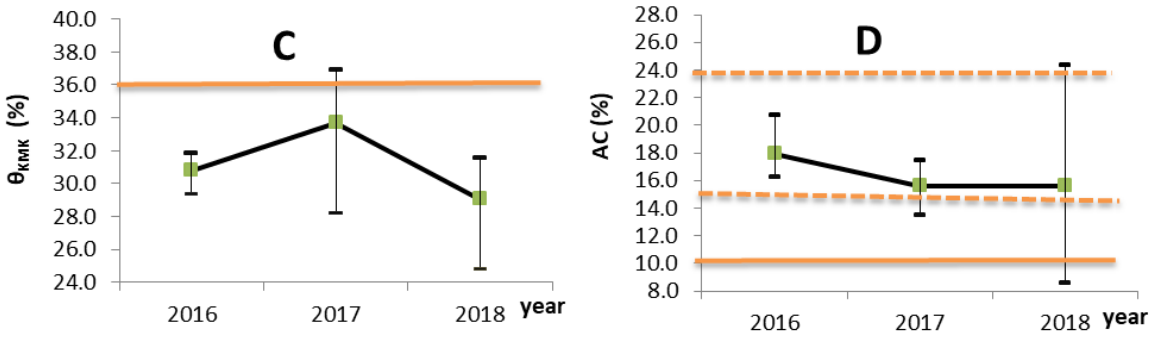

Fig. 2. C) average θ_{KMK} values in the 0–10 cm depth from the plot K1 with RT. The horizontal line demarks a critical value for loamy soils. D) average AC values in the 0–10 cm depth from the plot K1 with RT. The horizontal lines demark a proposed minimum and optimal AC values for adequate root-aeration. In both pictures the vertical T-bars indicate range of measured values.

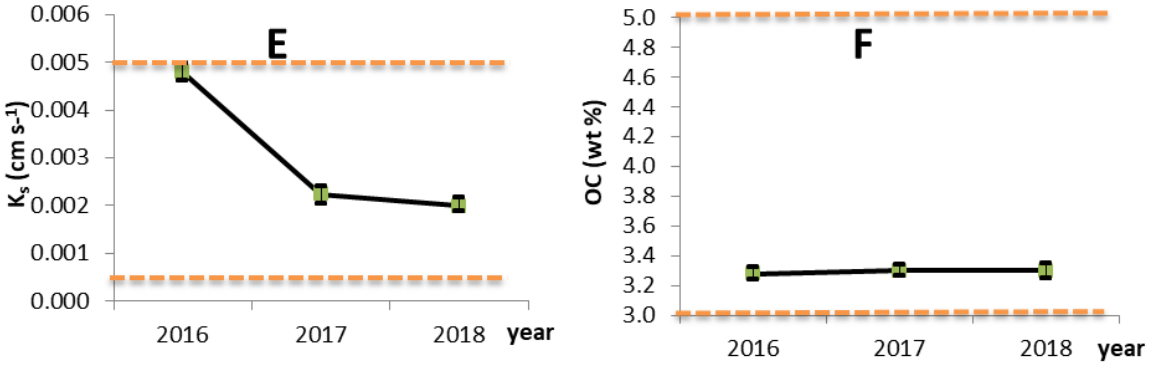

Fig. 2. E) average K_s values in the 0–10 cm depth from the plot K1 with RT. The two horizontal lines demark a proposed optimum K_s range. F) average OC values in the 0–10 cm depth from the plot K1 with RT. The horizontal lines demark a proposed optimal OC range (Reynolds et al., 2007). In both pictures the vertical T-bars indicate range of measured values.

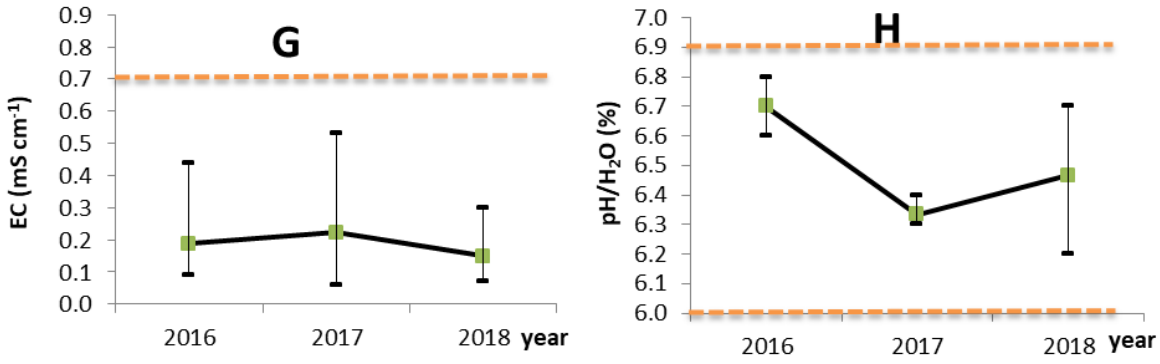

Fig. 2. G) average EC values in the 0–10 cm depth from the plot K1 with RT. The horizontal line demarks a boundary for salinity. H) average pH/H_2O values in the 0–10 cm depth from the plot K1 with RT. The horizontal lines demark boundary for a weakly acid reaction. In both pictures the vertical T-bars indicate range of measured values.

conductivity is shown in Fig. 2G, with average EC values ranging from 0.15 to 0.22 mS cm^{-1}, without negative effect of fertilization on the soil. The course of the soil reaction including the range for the weakly acidic reaction is shown in Figure 2H, the average pH/H_2O values ranged from 6.33 to 6.7, the active soil reaction was weakly acidic. The results of chemical indicators are not consistent with the results of the evaluation of basal monitoring of agricultural soils (Kňákal, 2000: pH/H_2O=7.0, humus=2.72%).

Locality K2 Bohaté Málkovice

The physical properties of the upper soil layer on plot K2 are also in good condition. The average soil texture in the Ap horizon (0–30 cm): 9.7% sand, 75.49% silt and 14.81% clay. The soil is classified by Novák as a medium-heavy loamy soil, by USDA classification as a silty loam.

Course of BD in the years 2016–2018 is shown in Fig. 3A, the average BD values ranged from 1.35 to 1.50 g cm^{-3} and exceeded the agro-ecological limit (1.45 g cm^{-3}) only in 2018. Critical value according to Arshad was not reached. In 2016–2017 the structural condition of the humus horizon was good, in 2018 it deteriorated and was unsufficient. The course of porosity including exceeding the critical value for loamy soil is evident from Fig. 3B, the average P values ranged from 43.58 to 49.31%, the critical value was exceeded in 2018. In 2016–2017 the state of the topsoil was compact, in 2018 was very compact.

The course of maximum capillary water capacity, including reaching or exceeding the critical value for loamy soil is shown in Fig. 3C, the θ_{KMK} values ranged from 28.34 to 34.89% and was not exceeded the critical value (36%).The course of the minimum air capacity, including the minimum and optimal AC range for adequate root aeration, is shown in Fig. 3D. The average AC values ranged from 12.15% to 15.64% and did not fall below the 12% minimum level. The optimum range was reached only in 2018. The results of the physical parameters are not consistent with the results of the evaluation of the basal monitoring program for agricultural soils (Kňákal, 2000).

The course of K_s is shown in Fig. 3E and average K_s are without significant changes (0.0020–0.0021 cm s^{-1}). The soil was classified according Kutilek (Holý et al., 1984) as moderately permeable (0.5–2 m day^{-1}). The average K_s values meet the condition of optimal values and can be considered "ideal" (Reynolds et al., 2003).

Chemical properties are good and do not require treatment. The course of OC is shown in Fig. 3F. The humus content is high (5.24–5.38%), the soil is highly humous (Kutílek, 1978). According average SI values (5.95 to 7.0), the soil in the first year indicate a high risk of structural degradation (5%<≤7% SI) and in 2017–2018 move between high and low risk of structural degradation. The course of electrical conductivity is shown in Fig. 3G, the average OC values were low (0.08–0.21 mS cm^{-1}) and without the effect of fertilization on soil quality (Pokorný et al., 2007). The course of the soil reaction including the range for the weakly alkaline reaction is shown in Figure 3 H, the average pH/H_2O values ranged from 7.39 to 7.58, the soil reaction was weakly alkaline (7.1–8.0). The results of chemical indicators are not consistent with the results of basal monitoring of agricultural soils (Kňákal, 2000).

Conclusion

The long-term reduced tillage technology showed small changes in selected physical parameters of soil quality. The critical *BD* and *P* value were exceeded only in 2018 and the average θ_{KMK} values did not exceed the limit for loamy soil. The minimum air capacity was better on the plot K1with optimal values, on the plot K2 did not drop below the minimum limit. The average K_s values for both plots meet the optimum condition and can be considered " ideal. With regard to achieving or exceeding

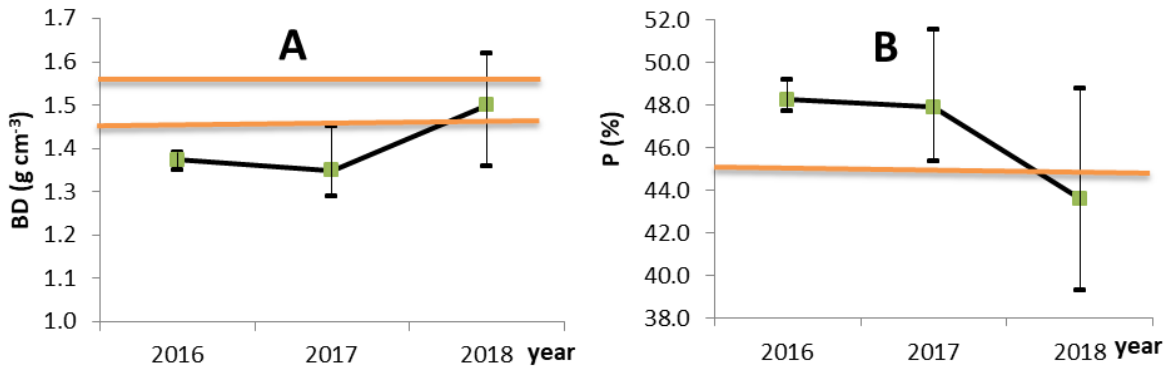

Fig. 3. A) average BD values in the 0–10 cm depth from the plot K2 with RT. The two horizontal lines demark a critical value according Lhotský et al. (1984) and Arshad et al. (1996). B) average P values in the 0–10 cm from the plot K2 with RT. The horizontal line demarks a critical value according Lhotský et al. (1984). In both pictures the vertical T-bars indicate range of measured values.

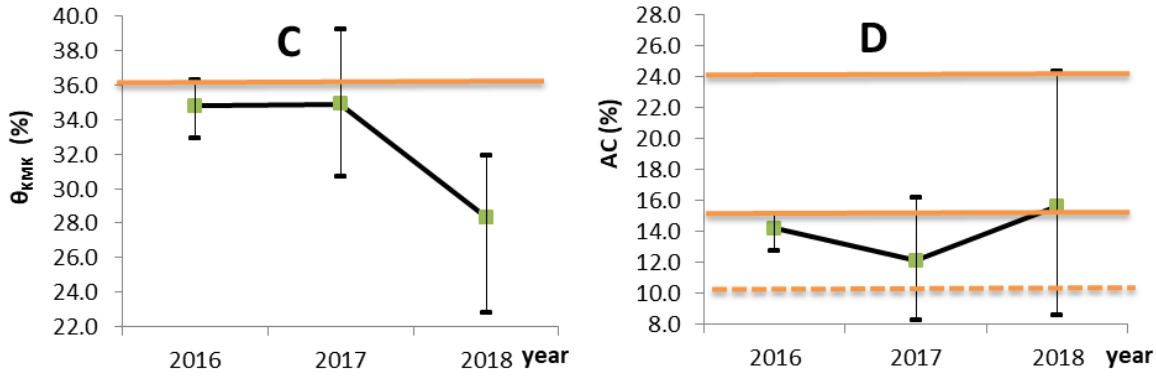

Fig. 3. C) average θ_{KMK} values in the 0–10 cm depth from the plot K2 with RT. The horizontal line demarks a critical value for loamy soils. D) average AC values in the 0–10 cm depth from the plot K2 with RT. The horizontal lines demark a proposed optimal and minimum AC value range for adequate root-aeration. In both pictures the vertical T-bars indicate range of measured values.

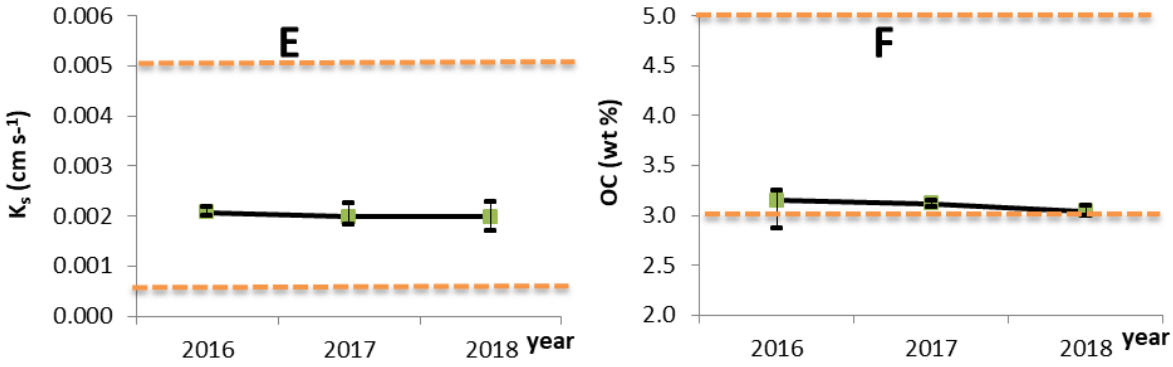

Fig. 3. E) average K_s values in the 0–10 cm depth from plot K2 with RT. The two horizontal lines demark a proposed optimum K_s range. F) average OC values in the 0–10 cm depth from the plot K2 with RT. The horizontal lines demark a proposed optimal OC range for landscaping soils. In both pictures the vertical T-bars indicate range of measured values.

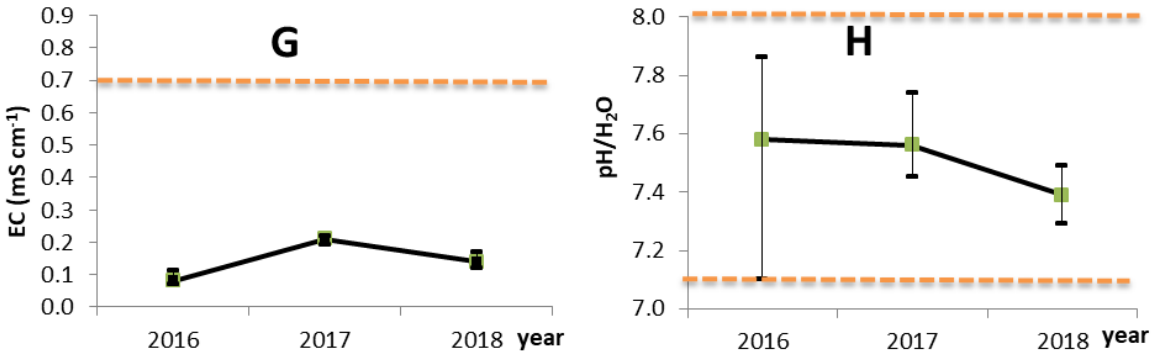

Fig. 3. G) average EC in the 0–10 cm depth for soil from plot K2 with RT. The horizontal line demarks a boundary for salinity. H) average pH/H_2O in the 0–10 cm depth for y soil from plot K2 with RT. The horizontal lines demark boundary for weakly alkaline reaction. In both pictures the vertical T-bars indicate range of measured values.

the critical values of the measured physical soil quality indicators, the experimental plot K1 near the village of Šardičky showed better quality of the upper layer. Soil chemical properties are good and do not require treatment. Both plots show a high proportion of humus, the plot K1 showed a higher stability index SI and a low risk of soil structure degradation. EC is low in both plots, without the effect of fertilization on soil quality. For the plot K1 the soil reaction was slightly acidic, for the plot K2 was slightly alkaline. If we compare the results of the research with the results of the evaluation of the basal monitoring of agricultural soils, the agreement is not evident in physical or chemical soil parameters. To assess soil quality in general, it is necessary to assess not only the physical and chemical properties of the soil, but also the biological ones. A comprehensive assessment will then help to identify the causes of the failures and to suggest effective measures to eliminate them.

Acknowledgment

This paper was supported with the specific research Brno University of Technology FCE-S-18-5345 "Evaluation of soil quality based on selected physical and chemical indicators". Thanks belong to Ing. Jiří Brňák from co-operative farm Zemo, spol. sr.o., Bohaté Málkovice, (on whose plots were conducted field experiments) and anonymous reviewers for their valuable comments to the manuscript.

References

Arshad, M. A., Lowery, B., Grossman, B. (1996): Physical tests for monitoring soil quality. p. 123–142. In: J.W.

Arshad, M. A., Martin, S. (2002): Identifying critical limits for soil quality indicators in agro-ecosystems. Agric. Ecosyst. Environ. 88, 153–160.

Dexter, A.R. (2004): Soil physical quality. Soil Tillage Res. 79, 129-130.

Drewry, J.J. and Paton, R.J. (2006): Soil physical quality under cattle grazing of a winter-fed brassica crop. Austr. J. Soil Res. 43, 525-531.

Holý, M. et al. (1984): Drainage constructions. SNTL/ALFA Praha, 472 p.

Doran, J. W., Parkin, T. B. (1996): Quantitative indicators of soil quality a minimum data set. In Doran, J.W and Jones, A. J., Eds., Method for assessing soil quality. Soil Sci. Soc. Am. Spec. Publ. 49. SSSA, Madison, WI.

Carter, M. R. (1988): Temporal variability of soil macro-porosity in a fine sandy loam under mouldboard ploughing and direct drilling. Soil Tillage Res. 12, 37–51.

Carter, M. R. (1990): Relative measures of soil bulk density to characterize compaction in tillage studies on fine sandy loams. Can. J. soil Sci. 70, 425–433.

Climate atlas ČSSR, Hydrometeorologický ústav Praha, 1961.

de Witt, N. M. M., McQueen, D. J. (1992): Compactibility Of Materials For Land Rehabilitation. DSIR Land Resources Scientific Report 7.

Jandák, J. et al. (2003): Pedology exercises. MZLU v Brně, ISBN 80-7157-733-2, 215 p.

Kňákal, P. (2000): Physical properties assessed on observated areas of basal monitoring of agricultural soils. Report ÚKZÚZ.

Kutílek, M. (1978): Water management pedology. SNTL, Praha. ISBN 04-721-78, 296 p.

Lhotský, J. et al. (1984): A set of measures for the fertilization of compacted soils]. Metodika ÚVTIZ 14/1984, 11–12.

Mapy.cz, (2015): Letecká mapa, Praha: Seznam.cz, a.s., www.basemap.at, Microsoft Corporation, OpenStreet Map, TopGis.

O'Connell, D. J. (1975): The measurement of apparent specific gravity of soils and its relationship to mechanical composition and plant root growth. Soil Physical Conditions and Crop Production. Tech. Bull. 29 MAFF, HMSO, London, 298–313.

Pokorný, E., Šarapatka, B., Hejátková, K. (2007): Assessment of soil quality in ecologically-farming company: methodical tool. Náměšť nad Oslavou: ZERA – Zemědělská a ekologická regionální agentura, 2007. ISBN 80-903-5485-8, 26 p.

Reynolds, W. D., Yang, X. M., Drury, C. F., Zhang, T. Q., Tan, C. S. (2003): Effects of selected conditioners and tillage on the physical quality of a clay loam soil. Can. J.

Soil Sci. 83, 318–393.

Reynolds, W. D., Drury, C. F., Yang, X. M., Fox, C. A., Tan, C. S., Zhang,T. Q. (2007): Land management effects on the near-surface physical quality of a clay loam soil. Soil and Tillage Res. 96, 316–330.

Topp, G. C., Reynolds, W. D., Cook, F. J., Kirby, J. M., Carter, M. R. (1997): Physical attributes of soil quality. In: Gregorich, E. G., Carter, M. R. (Eds.). Soil Quality for Crop Production and Ecosystem Health. Developments in Soil Science, vol. 25. Elsevier, New York, NY, 21–58.

Ing. Ivana Kameníčková, Ph.D.
Ing. Šárka Schneiderová
Ing. Kateřina Suchá
Institute of Landscape Water Management
Brno University of Technology
Faculty of Civil Engineering
Veveří 95, 662 37 Brno
Czech Republic
E-mail: kamenickova.i@fce.vutbr.cz

DOI: 10.31577/ahs-2019-0020.02.0025

ACTA HYDROLOGICA SLOVACA

Volume 20, No. 2, 2019, 204–209

SOYBEAN YIELD AND SEED QUALITY UNDER MODERATE DROUGHT STRESS AS AFFECTED BY P FERTILIZER

Oqba Basal, András Szabó

Providing nutritional sources is crucial in order for plants to achieve optimum yield and quality of the produced yield; this becomes more important under stress conditions, to which drought belongs, representing one of the mainly increasing abiotic stresses. P fertilizer has a special role in enhancing the rooting system of plants, which might help in overcoming negative drought influence by enhancing water and nutrient uptake. Soybean is classified as a drought-sensitive legume, providing cheap source of both protein and oil. To evaluate the influence of P fertilizer on soybean yield and quality under moderate drought, an experiment was conducted in 2018 by applying three P fertilizer rates (0, 45 and 90 kg ha^{-1} of P_2O_5) to soybean (cv. Boglár) under two irrigation regimes; irrigated and moderate-drought-stressed regimes. Results showed that drought had negative effects on both yield and oil concentration; however, P application could alleviate drought's effects by enhancing both traits, moreover, it could enhance these traits when drought was waived off as well. P application had very small effect on protein concentration which was significantly higher under moderate drought conditions. Applying relatively-high rate of P could further increase oil concentration compared to lower P rate, however, it did not enhance yield or protein concentration. It was concluded that applying P fertilizer has positive effects on both yield and seed quality of soybean, especially under moderate drought, however, higher rate of P fertilizer had little influence on oil concentration only.

KEY WORDS: drought stress; irrigation regimes; P fertilizer; seed quality; soybean; yield

Introduction

Soybean (*Glycine max* (L.) Merrill) is among the most grown crops worldwide (He et al., 2017), and the most widely grown seed legume that provides an inexpensive source of protein (Hao et al., 2013), in addition to being the most widely grown oilseed crop (Cerezini et al., 2016).

One of the major abiotic stresses affecting soybean plants is drought stress (Fan et al., 2013) as soybean is widely sown under rain fed conditions that are noticeably influenced by the current global climatic changes. Soybean is highly sensitive to drought, especially during the reproductive stages (Sinclair and Serraj, 1995; Brevedan and Egli, 2003; Oya et al., 2004). At this period, drought stress reduces pod number and accelerates leaf senescence, shortens seed-filling period and results in smaller and lighter seeds (Frederick et al., 2001; Egli and Bruening, 2004; Liu et al., 2004; Manavalan et al., 2009). The annual soybean yield reductions caused by drought are enormous (Sinclair et al., 2007; Sincik et al., 2008), reaching up to 40% (Manavalan et al., 2009). Under drought stress conditions, P can enhance vegetative development, net photosynthetic rate, carbohydrate metabolism, root morphology and P uptake which, in part, positively affects seed number and size and, consequently, seed yield (Gutierrez-Boem and Thomas, 1999; Garg et al., 2004; Jin et al., 2006).

Phosphorus (P) is one of the most important limiting nutrients in plant growth and production (Elser et al., 2007); it plays an important role in chloroplast composition and in photosynthesis (Hernández and Munné-Bosch, 2015). Soybean is a Phosphorus-dependent crop, and proper applied rates of phosphorus improve physiological characteristics and enhance nutrient uptake and production (Yan et al., 1995), consequently, deficiency in available phosphorus in the soil results in limitations in soybean development and final yield (Suman and Singh, 1985; Wissuwa, 2003).

It was previously reported that phosphorus application enhanced mean plant height (Dadson and Acquaah, 1984), photosynthesis (Robson et al., 1981), node number per plant and pod number per plant (Dadson and Acquaah, 1984), dry matter accumulation (Hu et al., 2002; Dong, 2009), biomass and P uptake (Goswami et al., 1999; Andraski and Bundy, 2003) and yield (Hu et al., 2002; Dong, 2009). The positive role of P in plant's growth and development was differently justified; Xue et al. (2014) concluded that suitable P concentrations

resulted in distributing dry matter more effectively in the pods of the soybean plants, which resulted in yield enhancement, whereas Ankomah et al. (1996) reported that the positive effect of added P on cowpea grain yield was most probably due to its role in increasing nodules mass and consequently the amount of fixed N_2; this was confirmed by the findings of Al-Chammaa et al. (2014) who reported quantities of N derived from atmosphere through fixation process to increase from 30.3 kg N ha^{-1} when P fertilizer was not applied to 35.6 and 37.2 kg N ha^{-1} when 40 and 80 kg ha^{-1} P, respectively, were applied to soybean plants. Also for beans, P fertilizer resulted in consistent responses in grain yield (Hungria et al., 2000).

Furthermore, Zheng et al. (2009) concluded that enhanced rates of P in the fields with lower soybean yields were the most practice needed for increasing soybean yield. Applying P fertilizer to soybean in a soybean-maize rotation cropping system lead to high biomass and grain yield of soybean, and also to better performance of the subsequent maize crop (Kihara et al., 2010; Vandamme et al., 2014). However, excessive P rates negatively-affected soybean development (Cai et al., 2004).

Zheng et al. (2009) concluded that applying P fertilizer under drought stress conditions can alleviate yield reduction resulted from N_2 fixation decline as P stimulates biological N_2 fixation and increases N accumulation in seeds (Graham and Vance, 2000; Ogoke et al., 2003). Zheng et al. (2015) investigated the different factors that affects soybean yield variability in Hailun County, China; the number of the analyzed fields was 101 in 2009 and 109 in 2010; they reported that available P in the soil was the most important soil variable controlling yield variations in both years. Although some controlled-chamber studies focused on P ability to alleviate soybean yield-loss under drought conditions (e.g. Gutierrez-Boem and Thomas, 1999; Jin et al., 2006), yet field experiments that investigated the combined effects of drought and phosphorus on soybean are scarce. The aim of our research was to investigate the influence of different phosphorus rates on both the yield and the seed quality of soybean (*cv. Boglár*) under irrigated and moderate drought-stressed regimes.

Material and methods

Soybean (*cv. Boglár*) was sown in Debrecen University's experimental site (Látókép) (N. latitude 47°33', E. longitude 21°27') on April 23rd and was harvested on September 20th, 2018. The soil type is calcareous chernozem, the 10-year-average annual precipitation (2001–2010) is 520.7 mm, whereas the precipitation between sowing and harvesting dates was 266.8 mm (Fig. 1).

Three P fertilizer rates; 0, 45 and 90 kg ha^{-1} P_2O_5 (0P, 45P and 90P, respectively) were applied under two irrigation regimes; moderate drought stress regime (accounting only on the precipitation as the only source of water supply) and irrigated regime (where an additional 50 mm of irrigation water was applied during full pod (R4) stage (Fehr and Caviness, 1977). Each treatment consisted of three replications.

The statistical analysis was made using SPSS (ver.25) software.

Results and discussion

The precipitation during the months of May and June, which were adequate to the vegetative stages V1 to V6 besides the blooming stages R1 and R2, was very close to the monthly average; however, a noticeable reduction (by 47.1%) in the precipitation amount happened during July where the plants were at full pod R4 stage (particularly between 8th and 15th, where only 4.8 mm of precipitation was recorded, so an additional 50 mm of irrigation water was provided to the irrigated plots on July 9th so the total water amount received was adequate to the monthly average).

On the other hand, August recorded higher precipitation amount than average (Fig. 1); plants, however, were at the beginning of full maturity stage (R7) by that time.

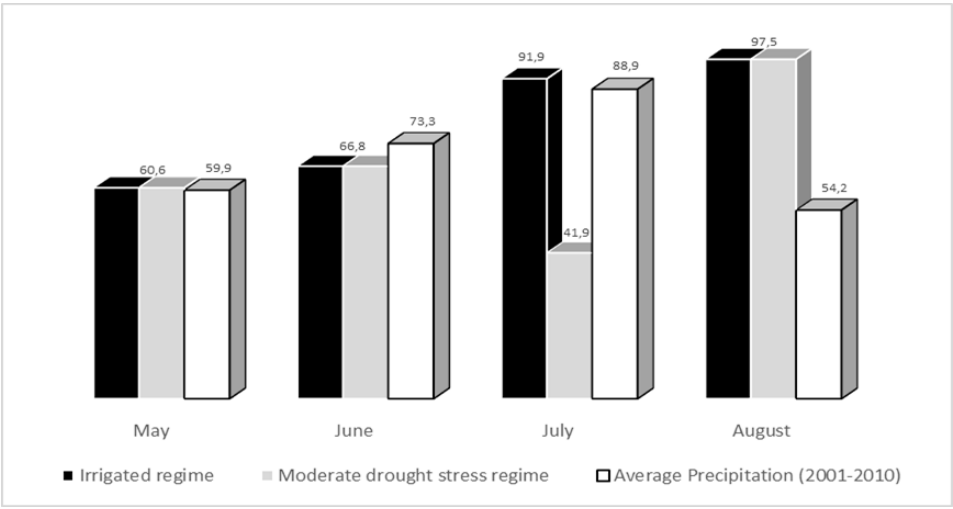

Fig. 1. Water amounts [mm] of both irrigation regimes in 2018 as compared to the average precipitation [mm] during (2001–2010) in Debrecen, Hungary.

Yield [t ha^{-1}]

Under drought stress, (45P) treatment resulted in significantly higher yield (4.47 t ha^{-1}) compared to (0P) (3.80 t ha^{-1}) treatment, however, increasing P rate to 90 kg ha^{-1} (90P) did not result in noticeable yield enhancement (4.50 t ha^{-1}) (Table 1). These results can lead to a conclusion that applying P fertilizer could alleviate the negative effect of drought stress on the yield.

Under irrigated regime, applying P fertilizer resulted in relatively better yield (5.13 and 5.23 t ha^{-1} for 45P and 90P treatments, respectively) compared to control (4.60 t ha^{-1}), however, the differences were insignificant (Table 1). Previously, Li et al. (2001) reported that the application of P fertilizer (in a rate of 33 kg ha^{-1}) resulted in an increase in soybean's seed yield by 6.7%. Similar conclusion was reported earlier (Dadson and Acquaah, 1984; Seneviratne et al., 2000). Al-Chammaa et al. (2014) recorded an increase by 7% and 12% in seed yield when P fertilizer was applied at rates of 40 and 80 kg ha^{-1}, respectively relative to control treatments (without P). Moreover, Aulakh et al. (2003) reported significant increases in seed yield as a result to direct application of P to soybean at rates up to 80 kg ha^{-1} (reaching 2.56 t ha^{-1}); however, higher rate of P (100 kg ha^{-1}) did not increase grain yield (2.53 t ha^{-1}).

Similar conclusions were also reported (Dong, 2000; Ogoke et al., 2003; Wang et al., 2006). In general, the high rates of P fertilizers do not always effectively-improve crop yield, as crops readily use only 10–45% of applied P (Adesemoye and Kloepper, 2009). In soybean, high P rates decrease nitrogen and protein accumulation in the seeds (Zheng et al., 2015), which is relatively demonstrated by our results on protein concentration under high P rate (Table 1), as N accumulation plays a key role in protein concentration in the seeds as reported by many papers (e.g. Rotundo and Westgate, 2009). Yield was significantly (<0.05), positively correlated with P rate (Table 2).

The effect of drought was obvious when no P fertilizer was applied (0P); the drought-stressed treatment resulted in significantly less yield (3.80 t ha^{-1} relative to 4.60 t ha^{-1} under irrigated regime). On the other hand, the irrigated plots which received P fertilizer were better than the drought-stressed counterparts, though the increases were insignificant (Table 1).

This comparison demonstrates the negative effect of drought stress on soybean yield, with an additional evidence of the ability of P fertilizer to reduce the negative influence caused by drought stress on soybean yield.

Many papers reported drought stress (regardless of its severity) to reduce soybean yield (e.g. Sadeghipour and Abbasi, 2012; Li et al., 2013; He et al., 2017). Also, it was previously reported that under drought stress conditions, the fields that received P fertilizer achieved greater yield than those that did not receive P fertilizer. Similarly, many papers reported that applying P fertilizer can enhance drought tolerance in soybean (Gutierrez-Boem and Thomas, 1999; Jin et al., 2006).

Under severe drought stress in 2007 in China, applied P rate to a study area of 43 fields was the most important factor in determining yield; applying lower P rate resulted in an average yield of 2.13 t ha^{-1}, whereas higher P rate increased the average yield to 2.65 t ha^{-1}; it accounted for 60.6% of the total variation in yield (Zheng et al., 2009). Yield was significantly (<0.05), positively correlated with irrigation regime (Table 3).

Table 1. The effect of different P fertilizer rates on yield [t ha^{-1}], protein concentration [%] and oil concentration [%] of soybean (*cv. Bolgár*) under two irrigation regimes

Trait	Moderate Drought Stress Regime			Irrigated Regime		
	0P	45P	90P	0P	45P	90P
Yield [t ha^{-1}]	3.80^{b2}	4.47^{a1}	4.50^{a1}	4.60^{a1}	5.13^{a1}	5.23^{a1}
Protein Concentration [%]	39.7^{a1}	40.6^{a1}	40.3^{a1}	33.6^{a1}	34.0^{a2}	33.6^{a2}
Oil Concentration [%]	21.8^{b2}	22.8^{ab2}	24.2^{a1}	23.5^{b1}	24.8^{ab1}	25.2^{a1}

- Same letter indicates no significant difference at .05 level among P rates within certain irrigation regime.
- Same number indicates no significant difference at .05 level between the two irrigation regimes within certain P rate.

Table 2. Correlation of P fertilizer treatment with yield, protein concentration and oil concentration under irrigated and moderate drought-stressed regimes

Trait	Moderate Drought Stress Regime	Irrigated Regime
Yield [t ha^{-1}]	.788*	.724*
Protein Concentration [%]	.161	.009
Oil Concentration [%]	.853**	.923**

- *. Correlation is significant at the 0.05 level (2-tailed).
- **. Correlation is significant at the 0.01 level (2-tailed).

Table 3. Correlation of irrigation regime treatment with yield, protein concentration and oil concentration under different rates of P fertilizer

Trait	0P	45P	90P
Yield [t ha^{-1}]	.902*	.891*	.851*
Protein Concentration [%]	-.883*	-.947**	-.904*
Oil Concentration [%]	.923**	.969**	.613

- *. Correlation is significant at the 0.05 level (2-tailed).
- **. Correlation is significant at the 0.01 level (2-tailed).

Protein Concentration [%]

Under both irrigation regimes, protein concentration was insignificantly enhanced in (45P) treatments, whereas (90P) treatments resulted in a very slight decrease (compared to 45P treatments) (yet they were better than 0P treatments) (Table 1). Dadson and Acquaah (1984) concluded that P application has lead, in general, to increased protein concentration in the seeds. Idris (1987) reported increased N accumulation in Lucerne (*Medicago sativum* L.) plants as a response to P application, which, in part, will lead to increased protein concentrations. The correlation with P rate was very small an insignificant (Table 2).

The effect of drought was more obvious; the drought-stressed plots resulted in better protein concentration relative to irrigated counterparts. Moreover, the increase was significant when P was applied (regardless of rate), whereas it was noticeable, yet not significant, when P was not applied (Table 1). These results suggest that drought has a major positive effect on protein concentration. Increased protein concentration under drought stress compared to well-irrigated counterpart was previously reported in many papers (e.g. Bellaloui and Mengistu, 2008; Rotundo and Westgate, 2009; Wang and Frei, 2011). This increase was explained in some reports as a result to a reduction in seed number associated with an increase in seed size (Borras et al., 2004), whereas other papers concluded it to be caused by drought stress rapidly remobilizing nitrogen from leaves to seeds (Brevedan and Egli, 2003) which leads to enhanced protein concentration. The correlation with irrigation regime was significantly negative under all P rates (Table 3).

Regardless of P application or rate, the decrease of yield, caused by drought stress, was accompanied by an increase in protein concentration (Table 1). Previously, Liang et al. (2010) reported that high protein concentration is negatively correlated with the yield in most cases; same conclusion was demonstrated later (Miransari, 2016).

Oil Concentration [%]

Under both irrigation regimes, applying P fertilizer noticeably enhanced oil concentration in the seeds; more particularly, (45P) treatment resulted in better oil concentration relative to (0P) treatment, and further increase of P rate (90P) resulted in further increase in oil concentration, and though this increase was insignificant relative to the (45P) treatment, yet it was significantly better as compared to the (0P) counterpart treatments (Table 1). Our results are consistent with those of Costache and Nica (1968) and Dadson and Acquaah (1984) who concluded that increasing P rate significantly increased oil concentration in the seeds. The correlation with P rate was highly significant (<0.01) (Table 2).

The effect of drought on oil concentration was also measurable regardless of P application and rate; irrigation significantly increased oil concentration for both (0P) and (45P) treatments, whereas the increase was insignificant when applying higher P rate (90P) (Table 1). Results of many studies indicated that drought stress reduced oil concentration in soybean seeds (e.g. Bellaloui and Mengistu, 2008; Maleki et al., 2013). Oil concentration correlation with irrigation regime was highly significant (< 0.01) under (0P) and (45P) rates and insignificantly positive under (90P) rate (Table 3).

Our results showed a negative relationship between oil and protein concentrations; the increase in oil concentration was accompanied by a reduction in protein concentration (Table 1). Chung et al. (2003) and Miransari (2016) reported similar conclusion.

Conclusion

Drought stress had noticeable effects on soybean; it resulted in reducing the yield to distinctive levels; however, it increased protein concentration and slightly decreased oil concentration. P fertilization had positive effects on both yield and seed quality of soybean; its influence was more obvious on the yield and the oil concentration. Moreover, P fertilization was extremely important and useful under drought stress conditions as it could alleviate the negative effects on the yield. However, high rate of P fertilizer did not lead to significant increases in soybean's yield and seed quality as compared to moderate rate. An extension of this research to involve different drought stress severities during different stages of soybean's vegetative period will provide more accurate data and more understanding of the different reactions of soybean plants to P under drought stress conditions. In addition, involving both physiological and production traits will provide even more integrated data on how drought stress affects soybean's development and final yield and seed quality.

Acknowledgement

The work/publication was supported by the EFOP-3.6.3-VEKOP-16-2017-00008 project. The project was co-financed by the European Union and the European Social Fund.

References

Adesemoye, A. O., Kloepper, J. W. (2009): Plant-microbes interactions in enhanced fertilizer-use efficiency. Appl Microbiol Biotechnol 85: 1–12

Al-Chammaa, M., Al-Ain, F., Khalifa, K. (2014): Growth and nitrogen fixation in soybean as affected by phosphorus fertilizer and sheep manure using ^{15}N isotopic dilution. Commun Soil Sci Plant Anal 45: 487–497

Andraski, T. W., Bundy, L. G. (2003): Relationships between phosphorus levels in soil and in runoff from corn production systems. Journal of Environ. Quality 32: 310–316

Ankomah, A. B., Zapata, F., Hadarson, G., Danso, S. K. A. (1996): Yield, nodulation, and N2 fixation by cowpea cultivars at different phosphorus levels. Biology and Fertility of Soils 22: 10–15

Aulakh, M., Pasricha, N., Bahl, G. (2003): Phosphorus fertilizer response in an irrigated soybean-wheat production system on a subtropical, semiarid soil. Field Crop Res 80: 99–109

Bellaloui, N., Mengistu, A. (2008): Seed composition is influenced by irrigation regimes and cultivar differences in soybean. Irrig Sci 26: 261–268

Borras, L., Slafer, G. A., Otegui, M. (2004): Seed dry weight response to source-sink manipulations in wheat, maize and soybean: a quantitative reappraisal. Field Crops Research 86: 131–146

Brevedan, R. E., Egli, D. B. (2003): Short periods of water stress during seed filling, leaf senescence, and yield of soybean. Crop Science 43: 2083–2088

Cai, B. Y., Zu, W., Ge, J. P. (2004): Influence on phosphorus amount to dry matter accumulation and distribution of different soybean cultivars. Soybean Science 23: 73–280

Cerezini, P., Kuwano, B., Santos, M., Terassi, F., Hungria, M., Nogueira, M. A. (2016): Strategies to promote early nodulation in soybean under drought. Field Crops Research 196: 160–167

Chung, J., Babka, H. L., Graef, G. L., Staswick, P. E., Lee, D. J., Cregan, P. B., Shoemaker, R. C., Specht, J. E. (2003): The seed protein, oil, and yield QTL on soybean linkage group I. Crop Science 43 (3): 1053–1067

Costache, D., Nica, O. (1968): Protein and oil content of soybeans as affected by variety, fertilizers, and nutritive environment. Lucr. Stiint. Inst. Agron. Bucuresti Ser. A 11, 113–147. Field Crop Abstracts 22: 1255

Dadson, R. B., Acquaah, G. (1984): *Rhizobium japonicum*, nitrogen and phosphorus effects on nodulation, symbiotic nitrogen fixation and yield of soybean (*Glycine max* (L.) Merill) in the southern savanna of Ghana. Field Crops Res 9: 101–108

Dong, Z. (2000): Soybean yield physiology. China Agriculture Press, Beijing. (in Chinese)

Dong, Z. (2009): Yield Physiology on Soybean. China Agriculture Press, Beijing. pp. 63-115 (in Chinese)

Egli, D. B., Bruening, W. P. (2004): Water stress, photosynthesis, seed sucrose levels and seed growth in soybean. Journal of Agricultural Science 142: 1–8

Elser, J. J., Bracken, M. E. S., Cleland, E. E., Gruner, D. S., Harpole, W. S., Hillebrand, H., Ngai, J. T., Seabloom, E. W., Shurin, J. B., Smith, J. E. (2007): Global analysis of nitrogen and phosphorus limitation of primary producers in freshwater, marine and terrestrial ecosystems. Ecol Lett 10: 1135–1142

Fan, X. D., Wang, J. Q., Yang, N., Dong, Y. Y., Liu, L., Wang, F. W., Wang, N., Chen, H., Liu, W. C., Sun, Y. P., Wu, J. Y., Li, H. Y. (2013): Gene expression profiling of soybean leaves and roots under salt, saline–alkali and drought stress by high-throughput Illumina sequencing. Gene 512: 392–402

Fehr, W. R., Caviness, C. E. (1977): Stages of soybean development. Special Report. 87. available online at: http://lib.dr.iastate.edu/specialreports/87.

Frederick, J. R., Camp, C. R., Bauer, P. J. (2001): Drought-Stress effects on branch and main stem seed yield and yield components of determinate soybean. Crop Sci 41: 759–763

Garg, B. K., Burman, U., Kathju, S. (2004): The influence of phosphorus nutrition on the physiological response of moth bean genotypes to drought. Journal of Plant Nutrition and Soil Science 167: 503–508

Goswami, S., Khan, R. A., Vyas, K. M. (1999): Response of soybean (*Glycine max*) to levels, sources and methods of phosphorus application. Indian Journal Agronomy 44: 126–129

Graham, P. H., Vance, C. P. (2000): Nitrogen fixation in perspective: an overview of research and extension needs. Field Crop Res 65: 93–106

Gutierrez-Boem, F.H., Thomas, G.W. (1999): Phosphorus nutrition and water deficits in field-grown soybeans. Plant and Soil 207: 87–96

Hao, L., Wang, Y., Zhang, J., Xie, Y., Zhang, M., Duan, L., Li, Z. (2013): Coronatine enhances drought tolerance via improving antioxidative capacity to maintaining higher photosynthetic performance in soybean. Plant Science 210: 1–9

He, J., Du, Y. L., Wang, T., Turner, N. C., Yang, R. P., Jin, Y., Xi, Y., Zhang, C., Cui, T., Fang, X. W., Li, F. M. (2017): Conserved water use improves the yield performance of soybean (*Glycine max* (L.) Merr.) under drought. Agric Water Manage 179: 236–245

Hernández, I., Munné-Bosch, S. (2015): Linking phosphorus availability with photo-oxidative stress in plants. J Exp Bot 66: 2889–2900

Hu, G.H., Zhang, J.X., Tang, C.Q. (2002): Growth Changing and Dry Matter Accumulation and Distribution in Spring Soybean. Xinjiang Agricultural Sciences, Beijing. 264–267 (in Chinese)

Hungria, M., Andrade, D. S., Chueire, L. M. O., Probanza, A., Guttierrez-Manero, F. J., Megias, M. (2000): Isolation and characterization of new efficient and competitive bean (Phaseolus vulgaris L.) rhizobia from Brazil. Soil Biol Biochem 32: 1515–1528

Idris, M. (1987): The effect of phosphorus and potash on the growth, nodulation and nitrogen fixing efficiency of lucerne (*Medicago sativum* L.). Pakistan Journal of Soil Science 2: 33–36

Jin, J., Wang, G. H., Liu, X. B., Pan, X. W., Herbert, S. J., Tang, C. X. (2006): Interaction between phosphorus nutrition and drought on grain yield, and assimilation of phosphorus and nitrogen in two soybean cultivars differing in protein concentration in grains. Journal of Plant Nutrition 29: 1433–1449

Kihara, J., Vanlauwe, B., Waswa, B., Kimetu, J. M., Chianu, J., Bationo, A. (2010): Stragetic phosphorus application in legume-cereal rotations increases land productivity and profitability in Western Kenya. Exp Agric 46: 35–52

Li, D., Liu, H., Qiao, Y., Wang, Y., Cai, Z., Dong, B., Shi, Ch., Liu, Y., Li, X., Liu, M. (2013): Effects of elevated CO_2 on the growth, seed yield, and water use efficiency of soybean (*Glycine max* (L.) Merr.) under drought stress. Agricultu-

ral Water Management 129: 105–112

Li, L., Sun, J. H., Zhang, F. S., Li, X. L., Yang, S. C., Rengel, Z. (2001): Wheat/maize or wheat/soybean strip intercropping. I. Yield advantage and interspecific interactions on nutrients. Field Crops Res 71: 123–137

Liang, H., Yu, Y., Wang, S., Yun, L., Wang, T., Wei, Y., Gong, P., Liu, X., Fang, X., Zhang, M. (2010): QTL Mapping of Isoflavone, Oil and Protein Contents in Soybean (*Glycine max* L. Merr.). Agricultural Sciences in China 9: 1108–1116

Liu, F., Jensen, Ch. R., Andersen, M. N. (2004): Pod Set Related to Photosynthetic Rate and Endogenous ABA in Soybeans Subjected to Different Water Regimes and Exogenous ABA and BA at Early Reproductive Stages. Annals of Botany 94: 405–411

Maleki, A., Naderi, A., Naseri, R., Fathi, A., Bahamin, S., Maleki, R. (2013): Physiological Performance of Soybean Cultivars under Drought Stress. Bull Env Pharmacol Life Sci 2 (6): 38–44

Manavalan, L. P., Guttikonda, S. K., Tran, L. S. P., Nguyen, H. T. (2009): Physiological and Molecular Approaches to Improve Drought Resistance in Soybean. Plant and Cell Physiology 50: 1260–1276

Miransari, M. (2016): Soybeans, Stress, and Nutrients. in Mohammad Miransari (Eds.), Environmental Stresses in Soybean Production. Soybean Production Volume 2 (273–298). Chippenham: Nikki Levy

Ogoke, I. J., Carsky, R. J., Togun, A. O., Dashiell, K. (2003): Effect of P fertilizer application on N balance of soybean crop in the guinea savanna of Nigeria. Agric Ecosyst Environ 100: 153–159

Oya, T., Nepomuceno, A. L., Neumaier, N., Farias, J. R. B., Tobita, S., Ito, O. (2004): Drought Tolerance Characteristics of Brazilian soybean cultivars – Evaluation and characterization of drought tolerance of various Brazilian soybean cultivars in the field. Plant Production Science 7: 129–137

Robson, A. D., O'Hara, G. W., Abbott, L. K. (1981): Involvement of phosphorus in nitrogen fixation by subterranean clover (*Trifolium subterranean* L.). Australian Journal of Plant Physiology 8: 427–436

Rotundo, J. L., Westgate, M. E. (2009): Meta-analysis of environmental effects on soybean seed composition. Field Crop Res 110: 147–156

Sadeghipour, O., Abbasi, S. (2012): Soybean Response to Drought and Seed Inoculation. World Applied Sciences Journal 17 (1): 55–60

Seneviratne, G., Van Holm, L. H. J., Ekanayake, E. M. S. (2000): Agronomic benefits of rhizobial inoculants use over nitrogen fertilizer application in tropical soybean. Field Crops Research 68: 199–203

Sincik, M., Candogan, B. N., Demirtas, C., Büyükacangaz, H., Yazgan, S., Gksoy, A. T. (2008): Deficit irrigation of soybean [Glycine max (L.) Merr.] in a sub-humid climate. J Agron Crop Sci 194: 200–205

Sinclair, T., Serraj, R. (1995): Legume Nitrogen-Fixation and Drought. Nature 378: 344

Sinclair, T. R., Purcell, L. C., King, C. A., Sneller, C. H., Chen, P., Vadez, V. (2007): Drought tolerance and yield increase of soybean resulting from improved symbiotic N2 fixation. Field Crops Res 101: 68–71

Suman, B., Singh, O. S. (1985): Response of lentil to VA mycorrhizal inoculation and plant available P levels of unsterile soils. Plant and Soil 87: 445–447

Vandamme, E., Pypers, P., Vanlauwe, B., Baijukya, F., Smolders, E., Merckx, R. (2014): Residual phosphorus effects and nitrogen x phosphorus interactions in soybean–maize rotations on a P-deficient Ferralsol. Nutr. Cycle Agroecosyst 98: 187–201

Wang, J. G., Li, Z. L., Li, W. B., Li, X., Li, Y. L., Li, C. J. (2006): Application of phosphorus in relation to soybean yield and quality. System Sciences and Comprehensive Studies in Agriculture 1: 55–57. (In Chinese)

Wang, Y., Frei, M. (2011): Stressed food – The impact of abiotic environmental stresses on crop quality. Agriculture, Ecosystems and Environment 141: 271–286

Wissuwa, M. (2003): How do plants achieve tolerance to phosphorus deficiency? Small causes with big Effects. Plant Physiology 133: 1947–1958

Xue, A. O., Guo, X. H., Qian, Z. H. U., Zhang, H. J., Wang, H. Y., Han, X. R., Zhao, M. H., Xie, F. T. (2014): Effect of phosphorus fertilization to P uptake and dry matter accumulation in soybean with different P efficiencies. J Integr Agric 13: 326–334

Yan, X. L., Beebe, S. E., Lynch, J. P. (1995): Phosphorus efficiency in common bean genotypes in contrasting soil types II. Yield response. Crop Science 35: 1094–1099

Zheng, H., Chen, L., Han, X., Zhao, X., Ma, Y. (2009): Classification and regression tree (CART) for analysis of soybean yield variability among fields in Northeast China: The importance of phosphorus application rates under drought conditions. Agriculture, Ecosystems & Environment 132 (1–2): 98–105

Zheng, H.F., Chen, L.D., Yu, X.Y., Zhao, X.F., Ma, Y., Ren, Z.B. (2015): Phosphorus control as an effective strategy to adapt soybean to reproductive-stage drought: Evidence from field experiments across Northeast China. Soil Use & Management 31: 19–28

Oqba Basal, PhD student,
Dr. András Szabó, PhD., Lecturer,
Institute of Crop Sciences,
University of Debrecen,
4032 Böszörményi road 138/A
E-mail: oqba@agr.unideb.hu;
oqbabasal@gmail.com
szabo@agr.unideb.hu

DOI: 10.31577/ahs-2019-0020.02.0026

ACTA HYDROLOGICA SLOVACA

Volume 20, No. 2, 2019, 210–217

THE MIGRATION OF POTENTIALLY TOXIC ELEMENTS DURING THE RECULTIVATION OF THE URANIUM MINING DEPOSIT IN MECSEK

Lamlile Khumalo, György Heltai, Márk Horváth

The ecological risk caused by the potential migration of potentially toxic elements (PTEs) during the recultivation of the abandoned uranium mining deposit in Mecsek in Hungary was estimated by developing a sample strategy. To study the effectiveness of soil covering layer in retardation of migration of PTEs (Ca, Cd, Co, Cr, Cu, Fe, K, Mg, Mn, Na, Ni, P, Pb, and Zn) on the covering soil of deposit No.1, sampling locations were selected based on the results of the running monitoring program at the deposit No.1, where erosion wounding occurred during the recultivation. Top to bottom soil core samples (0–25, 25–50, 50–75 and 75–100 cm depths) and covering plant (grass) samples were taken and analyzed using Inductively Coupled Plasma – Optical Emission Spectrometer. Overall the results of the soil samples collected indicated that there is a possibility of migration of PTEs as water infiltrates from the top to the bottom of the deposit. Transfer factor, TF ≥1 for Cu might be an indication of trace elements' availability to be taken up by the plants. The fractionation by sequential extraction of PTEs is still in progress which should give more information on their migration.

KEY WORDS: uranium mining, potentially toxic elements, migration, soil, plants

Introduction

Mecsek mine produced 21,000 t of uranium until it was shutdown in 1997 due to being uneconomical (Wallner and Stein, 2012; Malovics, 2014). In 2006, there was a feasibility study of restarting uranium mining in the Mecsek Hills near Pécs in Hungary (Malovics, 2014). Uranium mining poses some unique risks due to the presence of radioactive substances and co-occurring minerals which can contain potentially toxic elements (PTEs) (Sahoo et al., 2014; National Research of The National Academies, 2012). Pollution by PTEs is a significant issue owing to their transport to soils, biota, and water streams (Soltani et al., 2017). The natural weathering is considered to be significantly responsible too for elevated trace metals concentrations in soils (Fite and Leta, 2015). Soils of abandoned mining sites pose a serious environmental threat because of potential mobility of pollutants including PTEs creating a risk of groundwater contamination and health hazards for animals and humans by food chain (Gałuszka et al., 2016; Nazir et al., 2015). Elevated acidity contributes to increasing the mobility of PTEs in aqueous solution, including uranium, as well as copper, arsenic, cadmium (Skipperud and Salbu, 2015). It is important to take into consideration effects such as the chemical toxicity of PTEs and PTE-species (IAEA, 2004; Pérez-Moreno et al., 2018). Regulatory standards for PTE levels in soils have been established, but wide discrepancy exists among different countries regarding the critical value of each contaminant (He et al., 2015). This is relevant in order to better predict the risks of uranium mining discharges in more common and ecologically significant scenarios (Reis et al., 2018).

The present research is joining the large monitoring program that is currently running at abandoned and recultivated Mecsek uranium mine in Pécs. Every three to five years, samples are being taken from all spoil banks and from covering soil to monitor radionuclide migration. The main aim of present research is to study the effectiveness of soil covering layer in retardation of migration of PTEs on the covering soil of deposit No.1 and to estimate the potential risk caused by the migration of PTEs on the environment. During the formation of soil covering, there was an erosion wounding occurrence. To follow the long-term effect of uranium mining, an appropriate additional sampling strategy is developing. Soil and plant samples were collected from the top and the bottom of the slope of this spoil deposit. For this purpose, it is necessary to analyze PTEs and their solubility under given geochemical conditions. Hence, the total soluble PTE concentrations and solubility fractions will be determined by sequential extraction. This is a preliminary step of an extensive study, the research is still in progress. The determination of total soluble element concentration for three classes of

elements; macronutrients (Ca, K, P, and Mg), micronutrients (Co, Na, Fe, Cu, Ni, Mn, and Zn) and toxic elements (Cd, Cr, and Pb) in soil and plant samples were completed. However, the total concentration of PTEs often does not accurately represent their characteristics and toxicity (Okoro et al., 2017). Therefore, evaluation of the individual fractions to which the metals are bound is necessary to fully understand their actual and potential environmental effects. For this reason, fractionation by sequential extraction of PTEs is still in progress.

Material and methods

Sampling in Mecsek uranium deposit No.1

Soil and covering plant (grass) samples were collected on the 11th of July 2018 from four sampling points in Mecsek uranium mine deposit No.1 in Pecs, South-west of Hungary: (1) at the top of the deposit – Rn-M11, (2) on the slope of the deposit – Rn-M12, (3) at the bottom field – Rn-M13 and (4) at the bottom edge of the slope of the deposit – radioactive point. For simple reference, the samples were renamed as M11 for Rn-M11, M12 for Rn-M12, M13 for Rn-M13 and RA for radioactive point. The radioactive point was chosen based on the knowledge of its high gamma dose rate ranging between 100 and 200 nGy h^{-1} to give an indication of whether PTE concentrations would also be high on this location. Deposit No.1 was covered with a different type of soils taken from various locations. Underneath the soil covering layer, there were natural rocks.

Sampling and sample preparation for total trace element determination

Plant samples were collected by cutting from the surface of the plants with a knife from the same locations where soil samples were collected (M11, M12, M13 and RA) to determine if there is any biological uptake of radioactivity and PTEs from the soil. Plant sample collected from the radioactive location was divided into two portions, one half was washed in a shower for 5 minutes to simulate the rain. Plant samples were air-dried and grinded before microwave digestion preparation.
Soil samples were collected using a hand auger instrument labeled with different measurements. Each soil core sample was taken from different depths: 0–25 cm, 25–50 cm, 50–75 cm and 75–100 cm. For M11, 75–100 cm depth could not be sampled as this was hard rock. Radioactive soil was only sampled from the top layer. All samples collected were carefully placed in clean polyethylene bags before transported to the laboratory.
Soil samples were homogenized and grinded using Retch SM 100 with a 0.25 mm sieve instrument.

Determination of soil moisture content

Approximately 25 g of soil samples were dried at 105°C for 72 hours, cooled and weighed for the determination of the soil moisture content.

Soil and plant sample preparation using microwave digestion and analysis method according to Hungarian Standard MSZ 21470-50:2006 6 chapter

0.5 g of homogenized plant samples were weighed into the Teflon vessel using an analytical balance. 5 mL of nitric acid (65% Merck), 6 mL of hydrogen peroxide (30% Emsure®) and approximately 9 mL of distilled water were added into the Teflon vessel containing the samples, to make it up to 20 mL. Whereas, 0.5 g of homogenized soil samples were weighed into the Teflon vessel using an analytical balance. 5 mL of nitric acid (65% Merck), 3 mL of hydrogen peroxide (30% Emsure®) and approximately 2 mL of distilled water were added into the Teflon vessel containing the samples, to make it up to 10 mL. The reaction could subside completely before capping the vessels.
The microwave digestion vessels containing samples were assembled together and placed in a CEM Mars 5 Xtraction 230/60 Microwave Accelerated Reaction System 907501. The microwave digestion system was set at the following parameters: Ramp time – 20 minutes (450 Psi or 180°C), Hold time – 18 minutes, Still time – 5 minutes (0 Watt), Hold time – 10 minutes (800 Watt, 450 Psi and/or 180 °C) and Cooling time – 20 minutes.
When the digestion was completed, each sample was filtered using a 90 mm Filter Discs (Quant.) Grade: 389 into a 25 mL volumetric flask and made up to 25 mL with distilled water. Each sample was physically homogenized by shaking it and transferred into a centrifuge tube for the trace element analysis.

Elemental analysis

Ca, Cd, Co, Cr, Cu, Fe, K, Mg, Mn, Na, Ni, P, Pb, and Zn content of digested solutions were determined by a HORIBA Jobin Yvon ACTIVA M Inductively Coupled Plasma – Optical Emission Spectrometer (ICP-OES) using operation parameters proposed by the manufacturer and yttrium internal standard.

The soil/plant transfer factor (TF) determination

The soil/plant transfer factor (TF) was calculated using Formula 1 to determine the possibility of the trace elements being taken up from the soil by the plants. The TF was calculated only from the total concentrations obtained from the 0–25 depth of soil sample because the grass does not have deep roots to reach a deeper level of the soil. The higher the value of the TF, the more mobile/available the trace metal is (Intawongse et al., 2007; Lato et al., 2012). According to (Fite and Leta, 2015), if the TF ratios >1, the plants have accumulated elements, the TF ratios approximately 1 indicate that the plants are not influenced by the elements, and if the TF ratios <1, it is the indication that plants avoid the elements from the uptake.

Soil/Plant Transfer Factor:

$$TF = C_{plant} / C_{soil} \quad (1)$$

where
C_{plant} – concentration of an element in the plant material
C_{soil} – total concentration of the same element in the soil where the plant was grown.

Meteorological conditions

The average precipitation at Pécs was calculated based on the meteorological data extracted from the Website (https://www.ksh.hu/docs/eng/xstadat/xstadat_annual/i_met002c.html) of the Hungarian Central Statistical Office. The average precipitation was calculated from 1997 when the mine was shut down to 2018 when sampling took place. The average precipitation was 674 mm with a minimum of 405 mm in 2011 and the maximum of 981 mm in 2014. The groundwater level at the time of sampling 2018 was at 160 m from the Balti line.

Results and discussion

Total soluble element concentrations in soil

The results obtained from this study were compared to the Hungarian Regulation and World Health Organization (WHO) permissible limits of elements in soil and plants. The results of the element analysis in soil samples are presented in three different figures. These results are presented according to the elemental importance in soil e.g. macronutrients, micronutrients, and toxic elements. Macronutrients (Ca, K, Mg, and P) and Fe are presented in Figure 1. Iron is an essential micronutrient, however, within soils and plants, it is not toxic because its average concentration is generally greater than 100 mg kg^{-1} (Hooda, 2014), hence its placement with macronutrients in Figure 1. Iron may be the most difficult element to make available in the soil for plants because it is needed in relatively large amounts and soil chemical processes sometimes quickly make it unavailable (Lohry, 2007).

Plants require essential macronutrients (such as N, P, K, Ca, and Mg) and micronutrients (such as Fe, Zn, Mn, Ni and Cu) from soil to grow and complete the cycle of life (Kabata-pendias and Pendias, 2001), therefore they are not included on the table of permissible limits of PTEs in plants and soil in Table 1. Soil concentrations for PTEs in dry weight were compared with soil toxic element contamination limit that is regulated by the Hungarian Government (6/2009. IV. 14. 2009) based on the regulation of other European (EU) member countries (Rékási and Filep, 2012). The WHO (1996) permissible limits for elements in the soil are included for reference in comparison of the Hungarian limits to the World's limits. Results for the micronutrients in the soil are presented in *Fig. 2*. The concentration levels for Co, Cu and Zn were within Hungarian limits of 30 mg kg^{-1}, 75 mg kg^{-1} and 200 mg kg^{-1} respectively, however Zn concentration for samples M11 at 50–75 cm was 60.52 ± 0.08 mg kg^{-1}, M13 at 0–25 mg $kg^{-1}$was 67.43 ± 0.12 mg kg^{-1}, at 25–50 was 58.92 ± 0.08 mg kg^{-1} and at 50–75 was 54.51 ± 0.12 mg kg^{-1}. These Zn concentrations were above the WHO limit of 50 mg kg^{-1} but they were still below the intervention level of 720 mg kg^{-1} (VROM, 2000). Nickel concentration levels for sample M12 at 25–50 cm and for RA sample were above the limits recommended for soil by Hungary (limit of 40 mg kg^{-1}), which were 53,47 ± 0.75 mg kg^{-1} and 40.54 ± 0.10 mg kg^{-1} respectively. However, these Ni concentrations were still within the allowed concentrations of 35–75 mg kg^{-1} recommended by the Commission of the European Communities (1986). The elevated concentration levels of Ni at sampling points M13 and RA might be an indication of the mobility of elements from the top of the deposit to the bottom part of the deposit. As indicated in Table 1, although micronutrients from the soil are essential for plant growth and development (Voss, 1998), high concentration levels can be toxic (Stanojković-Sebić et al., 2017).

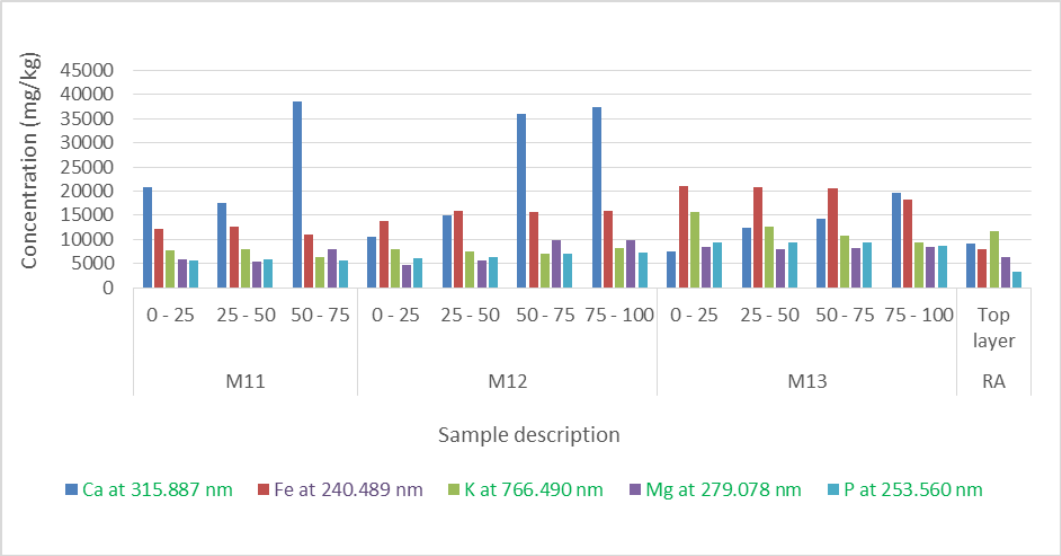

Fig. 1. Total concentration of Ca, Fe, K, Mg and P in soil samples.

Table 1. Permissible limits for PTEs in plant and soil

Trace elements	*[a]Target value of soil [mg kg^{-1}]*	*[b]Permissible value of plant [mg kg^{-1}]*	*[c]Concentration of elements in soil and contamination limit values [mg kg^{-1}]*	*[d]Allowed levels in soil [mg kg^{-1}]*	*[e]Intervention values [mg kg^{-1}]*
Cd	0.8	0.02	1	1 – 3	12
Co	-	-	30	-	240
Cr	100	1.3	75	100 – 150	380
Cu	36	10	75	50 – 140	190
Fe	-	-	-	-	-
Mn	-	-	-	-	-
Ni	35	10	40	35 – 75	210
Pb	85	2	100	50 – 300	530
Zn	50	0.6	200	150 – 300	720

[a]Target values are specified to indicate desirable maximum levels of elements in unpolluted soils (Denneman and Robberse 1990; Ministry of Housing, Netherlands, 1994).
[b]WHO permissible value of plant (WHO,1996; Adio, 2017).
[c]Contamination limit values for Hungarian soils (6/2009. IV. 14. 2009) (Rékási and Filep, 2012).
[d]Allowed levels in soil (Commission of the European Communities, 1986).
[e]Intervention values (Netherlands Ministry of Housing, Spatial Planning and the Environment (VROM), 2000).

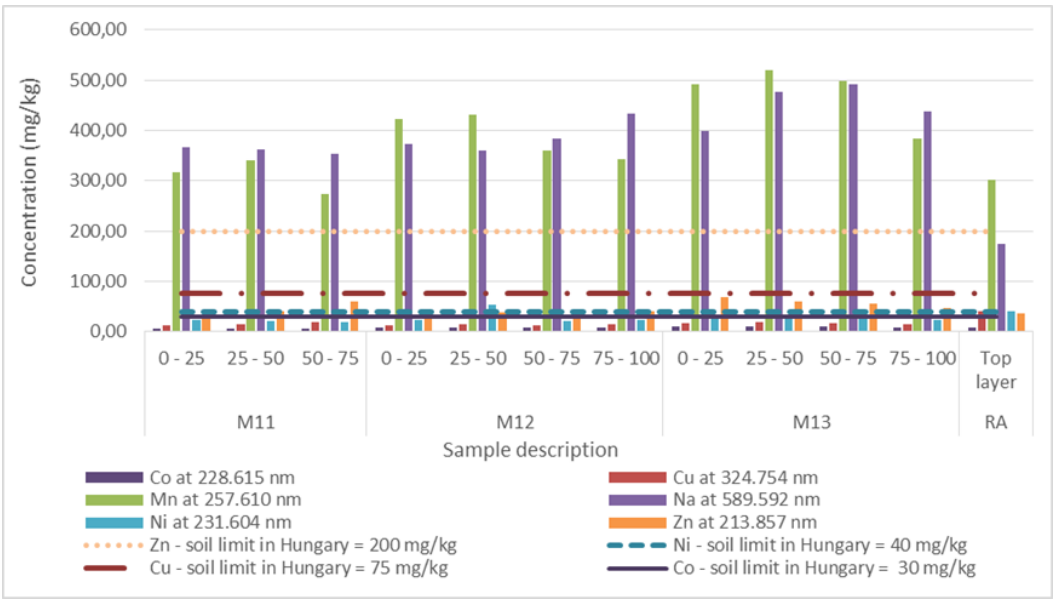

Fig. 2. Total concentration of Co, Cu, Mn, Na, Ni and Zn in soil samples.

The concentrations for toxic elements in the soil are obtained in Figure 3. The results for the analysis indicated that the soil from deposit No.1 did not contain Cd element and the Pb concentrations were below the Hungarian limits. Although Cr concentrations for sampling points M12 at 25–50 cm with 116 ± 0.36 mg kg^{-1} and RA with 127 ± 0.01 mg kg^{-1} were above the Hungarian limits of 75 mg kg^{-1}, these concentrations were still withing the allowed levels of 100–150 mg kg^{-1} (Commission of the European Communities, 1986). The elevated Cr concentrations in soils at the M12 and RA sampling locations might be an indication that plants did not take Cr from the soil.

ANOVA statistical analysis for the function of soil sampling points and different depths for each sample was determined, the results indicated that there was no significant difference among the means of concentrations for different depths for each sample and also for each of the sampling points at 95% confidence interval.

Element concentrations in plants

The results of the concentrations for the elements in plant samples are presented in Table 2. The concentrations for the elements in analyzed plants were compared to the WHO (1996) permissible limits for plants. Chromium results for the sample M11 with a concentration of 14.2 ± 0.02 mg kg^{-1} was observed to be above WHO (1996) limit of 1.3 mg kg^{-1}. This observation might be an indication that Cr was taken up by plant from the soil on

sampling point M1 which is located on top of the deposit. Copper concentrations for sampling points M12, M13, and RA (both unwashed and washed plant samples) were above the WHO permissible limit of 10 mg kg^{-1}. It was also observed that the concentrations for Cu increased as the topography changed from the top of the deposit to

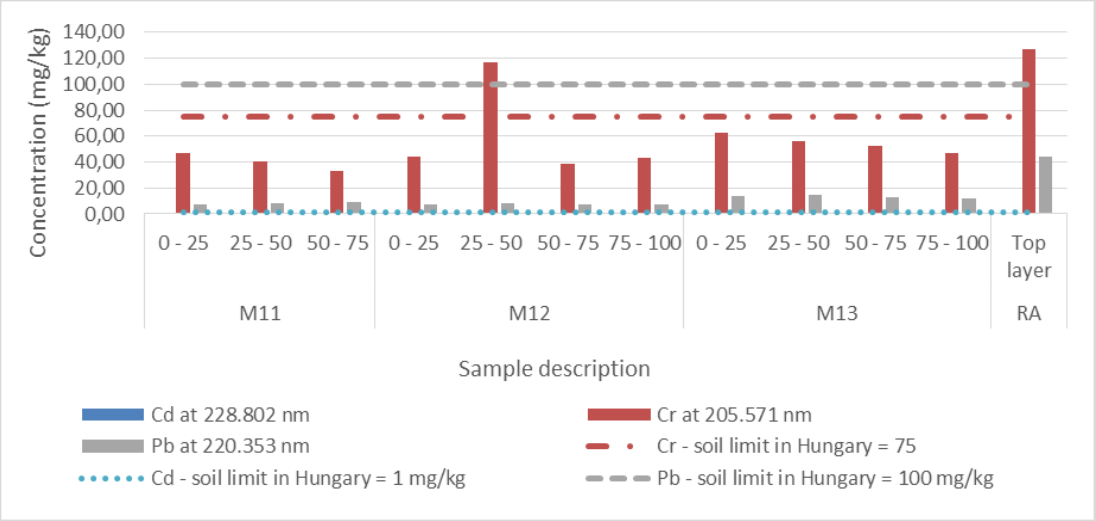

Fig. 3. Total concentration of Cr, Cd, and Pb in soil samples.

Table 2. Total concentrations for elements in plant samples

Element	*M11 Total Concentration [mg kg^{-1}]*	*M12 Total Concentration [mg kg^{-1}]*	*M13 Total Concentration [mg kg^{-1}]*	*Unwashed plant Total Concentration [mg kg^{-1}]*	*Washed plant Total Concentration [mg kg^{-1}]*	*Permissible value of plant (WHO, 1996) [mg kg^{-1}]*
Ca (315.887 nm)	5710 ± 54.26	4400 ± 15.61	2133 ± 11.94	5369 ± 0.43	5184 ± 43.05	-
Cd (228.802 nm)	0.00 ± 0.00	0.00 ± 0.00	0.00 ± 0.00	0.00 ± 0.00	0.00 ± 0.00	0.8
Co (228.615 nm)	0.00 ± 0.00	0.00 ± 0.00	0.00 ± 0.00	0.00 ± 0.00	0.00 ± 0.00	-
Cr (205.571 nm)	**14.2 ± 0.02**	0.00 ± 0.00	0.00 ± 0.00	0.00 ± 0.00	0.00 ± 0.00	1.3
Cu (324.754 nm)	5.89 ± 0.09	**18.3 ± 0.00**	**59.5 ± 0.11**	**21.7 ± 0.22**	**73.1 ± 0.17**	10
Fe (240.489 nm)	265 ± 3.60	94.93 ± 0.56	301 ± 2.01	52.39 ± 0.37	68.59 ± 0.35	-
K (766.490 nm)	7206 ± 20.60	7608 ± 151.90	8861 ± 27.63	13289 ± 12.76	14302 ± 5.50	-
Mg (279.078 nm)	1781 ± 13.81	1786 ± 8.77	785 ± 0.87	868 ± 7.44	925 ± 2.93	-
Mn (257.610 nm)	34.2 ± 0.13	21.5 ± 0.20	26.1 ± 0.50	3.68 ± 0.04	8.97 ± 0.10	-
Na (589.592 nm)	73.9 ± 0.53	43.0 ± 0.21	36.9 ± 0.43	33.5 ± 1.51	52.8 ± 0.50	-
Ni (231.604 nm)	5.48 ± 0.06	2.42 ± 0.02	0.00 ± 0.00	0.00 ± 0.00	0.00 ± 0.00	10
P (253.560 nm)	1411 ± 0.48	1150 ± 3.60	1307 ± 0.59	1489 ± 15.61	1631 ± 6.84	-
Pb (220.353 nm)	0.00 ± 0.00	0.00 ± 0.00	0.00 ± 0.00	0.00 ± 0.00	0.00 ± 0.00	2
Zn (213.857 nm)	**20.9 ± 0.05**	**9.41 ± 0.05**	**13.6 ± 0.05**	**8.87 ± 0.03**	**13.3 ± 0.39**	0.6

Results highlighted in bold, were above the permissible limits.

Table 3. Soil/Plant Transfer Factor (TF)

Trace elements	*M11*	*M12*	*M13*	*Active samples*
Ca 315.887	0.27	0.41	0.28	0.59
Cd 228.802	-	-	-	-
Co 228.615	0.00	0.00	0.00	0.00
Cr 205.571	0.30	0.00	0.00	0.00
Cu 324.754	0.52	**1.56**	**3.64**	0.54
Fe 240.489	0.02	0.01	0.01	0.01
K 766.490	0.93	0.95	0.56	**1.14**
Mg 279.078	0.30	0.39	0.09	0.14
Mn 257.610	0.11	0.05	0.05	0.01
Na 589.592	0.20	0.12	0.09	0.19
Ni 231.604	0.24	0.10	0.00	0.00
P 253.560	0.25	0.19	0.14	0.46
Pb 220.353	0.00	0.00	0.00	0.00
Zn 213.857	0.69	0.29	0.20	0.25

The TF values highlighted in bold are over the limit of 1.

the bottom of the deposit. The increase in Cu concentration at the bottom of the deposit might be an indication that Cu was transported down the slope of the deposit and have accumulated at the bottom of the deposit. Zinc concentrations for all the plant samples collected were above WHO permissible limits of 0.6 mg kg^{-1}. These results indicate that Zn may have been available from soil to be absorbed in large quantities by plant. Copper, Zn, Fe, Mn, and Ni are all more available at low pH levels than at high pH levels because metals are bound very tightly to the soil or exist in solid minerals at high pH (Jones and Jacobsen, 2001). When comparing the results for washed and unwashed plant samples collected from RA, there was no noticeable difference in concentration. This might be an indication that the concentrations of the elements obtained are not due to surface contamination but are due to biological uptake.

ANOVA statistical analysis for the function of plant sampling points was determined. The results indicated that there was no significant difference amongst the plant sampling points at a 95% confidence interval.

Plant/Soil transfer determination

To assess the availability/mobility of trace metals from soil to plant, TF ratios were calculated on dry weight for both plant and soil samples. The TF ratios are presented in Table 3.

The transfer factor (TF) ratios were calculated to determine the ability of a metal species to migrate from the soil into plant roots. Copper TF values indicated an increasing trend from the M11 with reported TF=0.52, M12 with TF=1.56 and to M13 with TF=3.64. This increasing trend might imply that there was a migration of Cu from the top of the deposit to the bottom of the deposit. Copper TF value for sampling points M12 and M13 were above the limit of 1, whereas the active sample reported the TF value of 1.14. This observation indicates that Cu and K trace metals are available to be taken up by plants (Intawongse et al., 2007, Agic et al., 2015).

Soil moisture content

The amount of water present in the soil was indicated by calculating the soil moisture content as indicated in Table 4. The results indicated that the soil sample which is located at the bottom of the deposit (M13) had the highest soil moisture content average of 14.94 % compared to M11 and M12 with the averages of 9.76 % and 8.77 % respectively. This observation might be an indication that water containing PTEs might be infiltrated through the soil from the top of the deposit to the bottom of the deposit.

Conclusion

Most elemental concentrations in soil samples collected from deposit No.1 were lower than the contamination limit values for Hungarian soils and within the permissible limits. The results for micronutrients indicated that there was a trend on the increase of concentrations of elements as the slope of the deposit decreased. Soil samples collected from the top of the deposit (M11) contained less average concentration followed by the sample collected from the slope (M12) and the sample collected from the bottom of the deposit (M13) had the highest average concentration. This observation might be an indication that there is a possibility of migration of these elements. The results for M13 were observed to have the combination of highest average for both soil moisture content PTE concentrations. This might be an indication that there is possibility of water infiltrating through the deposit while migrating PTEs.

The results for plant analysis indicated that Cu, Zn and Cr were above the WHO limits of 10 mg kg^{-1}, 0.6 mg kg^{-1} and 1.3 mg kg^{-1}respectively for some sampling

Table 4. Soil moisture content

Sample name	*Sample layer [cm]*	*Mass of empty container [g]*	*Mass of container + sample before drying [g]*	*Mass of container + sample after drying [g]*	*Moisture content [%]*
M11	0–25	51.8315	75.4234	73.2435	9.24
	25–50	51.3661	74.1878	72.4906	7.44
	50–75	49.9757	78.8825	75.2421	12.59
M12	0–25	50.5424	82.0956	79.1077	9.47
	25–50	48.7002	78.0861	75.4438	8.99
	50–75	48.0575	77.6417	75.2200	8.19
	75–100	49.3037	75.1385	72.9608	8.43
M13	0–25	49.8464	79.0846	74.0951	17.07
	25–50	50.4257	82.6054	77.9922	14.34
	50–75	48.6373	83.1727	78.2866	14.15
	75–100	48.8749	82.4759	77.7055	14.20
RA	Top layer	35.3620	82.9546	81.4488	3.16

location. This might be an indication that these elements were available for uptake from by plants. Even though these micronutrients are essential to plants, elevated concentrations may cause several problems, including the toxicity of the environment. The transfer factor values for Cu and K (≥1) indicate higher absorption of metal from the soil by the plant. The TF value for K in an active sample was above the TF limit of 1, however, K is a macronutrient and is needed in abundance for plants to grow.

The possibility of migration of these elements will be confirmed by fractionation by sequential extraction for PTEs. These results do not provide enough information to conclude on the migration of PTEs. However, based on the plant elemental uptake, it is apparent that 1 meter covering soil for deposit No.1 might not be effective. More information with regards to the mobility of PTEs will be revealed when the fractionation of PTEs in soil samples is completed. Additional samples will be collected from different sampling points of the deposit No.1 to ensure the representation of the samples. This investigation is planned to be repeated two times in the next years to ensure a more reliable conclusion.

Acknowledgement

This research is supported by Stipendium Hungaricum [Reg. No.: 238700], by the South African Department of Higher Education and Training and by the Higher Education Institutional Excellence Program [NKFIH-1159-6/2019] awarded by the Ministry for Innovation and Technology within the framework of water-related research of Szent István University.

References

Adio, A. (2017): 'Heavy Metal Concentrations in Plants and Soil along Heavy Traffic Roads in North Central Nigeria', (June). doi: 10.4172/2161-0525.1000334.

Agic, R., Mirecki, N., Šunić, L., Milenković, L., Ilić, Z. S. (2015): 'Transfer factor as indicator of heavy metal contetnt in plants', Fresenius Environmental Bulletin. (December). PSP Volume 24 – No 11c, 4212–4219.

Commission of the European Communities. (1986): 'Council Directive (86/278/EEC) of 12 June on the protection of the environment, and in particular of the soil, when sewage sludge is used in agriculture. Official Journal of the European Communities', L 181, 6–12.

Denneman, C. A. J., Robberse J.G. (1990): 'Ecotoxicological risk assessment as a base for development of soil quality criteria. In: Contaminated Soil'90; third international KfK/TNO conference on Contaminated Soil'; F. Arendt, M. Hinselveld and W.J. van den Brink eds; Kluwer academic publishers, Dordrecht/Boston/ London.

Fite, T., Leta, S. (2015): 'Determination of Levels of As, Cd, Cr, Hg and Pb in Soils and Some Vegetables Taken from River Mojo Water Irrigated Farmland at Koka Village, Oromia State, East Ethiopia', 4531, 352–372.

Gałuszka, A., Migaszewski, Z., Duczmal-Czernikiewicz, A., Dołęgowska, S. (2016). 'Geochemical background of potentially toxic trace elements in reclaimed soils of the abandoned pyrite – uranium mine', Int. J. Environ. Sci. Technol. (2016), 2649–2662. doi: 10.1007/s13762-016-1095-z.

He, Z., Shentu, J., Yang, X., Baligar ,V. C., Zhang, T., Stoffella, P. J. (2015): 'Soil pollution in the world (EEC', Journal of Environmental Indicators, 9(Table 2), 17–18. Available at: http://www.eea.europa.eu/data-and-maps/ indicators.

National Research of The National Academies. (2012): 'Uranium Mining in Virginia: Scientific, Technical, Environmental, Human Health and Safety, and Regulatory Aspects of Uranium Mining and Processing in Virginia'. doi: 10.17226/13266.

Hooda, P. S. (2014): Trace Elements in Soils. doi: 10.13140/ RG.2.1.3377.1123.

Hungarian Central Statistical Ofice. (no date): '5.10.4. Main data of meteorological observation stations (1985-) *', https://www.ksh.hu/docs/eng/xstadat/xstadat_annual/i_met002c.html. Retreaved (21 November 2019).

IAEA (2004): 'Environmental Contamination from Uranium Production Facilities and their Remediation', Enivironmental contamination from uranium production facilities and their remediation, (February), 11–13.

Intawongse, M., Dean, J. R. (2006): 'Uptake of heavy metals by vegetable plants grown on contaminated soil and their

bioavailability in the human gastrointestinal tract'. Food Additives and Contaminants. doi: 10.1080/02652030500387554.

Jones, C., Jacobsen, J. (2001): 'Plant Nutrition and Soil Fertility: Nutrient Management Module No.2', Nutrient Management Module, (2), p. 282. Available at: www.colostate.edu/Depts/CoopExt/TRA/PLANTS/nutrient.html.

Kabata-pendias, A., Pendias, H. (2001): Trace Elements in Soils and Plants Trace Elements in Soils and Plants.

Laţo, A. Radulov I., Berbecea, A., Laţo, K., Crista, F. (2012): 'The transfer factor of metals in soil-plant system', Research Journal of Agricultural Science, 44(119), 67–72.

Lohry, R. (2007): 'Micronutrients : Functions , Sources and Application Methods', 2007 Indiana CCA Conference Proceedings. Nutra Flo Company, Sioux City, Iowa.

Malovics, G. (2014): 'Uranium mine opening in Pecs, Hungary'. Retrieved 09 24, 2017, from Ejatlas.org: http://ejalas.org/conflict/uranium-mine-reopening-in-pecs-hungary.

Nazir, R., Khan, M., Masab, M., ur Rehman, H., ur Rauf, N., Shahab, S., Ameer, N., Sajed, M., Ullah, M., Rafeeq, M., Shaheen, Z. (2015): 'Accumulation of Heavy Metals (Ni, Cu, Cd, Cr, Pb, Zn, Fe) in the soil , water and plants and analysis of physico-chemical parameters of soil and water Collected from Tanda Dam kohat', Journal of Pharmaceutical Sciences and Research, 7(3), 89–97.

Okoro, H. K., Ige, J. O., Iyiola, O. A., Ngila, J. C. et al. (2017): 'Fractionation profile, mobility patterns and correlations of heavy metals in estuary sediments from olonkoro river, in tede catchment of western region, Nigeria', Environmental Nanotechnology, Monitoring and Management, 8. doi: 10.1016/j.enmm.2017.04.003.

Pérez-Moreno, S. M., Gázquez, M. J., Pérez-López, R., Bolivar J. P. (2018): 'Validation of the BCR sequential extraction procedure for natural radionuclides', Chemosphere, 198, 397–408. doi: 10.1016/j.chemosphere.2018.01.108.

Reis, P., Pereira, R., Carvalho, F. P., Oliveira, J., Malta, M., Mendod, S., Lourenço, J. (2018): 'Life history traits and genotoxic effects on Daphnia magna exposed to waterborne uranium and to a uranium mine effluent – A transgenerational study', Aquatic Toxicology, 202 (July), 16–25. doi: 10.1016/j.aquatox.2018.06.009.

Rékási, M., Filep, T. (2012): 'Fractions and background concentrations of potentially toxic elements in Hungarian surface soils', 7461–7471. doi: 10.1007/s10661-011-2513-9.

Sahoo, S. K., Mohapatra, S., Sethy, N. K., Patra, A. C., Shukla, A. K., Kumar, A. V., et al. (2010): Natural radioactivity in roadside soil along Jamshedpur-Musabani Road: A mineralised and mining region, Jharkhand and associated ris. Radiation Protection Dosimetry, 140(3), 281–286.

Skipperud, L., Salbu, B. (2015): 'Sequential extraction as a tool for mobility studies of radionuclides and metals in soils and sediments', Radiochimica Acta, 103(3), 187–197. doi: 10.1515/ract-2014-2342.

Stanojković-Sebić, A., Poštić, D., Pivic, R. (2017): 'Microelements and Heavy Metals Content in Frequently Utilized Medicinal Plants Collected from the Power Plant Area Microelements and Heavy Metals Content in Frequently Utilized Medicinal Plants Collected from the Power Plant Area', Microelements (February). Natural Product Communications.

Soltani, N., Keshavarzi, B., Moore, F., Sorooshian, A., Ahmadi, M. R (2017): 'Distribution of potentially toxic elements (PTEs) in tailings, soils, and plants around Gol-E-Gohar iron mine, a case study in Iran', Environ Sci Pollut Res Int. 24(23), 18798–18816. doi: 10.1007/s11356-017-9342-5.

Voss, R. (1998): 'Micronutrients'. Department of Agronomy, Iowa State University. Ames, IA 50011.

VROM (2000): 'Circular on target values and intervention values for soil remediation', Netherlands Government Gazette, 2000, p. 51.

Wallner, A., Stein, P. (2012): 'Uranium Mining in and for Europe'. Österreichisches Ökologie-Institut, Vienna.

WHO (1996): Permissible limits of heavy metals in soil and plants (Geneva: World Health Organization), Switzerland.

Lamlile Khumalo, PhD Student
Dr. György Heltai, DSc Professor Emeritus
Dr. Márk Horváth, PhD assistant Professor
Szent Istvan University Institute of environmental Sciences
Department of Chemistry
Gödöllő, Páter Károly u. 1, 2100, Hungary
E-mail: lamlilekhumalo@gmail.com
heltai.gyorgy@mkk.szie.hu
Horvath.Mark@mkk.szie.hu